Universitat de Barcelona

Departament d'Estructura i Constituents de la Matèria

# Interface dynamics in two-dimensional viscous flows

Eduard Pauné i Xuriguera

Barcelona, 2002

Universitat de Barcelona
Departament d'Estructura i Constituents de la Matèria
Programa de doctorat Física de la Matèria Condensada
Bienni 1997/99

# Interface dynamics in two-dimensional viscous flows

Memòria de la tesi presentada el novembre de 2002 per
Eduard Pauné i Xuriguera
per optar al títol de Doctor en Física,
dirigida pel Dr. Jaume Casademunt Viader

Dr. Jaume Casademunt Viader

*Als meus pares*

# Agraïments

Una tesi doctoral és fruit d'anys de feina, i no és només, com podria semblar, una obra individual, sinó que reflexa també en major o menor mesura el treball de molta altra gent que ha contribuït a la seva realització. A tots ells vull agrair la seva ajuda durant tot aquest temps.

Primer de tot el meu agraïment per en Jaume, que ha estat el meu director de tesi. Durant el darrer any de llicenciatura em va despertar l'interès per un camp de la física que jo havia injustament menystingut, i durant la tesi em va introduir a un problema interessant (i difícil), que ha suposat per a mi un repte apassionant. En Jaume m'ha ensenyat molta física, i d'ell també he après que tinc molt per aprendre. També he d'agrair-li la seva dedicació, i que la seva porta sempre hagi estat oberta als meus dubtes i preocupacions.

Vull donar les gràcies a tota aquella altra gent amb qui he col.laborat durant la tesi. En Jordi Ortín, amb qui no tan sols he treballat (si bé més breument del que hauria desitjat) sinó que sempre que ha calgut m'ha donat un cop de mà, ja fos informàtic o burocràtic. Agraïments igualment per en Michael Siegel, que em va ensenyar un bon grapat de coses de càlcul numèric i programació, i que va tenir la paciència suficient (que va ser molta) perquè la nostra col.laboració fos fructífera. Sense ell la meva tesi seria molt diferent del que és ara.

I de la mateixa manera seria molt diferent si no hagués estat per en Francesc Magdaleno, a qui tinc molt per agrair. D'ell vaig aprendre quasi tot el que sé de tècniques conformes, i aquesta tesi és en certa mesura una continuació del seu treball. Espero haver estat un digne continuador de la 'saga conforme', i lamento no haver pogut treballar més amb ell. I també li he d'agrair les molt bones estones que he passat amb ell, el seu bon humor i ànim en qualsevol circumstància.

Els meus agraïments per en Jordi Soriano, un treballador incansable sempre disposat a donar un cop de mà en qualsevol cosa que li demanés i a dedicar el seu temps per ajudar-me a resoldre qualsevol problema. I l'Enric, amb qui he col.laborat un temps i amb qui he passat bones estones en uns quants congressos. No puc oblidar-me tampoc d'en Roger, amb qui he treballat

harmònicament, compartit despatx i fins i tot habitació uns quants cops.

Fins ara m'he centrat sobretot en els agraïments científics i acadèmics, la qual cosa no vol dir pas que no siguin alhora en la majoria dels casos agraïments personals. De la facultat hi ha una petita llista de gent que han estat amics i companys meus bona part d'aquest temps. En Xavi, i en David, que van començar la tesi al mateix temps que jo, i amb qui he compartit converses, dinars i sobretot molts cafès. En Tomàs, amb el seu humor càustic sempre a punt, en Mateu, silenciós però no perquè li manquin coses per dir, i l'Iván i en Jose. I també l'Andrea Rocco, *claro*.

Vull donar les gràcies a algunes persones que vaig conèixer durant l'estada al NJIT. La Tudy i l'Amit, que em van acollir a casa seva, i l'Amir, i l'Urmi.

Els meus agraïments a D-Recerca, Associació de doctorands i becaris de recerca de Catalunya, així com a la Federación de jóvenes investigadores Precarios per tot l'esforç que han fet per aconseguir que els joves investigadors vegem reconeguts els nostres drets laborals bàsics, i el paper fonamental que representem en el sistema de recerca públic d'aquest país. Aquest agraïment va destinat sobretot a tots aquells que han dedicat generosament bona part del temps de la seva tesi a treballar per millorar les condicions de tots, sense fer cas d'aquells que, com el conseller Mas-Colell afirmen que: *Vostè el què ha de fer és preocupar-se d'acabar la seva tesi.* Si una memòria de tesi inclogués una secció de desagraïments en Mas-Colell ben segur que hi ocuparia un lloc destacat.

Per acabar la secció dedicada a la recerca, no vull oblidar que una eina fonamental per realitzar aquesta tesi, i de fet qualsevol altra en l'actualitat, ha estat la informàtica. I més en concret, GNU/Linux, el sistema operatiu lliure que he utilitzat durant la major part de la tesi. Per això vull agrair l'esforç de tots aquells que han treballat i continuen treballant per posar a l'abast de tothom aquest extraordinari sistema operatiu.

Hi ha també algunes persones que fins ara no he anomenat però que no poden deixar d'estar en aquests agraïments. Un record especial i afectuós per a la Neus, que em va acompanyar en els primers anys d'aquesta tesi. I un calorós agraïment per a l'Eva, l'Oriol i en Ramon, encara que aquests darrers més aviat han representat obstacles per la finalització de la tesi, si tenim en compte que el vi no és gaire compatible amb el treball inteł.lectual que una tesi requereix.

La Teresa ha estat durant aquests darrers temps de llarg el meu principal suport i inspiració. El seu somriure m'ha animat en tot moment. Moltes gràcies.

Finalment, la meva família, que sempre ha estat al meu costat. Els meus pares, la Carme i en Magí, la meva germana Gemma, l'Alberto i també el més petit de la família, el meu nebodet Tomàs.

# Contents

# Capítol 0

# Resum

## 0.1 Introducció

L'aparició espontània d'estructura i ordre en sistemes amb substrats que no en tenen ha fascinat i intrigat durant segles científics pertanyents a les més variades disciplines. Aquestes estructures es troben en un gran nombre de sistemes del camp de la física, la biologia o la química, i apareixen quan els sistemes són apartats de l'equilibri termodinàmic. L'estudi d'aquests fenòmens ha donat lloc al naixement d'un camp de la física que du per nom *formació d'estructures fora d'equilibri* [CH93, Man90, Wal97, NP77], que s'ocupa no només de sistemes físics sinó que també s'endinsa en la química i la biologia. La comprensió de la formació d'estructures ha avançat notablement gràcies al desenvolupament de les ciències no lineals, on conflueixen disciplines de caire matemàtic com la teoria de sistemes dinàmics [GH83, Cra91], o les geometries fractals [Man77] amb la tradició de la mecànica estadística fora d'equilibri o la hidrodinàmica.

Un dels camps inclosos dins dels marc general de la formació d'estructures és la formació d'estructures interficials [Lan80, Lan87, KKa88, Pel88, BM91], on l'estructura és descrita en termes d'una interfície entre dues fases macroscòpiques. En molts casos la dinàmica del problema complet es pot projectar sobre la interfície, tot reduint la dimensió i simplificant-lo, si bé la projecció sobre la interfície pot introduir no localitats al problema. En els problemes de dinàmica d'interfícies una de les dificultats des del punt de vista matemàtic és que aquests defineixen problemes anomenats de contorn lliure, ja que la solució involucra resoldre equacions diferencials en derivades parcials amb condicions de contorn sobre un contorn (la interfície) que és mòbil, i el moviment del qual ve determinat precisament per la pròpia solució de les equacions diferencials en el volum.

La dinàmica d'interfícies fora d'equilibri planteja qüestions fonamentals en el context de formació d'estructures i dinàmica no lineal en sistemes extesos en l'espai, així com en les matemàtiques dels problemes de contorn lliure. Malgrat això, el seu estudi ha estat motivat en molts casos per problemes industrials o aplicats. Una gran varietat de fenòmens estan inclosos en la dinàmica d'interfícies, com ara en desplaçament de fluids en medis porosos o digitació viscosa [BKL+86], solidificació [PA92], propagació de flames [Mar51, PC82], combustió sense flama [ZOM98] o descàrregues elèctriques en gasos [Rai91]. Més concretament, aquesta tesi es centra en la digitació viscosa en ceł.les de Hele-Shaw [BKL+86, Tan00] (conegut com fluxos de Hele-Shaw), amb la intenció d'avançar en la comprensió dels mecanismes universals que governen la dinàmica d'interfícies. L'objectiu és doble: d'una banda ens hem centrat en el paper de la tensió superficial i el contrast de viscositats en la dinàmica de les estructures en forma de dit, i de l'altra hem estudiat l'efecte del desordre en fluxos de Hele-Shaw, sobretot pel que fa a les propietats estadístiques de les interfícies rugoses que es formen en presència de desordre.

### 0.1.1 Fluxos de Hele-Shaw

Aquesta tesi tracta de la dinàmica de la interfície entre dos fluids confinats en una ceł.la de Hele-Shaw [Hel98]. Una ceł.la de Hele-Shaw consisteix en dues plaques planoparał.leles separades per una distància molt petita $b$, de manera que a l'interior de la ceł.la hom troba un flux potencial en dues dimensions. En la geometria clàssica, tal i com la van formular Saffman i Taylor [ST58], la ceł.la té forma rectangular, amb amplada $W$ i longitud $L$. D'un dels extrems s'injecta un fluid i per l'altre extrem s'extreu l'altre. A més de la geometria rectangular se n'han estudiat d'altres, com ara la radial [Pat81] o l'angular [TRHC89, Ben91].

El flux ve descrit per les equacions de Navier-Stokes i hom suposa que els fluids són incompressibles. Les condicions experimentals són tals que el sistema es troba en el límit d'alta fricció de manera que el terme inercial i el no lineal de Navier-Stokes són negligibles. El flux es pot considerar quasiestacionari, i tot junt equival a prendre valors petits del nombre de Reynolds. Considerant un flux de Poiseuille en la direcció perpendicular a les plaques s'arriba a que la velocitat $\mathbf{u}$ en dos dimensions (resultat de fer la mitjana a l'espaiat entre plaques) satisfà

$$\mathbf{u} = -\frac{b^2}{12\mu}\left(\nabla p - \mathbf{F}_{ext}\right) \tag{1}$$

on $\mu$ és la viscositat del fluid, $p$ és la pressió i $\mathbf{F}_{ext}$ és una força externa

que considerarem potencial amb $\nabla \mathbf{F}_{ext} = 0$. Aplicant que els fluids són incompressibles, $\nabla \cdot \mathbf{u} = 0$, s'obté que la pressió obeeix l'equació de Laplace

$$\nabla^2 p = 0. \tag{2}$$

L'Eq. (1) és la mateixa que satisfà la velocitat d'un fluid en un medi porós, si bé amb una constant de proporcionalitat diferent. L'Eq. (1) rep el nom de llei de Darcy.

A partir d'ara considerem la geometria rectangular clàssica: el fluid 1 és injectat a velocitat constant $V_\infty$ per un extrem de la ceł.la, desplaçant el fluid 2, i estan sotmesos a una gravetat efectiva $g_{eff} = g\cos\beta$ dirigida en la direcció $-\hat{\mathbf{x}}$. Si hom imposa igualtat de velocitats normals a la interfície s'obté la condició de contorn següent a la interfície

$$U = -\frac{b^2}{12\mu_1}\left(\partial_n p_1 + \rho_1\, g_{eff}\, \hat{\mathbf{n}}\cdot\hat{\mathbf{x}}\right) = -\frac{b^2}{12\mu_2}\left(\partial_n p_2 + \rho_2\, g_{eff}\, \hat{\mathbf{n}}\cdot\hat{\mathbf{x}}\right), \tag{3}$$

on $\hat{\mathbf{n}}$ és el vector unitari normal a la interfície i $\rho_{1,2}$ són les densitats del fluid 1 i 2 respectivament. La condició de contorn Eq. (3) es coneix com condició cinètica. Per determinar completament el problema cal una segona condició de contorn sobre la interfície, i aquesta ve donada (en la seva versió més simple) pel salt de pressions de Young-Laplace

$$p_1 - p_2 = \sigma\kappa, \tag{4}$$

essent $\sigma$ la tensió superficial i $\kappa$ la curvatura. Així doncs, el problema queda completament definit per les Eqs. (2, 3, 4), juntament amb la condició de contorn $\mathbf{u} = V_\infty\hat{\mathbf{x}}$ a $|x| \to \infty$ i les condicions adequades a les parets.

El problema també admet una formulació en termes de la funció corrent $\Psi$, l'harmònic conjugat de la pressió. Així, $\Psi$ satisfà l'equació de Poisson [TA83]

$$\Delta\Psi = -\Gamma \tag{5}$$

on $\Gamma$ és la distribució de vorticitat, singular i localitzada a la interfície: $\Gamma(\mathbf{r}) = \gamma(s)\delta\left[\mathbf{r} - \mathbf{r}(s)\right]$ on la vorticitat $\gamma$ té la forma [TA83]

$$\gamma = \frac{\Delta\mu}{\bar{\mu}}\mathbf{w}\cdot\hat{\mathbf{s}} + \left(\frac{\Delta\mu}{\bar{\mu}}V_\infty + \frac{\Delta\rho g b^2}{12\bar{\mu}}\right)\hat{\mathbf{x}}\cdot\hat{\mathbf{s}} + \frac{\sigma b^2}{12\bar{\mu}}\frac{\partial\kappa}{\partial s}. \tag{6}$$

En dues dimensions el camp de velocitats degut a un full de vòrtexs com el que tenim en aquest cas ve donat per la fórmula integral de Birkhoff [Bir54, TA83]

$$\mathbf{w} = \mathbf{w}(s,t) = \frac{1}{2\pi}\mathrm{P}\int ds' \frac{\hat{\mathbf{z}}\times\left[\mathbf{x}(s,t) - \mathbf{x}(s',t)\right]}{|\mathbf{x}(s,t) - \mathbf{x}(s',t)|^2}\gamma(s',t) \tag{7}$$

on la P indica que la integral s'ha d'avaluar segons la prescripció de part principal. Cal tenir en compte que l'expressió per $\mathbf{w}$ no inclou la contribució potencial (o irrotacional) $\mathbf{u_{pot}}$ originada per les condicions de contorn a l'infinit, de manera que la velocitat $\mathbf{u}$ d'un punt de la interfície ve donada per la suma $\mathbf{u} = \mathbf{w} + \mathbf{u_{pot}}$.

Les equacions es poden adimensionalitzar fent servir la quantitat $W/2\pi$ per les longituds i la combinació [TA83]

$$U_* = cV_\infty + g_{eff}\frac{b^2(\rho_2 - \rho_1)}{12(\mu_1 + \mu_2)} \tag{8}$$

per escalar les velocitats, de manera que en el problema només apareixen dues quantitats adimensionals, el contrast de viscositats $c$ i la tensió superficial adimensional $B$, donades per

$$B = \frac{\pi^2 b^2 \sigma}{3W^2(\mu_1 + \mu_2)U_*} \tag{9}$$

$$c = \frac{\mu_2 - \mu_1}{\mu_1 + \mu_2}. \tag{10}$$

### 0.1.2 L'experiment de Saffman i Taylor. Problema de selecció i dinàmica

Saffman i Taylor [ST58] van estudiar experimentalment el desplaçament d'un fluid viscós per un de menys viscós en una ceł.la de Hele-Shaw, amb valors de $c$ propers o molt propers a 1. Van observar que una interfície inicialment plana és inestable, de manera que els petits bonys que es formen inicialment ràpidament creixen en forma de dits d'aire que penetren en el líquid. Els dits competeixen entre ells i a temps llargs un únic dit d'amplada propera a la meitat de l'amplada del canal sobreviu. Aquest dit es coneix com a dit de Saffman-Taylor (ST), i la inestabilitat de la interfície plana rep el nom d'inestabilitat de Saffman-Taylor, equivalent a la inestabilitat de Mullins-Sekerka que apareix en solidificació [MS64]. La seva relació de dispersió en variables adimensionals és [Cvv59]

$$\omega(k) = |k|(1 - Bk^2) \tag{11}$$

i d'aquesta relació es veu que hi ha una banda de modes inestables (aquells amb $|k| < B^{1/2}$) l'amplada de la qual està controlada per la tensió superficial adimensional. D'altra banda, el fet que en la relació de dispersió aparegui el valor absolut de $k$ és una indicació del caràcter no local del problema.

La inestabilitat inicial dóna lloc a la formació d'una graella de dits que creixen independentment fins que s'inicia el règim no lineal, en el qual té

lloc un procés de competició entre dits (per contrast de viscositat alt) que finalitza amb un únic dit d'amplada propera a 1/2 de l'amplada del canal. Per contrast de viscositats baix la situació és diferent ja que el procés de competició està fortament inhibit [Mah85] de manera que el dit de Saffman-Taylor no és l'atractor universal per a qualsevol valor de $c$ [CJ91, CJ94].

Saffman i Taylor [ST58] van trobar una família uniparamètrica de solucions estacionàries exactes en forma de dit, en absència de tensió superficial. En aquestes solucions l'amplada relativa $\lambda$ del dit és el paràmetre continu que caracteritza les solucions. Aquestes reprodueixen bastant bé les formes observades experimentalment *si* l'amplada $\lambda$ s'escull d'acord amb l'observada experimentalment (que depèn del valor de $B$ utilitzat). Ara bé, la teoria de tensió superficial zero és incapaç de predir el valor observat de $\lambda$ en funció de $B$: aquest és el problema de la selecció, com la introducció d'una $B$ finita *selecciona* el valor de $\lambda$. Aquest problema no va ser resolt fins a mitjans dels anys 80 per diversos autors [HL86, Shr86, CDH$^+$86] que van demostrar que la tensió superficial selecciona un conjunt discret de valors de $\lambda$ del continu inicial, de manera que $\lambda = \lambda_n(B)$, amb $\lambda_n > 1/2$. Per $B \to 0$ es troba $\lambda_n \to 1/2$, i només la solució amb $n = 0$ (la més estreta) és linealment estable[1], tota la resta són inestables [Ben86]. Aquest escenari de selecció també s'aplica a d'altres problemes de formació d'estructures interficials, i és conegut com a Solvabilitat Microscòpica.

La Part II d'aquesta tesi està dedicada a la generalització d'aquest escenari a la dinàmica, tot partint de l'existència de solucions exactes sense tensió superficial i plantejant el paper selectiu de la tensió superficial. Prendrem com a base el formalisme i els resultats descrits per Siegel i Tanveer [ST96] entre d'altres, referents als efectes singulars de tensió superficial en la dinàmica.

La part III es centra en l'estudi del paper del contrast de viscositat en la dinàmica, tot comprovant una conjectura de Casademunt i Jasnow [CJ91, CJ94] i caracteritzant a nivell quantitatiu la sensibilitat de la dinàmica a aquell paràmetre, tot identificant nous atractors que competeixen amb el de Saffman-Taylor.

### 0.1.3 Dinàmica d'interfícies rugoses

La dinàmica d'una interfície propagant-se en un medi desordenat ha estat estudiada intensivament en els darrers anys [HHZ95, BS95, Kru97], sobretot pel que respecta a les seves propietats d'escala. S'ha trobat evidència d'invariància d'escala i universalitat en diversos sistemes, incloent fluxos de Hele-

[1] Però inestable a pertorbacions d'amplitud finita. L'amplitud $A$ de les pertorbacions que inestabilitzen el dit decreix ràpidament amb $B$, d'acord amb la relació [Ben86] $\ln A \sim -1/\sqrt{B}$.

Shaw amb desordre [REDG89, HFV91, HKzW92], creixement de colònies bacterianes [VCH90, MM92], combustió en absència de flama [ZZAL92], entre d'altres. En el cas que ens interessa, el del flux de Hele-Shaw en una ceł.la desordenada, l'experiment original [REDG89] consisteix en injectar aigua per un extrem d'una ceł.la plena de petites boles de vidre compactades. La presència de les boletes arruga la interfície, que seria estable en absència d'aquestes. La magnitud física rellevant en aquest tipus d'experiments és l'amplada $W$ de la interfície, definida com $W(t) = \langle \overline{[h(x,t) - \overline{h}]^2} \rangle^{1/2}$ on $h(x,t)$ és l'alçada de la interfície, $\overline{\quad}$ indica mitjana espacial i $\langle \quad \rangle$ mitjana sobre realitzacions. Per una interfície inicialment plana l'amplada $W(t)$ creix d'acord amb la llei de potències [FV85] següent $W(t) \sim t^{\beta}$ abans de saturar. L'amplada un cop el creixement ha saturat, $W_{sat}$, també satisfà una llei de potències amb la mida $L$ del sistema: $W_{sat}(L) \sim L^{\alpha}$. Els exponents $\beta$ i $\alpha$ reben el nom d'exponent de creixement i de rugositat respectivament.

Bona part del treball experimental i teòric dut a terme en el camp de la dinàmica d'interfícies rugoses des de finals dels anys 80 es basa en l'equació coneguda com a KPZ [KPZ86], que té la forma

$$\frac{\partial h(\mathbf{x},t)}{\partial t} = \nu \nabla^2 h(\mathbf{x},t) + \frac{\lambda}{2}[\nabla h(\mathbf{x},t)]^2 + \eta(\mathbf{x},t) \tag{12}$$

on $\lambda$ i $\nu$ són constants positives i $\eta(\mathbf{x},t)$ és un soroll. Aquesta equació suposadament descriu de manera universal les propietats d'escala d'interfícies rugoses en sistemes d'allò més variats, i està caracteritzada pels exponents $\alpha = 1/2$ i $\beta = 1/3$ en dimensió 1. L'experiment abans descrit [REDG89] va ser ideat precisament amb la intenció d'observar els exponents de KPZ, però en canvi l'exponent obtingut va ser $\alpha \simeq 3/4$, en clara discrepància amb l'exponent predit per a KPZ. L'experiment va ser repetit per altres autors [HFV91, HKzW92] que si bé van obtenir resultats no plenament coincidents amb els anteriors sí que van confirmar que l'Eq. (12) no descriu les propietats d'escala de la interfície en experiments d'invasió forçada d'una ceł.la de Hele-Shaw plena de boletes de vidre.

Nombroses modificacions de l'equació KPZ van ser proposades en anys següents que podrien explicar els resultats experimentals. Aquestes consisteixen en utilitzar un soroll $\eta(x,t)$ que no sigui gaussià i blanc. Així, diferents valors dels exponents s'obtenen amb soroll tipus llei de potències [Zha90] i soroll correlacionat [MHKZ89]. En ambdós casos es poden obtenir variant els paràmetres que controlen el soroll valors d'$\alpha$ en un ampli rang que inclou els resultats experimentals, ara bé, no està en absolut clar com connectar el soroll original dels experiments amb el soroll de l'equació. Una manera lleugerament diferent d'afrontar el problema consisteix en utilitzar un soroll congelat $\eta(h,x)$ enlloc de l'original soroll dinàmic. Aquest tipus de soroll

és força més semblant al soroll present als experiments, però l'equació KPZ amb soroll congelat tampoc explica satisfactòriament els resultats experimentals [Les96].

Hom no s'hauria de sorprendre del fet que l'equació KPZ no expliqui satisfactòriament els experiments d'invasió forçada d'una ceł.la de Hele-Shaw amb desordre, ja que KPZ és una equació completament fenomenològica per descriure el creixement d'interfícies rugoses on el creixement és essencialment local (com la mateixa equació), contràriament al que succeeix en una ceł.la de Hele-Shaw, on els efectes no locals són els dominants. Recentment [GB98] s'ha proposat una equació no local per estudiar el problema, i usant arguments de tipus Flory s'ha trobat $\alpha \simeq 3/4$. Una manera alternativa de tractar la no-localitat és mitjançant un camp de fase, tal i com s'ha fet a les Refs. [DRE+99, DRE+00, HMSL+01]. Ara bé, en ambdós casos el soroll és introduït de manera fenomenològica. Des d'un punt de vista experimental recentment s'han realitzat experiments [HMSL+01, SRR+02, SOHM02b] amb ceł.les de gap inhomogeni, de manera que el desordre és molt més controlat que en el cas de les boletes de vidre. Aquests experiments mostren que l'exponent $\alpha$ depèn fortament dels paràmetres experimentals, i en alguns casos la interfície no satisfà la hipòtesi d'escala de Family-Vicsek. La part IV d'aquesta tesi aporta un marc teòric unificat i general per a l'estudi de la invasió de ceł.les amb gap aleatori, en la línia dels experiments citats [HMSL+01, SRR+02, SOHM02b].

## 0.2 Preliminars

### 0.2.1 Formulació del mapatge conforme. Punt de vista de sistemes dinàmics

La tècnica analítica més utilitzada i que ha donat més fruits en el cas $c = 1$ és la tècnica matemàtica del mapatge conforme [BKL+86], que consisteix en mapar la regió ocupada pel fluid viscós a l'interior del cercle unitat del pla complex mitjançant una funció $f(\omega, t)$, de manera que la interfície és mapada en el contorn del cercle. Així, un punt $z$ del fluid està relacionat amb un punt de l'interior del cercle per $z = f(\omega)$. Si considerem condicions periòdiques de contorn en l'eix $y$ i de període $2\pi$ el mapa pren la forma $f(\omega, t) = -\ln \omega + h(\omega, t)$, amb $h(\omega, t)$ analítica a l'interior i $\partial_\omega f(\omega, t) \neq 0$ també a l'interior del cercle unitat. Es pot demostrar que l'evolució del mapa ha de satisfer [BKL+86, Mag00, CM00]

$$\mathrm{Re}\left[i\partial_s f(s,t)\partial_t f^*(s,t)\right] = 1 - B\partial_s \mathrm{H}[\kappa] \tag{13}$$

per $w = e^{is}$, on la curvatura $\kappa$ s'expressa en funció de $f$ com $\kappa(s) = -|\partial_s f|^{-1}\mathrm{Im}[\partial_s^2 f/\partial_s f]$ i H[$g$] és la transformada de Hilbert en el cercle unitat.

L'equació (13) pel mapa $f(w,t)$ és impossible de resoldre explícitament si $B \neq 0$, però en canvi en el cas $B = 0$ es coneixen classes molt generals de solucions de l'equació. Les dues famílies de solucions més estudiades són les polinòmiques i les de tipus pol o logarítmiques. Les transformacions polinòmiques sempre desenvolupen singularitats a temps finit (en forma de cúspides) [SB84, Sar85]. D'altra banda les solucions de tipus pol o logarítmiques tenen la forma

$$f(w,t) = -\ln w + d(t) + \sum_{j=1}^{N} \gamma_j \ln\left[1 - \alpha_j(t) w\right] \tag{14}$$

on les constants complexes del moviment $\gamma_j$ han de satisfer $\sum_{j=1}^{N} \gamma_j = 2(1-\lambda)$, on $\lambda$ és la fracció del canal ocupada pels dits asimptòtics. Les solucions exactes que estudiarem en aquesta tesi són d'aquesta forma, ja que contenen evolucions lliures de singularitats per tot temps. A més, amb els paràmetres apropiats reprodueixen la fenomenologia observada experimentalment i alguns autors han cregut que poden descriure tota la fenomenologia present per $B \neq 0$ [PMW94, MWD94, MW97]. Això ha estat rebatut tant des d'un punt de vista teòric [CM98, CM00, Mag00, PMC02] com numèric [KL01, PSC02]. Precisament, un dels principals objectius d'aquesta tesi ha estat precisar el paper de les solucions de $B = 0$ en la dinàmica del problema físic amb $B \neq 0$, tant des d'un punt de vista teòric com numèric.

La substitució del mapa Eq. (14) a l'equació d'evolució Eq. (13) defineix un sistema d'equacions diferencials ordinàries de dimensió finita, encastat en el sistema dinàmic de dimensió infinita del problema general. Això permet l'ús de les eines i els conceptes de la teoria de sistemes dinàmics, i des d'aquest punt de vista la utilització de les solucions Eq. (14) permet passar d'un problema definit en un espai de dimensió infinita (l'espai de configuracions interficials) a un problema en un espai de dimensió finita [MC98, CM00, Mag00, PMC02].

### 0.2.2 El model mínim de dos dits

La solució exacta amb $B = 0$ més simple que conté els punts fixes rellevants del problema, que són la interfície plana (PI), el dit de Saffman-Taylor (1ST) i el doble dit de Saffman-Taylor (2ST) va ser presentada a la referència [MC98] i estudiada àmpliament a les Refs. [CM00, Mag00]. Té la forma

$$f(\omega,t) = -\ln\omega + d(t) + (1-\lambda)\left\{\ln\left[1-\alpha(t)\omega\right] + \ln\left[1+\alpha(t)^*\omega\right]\right\} \tag{15}$$

i l'únic paràmetre que conté és l'amplada $\lambda$. El mapa Eq. (15) descriu una interfície amb un o dos dits d'amplada total $\lambda$.

La principal característica del flux de l'espai fàsic d'aquest model és el fet que la conca d'atracció de 1ST *no* és tot l'espai de les fases, sinó que existeix una separatriu que separa la seva conca d'atracció i la resta de l'espai. El flux que no és atret cap al dit de Saffman-Taylor evoluciona cap a un continu de punts fixes corresponents a solucions estacionàries de dos dits desiguals que avancen a la mateixa velocitat. El flux és tal que només apareix competició reeixida per $\lambda < 1/3$, i aquesta és poc significativa (s'eliminen dits molt petits).

L'interès des del punt de vista de sistemes dinàmics es troba en l'estudi de propietats globals del flux de l'espai fàsic i no en l'estudi de trajectòries particulars. Per comparar la dinàmica del problema amb i sense tensió superficial cal definir adequadament els sistemes dinàmics a comparar. Prenent un conjunt unidimensional de condicions inicials del tipus definit per l'Eq. (15) podem definir un sistema dinàmic $S^2(B)$ evolucionant-les en ambdós sentits temporals sota una tensió superficial finita $B$. El sistema dinàmic $S^2(B)$ és de dimensió 2 com el definit pel model mínim, que anomenarem $L^2(1/2)$ (prenem $\lambda = 1/2$, el valor seleccionat per tensió superficial petita). A la Ref. [MC98] es va mostrar que els dos sistemes dinàmics, $S^2(B)$ i $L^2(1/2)$ no són topològicament equivalents i que de cap manera $L^2(1/2)$ pot ser el límit de $S^2(B \to 0)$. Aquesta diferència és deguda a que el punt 2ST (el doble dit de ST) és un punt fix hiperbòlic (sella) en el sistema regularitzat amb tensió superficial petita i en canvi a $L^2(1/2)$ és un punt fix no hiperbòlic. D'altra banda, el flux del sistema dinàmic $L^2(1/2)$ és estructuralment inestable d'acord amb el teorema de Peixoto [GH83] degut a l'existència del continu de punts fixes, cosa que el fa inacceptable des d'un punt de vista físic.

## 0.3 Més enllà del model mínim

El model mínim de la secció anterior presenta característiques que el fan inacceptable des d'un punt de vista físic, en particular és estructuralment inestable. És clar que la introducció de la tensió superficial transformaria el flux en l'espai fàsic de manera que el sistema dinàmic seria estructuralment estable i el punt 2ST tindria el comportament sella desitjat, però el que cerquem és la possibilitat d'obtenir aquesta estructura *dins* de la classe de solucions exactes sense tensió superficial. Però com veurem, això no és possible, de manera que l'única manera d'obtenir la hiperbolicitat desitjada és mitjançant la inclusió de la tensió superficial. I aquest és el punt clau de l'escenari de solvabilitat dinàmica que proposarem.

### 0.3.1 Extensió en 2 dimensions

Una possible modificació de la solució Eq. (15) estudiada a la secció anterior és

$$f(\omega,t) = -\ln\omega + d(t) + (1-\lambda+i\epsilon)\ln[1-\alpha(t)\omega] \\ +(1-\lambda-i\epsilon)\ln[1+\alpha(t)^*\omega] \qquad (16)$$

on $\epsilon$ és una constant de moviment real i positiva. L'Eq. (16) és solució de l'equació d'evolució Eq. (13) amb $B = 0$, i descriu genèricament dos dits axisimètrics desiguals, amb la particularitat (en comparació amb el model mínim) que els dits poden presentar laterals no paral.lels i estretament a la base. A més, la solució Eq. (16) presenta singularitats a temps finit per un conjunt determinat de condicions inicials, així com situacions en les que la interfície es creua sobre ella mateixa, bé un cop (quan un zero de $\partial_\omega f(\omega)$ és a l'interior del cercle) o bé dos.

El flux en l'espai fàsic d'aquesta solució és força diferent del cas estudiat anteriorment: el continu de punts fixes existent per $\epsilon = 0$ desapareix, per tant aquesta solució sí que presenta competició reeixida per a qualsevol valor de $\lambda$ i $\epsilon \neq 0$. Els únics punts fixes existents són la interfície plana PI i el dit de Saffman-Taylor, que està degenerat en dos punts, 1ST(L) i 1ST(R) que representen les dues maneres d'aproximar-se al dit de Saffman-Taylor amb interfícies que originàriament tenen dos dits. Ara bé, en desaparèixer el continu de punts fixes també ha desaparegut el punt fix 2ST. Les conques d'atracció de 1ST(L) i 1ST(R) no estan separades per una trajectòria separatriu que neixi a PI i mori en un punt sella, com seria d'esperar, sinó per la regió de condicions inicials que desenvolupen singularitats a temps finit.

Per poder comparar la dinàmica de $B = 0$ amb la de $B \neq 0$ fem servir la construcció introduïda per Magdaleno i Casademunt [MC98], comentada prèviament. De la mateixa manera construïm el sistema dinàmic amb tensió superficial finita $S^2(B)$ que podem comparar amb el definit a partir de l'Eq. (16) amb $\lambda = 1/2$, $L^2(1/2,\epsilon)$. Ambdós sistemes tenen en comú (en el límit $B \to 0$) no només els punts fixes PI, 1ST(L) i 1ST(R) sinó també la trajectòria corresponent al dit de Saffman-Taylor depenent del temps. Però en canvi a $S^2(B)$ ha d'existir necessàriament un punt fix tipus sella connectat a una trajectòria separatriu fronterera entre les conques d'atracció de 1ST(L) i 1ST(R), ja sigui 2ST o un punt fix equivalent. Contràriament el sistema dinàmic de tensió superficial zero $L^2(1/2,\epsilon)$ no té aquest punt fix, i per tant no pot descriure en cap cas la dinàmica correcta (amb $B$ finita) d'una manera global encara que hi hagi competició reeixida. No obstant això, els nostres resultats no exclouen l'existència de trajectòries físicament acceptables ben descrites pel mapa Eq. (16).

### 0.3.2 Generalització a dimensions superiors

Fins ara hem demostrat que les solucions exactes Eqs. (15) i (16) *no* poden descriure la dinàmica del problema físic amb tensió superficial petita, però això no implica res sobre la resta de solucions exactes de $B = 0$. Per tant, el que s'ha fet és generalitzar els resultats anteriors al conjunt de solucions exactes de tipus logarítmic, la classe descrita per l'Eq. (14).

Les solucions estudiades fins ara són axisimètriques, i per verificar que aquesta propietat geomètrica no té cap influència en la dinàmica de competició de dits hem estudiat solucions exactes de dimensió baixa (2 i 3) amb dits no axisimètrics, obtenint que els diagrames fàsics són qualitativament iguals als de les solucions anteriors, i per tant les conclusions obtingudes no depenen de l'axisimetria dels dits.

Hem vist que en introduir una part imaginària (el terme $i\epsilon$) a la constant que multiplica el logaritme apareixien singularitats a temps finit en forma de cúspide. L'aparició de cúspides no és una particularitat de l'Eq. (16) sinó una propietat general de les solucions logarítmiques del tipus

$$f(w,t) = -\ln w + d(t) + \sum_{j=1}^{N} \gamma_j \ln\left[1 - \alpha_j(t) w\right] \tag{17}$$

presentades anteriorment (Eq. (14)). Hem demostrat que si algun $\gamma_j$ té una part imaginària no nul.la aleshores a l'evolució de $f(w,t)$ apareixeran cúspides per un conjunt de condicions inicials de mesura no nul.la, reproduint per tant les patologies que fan que la solució Eq. (16) no sigui físicament acceptable. D'altra banda, si tots els coeficients $\gamma_j$ són reals es pot demostrar [MWK99] que existeixen continus de punts fixes de manera que 2ST no és un punt sella i per tant l'estructura de punts fixes hiperbòlics necessària per descriure correctament la dinàmica és absent. Per tant, hem demostrat que les solucions exactes conegudes de tensió superficial zero no poden descriure en cap cas la dinàmica física d'una manera global, degut a que no contenen l'estructura de punt sella del doble dit, essencial per donar compte de la competició de dits.

### 0.3.3 Les solucions de $B = 0$ i la solvabilitat dinàmica

Les solucions de tensió superficial zero no són físiques d'una manera *global*, com acabem de veure. Aleshores, quin és el seu paper en la descripció dels fluxos de Hele-Shaw? El fet que els límits $B \to 0$ i $B = 0$ no coincideixin és una mostra del caràcter de pertorbació *singular* de la tensió superficial. Tanveer [Tan93] va demostrar que el seu efecte es manifesta a la interfície

en un temps d'ordre 1 fins i tot per valors de $B$ arbitràriament petits, i que després l'evolució amb i sense tensió superficial és dramàticament diferent en general. Però per a temps inferiors la tensió superficial actua com una pertorbació *regular* de la dinàmica de $B = 0$, i per tant per situacions no molt allunyades de la interfície plana (si bé dins del règim no lineal) les solucions de tensió superficial zero són una bona descripció del problema físic. A més, Siegel i Tanveer [ST96] van mostrar que l'evolució del dit de Saffman-Taylor depenent del temps convergia regularment a la solució física, triant és clar el valor de $\lambda$ d'acord amb la teoria de selecció. Tot plegat indica que existeixen trajectòries particulars, o conjunts de trajectòries que estan ben descrites per les solucions de $B = 0$, si més no qualitativament, i fins i tot quantitativament en alguns casos (com per exemple el dit ST depenent del temps), però aquestes trajectòries correctes no es poden distingir *a priori* de les incorrectes, i es fa necessari recórrer al càlcul numèric per saber si una trajectòria particular convergeix regularment a la dinàmica física.

Els resultats que hem exposat fins ara ens permeten concloure que el paper de la tensió superficial sobre les solucions exactes de $B = 0$ és restaurar la hiperbolicitat del punt fix del doble dit. D'acord amb la teoria de solvabilitat microscòpica que s'aplica al cas estacionari del dit de ST la tensió superficial transforma un continu de punts fixes (no hiperbòlics) en un conjunt discret de punts fixes inestables excepte un punt fix estable, i en solucions de dos dits estacionaris Magdaleno i Casademunt [MC99] van aplicar la teoria de solvabilitat obtenint que el continu de punts fixes es transforma sota l'acció de la tensió superficial en un conjunt discret de punts fixes inestables, llevat de 2ST que és un punt sella. Aquest darrer efecte és dinàmic en contrast amb la selecció de l'amplada del dit, i això ens du a proposar un *escenari de solvabilitat dinàmica* en el qual la tensió superficial transforma els continus de punts fixes corresponents a solucions amb N dits en conjunts discrets de punts fixes inestables i alguns de tipus sella, transformant radicalment el flux de l'espai fàsic i restaurant la hiperbolicitat del problema físic. L'anomenem dinàmica perquè contràriament al que succeeix en la selecció clàssica (estàtica) en aquest cas la dinàmica es veu fortament influïda per la tensió superficial, en implicar una profunda reestructuració de l'espai fàsic.

## 0.4 Efectes singulars de la tensió superficial en la dinàmica de dits

L'efecte de la tensió superficial en les solucions exactes de $B = 0$ i en particular en la solució Eq. (3.2) és poc conegut. Des d'un punt de vista teòric

l'única tècnica disponible per estudiar l'efecte d'una tensió superficial petita sobre les solucions exactes és la teoria asimptòtica desenvolupada per Tanveer [Tan93], que detalla com l'estructura analítica de les solucions es veu modificada per la tensió superficial i permet predir de manera quantitativa el rang de validesa de les solucions exactes, però no l'efecte de $B$ en la interfície. Per determinar aquests efectes s'ha de recórrer al càlcul numèric directe de l'evolució de la interfície.

La teoria de la selecció del dit estacionari fixa quin ha de ser el valor de l'amplada del dit, $1/2$ per $B \to 0$, de manera que aquelles solucions amb $\lambda \neq 0$ s'haurien de veure afectades notablement per la inclusió de tensió superficial. Però quin serà l'efecte sobre les solucions amb un valor de $\lambda$ compatible amb la selecció?

### 0.4.1 Teoria asimptòtica

La teoria pertorbativa asimptòtica [Tan93, ST96] és aplicable per $0 < B \ll 1$, i descriu els efectes de la introducció d'un valor petit de $B$ sobre condicions inicials $f(\omega, 0)$ especificades a *tot* el pla complex. Així, la teoria prediu els efectes sobre les singularitats i els zeros de $f$, que és el que determina en última instància la forma de la interfície.

Aplicada a les solucions exactes de tipus logarítmic, la teoria ens diu que la tensió superficial provoca l'aparició d'un nou tipus de singularitats, i al mateix temps deixa bàsicament inalterades les singularitats tipus pol i els zeros inicials. Aquest nou tipus de singularitats rep el nom de *singularitats filles*, i sorprenentment la seva dinàmica ve determinada únicament per la de la solució de $B = 0$, i no depèn de la tensió superficial. Quan les singularitats filles, inicialment formades lluny del cercle unitat (i per tant lluny del domini físic) s'atansen al cercle unitat el seu efecte sobre la interfície és gran, de manera que aquesta diferirà significativament de la solució de $B = 0$. A més, com que la dinàmica de les singularitats ve determinada únicament per la solució de $B = 0$ i és independent de $B$ l'impacte de la filla sobre el cercle unitat es produeix en un temps $t = \mathcal{O}(1)$ en el cas que l'impacte tingui lloc.

Hem aplicat la teoria pertorbativa asimptòtica a la solució Eq. (16), i un estudi qualitatiu ens ha permès concloure que per $\lambda < 1/2$ la singularitat filla *sempre* impacta, i per tant els efectes de la tensió superficial es manifesten en un temps d'ordre 1. En canvi, per $\lambda \geq 1/2$ un estudi qualitatiu no és concloent i cal recórrer al càlcul explícit de l'evolució de les filles. El resultat del càlcul numèric confirma els resultats qualitatius per $\lambda < 1/2$ i fa prediccions concretes per $\lambda \geq 1/2$, on segons els valors de $\lambda$, $\epsilon$ i la condició inicial l'impacte de la filla es produirà en $t = \mathcal{O}(1)$ o bé en $t = \mathcal{O}(-\ln B)$.

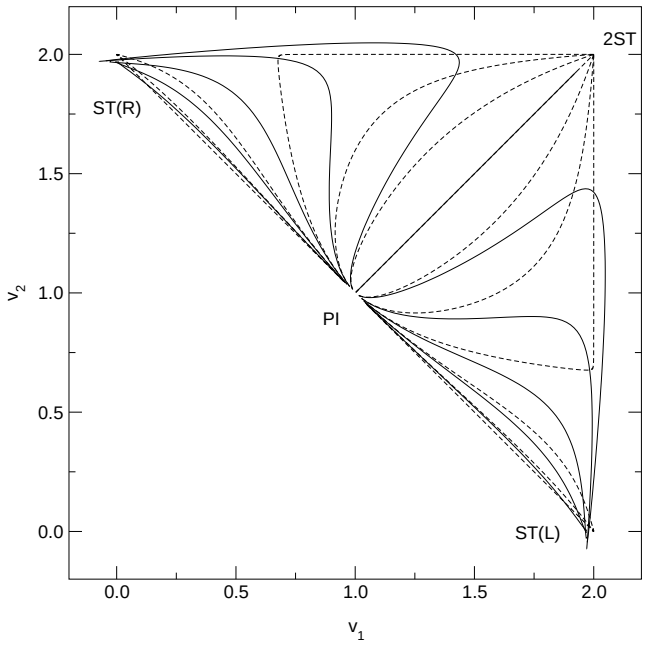


Figura 1: Evolució de condicions inicials amb la forma Eq. (16), amb $\lambda = 1/2$ i $\epsilon = 0$. $v_1$ i $v_2$ són les velocitats de la punta dels dits, les línies contínues corresponen a $B = 0.01$ i les discontinues a $B = 0$. En aquesta representació el continu de punts fixes ha col.lapsat en un únic punt (no hiperbòlic), el punt $(2, 2)$.

### 0.4.2 Càlcul numèric

La teoria asimptòtica només ens informa de quan es manifestarà l'efecte de la tensió superficial, però aporta molt poca informació sobre com es veu modificada la interfície. Per poder quantificar i precisar l'efecte de l'impacte de la filla sobre la interfície cal recórrer al càlcul numèric de les equacions d'evolució. Hem desenvolupat un codi numèric amb aquesta finalitat, seguint l'esquema desenvolupat per Hou, Lowengrub i Shelley [HLS94]. El codi integra les equacions fent ús del formalisme de la funció corrent, és espectralment acurat i no pateix encarcarament (les severes restriccions en el pas de temps degudes als termes de derivades espacials altes).

Les interfícies inicials tenen la forma de l'Eq. (16), properes a la interfície plana, i amb $\lambda = 1/2$, per intentar sostreure l'efecte de la tensió superficial degut a la selecció de l'amplada i poder estudiar únicament l'efecte en la dinàmica. Els valors de $B$ que hem estudiat són petits, en el rang $10^{-2}$–$10^{-4}$. Ens hem concentrat en els dos valors representatius $\epsilon = 0$ i $\epsilon = 0.1$, i hem estudiat tan condicions inicials concretes amb valors decreixents de $B$

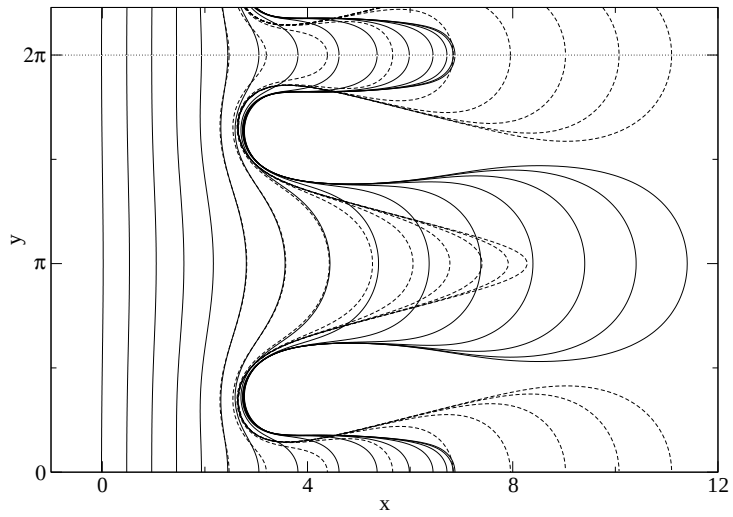


Figura 2: Evolució d'una condició inicial amb la forma Eq. (16), $\lambda = 1/2$ i $\epsilon = 0.1$. Les línies contínues corresponen a $B = 0.005$ i les discontinues a $B = 0$. L'interval temporal entre corbes és 0.5. Per apreciar millor l'evolució del dit lateral s'ha afegit una regió extra, i per tant el canal físic en la direcció $y$ s'extén des de l'origen fins a la línia de punts.

com conjunts amplis de condicions inicials aplicant un únic valor de $B$. Per a $\epsilon = 0$ hem observat que la introducció d'una tensió superficial petita té l'efecte d'alentir el dit petit, de manera que aquest és eliminat del procés de competició i el dit inicialment gran guanya i s'eixampla fins assolir l'amplada que li pertoca d'acord amb la teoria de selecció. És a dir, en introduir la tensió superficial el sistema no evoluciona cap als punts del continu de punts fixes sinó cap al dit de Saffman-Taylor, com es veu a la figura 1, restaurant la hiperbolicitat del flux en l'espai de les fases i confirmant l'escenari de solvabilitat dinàmica. A més, hem comprovat que l'efecte en la interfície és conseqüència de l'impacte de la singularitat filla verificant prediccions concretes de la teoria asimptòtica. En el cas de $\epsilon = 0.1$ (i en general per $\epsilon \neq 0$) hem observat dos tipus diferents de comportaments: en un la tensió superficial no canvia qualitativament la dinàmica, i en canvi en l'altre un valor de $B \neq 0$ té efectes dramàtics en l'evolució, ja que és capaç de modificar la dinàmica fins al punt d'invertir el resultat de la competició de dits, fent que el dit que guanya amb $B = 0$ perdi quan $B \neq 0$, com s'exemplifica a la figura 2. Això succeeix per un conjunt força significatiu de condicions inicials en les quals els dos dits tenen longituds comparables, és a dir, per configuracions interficials on hom espera que els mecanismes de competició siguin importants. Aquesta regió de condicions inicials on la competició està

erròniament descrita per la solució està limitada per la separatriu entre les conques d'atracció de 1ST(L) i 1ST(R) amb $B \neq 0$, i la posició concreta de la separatriu depèn de $B$. Però en fer $B \to 0$ hem observat evidències de l'existència d'una trajectòria separatriu límit, i la posició d'aquesta està clarament lluny de la regió separatriu de les solucions de $B = 0$: les solucions de $B = 0$ no convergeixen regularment a $B \neq 0$ encara que la seva evolució sigui suau per tot temps i tinguin l'amplada asimptòtica correcta. La raó d'això és el fet que les solucions de $B = 0$ no tenen l'estructura de punt sella del doble dit, essencial en el mecanisme de competició de dits, i per tant de cap manera poden descriure correctament el fenomen de competició. L'efecte de l'impacte d'una filla en la interfície és en general l'alentiment del dit on es produeix l'impacte, seguit de l'eixamplament del dit més avançat, de manera que com a recepta general el dit que va guanyant la competició en el moment de l'impacte és el que acaba vencent, i només quan no queda clar quin dit guanya (pot ser que un dit estigui més avançat però que tingui una velocitat menor) la regla pot no ser aplicable.

## 0.5 Dinàmica de dits viscosos amb contrast de viscositat arbitrari. Dits i bombolles.

Fins ara hem estudiat fluxos de Hele-Shaw en el límit de contrast de viscositats alt, on la interfície asimptòtica consisteix en un únic dit, el dit de Saffman-Taylor, al qual s'arriba després d'un procés de competició en el qual els altres dits presents inicialment són eliminats. Però aquesta fenomenologia no es produeix per qualsevol valor de $c$, com s'ha observat experimentalment [Mah85] i numèricament [TA83, CJ94], sinó que per valors del contrast de viscositat baixos el dit de Saffman-Taylor no és l'atractor universal del problema. A més, la mida de la conca d'atracció del dit de ST sembla dependre del valor de $c$. Aquesta fenomenologia és la que ens hem proposat d'estudiar, fent ús de l'adaptació del codi numèric desenvolupat per $c = 1$ a qualsevol valor de $c$, ja que la manca de solucions exactes del problema impedeix la utilització dels mètodes usats per $c = 1$.

### 0.5.1 La conca d'atracció del dit de Saffman-Taylor

El nostre objectiu és caracteritzar la conca d'atracció del dit de ST i els altres atractors del problema en funció del valor de $c$. Primer de tot cal triar una família de condicions inicials apropiada pel problema que volem estudiar, i donat que la competició de dits requereix com a mínim dos dits hem triat la

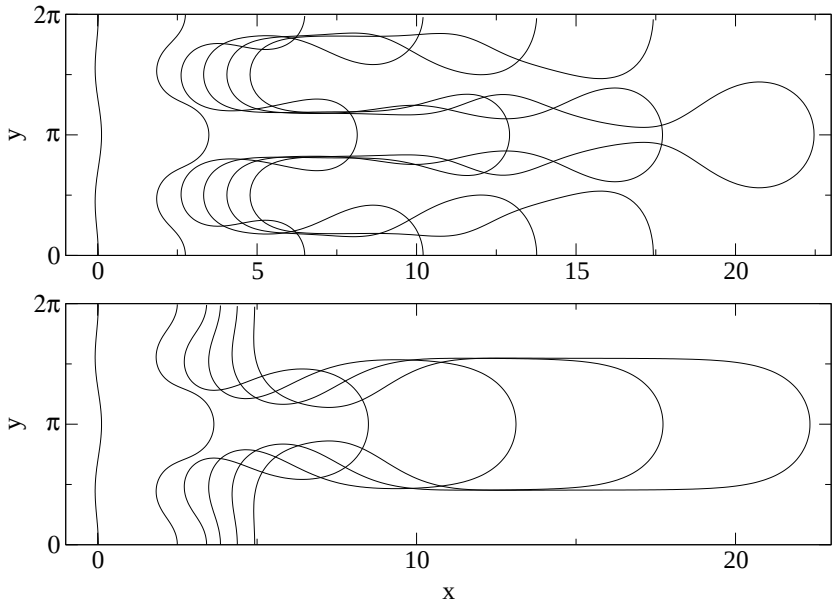


Figura 3: Evolució de condició inicial $a_1 = 0.05, a_2 = 0.07285$, amb $B = 1/7$ i $c = 0.0$ (gràfic superior), $c = 0.8$ (gràfic inferior).

següent condició inicial de dos modes:

$$x(y) = -a_1 \cos(y) + a_2 \cos(2y), \tag{18}$$

on $a_1$ i $a_2$ són reals i positius. La interfície inicial tindrà dos dits si $a_1 < 4a_2$, i ambdues amplituds es prenen prou petites com per assegurar que la interfície es troba en el règim lineal. En calcular l'evolució de la condició inicial Eq. (18) hem observat dos tipus diferents de comportament, que anomenarem tipus I i tipus II. En el tipus I el mecanisme de competició actua plenament i un dels dits 'guanya' la competició assolint la forma del dit de ST, i en canvi l'altre dit, el petit, veu alentit el seu creixement fins a quedar totalment aturat o fins i tot eliminat. A l'altre tipus de dinàmica la competició no arriba a dominar la dinàmica de manera que el dit petit no s'atura, encara que la seva velocitat pot ser menor que la de l'altre. En general, el dit gran desenvolupa un estretament a prop de la base del dit, i en alguns casos aquest estretament es fa extraordinàriament prim, fins al punt que la part avançada del dit té la forma d'una bombolla. Per al dit petit hem observat diferents tipus de dinàmica: desdoblament del dit, estretament aprop de la base que tendeix a la formació d'una bombolla, i creixement sense cap altre peculiaritat. Els dos tipus diferents de comportament estan il·lustrats a la figura 3. Donada una condició inicial i un valor de $B$ el sistema exhibirà un o altre comportament depenent del valor de $c$.

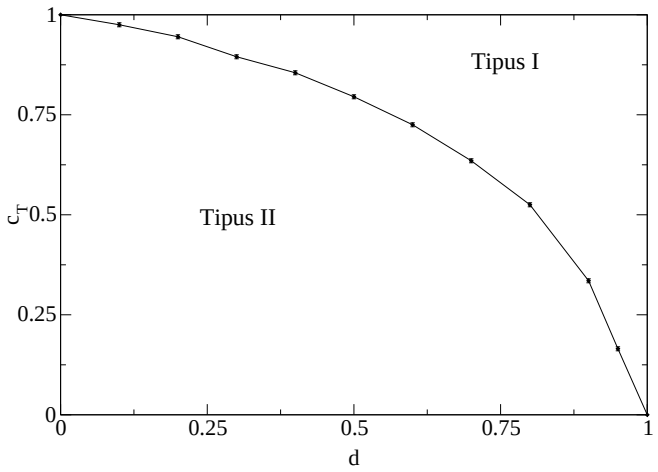


Figura 4: $c_T$ en funció de $d$, per a una condició inicial amb la forma de l'Eq. (18) i $B = 1/7$.

Per a caracteritzar com canvia la mida de la conca d'atracció del dit de Saffman-Taylor hem realitzat un estudi sistemàtic del comportament del sistema a temps llargs per a diferents valors de $c$ i diferents valors de $a_1$ i $a_2$. Per a reduir el nombre de possibles valors dels paràmetres hem triat el valor de la tensió superficial de manera que els dos modes de la condició inicial Eq. (18) creixen exactament a la mateixa velocitat, i així qualsevol condició inicial (dins del règim lineal) que tingui el quocient $a_1/a_2$ igual serà equivalent, en el sentit que el sistema pot anar d'una a l'altra simplement canviant l'origen temporal. D'aquesta manera les condicions inicials passen a ser un conjunt uniparamètric d'interfícies. Hem explorat el valor del contrast de viscositats en el qual es produeix la transició d'un tipus de comportament a l'altre, i els resultats es poden veure a la figura 4, on $c_T$ és el valor del contrast on es produeix el canvi de comportament i $d$ és el paràmetre que descriu la condició inicial. $d$ és el quocient entre la distància entre les puntes dels dits i l'amplada de la interfície, de manera que per $d = 0$ els dos dits són iguals i per $d = 1$ només hi ha un dit. Es pot veure clarament com en reduir el contrast la mida de la regió de condicions inicials en la qual el dit de ST és l'atractor es redueix ràpidament, de manera que el comportament genèric és més aviat el de contrast baix, i la sensibilitat de la dinàmica a $c$ és precisament en $c \simeq 1$. Els resultats exposats concorden qualitativament amb la teoria dèbilment no lineal [ALCO01], que prediu que per contrast alt el mode 2 reforça el creixement del mode 1, i en canvi per a contrast baix el debilita.

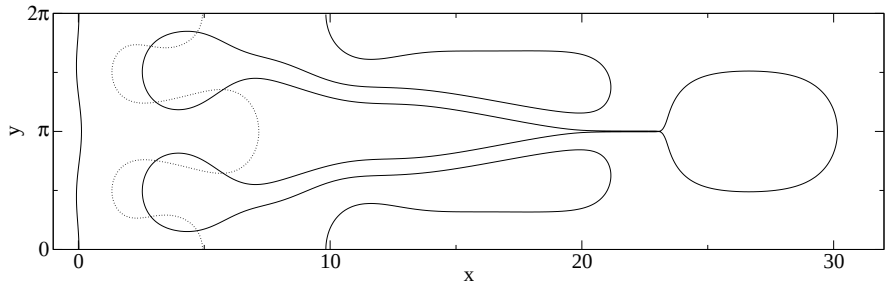


Figura 5: Evolució d'una condició inicial amb $d = 0.5$, $c = 0.8$ i $B = 1/7$. La corba de més a la dreta correspon a $t = 16$ i la intermèdia a $t = 4$.

### 0.5.2 La bombolla de Taylor-Saffman

S'ha observat que dins del comportament de tipus II en algunes ocasions el dit avançat per a temps llargs desenvolupa una quasibombolla a la seva part davantera, connectada a la resta de la interfície per un coll molt estret, com es pot veure a la figura 5. Aquesta quasibombolla té una forma molt similar a la de la solució exacta de $B = 0$ trobada per Taylor i Saffman [TS59], que és

$$x = \frac{2}{\pi}\frac{U-1}{U}\tanh^{-1}\left[\sin^2(\frac{\pi}{2}U\lambda) - \cos^2(\frac{\pi}{2}U\lambda)\tan^2(\frac{U}{4}y - \frac{\pi}{2}U)\right]^{\frac{1}{2}} \qquad (19)$$

i que té dos paràmetres, la velocitat $U$ de la bombolla i l'amplada $\lambda$. La solució Eq. (19) planteja un problema de selecció anàleg al del dit de Saffman-Taylor: donat un valor a l'àrea de la bombolla, $\lambda$ i $U$ no queden determinats, sinó que existeix un continu de solucions. Tanveer [Tan86, Tan87b] va demostrar que la introducció de la tensió superficial selecciona l'amplada (i per tant la velocitat) de la bombolla.

Hem comparat la forma de la solució Eq. (19) amb les quasibombolles observades, escollint $\lambda$ i $U$ de manera que l'acord entre les dues sigui el millor possible, i hem obtingut que l'acord és efectivament molt bo, i força millor que ajustant el dit de ST a la meitat frontal de la bombolla. Aquests resultats indiquen que la interfície, o com a mínim una part d'ella està essent atreta per la solució de la bombolla de Taylor-Saffman, encara que de fet la regió de bombolla està connectada a la resta de la interfície.

També s'ha estudiat l'evolució del coll de la bombolla, així com l'àrea d'aquesta. Ara bé, els resultats respecte a l'evolució del coll no són en absolut concloents, i no ens permeten dir si la interfície es trencarà o no, i si ho farà en un temps finit. D'altra banda, Almgren [Alm96] ha obtingut fortes evidències de l'existència de trencament en temps finit en fluxos de Hele-Shaw en configuracions sense injecció, i això ens suggereix que en el nostre

sistema també es produirà aquest trencament. Hem observat que l'àrea de la bombolla creix, però aquest creixement s'alenteix notablement quan la bombolla està ben formada, si bé els temps que duren els càlculs no permeten discernir si l'àrea acaba saturant a un valor estacionari o continua augmentant sense saturar.

Els nostres resultats no permeten decidir de manera concloent quin és l'estat estacionari de la interfície. Les possibilitats són variades: una configuració de dits estacionaris (similars als dits del continu de punts fixes descrits a la secció 0.2), un dit estacionari més avançat (el dit central) i una dinàmica persistent del(s) dit(s) petit(s), una situació estacionària amb una o dos bombolles col.locades al davant de dits estacionaris, una situació de dinàmica persistent en la qual la interfície emet gotes de manera periòdica o aperiòdica, etc. Per intentar reduir el nombre d'escenaris possibles segurament serien necessaris més resultats experimentals, ja que els disponibles fins ara [Mah85] són limitats i utilitzen una relació d'aspecte de la ceł.la massa petita com per estudiar configuracions a temps molt llargs. En qualsevol cas queda clar que el domini d'atracció del dit de ST és força reduït degut a la competició dels atractors tipus bombolla, malgrat que aquests tenen una topologia diferent.

## 0.6 Fluxos de Hele-Shaw amb desordre a l'espaiat. Propietats d'escala.

Els tractaments teòrics per estudiar la dinàmica d'interfícies rugoses s'han basat en general en l'equació KPZ [KPZ86], que és fenomenològica i local. En canvi, el problema de la invasió forçada d'un medi porós és fortament no local, i només recentment han aparegut treballs que tenen en compte aquesta no localitat del problema [GB98, DRE+99, HMSL+01], però aquests tracten el desordre des d'un punt de vista totalment fenomenològic. Nosaltres ens proposem estudiar un medi porós model, la ceł.la de Hele-Shaw amb desordre en l'espaiat, i derivar-ne *ab initio* una equació interficial que contingui la no localitat i tots els efectes del soroll d'una manera controlada (no fenomenològica), i estudiar-ne les propietats d'escala.

### 0.6.1 Modelització d'una ceł.la de Hele-Shaw d'espaiat inhomogeni

Considerem una ceł.la de Hele-Shaw amb espaiat no homogeni $b = b(x, y)$. Si la variació de $b$ és prou suau, $|\nabla b| \ll 1$, aleshores la llei de Darcy és vàlida

localment, de manera que

$$\mathbf{v} = -\frac{b(x,y)^2}{12\mu}\nabla p \tag{20}$$

i imposant incompressibilitat la velocitat (bidimensional) satisfà

$$\nabla \cdot (b\mathbf{v}) = 0. \tag{21}$$

Definim $p = p_0 + \delta p$, de manera que $\nabla p_0 = 0$, o sigui, separem la pressió en una part laplaciana i una part no laplaciana. Aleshores, la pressió obeeix

$$\nabla^2 p_0 = 0 \tag{22a}$$

$$\nabla^2 \delta p + \frac{3\nabla b}{b} \cdot \nabla p_0 = 0. \tag{22b}$$

on hem negligit un terme d'ordre $|\nabla b|^2$. El salt de pressions a la interfície ve donat per

$$p_2 - p_1 = \sigma(\kappa_\parallel + \kappa_\perp) = \sigma\left(\kappa_\parallel + \frac{2\cos\theta}{b(x,y)}\right) \tag{23}$$

on $\kappa_\parallel$ i $\kappa_\perp$ són respectivament la curvatura parał.lela i perpendicular al pla de les plaques, i $\theta$ és l'angle de contacte entre el menisc i les plaques, de manera que mullat perfecte implica $\cos\theta = 1$. L'altra condició de contorn a la interfície imposa que les velocitats normals són iguals, i això implica

$$\mu_2 \partial_n p_1 = \mu_1 \partial_n p_2. \tag{24}$$

Per resoldre l'equació (22) primer resolem l'Eq. (22a) amb la condició de contorn completa Eq. (23), i un cop resolta utilitzem $p_0$ per resoldre l'Eq. (22b) amb la condició de contorn a la interfície[2] $\delta p = 0$ mitjançant el teorema de Green. El fet d'haver triat $\delta p = 0$ a la interfície en facilita considerablement la resolució. Un cop trobat el camp de pressions total, la velocitat de la interfície s'obté mitjançant la llei de Darcy, Eq. (20).

### 0.6.2 Equació interficial

Un cop modelitzat el nostre sistema, ara considerem el problema de la invasió forçada de la ceł.la desordenada per un fluid injectat a velocitat constant $V_\infty$. L'espaiat pren la forma $b^2 = b_0^2[1 + \zeta(x,y)]$ on el soroll és de mitjana nuł.la, $\langle\zeta(x,y)\rangle = 0$. En absència de soroll, la interfície és estable, però la presència de desordre introdueix rugositat a la interfície. Considerant que

[2]Per contrast arbitrari la condició és $\delta p_1 - \delta p_2 = 0$.

aquesta no es desvia gaire de la interfície plana i que el soroll és dèbil es pot trobar una equació que per l'alçada $h(x,t)$ de la interfície a partir del model descrit. Aquesta en espai de Fourier pren la forma per a qualsevol contrast $-1 \leq c \leq 0$

$$\frac{\partial \hat{h}_k}{\partial t} = V_\infty \left\{ \delta(k) + c|k|\hat{h}_k[1+(\ell_1 k)^2] - \hat{\zeta}(k)/2 - \ell_2|k|\hat{\zeta}(k) \right\}$$
$$+\hat{\Omega}_{LR}(k,t) - V_\infty c^2|k| \int_{-\infty}^{\infty} dq[1-\mathrm{sgn}(kq)]\hat{h}_{k-q}\hat{h}_q|q|[1+(\ell_1 q)^2] \qquad (25)$$

on

$$\hat{\Omega}_{LR}(k,t) = \frac{3V_\infty}{2}\frac{1-c}{2}|k| \int_{-\infty}^{\infty} dx' \int_{-\infty}^{0} dy \zeta(x', y+V_\infty t) e^{-ikx'} e^{y|k|}$$
$$+\frac{3V_\infty}{2}\frac{1+c}{2}|k| \int_{-\infty}^{\infty} dx' \int_{0}^{\infty} dy \zeta(x', y+V_\infty t) e^{-ikx'} e^{-y|k|}, \qquad (26)$$

$\hat{h}_k$ i $\hat{\zeta}(k)$ són respectivament les transformades de Fourier de $h(x)$ i $\zeta(x,h)$ i $\delta(k)$ és la distribució delta de Dirac. Per obtenir l'Eq. (25) s'ha fet servir la teoria dèbilment no lineal per als fluxos de Hele-Shaw desenvolupada a la Ref. [ALCO01] i s'han inclòs els termes lineals i quadràtics en $h$ i els lineals en el soroll $\zeta$.

Les longituds característiques $\ell_1$ i $\ell_2$ que apareixen a l'equació estan definides en termes del nombre de capił.laritat $\mathrm{Ca} = 12(\mu_1+\mu_2)V_\infty/\sigma$ com

$$\ell_1 = \frac{b_0}{\sqrt{|c|\mathrm{Ca}}} \quad \text{i} \quad \ell_2 = \frac{b_0 \cos\theta}{\mathrm{Ca}}. \qquad (27)$$

El soroll original en l'espaiat es manifesta en diferents termes (i efectes físics) en l'equació interficial (25). Primer, un terme de soroll conservat i no local $\ell_2|k|\hat{\zeta}(k)$ que anomenarem soroll capił.lar ja que és conseqüència de la variació en la capił.laritat deguda a la variació de l'espaiat. El terme de soroll no conservat local $\hat{\zeta}(k)/2$ en canvi és una combinació dels efectes de l'espaiat en la permeabilitat i de la conservació de volum de fluid. A més, és fàcil de verificar que aquest terme assegura la conservació del volum total de fluid injectat. Finalment, el terme $\hat{\Omega}_{LR}$ té en compte l'efecte del soroll en tota l'àrea ocupada per fluid. Aquest terme es mereix un comentari ja que introdueix correlacions de llarg abast, com es pot veure de l'expressió

$$\langle \hat{\Omega}_{LR}(k,t)\hat{\Omega}_{LR}(k',t')\rangle = \Delta \left(\frac{3V_\infty}{2}\right)^2 \pi|k|\delta(k+k')e^{-V_\infty|k||t-t'|}. \qquad (28)$$

pel cas en que $\zeta$ és un soroll blanc i on per simplicitat hem considerat $c=-1$. Per tant, $\hat{\Omega}_{LR}$ és de manera efectiva un soroll dinàmic i de llarg abast tant

en l'espai com en el temps. Aquest tipus de sorolls de llarg abast han estat proposats [GB98] qualitativament per explicar les propietats d'escala de la interfície, però aquesta és la primera derivació microscòpica d'aquest tipus de soroll.

La presència de les dues longituds $\ell_1$ i $\ell_2$ a l'Eq. (25) introdueix diferents règims d'escala a l'equació. La longitud $\ell_1$ marca la ben coneguda escala de longitud per a la qual les forces viscoses dominen sobre les forces capil.lars, i la nova escala $\ell_2$ controla la longitud en la qual el soroll no conservat passa a dominar sobre el soroll conservat capil.lar.

### 0.6.3 Propietats d'escala

La presència de soroll en el sistema provoca que la interfície s'arrugui, i són precisament les propietats d'escala d'aquesta interfície arrugada allò que ens proposem estudiar.

Les dues longituds $\ell_1$ i $\ell_2$ determinen la presència de fins a tres règims d'escala diferents, assumint és clar que $\ell_1$ i $\ell_2$ són molt diferents i que la mida $L$ del sistema és força més gran que ambdues longituds. Per simplicitat, considerarem el cas experimentalment més usual en el que un fluid viscós que mulla totalment en desplaça un de no viscós, de manera que hom té $c = -1$ i $\cos\theta = 1$. En aquest cas, $\ell_1 < \ell_2$. Aleshores el primer règim o règim capil.lar està definit per $\ell_1|k| \gg 1$, i en aquest dominen els termes capil.lars, tant el determinista com el de soroll. Hi ha un règim intermedi en el que dominen el terme determinista proporcional a $|k|$ i el terme de soroll capil.lar, i que ve definit per $\ell_1|k| \ll 1 \ll \ell_2|k|$. Finalment, existeix un tercer règim en el qual les forces viscoses dominen, és a dir, en que el comportament d'escala de l'equació ve donat pel terme determinista proporcional a $|k|$ i el soroll no conservat. En aquest darrer règim es satisfà $\ell_2|k| \ll 1$. En aquesta discussió no s'ha tingut en compte el terme de soroll de llarg abast $\hat{\Omega}_{LR}$ ni els termes quadràtics, ja que es pot veure que $\hat{\Omega}_{LR}$ no afecta habitualment l'escalat asimptòtic i els termes quadràtics només podrien afectar-lo en el règim capil.lar, com mostren arguments de recompte de potències.

En el cas de soroll dinàmic $\zeta = \zeta(x,t)$ o columnar $\zeta = \zeta(x)$ l'Eq. (25) es pot resoldre exactament[3]. Així, en el règim capil.lar s'obté $\alpha = 3/2$ i $\beta = 1/2$ per soroll columnar i $\alpha = \beta = 0$ per soroll dinàmic; en el règim intermedi la interfície no és rugosa (els exponents són negatius); i en el règim dominat per les forces viscoses els exponents són $\alpha = 1/2$ i $\beta = 1/2$ per soroll columnar i $\alpha = \beta = 0$ per dinàmic. Ara bé, cal tenir en compte que en el règim capil.lar el terme quadràtic és rellevant i la seva inclusió podria

[3]Negligint els termes quadràtics i el terme de soroll de llarg abast $\hat{\Omega}_{LR}$.

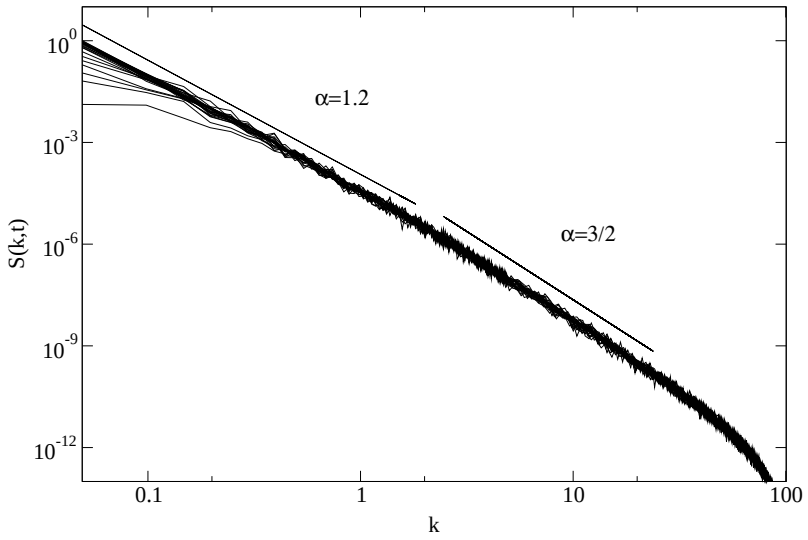


Figura 6: Factor d'estructura per un sistema amb $L = 128$, $V_\infty = 0.18$, $\ell_1 = 250\sqrt{2}/3$ i $\ell_2 = 50000/3$. Els temps van de $t = 2$ (corba inferior) fins $t = 50$ en intervals $\Delta t = 2$. La recta de pendent $-3.3$ ($\alpha = 1.2$) és un ajust, i l'altra recta té pendent $-4$ ($\alpha = 3/2$).

modificar els exponents que hem donat.

En canvi, per soroll congelat $\zeta = \zeta(x, h)$ l'Eq. (25) no té solució exacta, i per intentar determinar el seu comportament d'escala hem recorregut a la simulació numèrica. Per tant, hem simulat l'Eq. (25) en cadascun dels tres règims, incloent només els termes (lineals) rellevants.

A la figura 6 es mostra un exemple del factor d'estructura obtingut de la simulació. El comportament a $k$ gran (longituds petites) $\alpha \simeq 1.5$ correspon a tenir soroll columnar, i a $k$ intermèdies o petites hem obtingut uns exponents de rugositat en el rang $\alpha \simeq 1.2 - 1.3$ escombrant un ampli rang de mides de sistema i diferents valors de $Ca$ i $V_\infty$. Per velocitats grans també hem observat $\alpha \simeq 0$ per $k$ petita, que és el valor que correspon a soroll dinàmic. Finalment, en algun cas també hem observat per $k$ petita valors $\alpha < 1$ però clarament diferents dels comportaments citats, però seria necessari simular sistemes més grans i temps més llargs per acabar de precisar aquest comportament. També hem estudiat com els termes quadràtics no lineals afecten els resultats anteriors, i hem observat que la introducció de termes quadràtics no canvia apreciablement els exponents, almenys en els temps que hem simulat, si bé aquest estudi no ha estat realitzat de manera sistemàtica.

En el règim intermedi els resultats de la simulació mostren que la interfície no és rugosa, cosa previsible vist el comportament pels sorolls dinàmic i

columnar.

En el règim viscós caracteritzat per $\ell_2|k| \ll 1$ hem obtingut que la interfície és logarítmicament rugosa, encara que per sorolls molt intensos aquest comportament es pot veure modificat.

Finalment, hem comparat els nostres resultats amb els obtinguts experimentalment per en Soriano i col.laboradors [HMSL+01, SRR+02, SOHM02b, SOHM02a]. En aquests experiments s'utilitza una cel.la de Hele-Shaw on l'espaiat pot prendre únicament dos valors, de manera que el soroll és dicotòmic i presenta pendents grans. Això implica que la llei de Darcy local no serà vàlida a tot arreu, i en particular en els punts on l'espaiat canvia bruscament de valor, on es donen fenòmens d'ancoratge. Malgrat tot, com que aquests són els únics experiments disponibles d'espaiat desordenat (en alçada) compararem breument els nostres resultats amb els seus. Experimentalment observen tres règims d'escala diferents en funció dels paràmetres experimentals, que són la velocitat d'injecció i l'espaiat. Per a velocitats grans o espaiats grans (que correspon a sorolls dèbils) obtenen que per $k$ petit l'exponent de rugositat és $\alpha \simeq 0$ i per $k$ grans $\alpha \simeq 1.3$. D'acord amb els seus paràmetres experimentals el règim on es troben és el capil.lar, i els nostres resultats són plenament compatibles amb els seus, per tant el nostre model descriu la física del seu experiment en el règim de velocitats altes o espaiats grans (sorolls dèbils). En canvi per espaiats petits o velocitats petites els resultats experimentals no coincideixen amb les nostres prediccions. Tampoc no és satisfactori l'acord entre experiment i teoria en el cas de soroll columnar, però en aquest cas és clarament atribuïble a l'ancorament de la interfície a les vores, el qual juga un paper determinant donada la persistència del soroll.

## 0.7 Conclusions i perspectives

Els principals objectius d'aquesta tesi han estat d'una banda l'estudi de la influència de la tensió superficial, i en menor mesura del contrast de viscositats en la dinàmica de Saffman-Taylor, i de l'altra la formulació de les equacions de Hele-Shaw en presència de desordre, així com les seves propietats d'escalat.

Per assolir el primer objectiu hem estudiat exhaustivament, des del punt de vista de sistemes dinàmics, solucions exactes del problema amb tensió superficial zero i contrast de viscositat unitat que exhibeixen competició reeixida i que contenen els atractors físics del problema amb tensió superficial finita. La comparació de les propietats del flux a l'espai de les fases d'aquestes solucions exactes amb el flux fàsic de les solucions de tensió superficial arbitràriament petita (però finita) associades, ens ha permès concloure que

el flux fàsic d'aquelles solucions exactes no és topològicament equivalent al de les solucions de tensió superficial petita, i que per tant les solucions exactes de tensió superficial zero no són una bona descripció de la dinàmica del problema regularitzat. Aquestes conclusions s'han estès a la classe de solucions exactes amb trajectòries lliures de singularitats, de manera que s'ha pogut concloure de manera general que la dinàmica de tensió superficial zero és essencialment diferent de la dinàmica de tensió superficial finita, degut a que en la dinàmica de tensió superficial zero no és present cap punt fix tipus sella, i sí en canvi punts fixes no hiperbòlics o singularitats a temps finit. Hem proposat un escenari de selecció dinàmica per explicar l'efecte de la tensió superficial en les solucions exactes. En aquest marc el paper de la tensió superficial seria el de restaurar la hiperbolicitat dels punts fixes no hiperbòlics, recuperant l'estructura de punt fix tipus sella present en el problema regularitzat.

Per entendre els efectes concrets de la tensió superficial en les solucions exactes estudiades hem aplicat la teoria asimptòtica desenvolupada per Tanveer, i hem obtingut que la tensió superficial sempre afecta significativament en un temps d'ordre 1 aquelles solucions d'amplada asimptòtica menor que 1/2, i afecta significativament conjunts finits de trajectòries fàsiques de solucions d'amplada major o igual a 1/2, també en temps d'ordre 1. Per quantificar aquests efectes hem desenvolupat un codi numèric per calcular l'evolució de les solucions amb tensió superficial petita. Aquest codi és estable, espectralment acurat, no presenta restriccions en l'increment temporal associades a l'encarcarament de les equacions, permet assolir valors molt petits de la tensió superficial i controla la influència del soroll numèric. Fent ús d'aquest codi hem obtingut que la introducció de la tensió superficial restaura la hiperbolicitat del punt fix corresponent al doble dit de Saffman-Taylor, regularitza les singularitats a temps finit i canvia el resultat final de la competició de dits per amplis conjunts de condicions inicials. En conclusió, la tensió superficial afecta dramàticament la dinàmica de tensió superficial zero degut al seu caràcter de pertorbació singular, i és per tant essencial per a descriure la dinàmica dels fluxos de Hele-Shaw.

L'efecte del contrast de viscositats en la dinàmica ha estat menys estudiat, principalment degut a la pràctica absència de solucions exactes. Hem estudiat sistemàticament de manera numèrica l'evolució de condicions inicials amb un i dos dits utilitzant el codi numèric mencionat abans, i hem comprovat que el dit de Saffman-Taylor no és l'atractor universal del problema, i a més hem observat que la mida de la seva conca d'atracció disminueix ràpidament en disminuir el contrast no gaire per sota de la unitat. Hem quantificat la conca d'atracció del dit de Saffman-Taylor en funció del contrast, utilitzant una condició inicial triada de manera apropiada. L'atractor alternatiu al de

Saffman-Taylor és molt complex i no es pot caracteritzar de manera simple, si bé en alguns casos la dinàmica asimptòtica sembla atreta cap a solucions de tipus bombolla de Taylor-Saffman.

L'altre objectiu destacat de la tesi ha estat la formulació del flux de Hele-Shaw amb desordre a l'espaiat entre plaques, que es un sistema model per al flux a través d'un medi porós. Assumint que aquest desordre és dèbil i suau s'han pogut obtenir les equacions de Hele-Shaw amb desordre (o soroll) de manera tancada. Aquestes equacions s'han aplicat a l'estudi de la configuració experimental en la que un fluid viscós desplaça un no viscós i s'ha obtingut l'equació rellevant per l'alçada de la interfície. La principal novetat d'aquesta equació és que inclou tant un soroll conservat com no conservat, així com un soroll que inclou la contribució del desordre a tota la regió ocupada pel fluid, i que està correlacionat en el temps i l'espai. Aquesta equació pot explicar les dificultats per observar el comportament d'escalat en els sistemes experimentals, i també les discrepàncies entre diferents experiments. L'equació permet fer prediccions precises que són experimentalment realitzables. S'ha simulat per obtenir el seu comportament d'escalat, obtenint valors dels exponents de rugositat i creixement compatibles amb alguns dels resultats experimentals.

Diversos aspectes d'aquest treball han quedat sense resposta, i s'han obert noves qüestions que han quedat fora de l'abast de la tesi. Les perspectives futures més generals són les següents:

El model de ceł.la d'espaiat inhomogeni ha estat aplicat al problema de la invasió forçada d'una ceł.la de Hele-Shaw desordenada, però un altre problema d'interès igual o superior al que es podria aplicar és el de pressió constant o imbibició, en el qual tampoc es disposa d'una modelització teòrica apropiada dels efectes del soroll.

L'equació interficial que hem derivat requereix un estudi numèric més intensiu del que hem pogut realitzar, en particular dels termes quadràtics i de situacions a prop de les transicions entre règims.

La possible existència de trencament de gotes en el cas de contrast de viscositat petit és una qüestió de notable interès, i per poder concloure quelcom caldria utilitzar l'aproximació del lubricant per descriure la zona on es troba l'estretament, i la solució s'hauria de acoblar a la solució completa per la resta de la interfície.

Altres qüestions més específiques que han quedat obertes són:

Hem observat que en alguns casos les solucions exactes presenten trencament de la interfície ('pinchoff') en la configuració estable del problema, i seria molt interessant estudiar si el trencament sobreviu a la introducció de la tensió superficial, aplicant la teoria asimptòtica i el càlcul directe de

l'evolució.

Per comprendre millor el comportament asimptòtic de la interfície seria bo poder allargar l'extensió dels càlculs numèrics, així com buscar noves solucions exactes de $B = 0$ consistents en una bombolla coexistint amb un o dos dits situats en eixos de simetria diferents.

En aquesta tesi s'han estudiat numèricament solucions exactes de $B = 0$ i $\lambda = 1/2$, però també seria prou interessant l'estudi de les solucions amb $\lambda > 1/2$ per aclarir el mecanisme que actua per fer que les solucions assoleixin l'amplada asimptòtica $1/2$.

L'estudi de la dinàmica de la interfície en el cas inestable amb soroll d'origen físic com el de la Sec. 0.6, sobretot en el cas de $B$ petita és un altre tema pendent que queda per al futur.

# Part I

# Introduction

# Chapter 1

# Introduction

The spontaneous emergence of macroscopic structure and spatio-temporal order in spatially extended systems out of uniform, structureless states has fascinated and puzzled scientists for a long time. These structures are found in a large number of systems in the fields of physics, chemistry or biology, and appear when the systems are driven out of thermodynamic equilibrium. A prototypical example of structure formation out of equilibrium is provided by the formation of snowflakes (see Fig. 1.1), that from the very beginning of modern science attracted the interest of scientists such as Kepler (1611) [Kep11]. At the beginning of the twentieth century the landmark book by D'Arcy Thompson *On Growth and Form* (1917) [Tho17] set the stage for a new way of thinking these problems, but it was not until the late century that both the mathematical tools and the physical thinking were sufficiently mature to solidify in a well established field. The modern study of the emergence of structure as a field of physics goes often under the label of *pattern formation out of equilibrium* [CH93, Man90, Wal97, NP77], and its applications extend far beyond traditional physical systems into chemical or biological ones. Such maturity has been attained in the last few decades thanks to the confluence of mathematical disciplines such as qualitative analysis (bifurcation theory) [Cra91] and dynamical systems theory [GH83], the geometry of fractals [Man77] and the development of nonequilibrium physics rooted in statistical mechanics and other classical disciplines such as hydrodynamics. The rather interdisciplinary character of the field is sometimes referred to as Nonlinear Science.

One of the subjects included within this general framework is *interfacial* pattern formation [Lan80, Lan87, KKa88, Pel88, BM91], where the structure formed is described in terms of an interface between two or more macroscopic phases or domains. In many cases the dynamics of the whole problem can be reduced or projected on the interface, thus reducing the dimensionality

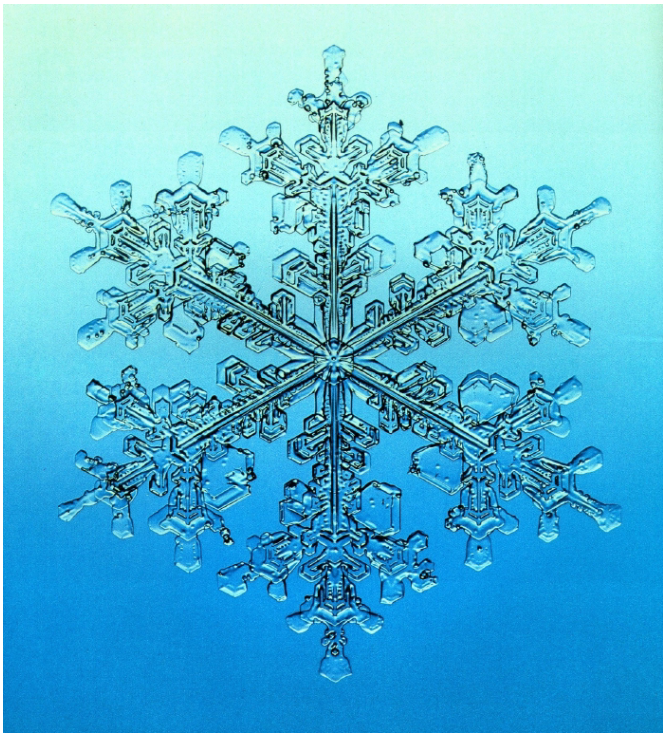

Figure 1.1: Snow crystal

of the original problem and simplifying its study. But this projection of the dynamics on the interface may also introduce new aspects that were absent in the original formulation, typically some degree of nonlocality. From a mathematical point of view this procedure defines what is known as a free-boundary problem, in which the object where boundary conditions for PDE's are specified is actually moving, and its motion is part of the solution of the problem.

The motion of interfaces under nonequilibrium conditions poses fundamental questions in pattern formation and nonlinear phenomena, as well as in the mathematics of free-boundary problems. From a historical perspective, most of them have been motivated by problems encountered in industry or engineering. Interfacial pattern formation include a variety of systems and phenomena, such as displacement of fluid interfaces in porous media or confined geometries (viscous fingering) [BKL+86], solidification of an undercooled melt [CCR92, PA92], electrodeposition [LSSC+97], flame propagation [Mar51, PC82], or electrical gas discharges (streamers) [Rai91].

Among interfacial pattern formation problems, the case of viscous fingering or Hele-Shaw flows arises as a model system which has become instrumen-

tal for many years in the search for generic phenomena in related problems. Due to its relative simplicity, which allows deeper analytical insights but also a better experimental control, it has become a paradigm of pattern formation in nonequilibrium interfaces. A Hele-Shaw cell consists of two parallel plates separated by a very small gap, in such a way that the flow of a viscous fluid inside the cell can be considered effectively two-dimensional. In a typical experiment a viscous fluid is displaced by a less viscous one, forming a nontrivial interfacial pattern. This relatively simple experimental setup gives rise to a rich variety of nonlinear phenomena and nonequilibrium patterns. In addition to its experimentally simple conception, it also allows a compact mathematical formulation, in terms of a field (the pressure) that satisfies the Laplace equation in the bulk of the fluid, and that must fulfill certain conditions at the boundaries. In particular, the pressure jump at the interface is proportional to the curvature of the interface[1]. Once the pressure field is known, the velocity of the interface is easily computed and the evolution of the interfacial shape determined. At first sight it does not seem a complicated problem, but a closer look changes this view: as a prototype free-boundary problem it faces strong nonlocality due to the laplacian nature of the pressure field and also strong nonlinearity. In addition, the surface tension acts as a particularly severe singular perturbation in the problem. In the absence of surface tension, however, and if the viscosity of one of the fluids is neglected, the initial value problem can be explicitly solved for some classes of initial conditions. This surprising fact is one of the most appealing features of Hele-Shaw flows to the theorist, but also poses a new question: to what extent do the solutions of the idealized (zero-surface-tension) problem describe the physical problem with positive surface tension? When one tries to work out an answer to this question the singular character of surface tension appears dramatically, challenging theorists to struggle in order to extract the physical content from the idealized problem. Moreover, in addition to surface tension there is another important parameter in the problem, the viscosity contrast, that measures the relative viscosity difference of the fluids. When one of the two viscosities is not neglected, different and richer dynamics appear, but at the same time the exact solutions of the idealized problem are no longer available, making the study of the arbitrary viscosity contrast much more difficult. Due to the its increased difficulty this case has been neglected for a long time, and many aspects of its dynamics are still unknown. Another aspect that has not received sufficient attention is the effect of noise on the

[1]This is the simpler boundary condition for the pressure jump at the interface. To complete the formulation of the problem additional conditions at the different boundaries are necessary, and this will be discussed later on.

interfacial patterns. Noise of various origins (fluctuations in the distance between the plates, dust or residual fluids in the plates, deformations of the plates, inhomogeneous wetting conditions etc.) as well as other deterministic perturbations of the original problem have an important influence in the stability and the shape of the patterns formed. The inclusion of a significant amount of noise in the stable configuration of the problem[2] gives rise to a set of phenomena totally different from the ones discussed above, and connects with the field of kinetic roughening of interfaces and universality of growth.

The subject of this thesis is viscous fingering in Hele-Shaw cells, or Hele-Shaw flows [BKL+86, Tan00]. We look for insights into the fundamental mechanisms underlying the physics of interface dynamics, which we hope will exhibit some degree of universality. The aim is twofold: on the one hand we focus our attention on the role of surface tension and viscosity contrast in the dynamics of fingering patterns, using a variety of mathematical tools and approaches, namely concepts of dynamical systems theory, a perturbative approach and direct numerical computation of the initial value problem. On the other hand we introduce a modification of the original problem in the spirit of Ref. [MM95] and study the effects of a inhomogeneous gap between the plates of a Hele-Shaw cell. We formulate the problem and obtain an interface equation, that is applied to study the statistical properties of interfaces roughened due to the presence of quenched disorder.

In the next four sections we motivate the different contributions of this thesis within a historical perspective. We provide the basic background of the problem of viscous fingering, including definitions, mathematical formulations and basic facts, and we highlight the key contributions that have directly motivated the present work.

## 1.1 Viscous fingering in Hele-Shaw cells

The present work deals with the time evolution of the interface between two immiscible fluids confined in a Hele-Shaw cell [Hel98]. A Hele-Shaw cell (see Fig. 1.2) consists in two parallel plates separated a very small distance $b$ (gap), much smaller than any other length of the system. The configuration is such that the flow becomes effectively two-dimensional and potential with boundary conditions set in a moving boundary, the interface. In the classical configuration the cell has a rectangular shape, with width $W$ and length $L$, defining a channel of width $W$ [ST58]. A fluid is injected from one end of the cell and the other fluid is extracted from the other end. The other

[2] A planar interface between a viscous fluid that is being displaced by a less viscous one is unstable, while in the opposite situation the interface is stable.

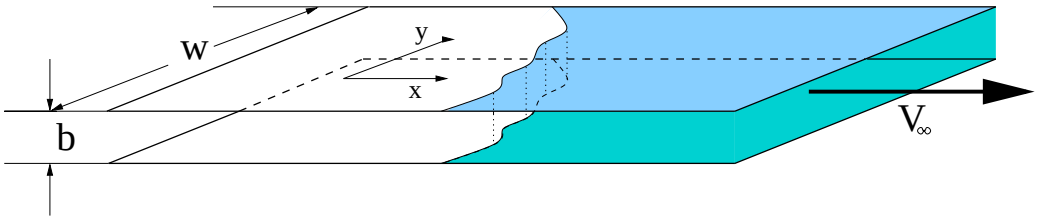


Figure 1.2: Hele-Shaw cell, in the rectangular configuration.

much studied geometry is the so called radial configuration [Pat81], where fluid is injected (extracted) through a small hole in one of the plates, but there are other experimental setups that have also received some attention, in particular the wedge geometry [TRHC89, Ben91].

The flow is described by the Navier-Stokes equation, we consider incompressible fluids and the conditions are such that the system is in the high friction limit, the inertial term of the Navier-Stokes equation is negligible. Since the flow is assumed to be quasi-stationary this is equivalent to consider small values of the Reynolds number. Taking into account that the gap spacing $b$ is much smaller than $W$ and $L$ and imposing no-slip boundary conditions on the plates it is obtained that the velocity profile in the $z$ direction (perpendicular to the plates) is given by the Poiseuille flow. Averaging the velocity of the fluid in the $z$ direction the resulting equation for the two dimensional flow is

$$\mathbf{u} = -\frac{b^2}{12\mu}\left(\nabla p - \mathbf{F}_{ext}\right) \tag{1.1}$$

where $\mathbf{u} = \mathbf{u}(\mathbf{r})$ is the averaged two dimensional velocity, $\mu$ is the viscosity of the fluid, $p = p(\mathbf{r})$ is the pressure and $\mathbf{F}_{ext} = \mathbf{F}_{ext}(\mathbf{r})$ is an external force. We will consider potential forces, $\mathbf{F}_{ext} = \nabla V_{ext}$ with $\nabla^2 V_{ext} = 0$, and applying the incompressibility condition $\nabla \cdot \mathbf{u} = 0$ it is obtained that the pressure satisfies Laplace equation

$$\nabla^2 p = 0. \tag{1.2}$$

It is important to note that Eq. (1.1) is the same equation that applies to flow in porous media, known as Darcy law, with a mobility $m$ given by $m = b^2/12\mu$.

We consider the classical channel geometry where the fluid is injected at a constant rate from one end of the cell with a velocity $V_\infty$, under an effective gravity $g_{eff} = g\cos\beta$ directed in the $-\hat{\mathbf{x}}$ direction. Fluid 1 is injected at $x = -\infty$ and displaces fluid 2. The channel is considered to be of infinite

length, and the boundary condition at infinity is then

$$\left.\frac{\partial p}{\partial x}\right|_{|x|\to\infty} = -\frac{12\mu_{1,2}}{b^2}V_\infty - \rho_{1,2}\, g_{eff} \tag{1.3}$$

where $\rho_{1,2}$ are the densities of fluid 1 and 2 respectively. Imposing the continuity of the normal velocities on the interface yields

$$U = -\frac{b^2}{12\mu_1}\left(\partial_n p_1 + \rho_1\, g_{eff}\, \hat{\mathbf{n}}\cdot\hat{\mathbf{x}}\right) = -\frac{b^2}{12\mu_2}\left(\partial_n p_2 + \rho_2\, g_{eff}\, \hat{\mathbf{n}}\cdot\hat{\mathbf{x}}\right) \tag{1.4}$$

where $\hat{\mathbf{n}}$ is the unit vector normal to the interface. Eq. (1.4) relates the gradients of the pressure on the interface, and an additional condition on the interface is needed to close the problem. This new boundary condition is given by the Young-Laplace pressure jump at the interface due to local equilibrium:

$$p_1 - p_2 = \sigma\kappa. \tag{1.5}$$

$\sigma$ stands for the surface tension and $\kappa$ for the curvature. In Eq. (1.5) $\kappa$ is the total curvature of the interface, but the curvature in the plane perpendicular to the plates is approximately constant and of order $b/2$, and therefore does not affect the dynamics. From now on $\kappa$ refers to the curvature in the plane parallel to the plates. When a fluid that does not wet the plates displaces a wetting one the expulsion is not complete and a film of the displaced fluid is left behind on the plates. To account for this effect Park and Homsy [PH84] proposed the following modified boundary condition instead of Eq. (1.5):

$$p_1 - p_2 = \frac{\sigma}{b/2}\left[1 + 3.80\left(\frac{\mu v_n}{\sigma}\right)^{\frac{2}{3}}\right] + \frac{\pi}{4}\sigma\kappa. \tag{1.6}$$

However, the kinetic boundary condition Eq. (1.6) is only necessary if a precise quantitative test of the model is required. In the present work we will restrict ourselves to the simpler boundary condition Eq. (1.5). The problem is then defined with Eq. (1.2) in the bulk and boundary conditions given by Eqs. (1.3, 1.4, 1.5).

The pressure $p$ obeys Laplace equation, Eq. (1.2), and its harmonic conjugate, the stream function $\Psi$ satisfies the Poisson equation [TA83]

$$\Delta\Psi = -\Gamma \tag{1.7}$$

where $\Gamma$ is the vorticity distribution, singular and localized on the interface: $\Gamma(\mathbf{r}) = \gamma(s)\delta\left[\mathbf{r} - \mathbf{r}(s)\right]$. The interface is parameterized with the arclength $s$, and the vorticity $\gamma$ reads [TA83]

$$\gamma = \frac{\Delta\mu}{\bar{\mu}}\mathbf{w}\cdot\hat{\mathbf{s}} + \left(\frac{\Delta\mu}{\bar{\mu}}V_\infty + \frac{\Delta\rho g_{eff} b^2}{12\bar{\mu}}\right)\hat{\mathbf{x}}\cdot\hat{\mathbf{s}} + \frac{\sigma b^2}{12\bar{\mu}}\frac{\partial\kappa}{\partial s} \tag{1.8}$$

with $\bar{\mu} = (\mu_1 + \mu_2)/2$. In two dimensions the velocity $\mathbf{w}$ of the interface due to a vortex sheet is given by Birkhoff integral formula [Bir54, TA83]

$$\mathbf{w} = \mathbf{w}(s,t) = \frac{1}{2\pi} \mathrm{P} \int ds' \frac{\hat{\mathbf{z}} \times [\mathbf{r}(s,t) - \mathbf{r}(s',t)]}{|\mathbf{r}(s,t) - \mathbf{r}(s',t)|^2} \gamma(s',t) \tag{1.9}$$

where P indicates Cauchy's principal value. Eq. (1.9) only accounts for the rotational part of the velocity, $\mathbf{w}$, the velocity induced by the vortex sheet. In general, the velocity of the interface has also a contribution $\mathbf{u_{pot}}$ from a potential velocity field, in our case $V_\infty \hat{\mathbf{x}}$, so that the velocity of the interface is $\mathbf{u} = \mathbf{u_{pot}} + \mathbf{w}$.

These equations can be nondimensionalized using $W/2\pi$ to scale lengths and the combination

$$U_* = cV_\infty + g_{eff} \frac{b^2(\rho_2 - \rho_1)}{12(\mu_1 + \mu_2)} \tag{1.10}$$

to scale velocities [TA83]. After this nondimensionalization the dynamics is controlled by only two nondimensional parameters: the nondimensional surface tension $B$ given by

$$B = \frac{\pi^2 b^2 \sigma}{3W^2 (\mu_1 + \mu_2) U_*} \tag{1.11}$$

and the viscosity contrast or Atwood ratio $c$:

$$c = \frac{\mu_2 - \mu_1}{\mu_2 + \mu_1}. \tag{1.12}$$

The nondimensional vorticity $\gamma$ reads then

$$\gamma = 2c\, \mathbf{w} \cdot \hat{\mathbf{s}} + 2\hat{\mathbf{x}} \cdot \hat{\mathbf{s}} + 2B\partial_s \kappa \tag{1.13}$$

where all quantities are now dimensionless.

## 1.2 Experimental observations

Saffman and Taylor [ST58] studied experimentally the displacement of a viscous fluid (glycerine or oil) by a less viscous one[3] in a Hele-Shaw cell with $g_{eff} = 0$ for various values of the control parameter $B$. They observed that a initially flat interface is unstable, then the initially small bumps that form on the interface grow into fingers and after a competition process only one

[3] In their experiments they displaced glycerine with air and oil, and oil by water.

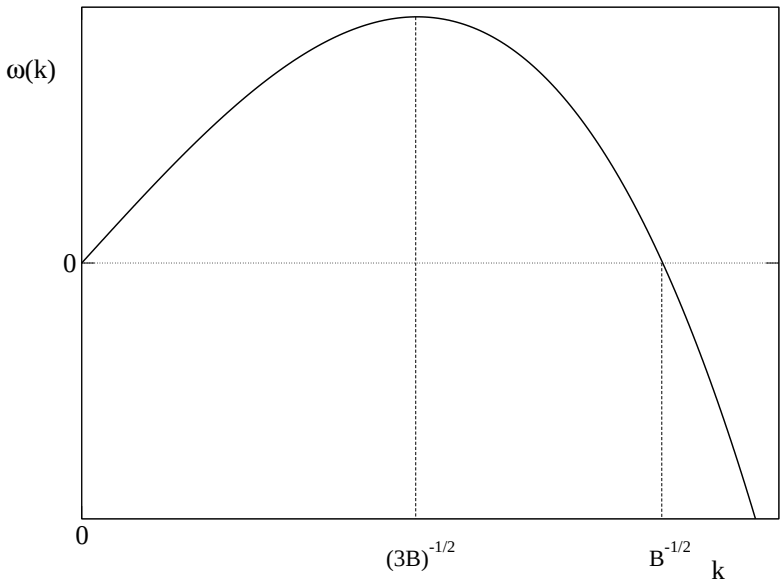


Figure 1.3: Linear dispersion relation.

finger survives. This finger has a width of roughly half the channel width and is centered in the middle of the cell, and is known as the Saffman-Taylor finger.

The initial linear regime was studied by Chuoke *et al.* [Cvv59] and it was found that the linear dispersion relation has in nondimensional variables the form

$$\omega(k) = |k|(1 - Bk^2). \tag{1.14}$$

From the linear dispersion relation Eq. (1.14) it is seen that a band of modes (those with $|k| < B^{-1/2}$) is unstable[4], and that the nondimensional surface tension $B$ is the relevant parameter in the initial linear regime. The viscosity contrast $c$ drops from this initial regime or has a trivial role depending on whether the experiments is gravity-driven or pressure-driven. The role of $B$, instead, is fundamental: it controls the modes that are unstable. Actually, $B$ is the ratio between the stabilizing *forces* (the surface tension $\sigma$) and the unstabilizing *forces* (injection plus gravity). The quantity $U_*$ determines the stability of the planar interface: for $U_* > 0$ the interface is unstable (as described above) and for $U_* < 0$ it is stable. The instability of the planar interface is known as the Saffman-Taylor instability, and is analogous to the so-called Mullins-Sekerka instability [MS64] found in solidification. The presence of an absolute value of the wave number in Eq. (1.14) is a manifestation of the nonlocal nature of the problem.

[4]For positive $B$, that is, for $U^* > 0$.

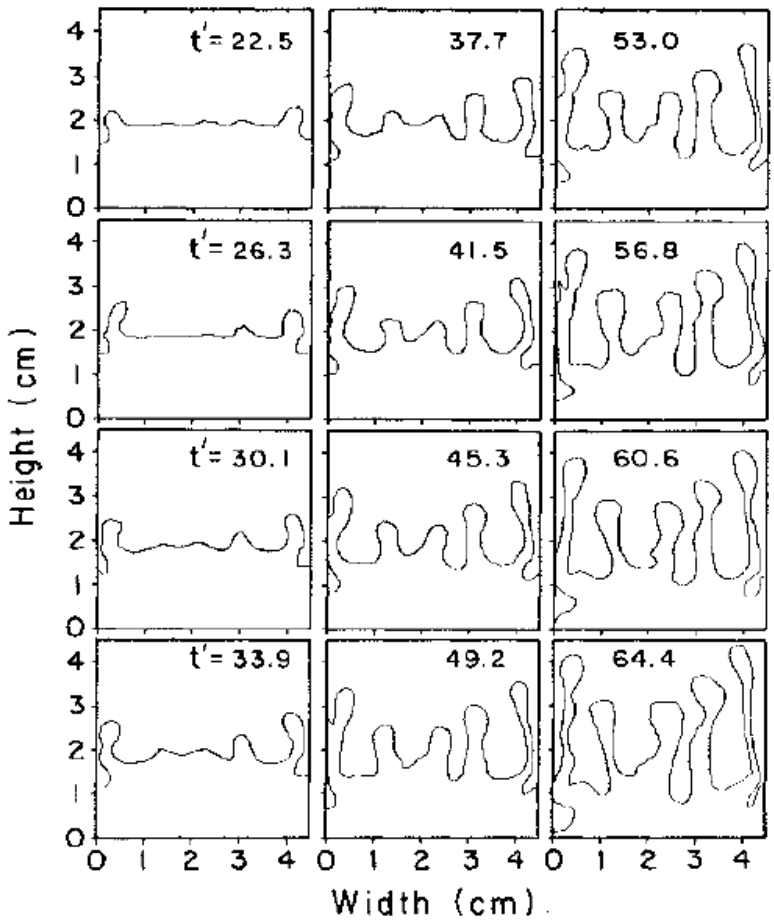


Figure 1.4: Time series of fingering patterns for low viscosity contrast ($c = 0.015$). Dimensionless time, $t'$, is indicated for each frame. Taken from [Mah85].

The instability gives rise to an irregular array of bumps or small fingers on a scale fixed by $B$ that grow independently until a nonlinear regime sets in. A systematic weakly nonlinear theory has been recently developed for the early stages of nonlinear growth [ALCO01]. However, the deeply nonlinear regime where fingers are well developed, usually with overhangs, and compete, is far more difficult to understand beyond simple qualitative observation. A common picture emerged from observations of high viscosity contrast experiments, according to which the leading fingers grow faster than the trailing ones, producing a coarsening regime [CM89, VnJ92] that ends with a unique finger of width about 1/2 of the channel width. This regime that connects the initial linear stage with the stationary finger is called finger competition

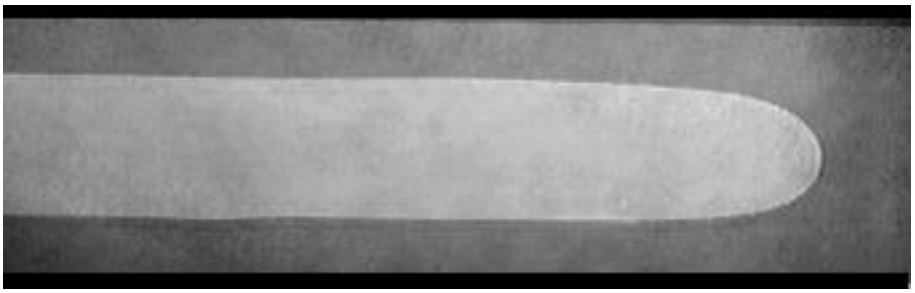

Figure 1.5: Example of Saffman-Taylor finger (high viscosity contrast).

regime. Indeed, experimental results [ST58, TL86] showed that for a range of experimental conditions a steady state pattern consisting of a single finger emerges (see Fig. 1.5). This so-called Saffman-Taylor finger has a width that depends weakly on surface tension and viscosity contrast in the limit of small $B$. In this limit the width $\lambda$ of the finger is around half the channel width. This steady Saffman-Taylor finger will be discussed next.

The qualitative understanding of the finger competition regime leading to the asymptotic solution is based on the idea of laplacian screening, where larger fingers 'screen out' the pressure field impeding the growth of smaller ones, in analogy to the growth of Diffusion Limited Growth branches of aggregates of random walkers [WS81]. This picture has shown to be too naive even within the high-contrast limit because it neglects surface tension. Part II of this thesis will be devoted precisely to the study of the subtle but dramatic effects of this parameter in the dynamics (see also next section of this introduction). On the other hand, the viscosity contrast, which is not a singular perturbation in the sense surface tension is, has been known since early numerical studies [TA83] and later experimentally confirmation [Mah85] to play a rather nontrivial role in the dynamics of finger competition, which appears to strongly depend on this parameter. For low viscosity contrast the growth of trailing fingers is not suppressed, for instance, and there seems to be no progress towards the Saffman-Taylor finger. This is illustrated in Fig. 1.4. Later numerical studies and the development of a more elaborated qualitative analysis (based on a topological approach) [CJ91, CJ94] gave support to the possibility that the Saffman-Taylor finger was *not* the universal attractor of the problem for low viscosity contrast. The conjecture of Refs. [CJ91, CJ94] that the basin of attraction of the Saffman-Taylor finger depended on viscosity contrast, and the consequent question about the alternative attractor competing with the single finger solution remained open and have been addressed in Part III of this thesis.

## 1.3 Surface tension as a singular perturbation in the problem

Surface tension $B$ is a singular perturbation to the $B = 0$ equations since it multiplies the higher derivatives of the problem, contained in the curvature term. Then, if one finds a $B = 0$ explicit solution and tries to apply a regular perturbation scheme for small $B$ assuming than the perturbed solution is 'close' to the unperturbed one, the attempt will not succeed, as McLean and Saffman [MS81] painfully learned. The singular character of surface tension manifests both in the statics and the dynamics, surprisingly even if the term $B\kappa$ is small and bounded everywhere and at any time. In this section we will then describe the singular effect of surface tension both in the selection of the steady state finger solution and in the dynamics of the problem.

### 1.3.1 The selection problem

In their classic paper, Saffman and Taylor [ST58] found a uni-parametric family of finger-shaped steady-state exact solutions, in the absence of surface tension and for any value of the viscosity contrast. In their solutions, the ratio $\lambda$ of the finger width to the width of the cell is the single (continuous) parameter. The finger shape is given by

$$x = \frac{1-\lambda}{\pi} \ln \cos\left(\frac{\pi y}{\lambda}\right), \tag{1.15}$$

and it can be seen in Fig. 1.6 for various values of $\lambda$. These shapes were quite similar to those observed experimentally if the value of $\lambda$ was chosen according to the experimental observation. In the experiment the width $\lambda$ depended on the value of the surface tension $B$, but the zero surface tension theory could not account for that. Although Saffman and Taylor guessed that surface tension was responsible for the selection of the value of $\lambda$, they could not give an explanation for it. The selection problem of the Saffman-Taylor finger width is equivalent to the selection problem present in free dendritic solidification, where steady state solutions also exist, known as Ivantsov parabolas. In this case the product of the tip radius and the velocity is fixed, but this is not enough to determine the tip velocity.

The question of the finger width selection was again taken up by McLean and Saffman [MS81], who looked for steady state solutions in the presence of a small surface tension. They numerically solved an integral equation for the interface shape, finding for any value of the surface tension parameter $B$ a unique solution (that is, a unique $\lambda$), instead of the continuum of solutions

present for $B = 0$. Later, it was found that for any value of $B$ it existed not a unique solution but a discrete set of solutions [VB83]. However, for all of these solutions, as $B$ is decreased to zero $\lambda$ goes to one-half. Most importantly for a fixed $B$ only the smallest finger width (the fastest propagating finger) corresponded to a linearly stable (therefore observable) solution.

Finally, it was not until the mid-eighties that the subtle analytical mechanism responsible for selection was fully understood as effect 'beyond all orders'. Several authors [HL86, HL87, Shr86, CDH$^+$86, CHD$^+$88, Tan87a, DM87] contributed to this understanding through different formulations of the underlying nonlinear eigenvalue problem leading to a *discrete* set of solutions. It was found that $\lambda$ must satisfy the selection criteria $\lambda = \lambda_n(B)$ where $\lambda_n(B)$ is given to leading order by

$$\lambda_n(B) = \frac{1}{2}\left[1 + \left(\frac{1}{8}\pi^2 C_n\right)^{2/3}\right], \quad n = 0, 1, 2, \ldots \tag{1.16}$$

where the integer $n$ parameterizes the family of solutions. The narrowest finger corresponds to $n = 0$ and $C_0 = 1.47$ [CHD$^+$88, Tan87a, DM87]. This scenario of selection also applies to other interfacial pattern forming systems, such as in dendritic growth, and is sometimes referred to as Microscopic Solvability (MS) scenario of selection. The MS scenario was studied in depth both theoretically and experimentally in modified boundary conditions of the Hele-Shaw problem [TL86, DM87, Tan91, BACC93], including the more accurate

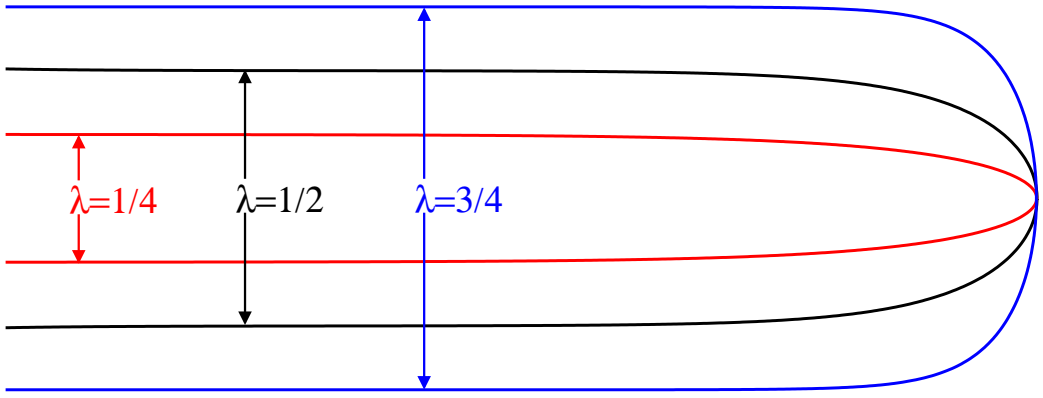


Figure 1.6: Profile of the Saffman-Taylor steady state solution for three values of the finger width $\lambda$.

boundary condition Eq. (1.6), until a complete quantitative understanding of the selection mechanism was achieved.

An important issue concerning the steady Saffman-Taylor (ST) finger is its stability. It has been experimentally observed that for small values of $B$ the ST finger becomes unstable, and a secondary transition to complex patterns of tip-splitting has been observed [TZL87, PH85, KH88, Max87]. In the absence of surface tension the ST finger is unstable, but in the presence of a finite value of $B$ the finger is linearly stable but nonlinearly unstable [Ben86]: the ST finger is stable under infinitesimal perturbations but unstable under perturbations of amplitude greater than a threshold that depends on surface tension. Then, the experimentally observed behavior is due to a finite-amplitude instability. The noise amplitude $A_{noi}$ required for destabilization decreases rapidly with $B$ and is consistent with the expression [Ben86]

$$\ln A_{noi} \sim -\frac{1}{\sqrt{B}}. \tag{1.17}$$

The celebrated generic scenario of selection that has emerged from all these studies has been often highlighted, in particular in the context of dendritic growth, as a major achievement in the recent history of pattern formation. As an example we quote Gollub and Langer, who chose it together with two other examples in their contribution on pattern formation in the centenary issue of Reviews of Modern Physics in 1999 [GL99]:

*It is here that some of the deepest questions in this field —the mathematical subtlety of the selection problem and the sensitivity to small perturbations— have emerged most clearly in recent research.*

J.P. Gollub and J.S. Langer[5]

### 1.3.2 Singular effects in the dynamics

The selection problem described in the previous section did receive much attention both as a mathematical challenge and for its implications in other more complicated problems in the physics of nonequilibrium interfaces. The rather counterintuitive fact that the velocity is 'quantized' came as a surprise, but other surprises were waiting in the backstage, which needed for a deeper analysis of the dynamics of the problem.

[5]Pattern formation in nonequilibrium physics, *Rev. Mod. Phys.*, **71**, 396, Centenary (1999)

As a matter of fact, one could object that the term 'selection problem' is not strictly appropriate, in the sense that the full problem, without neglecting surface tension, does not have the continuum degeneracy, and it is only when the problem is simplified (changed) that the problem of degeneracy arises. Nevertheless, we would like to emphasize that, through the process of neglecting and reintroducing surface tension, deep understanding has been gained indeed. The same spirit is what motivates a big part of this thesis (Part I), which will try to follow a similar scheme but now for the dynamics. This will be possible because large classes of exact time-dependent solutions of the problem in the absence of surface tension have been discovered [Saf59, How86, PMW94]. Some solutions are known to develop finite-time singularities in the form of cusps and are thus not of much interest in the physics of viscous fingering, since surface tension regularization will obviously remove such singularities. Nevertheless, a still remarkably large class of known solutions is free from singularities and therefore physically acceptable, *in principle*. They include interfacial shapes that smoothly evolve from a quasi-planar interface to the Saffman-Taylor finger, reproducing shapes quite similar to those observed in experiments and numerics. With the experience of the selection problem it is thus natural to ask to what extent will these solutions capture the correct physics, or what would be the effect of introducing a small surface tension. In a sense we could be asking whether there is some kind of *dynamical* selection principle which discriminates the correct dynamics, leading to some form of a Dynamical Solvability scenario. An important part of the thesis is devoted to this aim. The basic question on the dynamical role of introducing surface tension was first raised by Dai, Kadanoff and Zhou [DKZ91], who showed that in some situations surface tension acted as a regular perturbation while for other situations the singular character of surface tension showed up dramatically in the dynamics. The question on the possible formulation of a Dynamical Solvability theory was first posed in [MC98] and more explicitly in [SL98]. A crucial first step towards this direction was the finding of Magdaleno and Casademunt [MC99] that continua of multifinger stationary solutions existed and, remarkably, they were subject to a selection mechanism analogous to that of the single finger problem, but with additional parameters. The PhD thesis of F.X. Magdaleno [Mag00] thus set the stage for the present work (see also Ref. [CM00]).

A key result a large part of this thesis stems from is due to Siegel and Tanveer [ST96], and is quoted by Tanveer [Tan00] as one of the big 'surprises' in viscous fingering, now referring to the dynamics. This work was based on a perturbative approach for small $B$ which is rather involved because of the ill-posedness of the zero surface tension problem. In fact, the initial value

problem is known to be ill-posed [How86] for zero surface tension in the sense that arbitrarily small differences in the initial interface generally lead to radically different interfaces at later times, even a short time later. The solution to an ill-posed problem needs not be physically meaningful, since one does not have exact control over initial conditions in real (or even numerical) experiments. Therefore, the regularization effect of surface tension has to be considered to see how deeply the solutions are affected. Tanveer [Tan93] was able to overcome the obstacle of the ill-posedness by embedding the zero surface tension problem in a well-posed one. In addition, this well-posed extension of the $B = 0$ problem allowed Baker *et al.* [BST95] to develop a numerical method to compute the time evolution of zero surface tension dynamics in a well-posed manner. Once the $B = 0$ problem is formulated in a well-posed way the $B \neq 0$ case can be studied using a perturbative approach.

The main result of the asymptotic perturbative theory developed by Tanveer [Tan93] is that the effect of surface tension may be manifest in a $\mathcal{O}(1) = \mathcal{O}(B^0)$ time: the evolution of the same initial interface for $B = 0$ and $B \neq 0$ will in general differ after a time of order one, even if the $B = 0$ solution is smooth for all time. Siegel *et al.* [ST96, STD96] have extended the work of Ref. [Tan93] to later stages of the evolution, and through numerical computation for very small values of $B$ they showed that smooth $B = 0$ solutions are indeed significantly affected by the presence of arbitrarily small $B$ in order-one time, thus confirming the predictions of the perturbative theory. The zero surface tension solutions studied by Siegel *et al.* [STD96, ST96] in the channel geometry were single-finger solutions with an asymptotic width $\lambda$, specifically chosen to be incompatible with selection theory for vanishing surface tension. They found that the singular effect of surface tension was to widen the finger in order to reach the selected width. The surprising feature here is that the effect of surface tension is felt in order-one time, i.e., that the time lapse for which the regularized solution approaches the unperturbed one as $B \to 0$ is bounded. The general implication is that the perturbative scheme breaks down at relatively small times and that nothing can be said *a priori* for the later evolution.

## 1.4 Kinetic roughening of growing interfaces

The dynamics of an interface propagating in a disordered substrate has been object of intensive study in recent years [HHZ95, BS95, Kru97], specially regarding the scaling properties of the rough interface. It has been found evidence of scale invariance and universality in a variety of systems, including

fluid flow in a Hele-Shaw cell with quenched disorder [REDG89, HFV91, HKzW92], spontaneous imbibition of water in paper [BBC+92, ABB+95, HS95], self-affine bacterial colonies [VCH90, MM92], slow electrochemical deposition [KqZFzW92] or flame-less fire lines [ZZAL92].

Our interest here is focussed on fluid flow through a disordered Hele-Shaw cell, as a model system of forced fluid invasion (FFI) in porous media. In the seminal experiment done by Rubio *et al.* [REDG89] and which triggered intense research in this field for many years, water was injected from one end of a Hele-Shaw cell filled with a dense packing of small glass beads. Since water displaced air, the interface was on a stable configuration, but the presence of the disorder introduced by the glass beads roughened the interface. The focus was on the scaling properties of the rough interface, and these were studied by means of the local width $w(l,t)$ of the interface, which is defined as the root mean square (rms) value of the deviations of the interfacial height $h(x)$ with respect the mean value $\overline{h}_l$ over a length scale $l$. They found a power law behavior at long times, $w(l) \sim l^{\alpha}$ with a *roughness* exponent $\alpha = 0.73 \pm 0.03$. This result was in clear contradiction with the value expected from previous theoretical work. Most of the theoretical and numerical work done on interfacial kinetic roughening in the late eighties was based in the noise driven Burgers equation [Bur74], or Kardar-Parisi-Zhang (KPZ) equation [KPZ86]. It reads

$$\frac{\partial h(\mathbf{x},t)}{\partial t} = \nu \nabla^2 h(\mathbf{x},t) + \frac{\lambda}{2}[\nabla h(\mathbf{x},t)]^2 + \eta(\mathbf{x},t) \tag{1.18}$$

where $\nu$ and $\lambda$ are positive constants and $\eta(\mathbf{x},t)$ is a noise. This nonlinear differential equation has been proposed as a paradigm for interfacial growth and claimed to describe the asymptotic scaling of a large class of problems. From a theoretical point of view this is argued upon the fact that this equation contains the only nonlinearity which is relevant within a Renormalization Group framework. In $1+1$ dimensions it can be solved exactly and it is found [KPZ86] that $\alpha = 1/2$ and $\beta = 1/3$. If $\lambda = 0$ the resulting equation is known as Edwards-Wilkinson (EW) equation [EW82]. It belongs to a different universality class, with exponents $\alpha = 1/2$ and $\beta = 1/4$. There is an enormous body of literature on theoretical aspects of the KPZ equation, including RG treatments and extensive numerical simulation. Unfortunately, there is very little experimental evidence of KPZ scaling in real systems. It is not here the place to review this issue, but let us mention two specific results which are relevant to questions that will arise in Part IV of this thesis and that refer to the actual difficulties to observe the asymptotic scaling, namely the simulations of Beccaria *et al.* [BC94] of the KPZ equation and more recently the work by Cuerno and Castro [CC01] on the existence of transients

which hinder the observation of KPZ scaling. The latter shares a big deal of the spirit that moved us into elucidating these type of questions through a better understanding based on more microscopic derivations.

When Rubio's experiment [REDG89] was done, the expected behavior was that of KPZ, but the result $\alpha_{\rm exp} \simeq 3/4$ contradicted the KPZ prediction. The experiment was done again by Horvath *et al.* [HFV91] and He *et al.* [HKzW92]. The former found $\alpha = 0.81$ and the latter that $\alpha$ varied over a wide range (0.65–0.91), with capillary number $Ca$ notably spanning the range $10^{-5} < Ca < 10^{-2}$. The capillary number is the ratio between viscous forces to the capillary forces, and its particular form will depend on the system being considered. These experimental results clearly disagree with the scaling behavior exhibited by KPZ equation. It was believed, before the results of Refs. [REDG89, HFV91, HKzW92] that Eq. (1.18) provided a universal description of the growth of rough interfaces, but the discrepancy between theory and experiments forced theorists to look for alternatives, but within the framework provided by the almighty KPZ equation. These were essentially based on changing the nature of the noise $\eta$ present in the original KPZ equation (1.18). If noise is considered to be power-law instead of Gaussian distributed, a different scaling behavior is obtained [Zha90] from Eq. (1.18): $\alpha$ seems to be in the range 0.5–1, depending on the exponent of the power law distribution, implying that with an appropriate choice of this exponent the values of $\alpha$ obtained experimentally could be reproduced. A different way to change the scaling exponents of Eq. (1.18) is to use correlated noise [MHKZ89]. Dynamic RG group analysis showed that the introduction of both spatial or temporal correlations does change the exponents, allowing them to reach values well above those obtained with uncorrelated noise.

One of the main differences between the forced fluid invasion experiments and a description based on the KPZ equation is the nature of the noise term. The dominant noise in the experiments is quenched, but the noise appearing in KPZ is annealed (dynamical). Then, Eq. (1.18) has been also studied with a noise $\eta = \eta(h, x)$. In the case relevant to FFI where the interface has a finite velocity it has been found that KPZ with quenched disorder yields an interface that is not self-affine [Les96], since it consists of pinned segments with $\alpha \simeq 0.633$ joined by advancing segments with $\alpha \simeq 1$. More details on QKPZ can be found for instance in Ref. [HHZ95].

To sum up, the KPZ equation is capable of presenting a roughness exponent similar to the experimental ones choosing appropriately the properties of the noise term, but does not provide a satisfactory explanation to the observed dependence of $\alpha$ with $Ca$, nor is capable to make a clear prediction of the exponents of a given experiment. In addition, it is unclear how the distribution of glass bead sizes could give rise to a power law or correlated

noise. This failure is not surprising: the KPZ equation is local and fully phenomenological, and misses ingredients essential to describe fluid flow in a Hele-Shaw cell, most notably nonlocality. This point has been recently recognized by several authors. It has been recently addressed by Ganesan and Brener [GB98], who proposed a nonlocal interface equation to describe fluid flow in a random Hele-Shaw cell and obtained an exponent $\alpha = 3/4$ using Flory type arguments, and by Dubé *et al.* in Refs. [DRE+99, DRE+00], where a phase-field model is developed and simulated for the viscous imbibition problem. However, in these works noise is introduced at a phenomenological level, and does not include all the physical ingredients present in experiments, in particular the effects on the viscous flow due to fluctuating permeability. A first attempt to model permeability fluctuations within a phase-field scheme was reported by Hernández-Machado *et al.* [HMSL+01]. From the experimental point of view, new experimental realizations of fluid flow in a disordered Hele-Shaw cell have been carried out by Ortín and coworkers [HMSL+01, SRR+02, SOHM02b] that could shed some light into the problem and directly motivate the work done here in this subject. These experiments introduce disorder in a different and more controlled way than previous ones [REDG89, HFV91, HKzW92]: a Hele-Shaw cell with a spatially variable gap is used, in such a way that the statistical properties of the noise are perfectly known. Their results show a clear dependence of the exponent $\alpha$ with experimental parameters, as well as the appearance of the so-called 'anomalous' roughening (see sections 7.1 and 7.3). The Hele-Shaw cell with random gap is not only a valuable model system from an experimental point of view, but it is also very interesting from a theoretical standpoint since it allows a full 'microscopic' treatment. This will lead us in Part IV of this thesis to go one step further the recent nonlocal but phenomenological approaches, and develop a unified theoretical framework which includes all physical effects related to the spatial variation of the gap, and with complete generality concerning viscosity contrast and wetting conditions, hopefully leading to new insights which are not possible from a phase-field formulation.

# Part II

# Surface tension

# Chapter 2

# Methodological preliminaries

In this chapter we summarize the basic methodological aspects which will be used in Part II, including formulation, conceptual tools, analytical techniques and numerical methods. The conformal mapping formulation of the problem for high viscosity contrast is recalled, and its equivalent for low viscosity contrast is presented, together with the characterization of finger competition. The Dynamical Systems approach to the problem is presented and discussed in detail. The basic results of the perturbative asymptotic theory for Hele-Shaw flows are recalled, and the Hou-Lowengrub-Shelley (HLS) boundary integral numerical method for Hele-Shaw flows is described.

## 2.1 Conformal mapping formulation. Characterization of finger competition

In this section the conformal mapping formulation used to study Hele-Shaw flows in channel geometry is recalled. The finger competition phenomenon is described and the relevant quantities to characterize it are presented.

Here we consider the case with the nonviscous fluid displacing the viscous one ($c = 1$), therefore the pressure in the nonviscous fluid is constant, and we choose it to be zero. We assume periodicity at the sidewalls of the channel. Except for configurations symmetric with respect to the center axis of the channel, periodic boundary conditions define different dynamics from the more physical case of rigid sidewalls (with no-flux through them). Strictly speaking our case describes an infinite periodic array of unit channels. We will argue that nothing essential is lost with respect to competition in a rigid-wall channel, while the analysis is significantly simplified.

We use conformal mapping techniques to formulate the problem, following the formulation of Ref. [BKL+86]. We define a function $f(\omega, t)$ that

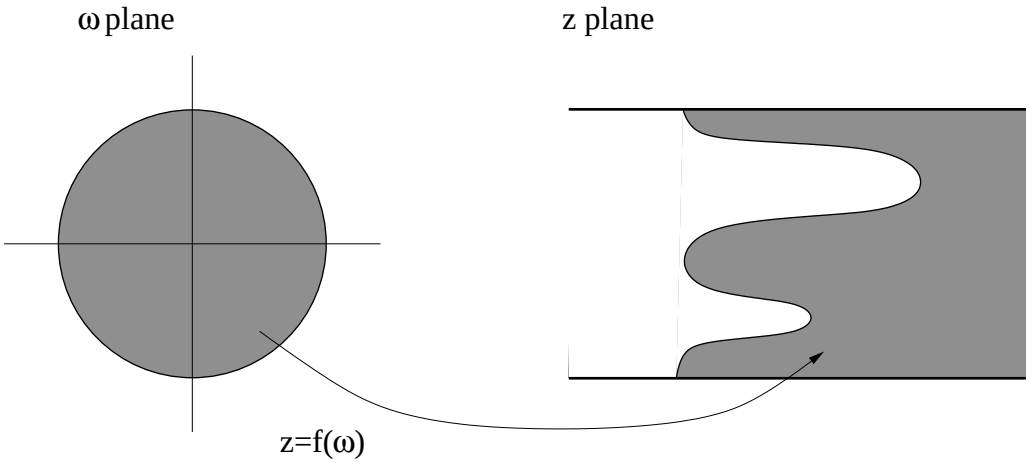


Figure 2.1: The interior of the unit circle is mapped into the viscous fluid.

conformally maps the unit disk in the complex plane $\omega$ into the viscous fluid in the physical plane $z = x + iy$, as schematically depicted in Fig. 2.1. We assume an infinite channel in the $x$ direction. The mapping $f(\omega, t)$ must satisfy $\partial_\omega f(\omega, t) \neq 0$ inside the unit circle, $|\omega| \leq 1$, and moreover, $h(\omega, t) = f(\omega, t) + \ln \omega$ must be analytic in the interior. The velocity potential $\varphi$ is defined as $\varphi = -(b^2/12\mu)p$, so that the velocity $\mathbf{u}$ reads $\mathbf{u} = \nabla\varphi$. We define the complex potential as the analytic function $\Phi = \varphi + i\psi$, where the harmonic conjugate $\psi$ of $\varphi$ is the stream function. The width of the channel is $W = 2\pi$ and the velocity of the fluid at infinity is $V_\infty = 1$, according to the nondimensionalization introduced in previous Chapter. It can be shown then that the evolution equation for the mapping $f(\omega, t)$ reads [BKL+86]

$$\partial_t f(\omega, t) = \omega \partial_\omega f(\omega, t) \mathrm{A}\left\{ \frac{\mathrm{Re}\left[ i\partial_\phi \Phi(e^{i\phi}, t) \right]}{|\partial_\phi f(e^{i\phi}, t)|^2} \right\} \tag{2.1}$$

where $\mathrm{A}[g]$ is an integral operator that acts on a real function $g(\phi)$ defined on the unit circle, and yields a complex function analytic in the unit disk, whose real part on the circle is $g(\phi)$. $\mathrm{A}[g]$ has the form

$$\mathrm{A}[g](\omega) = \frac{1}{2\pi} \int_0^{2\pi} g(\theta) \frac{e^{i\theta} + \omega}{e^{i\theta} - \omega} d\theta, \tag{2.2}$$

and on the unit circle $\omega = e^{i\phi}$ it reads

$$\mathrm{A}[g](\omega = e^{i\phi}) = g(\phi) + i\mathrm{H}_\phi[g] \tag{2.3}$$

where $\mathrm{H}_\phi[g]$ is the so-called Hilbert transform of $g(\phi)$ defined by

$$\mathrm{H}_\phi[g] = \frac{1}{2\pi} P \int_0^{2\pi} g(\theta) \cot\left(\frac{\phi-\theta}{2}\right) d\theta \tag{2.4}$$

where $P$ stands for the principal value prescription. The complex potential $\Phi$ satisfies

$$\Phi(\omega, t) = -\ln\omega + B\mathrm{A}[\kappa] \tag{2.5}$$

where the curvature $\kappa$ given in terms of $f(e^{i\phi}, t)$ is

$$\kappa = -\frac{1}{|\partial_\phi f|} \mathrm{Im}\left[\frac{\partial_\phi^2 f}{\partial_\phi f}\right]. \tag{2.6}$$

The evolution equation (2.1) written on the unit circle $\omega = e^{i\phi}$ is

$$\mathrm{Re}\left[i\partial_\phi f(\phi,t)\partial_t f^*(\phi,t)\right] = 1 - B\partial_\phi \mathrm{H}_\phi[\kappa] \tag{2.7}$$

where $f(\phi,t) \equiv f(e^{i\phi},t)$. In the zero surface tension case $B = 0$ the integro-differential equation (2.7) reduces to a much simpler equation, and the evolution of $f(\phi,t)$ for $B = 0$ is then given by

$$\mathrm{Re}\left[i\partial_\phi f(\phi,t)\partial_t f^*(\phi,t)\right] = 1. \tag{2.8}$$

The direct motivation of the present study is that, despite the fact that neglecting surface tension is in principle incorrect from a physical standpoint, the $B = 0$ case can be solved explicitly in many cases [Saf59, How86, PMW94] including solutions which, although being unstable, they exhibit a smooth and physically acceptable (nonsingular) behavior, quite similar to what is observed in experiments and simulations of the full problem.

The conformal mapping formulation we have just described has revealed as a powerful tool to study Hele-Shaw flows in the high viscosity contrast limit. More recently, a conformal mapping formalism for arbitrary viscosity contrast has been developed [PFC02], but the formalism is rather complicated since it involves two coupled mapping functions. But we have found that for the particular case of zero viscosity contrast the general formalism is notably simplified [PFC02] since only one mapping function is necessary to describe the evolution of the interface. Then, the evolution equation of the conformal mapping $f$, that maps the interior of the unit circle into the displaced fluid (fluid 2) is

$$\partial_t f = -\frac{1}{4\pi}\omega\partial_\omega f\, A\left(\frac{\mathrm{Re}\left\{\partial_s f\, P\int_0^{2\pi} ds'\gamma(s')\mathrm{cotgh}\left[\frac{f(s)-f(s')}{2}\right]\right\}}{|\omega\partial_\omega f|^2}\right) \tag{2.9}$$

with

$$\gamma(s) = 2\mathrm{Re}(\partial_s f) + 2B\partial_s \kappa(s). \tag{2.10}$$

The derivation of this equation can be found in the Appendix A.

As opposed to the high viscosity contrast case, where several rather general families of solutions of Eq. (2.1) are known, Eq. (2.9) has only two known explicit solutions: the (steady) ST finger and the unsteady Saffman-Taylor finger of width 1/2 found by Jacquard and Séguier [JS62] to be solution for any value of the viscosity contrast.

Before proceeding to the description of the general approach and its application to specific solutions, let us first introduce some ideas and definitions which will be helpful in further discussion. To quantify finger competition it is useful to define individual growth rates of fingers [MC98]. In simple situations like those considered here, the growth rate of a finger can be simply defined (in the reference frame moving with the mean interface position) as the peak-to-peak difference of the stream function between the maximum and the minimum which are adjacent to the zero of the stream function located at (or near) the finger tip [CJ94] (the definition can be generalized to more complicated situations). According to this definition, one assigns a nonzero growth rate to the finger if the tip advances at a velocity which is larger than the mean interface position. Looking at individual growth rates one can easily distinguish two different stages of the dynamics in the process of finger competition. A first stage characterized by the monotonous growth of all individual finger growth rates and a second one dominated by the redistribution of the total growth rate among the fingers. We call these two stages *growth* and *competition* regimes respectively. For a configuration of two different fingers, which is practically the only one addressed throughout this part of the thesis, during the growth regime the two fingers develop from small bumps of the initially flat interface, while the total growth rate $\Delta\psi_T(t)$, defined as $\Delta\psi_T(t) = \Delta\psi_1(t) + \Delta\psi_2(t)$, grows until it reaches a value close to its asymptotic one $\Delta\psi_T(\infty)$. The decrease of the growth rate of one of the fingers signals the outcome of the competition regime: there is a redistribution of flux from one finger to the other one. We also define the existence of *successful* competition as the ability to completely suppress the growth rate of one finger. A finger is dynamically suppressed of the competition process when its growth rate $\Delta\psi$ is reduced to zero.

## 2.2 Dynamical systems approach

The dynamical systems approach to the problem is introduced in this section, together with the general formulation in connection with the conformal

mapping formalism.

### 2.2.1 Elements of Dynamical Systems Theory

The theory of Dynamical Systems is a mathematical discipline which studies ordinary differential equations or flows (and difference equations or maps) with stress on geometrical and topological properties of solutions [GH83]. The approach is sometimes referred to as qualitative theory of differential equations. The focus is not on the study of individual solutions or trajectories of the differential equation, but on global properties of families of solutions. This point of view has become very fruitful in searching for universality in the context of nonlinear phenomena.

A dynamical systems approach seems thus appropriate to study in a mathematically precise way, the qualitative properties of the dynamics of our problem, and the qualitative differences associated to the presence or absence of surface tension. One of the important concepts in dynamical systems theory is that of *structural stability*, which captures the physically reasonable requirement of robustness of the mathematical description to slight changes in the equations. Roughly speaking, a system is said to be structurally stable if slight perturbations of the equations yield a topologically equivalent phase space flow. Although the structural stability 'dogma' must be taken with some caution [GH83], a structurally unstable description of a physical problem must be seen in principle as suspect. When a dynamical system (DS) depends on a set of parameters, the bifurcation set is defined as those points in parameter space where it is structurally unstable. In this case the structural instability at an isolated point in parameter space is the property necessary for the system to change its qualitative behavior. At a bifurcation point, adding perturbations to the equations to make the system structurally stable is called an *unfolding* [GH83]. For dimension higher than two, the mathematical definition of structural stability is usually too stringent. For the purposes of the present discussion and most physical applications it is sufficient to consider the notion of *hyperbolicity* of fixed points, which in 2 dimensions is directly associated to structural stability through the Peixoto theorem [GH83]. A fixed point is hyperbolic when the linearized flow has no marginal directions, that is, all eigenvalues of the linearized dynamics are nonzero. We will see that the nonhyperbolicity of the double-finger fixed point (in general the $n$-equal-finger fixed point) and the nonexistence of an unfolding of it within the known class of solutions is at the heart of the unphysical nature of this class of solutions.

In the approach to the Saffman-Taylor problem with concepts of DS theory, there is, however, an important additional difficulty in the fact that our

problem is infinite-dimensional and unbounded. In similar spatially extended systems, such as described by PDE's, it is customary to project the dynamics onto effective low-dimensional dynamical systems based on the so-called center manifold reduction theorem [GH83]. This is possible near the instability threshold and, for truly low-dimensional reduction, only for strongly confined systems, with a discrete set of modes. The ST problem however is both unbounded and will operate in general far from threshold. On the other hand, since the growth is never saturated to a finite amplitude, any weakly nonlinear analysis is necessarily limited to a rather early transient [ALCO01]. All the above techniques are thus of no much use for our purpose of studying the strongly nonlinear dynamics of competing fingers in their way to the ST stationary solution.

### 2.2.2 Dynamical systems and integrability of the ST problem

The basic point that we will exploit here to gain some analytical insight into the dynamics of the ST problems as a dynamical system is the fact that all exact solutions known explicitly for the idealized problem ($B = 0$) are defined in terms of ODE's for a finite number of parameters, and thus define finite-dimensional DS's in the phase space defined by those parameters[1]. The complete ST problem, for any finite $B$, defines a DS in an infinite dimensional phase space. We will refer to this DS as $S^\infty(B)$. The limit $B \to 0$ defines a limiting DS which we will refer to as $S^\infty(0^+)$, which, as we will see, is different from $S^\infty(0)$.

The conformal mapping $f(\omega, t)$ of the reference unit disk in the complex $\omega$-plane into the physical region occupied by the viscous fluid $z = x + iy = f(\omega)$ has the form

$$f(\omega, t) = -\ln \omega + h(\omega, t) \tag{2.11}$$

where $h(\omega, t)$ is an analytic function in the whole unit disk, and therefore has a Taylor expansion

$$h(\omega, t) = \Sigma_{k=0}^{\infty} a_k(t)\omega^k \tag{2.12}$$

which is convergent in the whole unit disk. Inserting Eq. (2.12) into the equation for the mapping $f(\omega, t)$, Eq. (2.1), we find an infinite set of equations

[1] In principle, the compactness of the resulting dynamical system could be troublesome for the present analysis due to the unboundedness of the original problem. Unlike what happens for instance for low viscosity contrast Hele-Shaw flows, where persistent dynamics of all regions of the interface may occur (see Chapter 5), the dynamics of high viscosity contrast is sufficiently simple, that is, compatible with low-dimensional dynamical systems in a compact space, that no such subtleties are relevant to the cases studied in this chapter.

of the form

$$\dot{a}_k = g_k(a_0, ..., a_k; B). \tag{2.13}$$

In the co-moving frame of reference the precise form of the infinite set of equations (2.13) is

$$\dot{a}_0 = C_0 \tag{2.14a}$$

$$\dot{a}_k = C_k - kC_0 a_k - \sum_{j=0}^{k-1} j a_j C_{k-j} \tag{2.14b}$$

where

$$C_0 = \frac{1}{2\pi}\int_0^{2\pi} \nu(\theta, t) d\theta \tag{2.15a}$$

$$C_k = \frac{1}{\pi}\int_0^{2\pi} \nu(\theta, t) e^{ik\theta} d\theta \tag{2.15b}$$

and

$$\nu(\theta, t) = \left.\frac{\mathrm{Re}\{\omega\partial_\omega h(\omega, t)] - B\mathrm{Re}[\omega\partial_\omega \mathrm{A}[\kappa](\omega, t)\}}{|\omega\partial_\omega f(\omega, t)|^2}\right|_{\omega=e^{i\theta}} \tag{2.16}$$

The infinite set of equations (2.13) defines the DS $S^\infty(B)$. In the special case of strictly zero surface tension, the DS $S^\infty(0)$ can be explicitly solved for some classes of initial conditions. These classes define invariant manifolds of $S^\infty(0)$ of *finite* dimension. In this context, finding explicit solutions implies identifying a specific analytic structure of $h(\omega)$, with a finite number of parameters, which is preserved under the time evolution. If this condition is fulfilled, then a set of ODE's for those parameters can be closed, and defines a certain DS on a finite-dimension space. For instance, for $B = 0$ the truncation of $h(\omega)$ into a polynomial form is preserved by the time evolution, so Eqs. (2.13) themselves remain a finite set of ODE's. This simple case, however, is known to lead to finite-time singularities. The evolution is in general not defined after some finite time and cannot be considered as sufficiently well behaved as a DS's. On the other hand, classes of solutions have been reported which are smooth (nonsingular) for all the time evolution. The corresponding conformal mapping takes the general form [How86, PMW94]

$$h(\omega) = d(t) + \sum_{j=1}^{N} \gamma_j \ln[1 - \alpha_j(t)\omega] \tag{2.17}$$

where $\gamma_j$ are constants of motion with the restriction $\sum_{j=1}^{N} \gamma_j = 2(1 - \lambda)$ where $\lambda$ is the asymptotic filling fraction of the channel occupied by fingers.

If all $\gamma_j$ are real the evolution is free of finite-time singularities, and if any $\gamma_j$ has an imaginary part then finite-time singularities may appear for some set of initial conditions (see Sec. 3.3.3). Although this form of the mapping contains all orders of the Taylor expansion of $h(\omega)$, it defines finite dimension invariant manifolds, since the superposition of logarithmic terms of Eq. (2.17) is preserved under the dynamics. This means that a closed set of ODE's for the finite number of parameters $\alpha_j(t)$ can be found. In addition, the region which is physically meaningful is that in which $|\alpha_j| \leq 1$ (including the equal sign allows for the limiting case of infinite fingers, and makes the phase space compact). The DS defined by Eq. (2.17) in the $2N$-dimensional hyper-volume will be denoted as $L^{2N}(\{\gamma_j\})$

For the sake of discussion throughout this work it is important to have in mind that modifying parameters $\{\gamma_j\}$, which are constants of motion under the dynamics defined through Eq. (2.8) corresponds to varying initial conditions in the phase space of $S^{\infty}(0)$, while, from the standpoint of the finite-dimensional DS's denoted by $L^{2N}(\{\gamma_j\})$ it corresponds to changing the DS itself, that is, changing the ODE's obeyed by the dynamical variables. In this sense, $\{\gamma_j\}$ label a set of DS's defined on a 2N-hyper-volume $|\alpha_j| \leq 1$.

Following Ref. [MC98], the key idea is to look for the simplest of the DS defined above which contains the three physically relevant fixed points, namely, the planar interface (PI), the single finger ST solution (1ST) and the double Saffman-Taylor finger solution (2ST). We will call this minimal DS as $L^2(\lambda, 0)$ or simply $L^2(\lambda)$, since it has only one constant of motion, namely $\lambda$. In Ref. [MC98] it was proposed to compare the global flow properties in phase space of such DS with those of a corresponding two-dimensional dynamical system defined by the regularized problem. The latter was obtained by restricting $S^{\infty}(B)$ to a one-dimensional set of initial conditions properly chosen in such a way that the invariant manifold of $S^{\infty}(0)$ which defines $L^2(\lambda)$ was tangent to $S^{\infty}(0^+)$ at the PI fixed point. The resulting DS $S^2(B)$ was then shown to have a topological structure nonequivalent to that of $L^2(\lambda)$. In particular in the limiting case, $S^2(0^+)$ intersected $L^2(1/2)$ not only at PI but also at the other fixed points 1ST and 2ST, and furthermore, at the two full trajectories connecting PI with 1ST and 2ST respectively. The basic conclusion was then that the regularized and the idealized problem were intrinsically different.

## 2.3 Asymptotic theory

The evolution equation for the mapping $f$ Eq. (2.1) can be explicitly solved in the absence of surface tension, as explained in previous section, but no solutions are known for $B > 0$. This makes the theoretical study of the $B > 0$ dynamics extremely difficult beyond the initial linear and weakly nonlinear [ALCO01] regimes. To close this gap, Tanveer [Tan93] developed an asymptotic perturbation theory that can be applied for $0 < B \ll 1$. The initial work was later on enlarged and numerically checked [STD96, ST96].

The conformal mapping formulation used by these authors differs slightly from the one used in previous sections, so prior to the description of the asymptotic theory we will briefly introduce their formulation.

### 2.3.1 Conformal mapping in the semicircle

Consider Hele-Shaw flows in the channel geometry, in which a fluid of negligible viscosity displaces a viscous liquid. The equations governing the interfacial evolution can be conveniently formulated by first introducing the conformal map $f(\zeta, t)$ which takes the interior of the unit *semicircle* in the $\zeta$ complex[2] plane into the region occupied by the viscous fluid in the complex plane $z = x + \mathrm{i}y$, in such a way that the arc $\zeta = e^{\mathrm{i}s}$ for $s \in [0, \pi]$ is mapped to the interface and the diameter of the semicircle is mapped to the channel walls[3]. Lengths are nondimensionalized using $W/2$ instead of $W/(2\pi)$, as done previously. The mapping function $f(\zeta, t)$ has the form $f(\zeta, t) = -(2/\pi)\ln\zeta + \mathrm{i} + f(\zeta, t)$, and inside and on the unit semicircle we require $f(\zeta, t)$ to be analytic and $f_\zeta(\zeta, t) \neq 0$. Here the subscript denotes derivative. In addition, we require that

$$\mathrm{Im}\ f = 0 \tag{2.18}$$

on the real diameter of the semicircle. This latter condition ensures that $f$ maps the diameter to the channel walls. Under suitable assumptions (see [Tan93]) the Schwartz reflection principle may be applied to show that $f$ is analytic and $f_\zeta \neq 0$ for $|\zeta| \leq 1$.

The form of the complex potential $\Phi(z, t)$ as a function of $\zeta$ is

$$\Phi(\zeta, t) = -(2/\pi)\ln\zeta + \mathrm{i} + \phi(\zeta, t) \tag{2.19}$$

[2]We use $\zeta$ instead of $w$ to emphasize that the interior of the unit semicircle is being mapped instead of the interior of the unit circle.

[3]For interfaces symmetric with respect to the central axis of the channel this formulation also describes periodic boundary conditions, that is, an infinite array of fingers.

where $\phi(\zeta, t)$ is an analytic function inside the unit circle. The condition that there is no flow through the walls implies that Im $\phi = 0$ must hold on the real diameter of the unit semicircle. In the absence of surface tension, $\phi = 0$ (see Eq. (2.21)).

The evolution equation for the mapping takes the form

$$\mathrm{Re}\left[\frac{f_t}{\zeta f_\zeta}\right] = \frac{1}{|f_\zeta|^2}\mathrm{Re}\left[\zeta\Phi_\zeta\right], \tag{2.20}$$

and the potential $\Phi$ is obtained from

$$\mathrm{Re}\ \phi = -\frac{\pi^{-2}B}{|f_\zeta|}\mathrm{Re}\left[1+\zeta\frac{f_{\zeta\zeta}}{f_\zeta}\right]. \tag{2.21}$$

### 2.3.2 Dynamics with small $B$: perturbative theory

The perturbation theory describes the effects of the introduction of a small amount of surface tension on initial data $f(\zeta, 0)$ specified in the extended complex plane, i.e., in a domain including the 'unphysical' region $|\zeta| > 1$ (the extended domain is required to make the $B = 0$ problem well-posed). The effect of finite $B$ is most important near isolated zeros and singularities of $f_\zeta(\zeta, 0)$, where a regular perturbation expansion in $B$ breaks down. (Away from these points the perturbation expansion is regular, at least initially). For the class of explicit solutions Eq. (2.17) that will be discussed in this thesis, the isolated singularities of $f_\zeta(\zeta, 0)$ are simple poles. The theory suggests that the introduction of finite surface tension modifies the poles $(\zeta_s)$ by transforming them into localized clusters of $-4/3$ singularities[4], but these clusters move at leading order according to the $B = 0$ dynamics. Thus the effect of one of these clusters on the interface is approximately equivalent to that of the unperturbed $(B = 0)$ pole-like singularity that has given birth to it.

The influence of surface tension on the zeros of $f_\zeta(\zeta, 0)$ is more complex. Each initial zero instantly gives birth to two localized inner regions, i.e., regions where the $B = 0$ and $B > 0$ solutions differ by $O(1)$. One of the two inner regions moves, at least initially, according to the $B = 0$ dynamics of the original zero $\zeta_0$[5]. Since the zero surface tension solutions of physical interest have zeros that are either bounded away from the unit disk for all time or impact the unit disk only after long times, the inner region around $\zeta_0(t)$ has a negligible influence on the interface. The second inner region created

[4]Branch points with a power $-4/3$

[5]This region can move differently from the $B = 0$ zero once the second inner region discussed below has impacted the unit disk. We do not consider this possibility here.

around $\zeta_0(0)$ moves differently. The theory suggests that this inner region consists of a cluster of singularities, whose size scales like $B^{1/3}$. Unlike the case discussed above this second inner region moves away from the $B = 0$ zero since, to leading order in $B$, it moves like a *singularity* of the zero surface tension problem and this speed is different form the speed of the zero $\zeta_0(t)$ which spawned the cluster. As this singularity cluster approaches the physical domain it may perturb the flow and the interface shape may differ significantly from that at $B = 0$. The location of this singularity cluster will be denoted by $\zeta_d(t)$, and following [Tan93] we shall call it the daughter singularity. We emphasize that the dynamics of the daughter singularity cluster is determined at lowest order solely by the $B = 0$ solution $f^0(\zeta, t)$, at least until it arrives at the surroundings of the unit circle, and therefore can be simply computed once the initial locations of the zeros of $f_\zeta(\zeta, 0)$ are determined.

The daughter singularity evolution equation is given by [Tan93]

$$\dot{\zeta}_d(t) = -q_1^0(\zeta_d(t), t); \quad \zeta_d(0) = \zeta_0(0) \tag{2.22}$$

where $q_1^0$ is defined by

$$q_1^0 = \frac{\zeta}{2\pi i} \oint_{|\zeta'|=1} \frac{d\zeta'}{\zeta'} \frac{\zeta + \zeta'}{\zeta' - \zeta} \frac{\mathrm{Re}\left[\zeta' \Phi_\zeta^0(\zeta', t)\right]}{|z_\zeta^0(\zeta', t)|^2} \tag{2.23}$$

and the superscript 0 denotes that the function evaluations are done using the corresponding $B = 0$ solution. The function $-q_1^0(\zeta, t)$ also gives the characteristic velocity of a pole or branch point singularity of $f_\zeta(\zeta, t)$ located at position $\zeta$ in the region $|\zeta| > 1$. The initial position $\zeta_d(0)$ is a consequence of the fact that each zero $\zeta_0(0)$ of the zero surface tension solution will give birth to a daughter singularity. From Eq. (2.22) it can be shown [Tan93] that $d|\zeta_d|/dt < 0$, so that the daughter singularity approaches the unit circle and it can impact it in a finite time $t_d$, the daughter singularity impact time, satisfying $|\zeta_d(t_d)| = 1$. In the limit $B \to 0$, the daughter singularity impact time $t_d$ signals the time when the effects of the surface tension are felt on the physical interface. For times larger than $t_d$ the $B = 0$ interface and the $B \to 0$ one are expected to differ significantly.

## 2.4 HLS numerical method

In this section the numerical method developed by Hou, Lowengrub and Shelley (HLS) [HLS94] is described. The method removes the stiffness of the equations in an efficient manner, is spectrally accurate and controls the effect

of numerical noise. HLS method has been used to develop the code used in Chapters 4 and 5.

Tryggvason and Aref [TA83] used the vortex sheet formalism to integrate the evolution, using a 'vortex-in-cell' algorithm. Later on, DeGregoria and Schwartz [DS85, DS86] applied also the vortex sheet formalism but with a different numerical algorithm, and observed tip-splitting of well developed fingers when surface tension was decreased. Dai and Shelley [DS93] showed that small $B$ numerical computations are extremely sensitive to the precision used in the computations, and as a consequence numerical noise has to be controlled with care in order to ensure that the computation is sufficiently accurate. Recently, phase-field methods originally developed in the solidification context [CL85, Lan86, Kob93] have been applied to Hele-Shaw flows by Folch *et al.* [FCHMRP99a, FCHMRP99b]. Although usually less accurate than boundary integral methods (at least for laplacian problems), phase-field models can naturally deal with multiply connected fluid domains and topological changes of the interface.

Numerical integration of Hele-Shaw flows is based on the vortex sheet formalism [TA83] introduced in Section 1.1. The velocity $\mathbf{w}$ due to the vortex sheet of a point of the interface is given by Birkhoff integral formula [Bir54, TA83]

$$\mathbf{w} = \mathbf{w}(s,t) = \frac{1}{2\pi}\mathrm{P}\int ds' \frac{\hat{\mathbf{z}} \times [\mathbf{r}(s,t) - \mathbf{r}(s',t)]}{|\mathbf{r}(s,t) - \mathbf{r}(s',t)|^2}\gamma(s',t) \tag{2.24}$$

where P indicates Cauchy's principal value and the vorticity $\gamma$ reads

$$\gamma = 2c\,\mathbf{w}\cdot\hat{\mathbf{s}} + 2\hat{\mathbf{x}}\cdot\hat{\mathbf{s}} + 2B\partial_s\kappa \tag{2.25}$$

To obtain the evolution of the interface Eq. (2.25) has to be solved with $\mathbf{w}$ given by Eq. (2.24), yielding an integro-differential equation for the vorticity $\gamma$. Once $\gamma$ is known, Eq. (2.24) is used again to obtain $\mathbf{w}$, and then its normal component together with the irrotational component of the velocity (if present) is used to update the position of the interface.

However, several problems arise in the practical implementation of this scheme. First, the integral that appears in Eq. (2.24) has a singular kernel that has to be evaluated carefully. Another important obstacle that represented a major problem for a decade to the numerical integration of the equations is its stiffness, that forced painfully slow numerical integrations. This stiffness is a consequence of the high order spatial derivatives of the curvature term. Finally, the problem is extremely sensitive to numerical noise, specially at small values of surface tension, and this sensitivity imposes the main limitation to computations at very small $B$.

### 2.4.1 $\theta - s_\alpha$ formalism

The evolution of an interface separating two fluids with surface tension is a complicated motion-by-curvature problem. The numerical treatment of this type of problems gets simplified by the use of appropriate dynamical variables instead of the original cartesian $x$ and $y$ variables to describe the interface position. The new variables are the interface's tangent angle $\theta$, defined as the angle between the $y$ axis and the tangent vector, and the derivative of the arclength $s_\alpha$, where $\alpha$ is the independent variable that parameterizes the interface. Then, given $\theta$ and $s_\alpha$ the interface in terms of the cartesian coordinates $(x(\alpha), y(\alpha))$ is obtained (up to a translation) from the integration of

$$\left(\frac{\partial x(\alpha)}{\partial \alpha}, \frac{\partial y(\alpha)}{\partial \alpha}\right) = s_\alpha \left(\cos\left[\theta(\alpha)\right], \sin\left[\theta(\alpha)\right]\right), \tag{2.26}$$

where $\mathbf{r}$ is assumed to be $2\pi$-periodic in $\alpha$. Note that we use the notation $b_a \equiv \partial b/\partial a$. One important advantage of the use of the $\theta - s_\alpha$ variables is that the curvature has the simple expression $\kappa = \theta_s$, in comparison to its expression in terms of $x - y$, that is

$$\kappa = \frac{\partial_\alpha x \partial_\alpha^2 y - \partial_\alpha^2 x \partial_\alpha y}{\left[(\partial_\alpha x)^2 + (\partial_\alpha y)^2\right]^{3/2}}. \tag{2.27}$$

The evolution of the interfacial shape is given solely by the normal component of the velocity, $U$, and the tangential component $T$ gives only a reparameterization of the interface, changing how the points are distributed along it. This allows one to introduce an arbitrary tangential component of the velocity without altering the dynamics of the interface. An appropriate election of $T$ may indeed simplify the integration of the equations of motion. The evolution of a point of the interface in terms of the components of the velocity is

$$\frac{\partial \mathbf{r}}{\partial t} = U\hat{\mathbf{n}} + T\hat{\mathbf{s}} \tag{2.28}$$

and in terms of $\theta - s_\alpha$ it reads [HLS94]

$$\theta_t = \frac{1}{s_\alpha} U_\alpha + \frac{T}{s_\alpha}\theta_\alpha \tag{2.29a}$$

$$s_{\alpha t} = T_\alpha - \theta_\alpha U. \tag{2.29b}$$

The freedom in the choice of $T$ allows us to choose tangential velocities that dynamically preserve a specific parameterization. In particular, one of the parameterizations that considerably simplifies the computation is [HLS94]

$$s_\alpha(\alpha, t) = \frac{1}{2\pi} L(t), \tag{2.30}$$

that makes $s_\alpha$ homogeneous all along the interface and equal to its mean value. This is the parameterization we will use, and then the dependent variables are the interface length $L(t)$ and the angle $\theta(\alpha, t)$. The tangential velocity $T(\alpha, t)$ that keeps the above equal-arclength parameterization is easily obtained from Eq. (2.29b) and reads

$$T(\alpha, t) = T(0, t) + \int_0^\alpha d\alpha' \theta_{\alpha'} U - \frac{\alpha}{2\pi} \int_0^{2\pi} d\alpha' \theta_{\alpha'} U. \tag{2.31}$$

The use of this parameterization transforms the partial differential equation (PDE) for $s_\alpha$, Eq. (2.29b) into a ordinary differential equation (ODE), simplifying its integration and the removal of the stiffness, as will be shown in next section.

### 2.4.2 Small scale decomposition

The main obstacle that appears when one integrates the motion equations Eq. (2.29) is the stiffness that arises from the presence of high order terms in Eq. (2.29a). It can be shown [BHLS93] that severe stability constraints are present. For an explicit time integration method the form of the constraint is

$$\Delta t < C \frac{(\bar{s}_\alpha h)^3}{B}, \tag{2.32}$$

where $C$ is a constant, $h$ is the spatial grid size, $\bar{s}_\alpha = \min_\alpha s_\alpha$ and $\Delta t$ is the time step. Hence, to improve spatial resolution (decreasing $h$) the time step has to be extraordinarily reduced. In addition, since the constraint depends on the minimum grid spacing in arclength that in turn is strongly time dependent (and can be very small if the points are not redistributed along the interface), the system can get very stiff. The constraint arises from the influence of high order derivatives at small length scales. To overcome these difficulties Hou, Lowengrub and Shelley [HLS94] studied the Birkhoff-Rott operator at small length scales and concluded that at small scales it can be considerably simplified. The term $\mathbf{w} \cdot \hat{\mathbf{s}}$ present in Eq. (2.25) is an operator on $\gamma$ that actually smoothes it. It can be assumed that at small length scales this term of Eq. (2.25) is negligible, and it can be proved [HLS94] that at small scales

$$\gamma(\alpha, t) \sim 2B\kappa_\alpha \tag{2.33}$$

where the notation $f \sim g$ is introduced to mean that the difference between $f$ and $g$ is smoother than $f$ and $g$. Now that the behavior expressed in Eq. (2.33) is known then in the PDE for $\theta$ the contribution at small scales

can be explicitely separated from the other contributions in the following way [HLS94]

$$\theta_t = \boxed{\frac{B}{s_\alpha}\left(\frac{1}{s_\alpha}\mathrm{H}\left[\frac{\theta_\alpha}{s_\alpha}\right]_\alpha\right)_\alpha} + \frac{1}{s_\alpha}U_\alpha - \frac{B}{s_\alpha}\left(\frac{1}{s_\alpha}\mathrm{H}\left[\frac{\theta_\alpha}{s_\alpha}\right]_\alpha\right)_\alpha + \frac{1}{s_\alpha}\theta_\alpha T, \quad (2.34)$$

so now in the numerical integration of $\theta_t$ an implicit scheme (free of the severe constraint given in Eq. (2.32)) can be applied to the boxed term of Eq. (2.34), removing the stiffness present with an explicit scheme. Taking into account the equal arclength parameterization Eq. (2.30) and applying the Fourier transform to Eq. (2.34), the evolution equation for the Fourier transform $\hat{\theta}$ of the angle is

$$\hat{\theta}_t(k) = -B\left(\frac{2\pi}{L}\right)^3 |k|^3\hat{\theta}(k) + \hat{N}(k), \quad (2.35)$$

where $\hat{N}(k)$ is the Fourier transform of the rhs of Eq. (2.34) except the boxed term. This expression is supplemented with the equation for $L$

$$L_t = -\int_0^{2\pi} d\alpha' \theta_{\alpha'} U. \quad (2.36)$$

### 2.4.3 Numerical method and discretization

The time integration methods applied to the equations of motion Eqs. (2.35, 2.36) have been chosen to be of second order in time. The ODE describing the evolution of $L$ has been integrated using the (explicit) second order Adams-Bashforth method:

$$L^{n+1} = L^n + \frac{\Delta t}{2}(3M^n - M^{n-1}), \quad (2.37)$$

where the superscript denotes the time step and $M$ is

$$M = -\int_0^{2\pi} d\alpha' \theta_{\alpha'} U. \quad (2.38)$$

The numerical time integration of Eq. (2.35) is more involved. The method we have used is the linear propagator method, one of the two proposed by Hou *et al.* [HLS94] and introduced by Rogallo [Rog77]. This method factor out the dominant linear term *prior* to discretization, providing stable methods to integrate diffusive problems. The method is applied as follows. Rewrite Eq. (2.35) as

$$\frac{\partial}{\partial t}\mathcal{F}(k,t) = \exp\left[B\,(2\pi|k|)^3 \int_0^t dt' L^{-3}(t')\right]\hat{N}(k,t) \quad (2.39)$$

where

$$\mathcal{F}(k,t) = \exp\left[B\left(2\pi|k|\right)^3 \int_0^t dt' L^{-3}(t')\right] \hat{\theta}(k,t). \tag{2.40}$$

Eq. (2.39) is discretized applying again the second order Adams-Bashforth method, and in terms of the original $\hat{\theta}$ it reads

$$\hat{\theta}^{n+1}(k) = e_k(t_n, t_{n+1})\hat{\theta}^n(k) + \frac{\Delta t}{2}\left[3e_k(t_n, t_{n+1})\hat{N}^n(k) - e_k(t_{n-1}, t_{n+1})\hat{N}^{n-1}(k)\right] \tag{2.41}$$

where $t_n = n\Delta t$, and

$$e_k(t_1, t_2) = \exp\left[-B\left(2\pi|k|\right)^3 \int_{t_1}^{t_2} \frac{dt'}{L^3(t')}\right]. \tag{2.42}$$

Eqs. (2.41) and (2.42) show the use of the linear propagator: at every time step $\hat{\theta}$ is propagated forward at the exact exponential rate corresponding to the linear term. If the nonlinear term $\hat{N}$ was absent, the method would give the *exact* solution. One still needs to compute the factor $e_k(t_1, t_2)$, that contains a continuous time dependence. To compute $e_k(t_1, t_2)$ the integral is evaluated using the trapezoidal rule approximation, that retains the second order of the time discretization. Then, at every time step $L^{n+1}$ is computed first using Eq. (2.37), and this $L^{n+1}$ is used to compute $\hat{\theta}^{n+1}$, since $L^{n+1}$ is needed to evaluate $e_k(t_n, t_{n+1})$.

The interface is initially discretized at points satisfying the equal arclength parameterization, and the election of $T$ given in Eq. (2.31) keeps it during the evolution. Spectrally accurate spatial discretizations are used, and any differentiation or partial integration is found at the mesh points by means of the Fourier transform. In the computation of the velocity at a point of the interface the singular kernel of the Birkhoff-Rott integral has to be evaluated. In this case we use the spectrally accurate alternate point discretization, and the lagrangian velocity (in complex form) is obtained as

$$u_j - iv_j = \frac{h}{2\pi i} \sum_{(j+l)\ odd} \gamma_l \cot\frac{z_j - z_l}{2} \tag{2.43}$$

where $z_j = x_j + iy_j$ is the $j$-th interfacial (mesh) point and $\mathbf{w}_j = (u_j, v_j)$ is its (rotational) velocity. Note that above we have written the Birkhoff-Rott integral for an interface $2\pi$-periodic, and for this reason the (singular) kernel of the integral in Eq. (2.24) is different from that of Eq. (2.43).

The vorticity is obtained from the numerical solution of Eq. (2.25). Formally, its discretized version is a system of ordinary linear equations, $\gamma_i(\delta^i_j -$

$M_j^i) = A_j$, and to solve it it would be necessary to invert the matrix $\delta_j^i - M_j^i$. However, this is very time consuming, and in practice the method used is the Generalized Minimal Residual (GMRES) [SS86] method. GMRES solves the system iteratively, starting from an initial guess, as close as possible to the solution. The numerical solution of Eq. (2.25) is the part of the numerical code that consumes most of the time, and to reduce the time devoted to obtain $\gamma$ it is important to supply a good initial guess, thus reducing the number of iterations needed by GMRES to reach convergence. The initial guess at every time step is obtained from extrapolation[6] of $\gamma$ at previous time steps. In addition, if the interface is symmetric along the mid-channel axis we can take advantage of this since only half of the points of $\gamma$ need to be computed with GMRES, and the rest are obtained from the symmetry condition, improving significantly the time performance of the total computation.

### 2.4.4 Noise filtering

The major limitation to the computation of the evolution at low values of $B$ is the extreme sensitivity of the system to noise. The Saffman-Taylor finger is linearly stable but unstable to perturbations of finite amplitude, or in other words, it is nonlinearly unstable [Ben86]. The amplitude $A_{noi}$ of the perturbation required to destabilize the finger decreases rapidly as $B$ is reduced, and is approximately described by [Ben86]

$$\ln A_{noi} \sim -\frac{1}{\sqrt{B}}. \tag{2.44}$$

This nonlinear instability of ST finger manifests also for fingers that are not well formed, but whose shape is close to the ST finger in its foremost region. Then, at low $B$ numerical noise originated at roundoff can trigger the instability, and has to be appropriately controlled to prevent the spurious growth of high order modes. The method we have used to control it is Krasny filtering: we set to 0 the amplitude of all Fourier modes below a filter level $\epsilon$. Krasny filtering is applied every time a derivative of any quantity is computed, and on $\hat{\theta}$ at every time step. The need of noise filtering is illustrated in Fig. 2.2, where $|\hat{\theta}(k)|$ corresponding to an interface consisting of a well developed finger very close to the ST finger is plotted. For large $k$ the effect of noise is clear: the amplitude of the modes decreases as $\log|\hat{\theta}| \sim -k$ for a range of wave numbers, but below a certain amplitude roundoff error becomes dominant. The application of Krasny filtering to the case depicted in the plot would set to zero all modes below the dashed line.

[6] We have typically used fourth-order extrapolation.

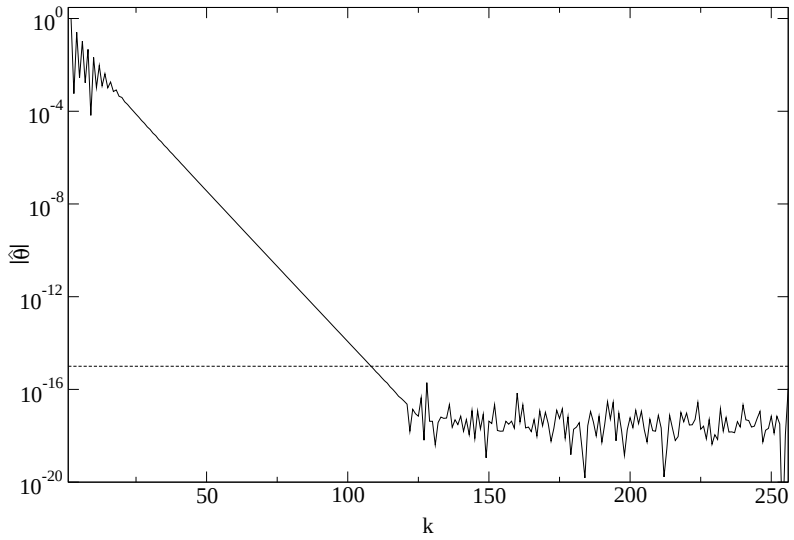


Figure 2.2: $|\hat{\theta}|$ for an interface corresponding to a well developed finger, with a shape close to ST finger. Below $k \approx 120$ numerical noise dominates $\hat{\theta}$. The dashed line represents a possible election of the noise filter $\epsilon$.

Krasny filtering reduces notably the effect of noise, but for very small values of $B$ numerical noise still has a dramatic effect on long time dynamics. In this case the only solution is to increase the arithmetic precision in order to lower the amplitude where roundoff noise is significant, thus allowing for a reduction on the value of the filter level $\epsilon$. Higher precision arithmetic (128-bit) combined with a lower value of $\epsilon$ notably delay or even suppress the appearance of noise effects on the interface, but at the cost of an important increase of CPU time. But even if higher precision is used noise appears again if $B$ is decreased further.

# Chapter 3

# Zero-surface tension dynamics. Towards a Dynamical Solvability Scenario

Previous work on finger competition is described, in particular the study of a two-finger exact solution of the problem without surface tension, that does not present successful finger competition. Some simple examples of exact solutions of the problem without surface tension that present successful finger competition are studied in detail in the framework of the Dynamical Systems approach. A general proof of the existence of finite-time singularities for broad classes of solutions is given. The main conclusion is that exact zero-surface tension solutions taken in a global sense are unphysical because the multifinger fixed points are nonhyperbolic, and an unfolding of them does not exist within the same class of solutions. Hyperbolicity (saddle-point structure) of the multifinger fixed points is argued to be essential to the physically correct qualitative description of finger competition. The restoring of hyperbolicity by surface tension is discussed as the key point for a generic Dynamical Solvability Scenario, which is proposed for a general context of interfacial pattern selection.

## 3.1 The two-finger minimal model

In this section the minimal class presented in Ref. [MC98] and studied in detail in [Mag00] is revisited. The comparison of its phase portrait with the known topology of the physical problem reveals that the minimal class dynamics is unphysical. The main reason for this unphysical behavior is the existence of a continuum of fixed points.

### 3.1.1 The model. Study of the dynamical system

The simplest class of exact time-dependent solutions of Eq. (2.8) containing the three physically relevant fixed points: the planar interface (PI), the single Saffman-Taylor (1ST) fixed point and the double Saffman-Taylor (2ST) fixed point was introduced in Ref. [MC98] and reads

$$f(\omega,t) = -\ln\omega + d(t) + (1-\lambda)\left\{\ln\left[1-\alpha(t)\omega\right] + \ln\left[1+\alpha(t)^*\omega\right]\right\} \qquad (3.1)$$

where $\lambda$ is a real-valued constant in the interval $(0,1)$, $\alpha(t) = \alpha'(t) + i\alpha''(t)$ and $d(t)$ is real. The relevant phase space for a given $\lambda$ is the first quadrant of the unit circle in the $(\alpha', \alpha'')$ space. The other three quadrants describe interface configurations that are equal or symmetrical to the interfaces contained in the first quadrant. In this section we will summarize the basic results discussed in detail in Refs. [MC98, CM00]. The interface described by this mapping consists generically of two unequal fingers, axisymmetric and without overhangs. The case $\alpha'(t) = 0$ gives the time-dependent ST finger solution, and $\alpha''(t) = 0$ corresponds to the double time-dependent ST

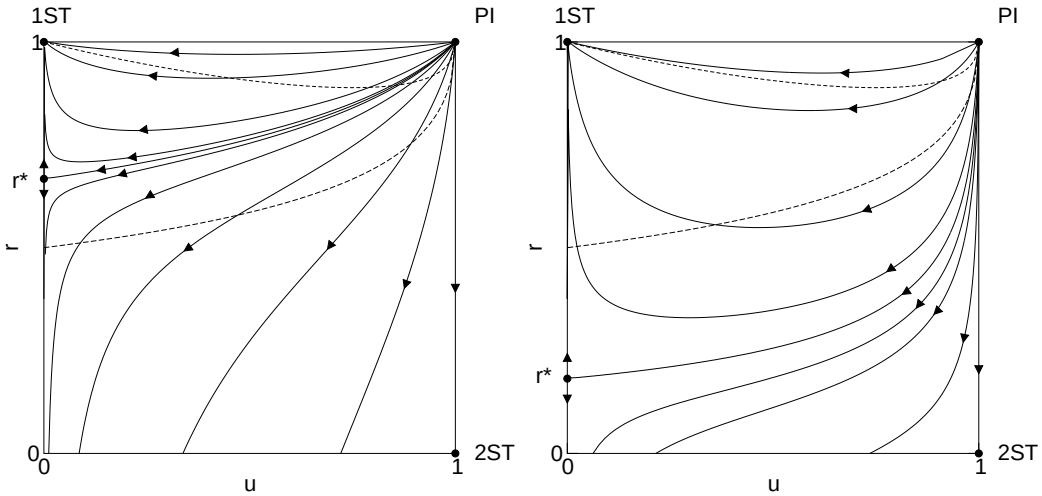


Figure 3.1: Phase portrait of the minimal model with (a) $\lambda = \frac{1}{2}$ and (b) $\lambda = \frac{1}{10}$. The one-finger (resp. two-finger) region is above (below) the short-dashed line. For the region above the long-dashed line the secondary finger has zero growth rate while for the region below the secondary finger has finite growth rate. Note that for $\lambda = \frac{1}{10}$ there are trajectories crossing from below the line separating the zero and finite growth rate regions. The phase space is parameterized with the variables $u = 1-\alpha''^2$ and $r = (\alpha'^2+\alpha''^2-1)/(\alpha''^2-1)$.

finger. For $|\alpha(t)| \ll 1$ the interface consists of a sinusoidal perturbation of the planar interface.

The phase portraits of the dynamical systems defined by the solutions of the form Eq. (3.1) for different $\lambda$ were studied in detail in Refs. [MC98, CM00, Mag00]. The most salient feature was that the basin of attraction of the Saffman-Taylor single finger is not the whole phase space (see Fig. 3.1). The separatrix between the basin of attraction of the ST finger and the rest of the flow starts in the planar interface fixed point and ends in a new fixed point whose location depends on $\lambda$. The flow not attracted to the single-finger fixed point, evolves to a continuum of fixed points, corresponding to stationary solutions with two unequal fingers advancing with the same velocity. The basin of attraction of the ST finger was shown to be larger for smaller $\lambda$ but never the full phase space. For $\lambda = 1/2$ there is no successful competition in the precise sense defined in Section 2.1. Successful competition is only possible for $\lambda < 1/3$ but, in any case, it is never very significant (only rather small fingers may be suppressed).

### 3.1.2 Comparison with the regularized dynamics

In this section we will extend the the analysis of Refs. [MC98, CM00, Mag00] to generalize and strengthen their conclusions. We are interested in the comparison between the $B = 0$ dynamics and the $B \neq 0$ one. The dynamical system defined by the mapping Eq. (3.1) is referred to as $L^2(\lambda)$. From now on we will restrict the analysis to the relevant case for $B \to 0$, namely $\lambda = 1/2$. In order to compare with the $B \neq 0$ dynamics we first have to define an appropriate invariant manifold of the full dynamical system $S^\infty(B)$. Following Ref. [MC98] we can take a uniparametric set of initial conditions of the form Eq. (3.1) in a neighborhood of the PI fixed point, say $\alpha(\theta) = \varepsilon e^{i\theta}$ and define a two-dimensional manifold as the set of trajectories generated by the forward and backward evolution of those initial conditions with the dynamics of finite $B$. The resulting DS, which we call $S^2(B)$, is thus defined on a two-dimensional invariant manifold $\mathcal{S}^2(B)$ of the infinite-dimensional phase space of $S^\infty(B)$. That manifold intersects the one where $L^2(1/2)$ is defined, denoted by $\mathcal{L}^2(1/2)$ at the line of initial conditions parameterized by $\theta$ above and at PI. By taking the limit $\varepsilon \to 0$ then the two manifolds become tangent at PI. A scheme of these construction is shown in Fig. 3.2. The basic conclusion of Ref. [MC98] was that the flow defined by the above DS's $L^2(1/2)$ and $S^2(B)$ are *not* topologically equivalent, in connection to the fact that $L^2(1/2)$ is structurally unstable. Accordingly, a generic perturbation of the equations, for instance the one provided by the introduction of a small surface tension, does yield a qualitatively different system. In this sense, the DS's defined by

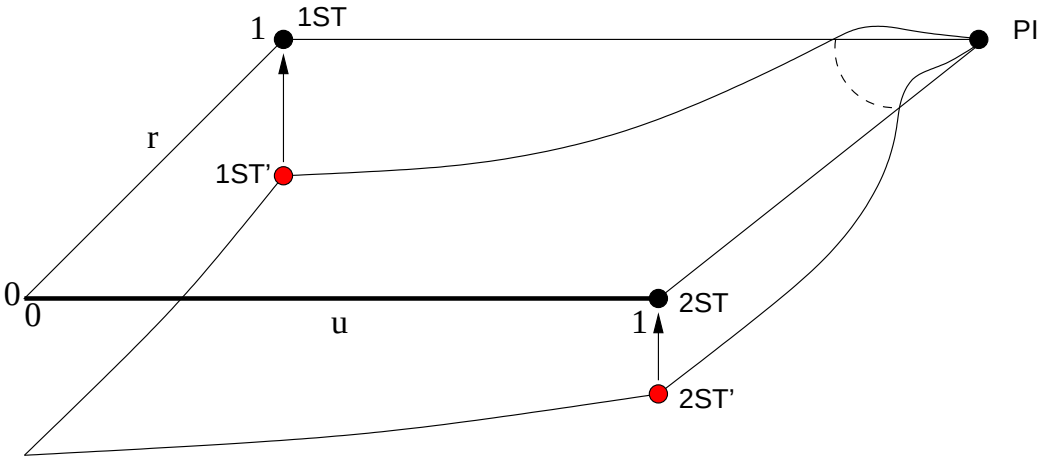


Figure 3.2: Schematic representation of the construction to define $S^2(B)$ (see text). In this scheme the two-dimensional phase space $S^2(B)$ is embedded in a three-dimensional phase space instead of the infinite-dimensional one $S^\infty(B)$. The dashed line represents the one dimensional set of initial conditions.

$L^2(1/2)$ in no way can be the limit of the regularized system $S^2(B)$ as $B \to 0$ since topological inequivalence means that there is no continuous deformation connecting the two phase portraits. Notice, however, that the manifold $\mathcal{S}^2(B)$ where $S^2(B)$ is defined is a different subset of the whole infinite-dimensional phase space for each value of $B$, all of them tangent at PI. This means that we are actually comparing interface configurations which are qualitatively similar but not quite the same. In order to strengthen the result, it is thus interesting to consider the limit $B \to 0$, as proposed in Ref. [MC98]. By doing this we will guarantee that the regularized dynamics will converge to the zero-surface tension dynamics in some parts of phase space, namely the trajectories connecting the PI fixed point respectively to the 1ST and the 2ST fixed points (selection theory does guarantee that, for $\lambda = 1/2$ 1ST' $\to$ 1ST and 2ST' $\to$2ST). Within the framework of the singular perturbative analysis of Refs. [STD96, ST96] it is now clear that the regularized dynamics will converge to the idealized one in a finite (nonzero measure) region of $L^2(1/2)$, which includes the three fixed points and a neighborhood of the trajectories connecting them (the region defined by the zero-surface tension dynamics until the impact at finite time on the unit circle of the so-called daughter singularities). The statement of the fundamental difference between the regularized and the idealized problems takes then a stronger form in that the two respective manifolds coincide at order one time but depart from each other for the long-time dynamics which defines finger competition. Knowing

the regions where the two manifolds coincide does unambiguously define the part of the dynamics which is correctly captured by the zero surface tension problem. Only for this part, introducing now a small but finite surface tension will behave as a regular perturbation. Hence although taking the limit of vanishing surface tension is not necessary to state the qualitative differences between the problem with and without surface tension, it clarifies and strengthens the conclusion on a quantitative basis. A detailed numerical study of this problem will be presented in Chapter 4. At this point, a word of caution is required concerning the distinction between intrinsic dynamics and noise effects when the limit of very small surface tension is considered. The well-known sensitivity to noise of the ST solution when surface tension is decreased in the presence of noise [Ben86] may modify in practice the present scenario making it virtually impossible for the dynamics to actually attain the fixed points [KL01]. It is important to stress, however, that while this is true for a fixed amount of local (high wavenumber) noise, either numerical or experimental, this effect is not contained in the intrinsic dynamics. That is, careful numerical studies have shown that the small surface tension limit can be approached to arbitrarily small values, provided that numerically generated noise is properly controlled [STD96, ST96, HLS01]. Furthermore it has conclusively been shown that, in the absence of noise, the single-finger fixed point is the universal attractor of the problem, at least for the classes of initial conditions here considered.

The flow topology of the regularized problem is thus very simple. PI is an unstable fixed point, 1ST' is a stable fixed point and 2ST' is a saddle point with a stable manifold connected to PI and an unstable manifold connected to 1ST'. The model $L^2(1/2)$ instead, contains, in addition to PI, 1ST and 2ST, an additional saddle fixed point which separates the basin of attraction of 1ST and the rest of the flow, which ends up in a continuum of fixed points corresponding to two unequal fingers. It is precisely the existence of this line of fixed points which causes the structural instability of the flow of $L^2(\lambda)$ according to Peixoto's theorem [GH83]. This is also responsible for the fact that the double finger 2ST fixed point is nonhyperbolic, that is, it misses the unstable direction which should connect 2ST to 1ST. From a physical point of view, it is clear that the saddle-point structure of the 2ST fixed point is essential to account correctly for finger competition, since it is the instability of this equal-finger configuration to symmetry-breaking perturbations which originates the phenomenon of finger competition. In this sense, we can associate 'growth' to the stable direction of 2ST and 'competition' to the unstable one. This saddle-point structure of the 2ST fixed point is thus expected to govern the crossover between these two regimes introduced above. In the following Chapter we will see that the failure of the minimal model $L^2(1/2)$

to properly account for finger competition is a generic property of the zero surface tension problem.

## 3.2 Extension within two dimensions: searching for an unfolding

In this section a perturbation of the minimal class described in Chapter 2 that removes the continuum of fixed points but keeps the dimensionality of the phase space unchanged is studied. We show that such perturbed exact solution presents finite-time singularities for broad sets of initial conditions, and it also exhibits finite-time interface pinchoff. This solution contains the main general features of zero surface tension, and it is shown that it does not describe in general the correct dynamics for finite surface tension. The main reason is that the dynamical system that it define lacks the saddle-point structure of the multifinger fixed point, necessary to account for the observed finite surface tension dynamics.

### 3.2.1 Modified minimal model

A possible modification of the ansatz (3.1) which is solvable and preserves the two-dimensionality of the phase space is the following:

$$f(\omega,t) = -\ln\omega + d(t) + (1-\lambda+i\epsilon)\ln[1-\alpha(t)\omega] \\ +(1-\lambda-i\epsilon)\ln[1+\alpha(t)^*\omega] \tag{3.2}$$

where the constant of motion $\epsilon$ is real and positive. If $\epsilon$ is set to zero then the minimal model Eq. (3.1) is retrieved. Solutions of this type have been reported before, for instance in Refs. [MWD94, MWK99, FPD01]. This mapping describes generically two axisymmetric unequal fingers, with the symmetry axis located in fixed channel positions separated a distance $\pi$, half the channel width. The main morphological difference between the interface described by the minimal class and the interface obtained from Eq. (3.2) is that the interface of the modified model may present overhangs. This can be understood from a geometrical point of view in the following manner: well developed fingers are separated from each other by fjords of the viscous phase, and the width and orientation of these fjords is determined by the constant $\gamma = 1-\lambda+i\epsilon$. If $\gamma$ is real, i.e. $\epsilon = 0$, the centerline of the fjords is parallel to the channel walls and the fingers do not present overhangs, but if the constant term has an imaginary part ($\epsilon \neq 0$) then the fjords form a finite angle with the walls [PMW94]. As a result of the inclination of the fjords

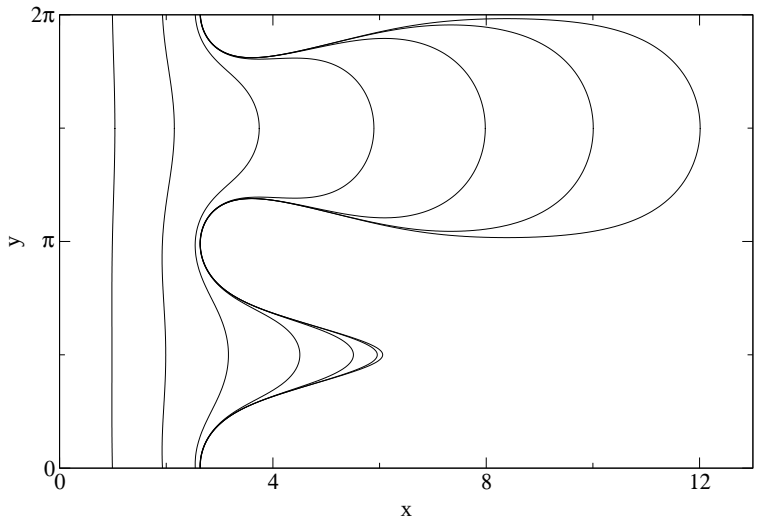


Figure 3.3: Time evolution of a configuration with $\lambda = 1/2$ and $\epsilon = 0.1$.

the fingers may present overhangs. An example of these solutions is shown in Fig. 3.3, with a series of snapshots of the corresponding time evolution. The class of solutions Eq. (3.2) contains also the single finger Saffman-Taylor solution ($\alpha' = 0$) but, remarkably enough, the introduction of a finite $\epsilon$ has removed the double Saffman-Taylor finger solution. As usual, the constant $\lambda$ is the asymptotic width of the advancing finger. The natural phase space in this case is the unit circle, $|\alpha| \leq 1$, but we will restrict the study to $\alpha' \geq 0$ because the flow in the $\alpha' \leq 0$ region can be obtained by a $\pi$ rotation of the $\alpha' \geq 0$ region. Physically, this rotation or the replacement $\alpha \to -\alpha$ corresponds to a shift of the interface by an amount $\pi$ (half the channel width) in the $y$ direction. Thus, the semi-circle $\alpha' \leq 0$ contains the same interfacial configurations and dynamics than the $\alpha' \geq 0$ region after a trivial transformation.

The zeros $\omega_0$ of $\partial_\omega f(\omega, t)$ laid outside the unit circle for the minimal model, but for the modified minimal model Eq. (3.2) the situation is different: for $|\alpha| < 1$ a zero of $\partial_\omega f(\omega, t)$ can be *inside* the unit circle. The position of the zeros in this case is

$$\omega_0 = \frac{-i(\lambda\alpha'' - \epsilon\alpha') \pm \sqrt{(2\lambda - 1)|\alpha|^2 - (\lambda\alpha'' - \epsilon\alpha')^2}}{(2\lambda - 1)|\alpha|^2} \tag{3.3}$$

for $\lambda \neq 1/2$ where $\alpha' = \text{Re } \alpha$ and $\alpha'' = \text{Im } \alpha$. For the particular value $\lambda = 1/2$ the position of the zero is

$$\omega_0 = \frac{1}{2i(\lambda\alpha'' - \epsilon\alpha')}. \tag{3.4}$$

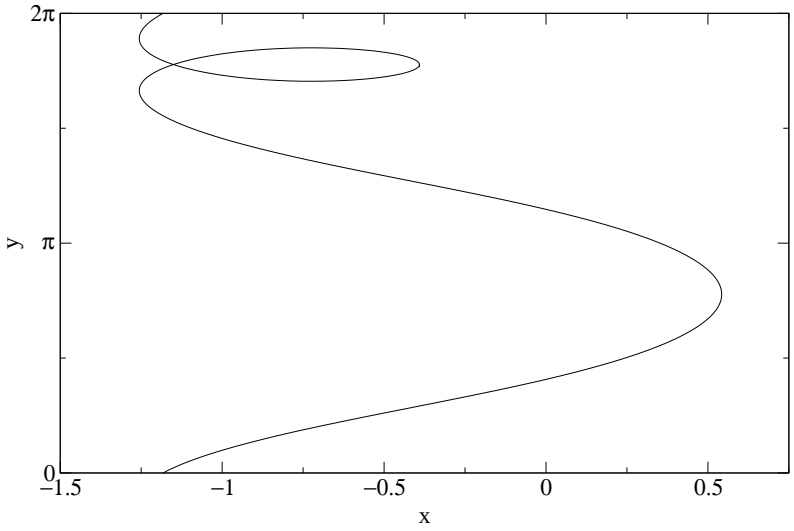


Figure 3.4: Interface with one crossing, with one zero inside the unit circle.

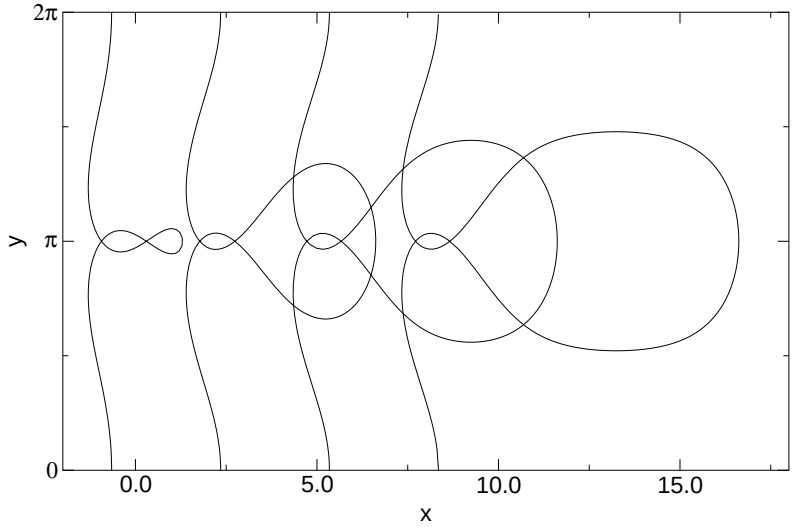


Figure 3.5: Time evolution of a configuration with a double crossing of the interface, with $\lambda = \frac{1}{2}$ and $\epsilon = \frac{1}{2}$. The the leftmost curve corresponds to $t = 0$ with $\alpha = 0.85 + i0.4$ and the rightmost one to $t = 3.0$. The spacing between the curves is $\Delta t = 1.0$. (The curves are plotted with its mean $x$ position shifted arbitrarily for better visualization).

It can be shown that for any $\lambda$ and $\epsilon \neq 0$ the zero $\omega_0$ can have a value such that $|\omega_0| < 1$ for some $|\alpha| < 1$. For instance, with $\lambda = 1/2$ the curve $|\omega_0(\alpha)| = 1$ is the line $\alpha'' = -1 + 2\epsilon\alpha'$, which clearly intersects the unit circle $|\alpha| = 1$, enclosing a region where $|\omega_0| < 1$. As a consequence of the presence of a zero inside the unit circle the parameter space $|\alpha| \leq 1$ contains unphysical regions, where the mapping Eq. (3.2) does not describe physically acceptable situations, with self-intersection of the interface associated to the fact that the mapping is not a single valued function. One of these regions is defined by the existence of a zero $\omega_0$ of $\partial_\omega f(\omega, t)$ inside the unit circle. In this region of phase space the interface crosses itself at one point, describing a single loop (see an example in Fig. 3.4). Most remarkably a second unphysical region containing interfaces with two intersections cannot be so easily detected since, in this case, the zeros of $\partial_\omega f(\omega, t)$ lay outside the unit circle. Zero surface tension solutions displaying this feature were also reported in Ref. [BST95]. Fig. 3.5 shows a configuration with this double crossing.

Substituting the mapping Eq. (3.2) in Eq. (2.8) it can be checked that this ansatz is a solution and that $\epsilon$ is a constant preserved by the dynamics. The system of differential equations resulting from the substitution takes the form

$$\begin{aligned}
1 + |\alpha|^4 + 4\,\mathrm{Im}[\alpha]^2 &= |\alpha|^2(2\lambda - 1)\{\dot{d}|\alpha|^2 + 2\,\mathrm{Re}[\gamma\alpha^*\dot{\alpha}]\} + \\
&\quad \dot{d} + 4\,\mathrm{Im}[\alpha(1-\gamma)]\{\dot{d}\,\mathrm{Im}[\alpha] + \mathrm{Im}[\gamma\dot{\alpha}]\} \qquad (3.5a) \\
4(1 + |\alpha|^2)\,\mathrm{Im}[\alpha] &= 2(2\lambda - 1)|\alpha|^2\{\dot{d}\,\mathrm{Im}[\alpha] + \mathrm{Im}[\gamma\dot{\alpha}]\} + \\
&\quad 2\{\dot{d}\,\mathrm{Im}[\alpha] + \mathrm{Im}[\gamma\dot{\alpha}]\} + 2\dot{d}\,\mathrm{Im}[\alpha(1-\gamma)] + \\
&\quad 2\,\mathrm{Im}[\alpha(1-\gamma)]\{\dot{d}|\alpha|^2 + \mathrm{Re}[\gamma\alpha^*\dot{\alpha}]\} \qquad (3.5b) \\
2\lambda\dot{d}|\alpha|^2 + 2\,\mathrm{Re}[\gamma\alpha^*\dot{\alpha}] &= 2|\alpha|^2 \qquad (3.5c)
\end{aligned}$$

where the time-dependence of $\alpha(t)$ and $d(t)$ has been dropped for sake of clarity and $\gamma = 1 - \lambda + i\epsilon$. Eqs. (3.5) can be integrated explicitely and the corresponding solutions for the variables $d(t)$ and $\alpha(t) = \alpha'(t) + i\alpha''(t)$ take the form

$$\begin{aligned}
\beta &= d(t) - \ln\alpha(t) + (1 - \lambda - i\epsilon)\ln[1 - |\alpha(t)|^2] \\
&\quad + (1 - \lambda + i\epsilon)\ln[1 + \alpha(t)^2] \qquad (3.6a) \\
t + C &= \lambda d(t) + (1 - \lambda)\ln|\alpha(t)| - \epsilon \arctan\frac{\alpha''(t)}{\alpha'(t)} \qquad (3.6b)
\end{aligned}$$

where $C$ is a real-valued constant and $\beta$ is a complex-valued constant. Notice that there is no apparent indication of the pathological situations described above in the form the explicit solutions above. The study of the dynamical systems defined by Eqs. (3.6) is the object of the next section.

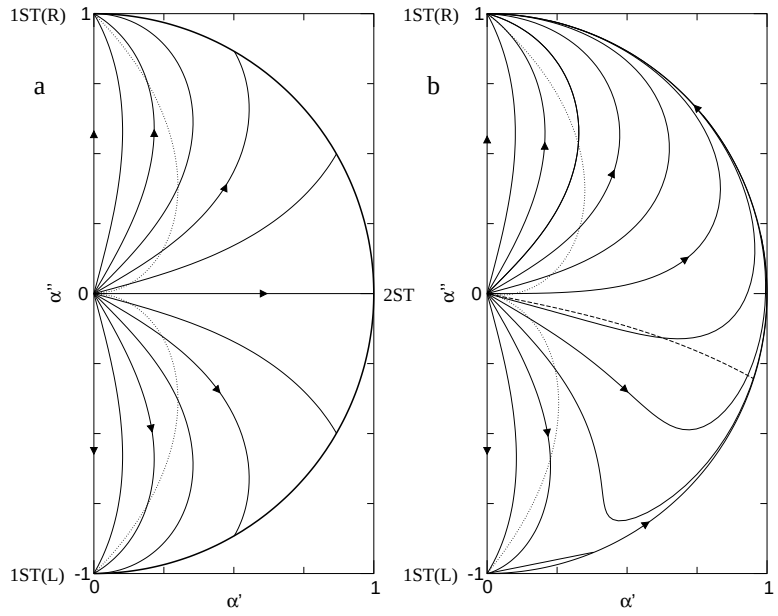


Figure 3.6: Phase portrait of the minimal model and the modified minimal model. $\lambda = \frac{1}{2}$ for both plots, the regions to the right of the dotted lines correspond to two-finger configurations (a) $\epsilon = 0$; note the continuum of fixed points (marked with a thick line) on $|\alpha| = 1$. (b) $\epsilon = 0.1$; the straight line in the lower left corner is a line of finite-time singularities and the two fingers have equal length on the dashed line.

### 3.2.2 Study of the dynamical system

The addition of an imaginary part $i\epsilon$ to the constant $(1 - \lambda)$ modifies dramatically the phase portrait of the minimal model, as can be seen in Fig. 3.6, where the phase portraits for $\epsilon = 0$ (in the variables $(\alpha', \alpha'')$) and $\epsilon = 0.1$ are depicted. The phase portrait of the modified minimal model is qualitatively different from the $\epsilon = 0$ one, as a direct consequence of the structural instability of the latter case [GH83], which implies that an arbitrary perturbation of the equations yields a flow which is not topologically equivalent (notice that a perturbation of an initial condition of the infinite-dimensional space of interface configurations is represented here as a perturbation of the equations themselves, that is, a displacement in the space of dynamical systems). One could have expected that the introduction of this $\epsilon$ would have provided an unfolding of the phase portrait of the minimal model into a structurally stable one (within the integrable class of mappings), hopefully with the saddle-point connection between the unstable and the stable fixed points, as corresponds to the the physical case with $B \neq 0$. The phase

portrait of the regularized flow (which is obviously the natural unfolding) would be similar to that of $\epsilon = 0$ in Fig. 3.6a, except that all trajectories other than the line $\alpha'' = 0$ would end up symmetrically to the upper ST fixed point or the lower one. Unfortunately, we must conclude that the resulting phase portrait for the modified minimal model does not provide the correct unfolding. This is particularly remarkable if one takes into account that, in two-dimensional systems, structurally stable dynamical systems are dense [GH83]. On the contrary, the perturbed equations contain finite-time singularities and, although they remove the continuum of double-finger fixed points, they also miss the equal-finger fixed point, which is an essential ingredient of the regularized flow.

Notice that in this representation, the 1ST fixed point has been split in two 1ST(R) and 1ST(L), corresponding to whether the right or the left finger approaches the single finger attractor. These two solutions correspond to having the ST finger located at two different positions (the symmetry axes of the fingers), owing to the translational invariance associated to the periodic boundary conditions. Since a $\pi$-shift in the transversal $y$-direction must yield an equivalent configuration, the identification of any point in the semicircle with the diametrically opposed which has reduced the actual phase space in half, implies also that the 1ST(R) and 1ST(L) must be topologically identified as the same point. Approaching one or the other thus means approaching from the left or from the right. With this identification the contact with the problem with rigid boundaries is clearer, since there, the attractor is clearly unique but the flow must also be symmetrically split into two parts, corresponding to whether the left or the right finger wins, owing to the symmetry of the system under parity (see a more detailed discussion in Sec. 3.3.4).

In Fig. 3.7 we plot the phase portrait for $\epsilon = 0.5$ and the different regions of phase space. For any other $\epsilon$ the flow is topologically equivalent but the shape and size of the different regions varies smoothly. The line of finite-time singularities collapses towards the lower fixed point 1ST(L) in the limit $\epsilon \to 0$ as shown in Fig. 3.6b. In the absence of the 2ST fixed point, the splitting of flow is made possible by the existence of the line of finite-time singularities. Instead of a separatrix between the respective basins of attraction of 1ST(R) and 1ST(L), there is an intermediate, nonzero measure region, connected to the PI fixed point, whose evolution ends up at that singularity line, defined by the condition $|\omega_0| = 1$. Similarly to the finite-time singularities occurring for polynomial mappings, this line is reached in a finite time and is associated to the formation of a cusp at the interface. The evolution is not defined after that time. The flow in the region below the singularity line (region III of Fig. 3.7b), defined by $|\omega_0| < 1$, is actually

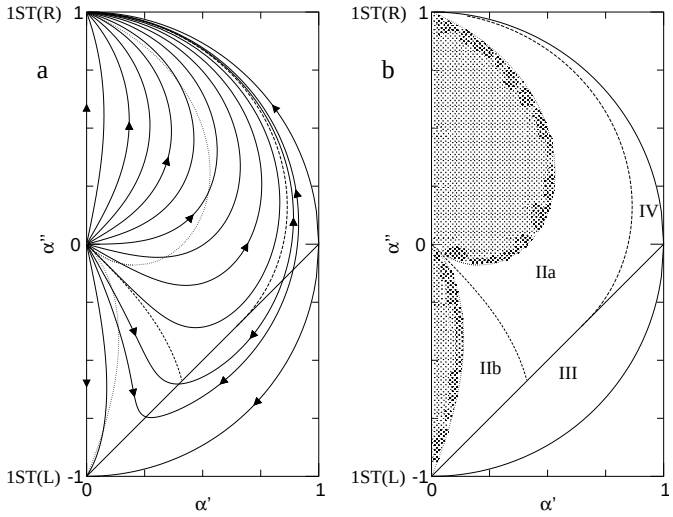


Figure 3.7: (a) Phase portrait of the modified minimal model with $\lambda = 1/2$ and $\epsilon = 1/2$. (b) Plot of different regions of phase space of case (a). The grey regions correspond to single finger interfaces and the other regions to two finger interfaces. Regions IIa and IIb differ in which of the two fingers is larger. Regions III and IV are unphysical regions described in the text. The straight boundary of region III is a line of cusp singularities.

well defined although it describes evolution of unphysical interfaces which intersect themselves forming a loop, (see Fig. 3.4). Their evolution originates and ends at different points of the singularity line. The region IV has double crossings of the interface (see Fig. 3.5) and also originates at the singularity line but, remarkably enough, it evolves asymptotically towards the ST finger despite their unphysical double crossing at the tail of the finger. This double-crossing is removed in a finite time in some subregion of IV and it remains up to infinite time in another subregion. Incidentally, this clearly illustrates how dangerous it may be to infer a physically correct dynamics from the fact that the interface evolves asymptotically towards a single ST finger, and that zero surface tension solutions must be dealt with extreme care since smooth and apparently physical interfaces may contain elements that yield them physically unacceptable when the time evolution is considered either forward or backward.

The double-crossing removal in some of the above solutions has some implications in the general study of topological singularities associated to interface pinchoff in fluid systems (for a recent review see Ref. [Egg97] and, in the context of Hele-Shaw flows, see for instance Ref. [GPS98]). Consider the stable Saffman-Taylor problem, in which the viscous fluid displaces the

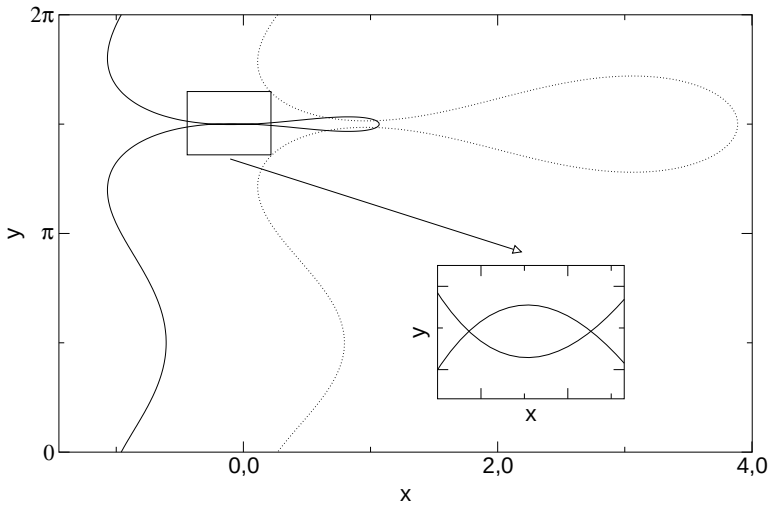


Figure 3.8: Time evolution of a configuration with a double crossing of the interface, showing the dynamical removal of the crossing. In this case, $\lambda = \frac{1}{2}$ and $\epsilon = \frac{1}{2}$. The initial interface with $\alpha = 0.865 + i0.2$ is the solid line, and the dotted line is the interface at $t = 0.5$. The mean $x$ position of the interface is shifted for better visualization. Time reversal of this evolution, corresponding to stably stratified Hele-Shaw flow, defines a finite-time interface pinchoff.

inviscid one. The planar interface is stable in this case and is the attractor of the dynamics. The conformal mapping obeys then an equation formally equivalent to Eq. (2.8), that applies to the unstable Hele-Shaw flow, with the only difference that time is reversed, $t$ is substituted by $-t$, in Eq. (2.8). Therefore, the dynamics of the stable case is obtained from the unstable one simply by a time reversal. As a consequence, the double-crossing removal we observed in the original problem encompasses a prediction of a finite-time interface pinchoff in the stable configuration of the problem, for some class of initial conditions. A similar pinchoff phenomenon for zero surface tension dynamics was detected numerically by Baker, Siegel and Tanveer [BST95] for other types of mapping singularities. Our result provides a very simple example of exactly solvable finite-time pinchoff. Notice that there is no singularity of the interface shape or velocity at the interface contact, so one could presume that surface tension may not affect significantly the phenomenon in this case, although this is an open question yet.

The evolution of a trajectory ending up in the cusp line cannot be continued beyond the impact time $t_0$ of the zero $\omega_0$ with the unit circle $|\omega| = 1$ because the cusp line attracts the flow from both sides, but the flow is indeed well defined in the interior of region III, where we have $|\dot{\alpha}| < 0$ in opposition

to the physical region where $|\dot{\alpha}| > 0$, so, in a sense, the temporal evolution inside the singularity region is reversed. As a matter of fact, the graph $\alpha''(\alpha')$ can be obtained and is smooth in all regions of phase space. Defining $\alpha = re^{i\theta}$, its substitution in Eqs. (3.6) yields after some algebra

$$\frac{d\theta}{dr} = \frac{4r\cos\theta}{1-r^2}\,\frac{(1-\lambda)(1-r^2)\sin\theta + \epsilon(1+r^2)\cos\theta}{1+(2\lambda-1)r^4 + 2\lambda r^2\cos 2\theta + 2\epsilon r^2\sin 2\theta} \tag{3.7}$$

and from this expression the trajectory can be obtained also in region III. The fact that the modified minimal model does not yield an unfolding of the minimal one is more deeply stressed by the fact that the field of directions defined by the above graph, even removing the singularities through a proper time reparameterization and time reversal in region III, is still a structurally unstable flow.

It is well known that the zero-surface tension problem is extremely sensitive to initial conditions: given a zero-surface tension solution at $t = 0$, another one can be found which is as close as desired to the interface of the first solution, and the evolution of the two solutions be completely different in general. This is a consequence of the ill-posedness of the initial-value problem [Tan93], which is most clearly manifest in polynomial mappings, which may arbitrarily approximate any initial condition, possibly one which does not develop singularities, but themselves always develop cusps. However, it is illustrative to see several striking examples of sensitivity to initial conditions within the class of logarithmic mappings which are much less predictive *a priori*.

*Example 1.* Consider two initial conditions $(\alpha_1', \alpha_1'')$ and $(\alpha_2', \alpha_2'')$ close to the PI fixed point, with $|\alpha_1|, |\alpha_2| \ll 1$, which differ only in nonlinear orders of their mode amplitudes[1], being equivalent to linear order. One can easily choose $(\alpha_2', \alpha_2'')$ (with $\alpha_1'\alpha_2' < 0$, that is, considering not only the semicircle $\alpha' > 0$ but the whole unit circle) such that the time evolution will be completely different from the evolution of the original initial condition, even though the two initial conditions where equivalent to linear order. In Fig. 3.9 we show an explicit example. While the two initial conditions for the interface configuration cannot be distinguished in the scale of the plot, the final outcome is dramatically different. One of the evolutions is an example of successful competition, where the finger in the initial condition is eventually approaching the ST solution, with a small secondary finger (not present in the initial condition) which is generated but screened out by the leading one. The other evolution is quite surprising since the secondary finger grows to the point of taking over and winning the competition.

[1]The amplitudes of the first two modes $k = 1, 2$ are $\delta_1 = 2(1-\lambda)\alpha'' + \epsilon\alpha'$ and $\delta_2 = 2\epsilon\alpha'\alpha'' + (1-\lambda)(\alpha''^2 - \alpha'^2)$.

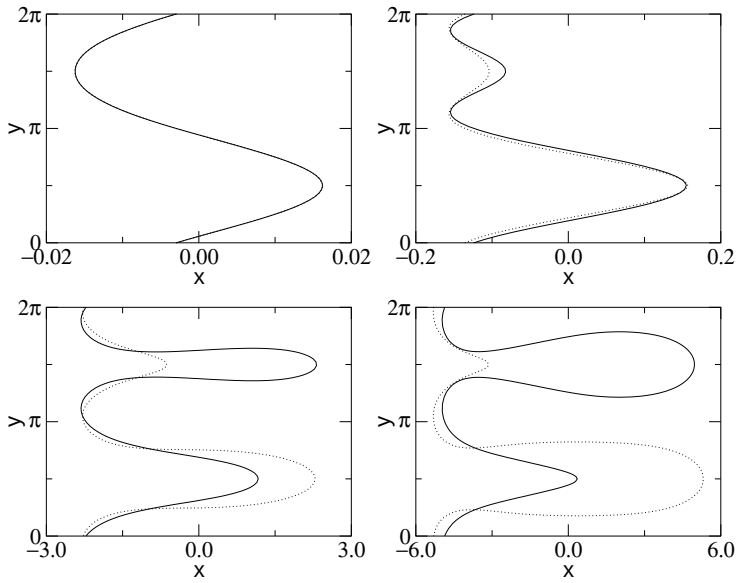


Figure 3.9: Evolution of two interfaces initially equal to linear order (see text), with $\lambda = 1/3$ and $\epsilon = 0.1$. $\alpha(0) = 0.04619398 - i0.01913417$ for the solid line and $\alpha(0) = -0.04619398 - i0.00527598$ for the dashed line. Upper left plot $t = 0$, upper right plot $t = 2.0$, lower left plot $t = 4.0$ and lower right plot $t = 6.0$.

*Example 2.* A similar situation is found if one compares two initial conditions equivalent to linear order up to a parity transformation. Pairs of initial conditions of this type, with the same values of $\lambda$ and $\epsilon$, can easily be found within the same semicircular phase space, and since the dynamics is indeed symmetric under mirror reflection, one should not expect, in principle, a very different behavior, even though such points are not close to each other in phase space. Fig. 3.10 shows an example in which one of the evolutions is smooth, with a leading finger and a small one being generated, and the other generates a cusp in finite time. As in the first example, no signature of the different fate of the system could apparently be seen in the initial conditions. In both cases the extremely small differences associated to higher orders in the mode amplitudes have thus been crucial. The sensitivity to initial conditions of these examples is more striking for decreasing values of $\epsilon$, since the time in which the two evolutions stay close to each other increases as $O(-\ln \epsilon)$. For instance, given an initial condition $\alpha_0$ close to PI, the difference between the $\epsilon = 0$ interface and the $\epsilon \to 0$ one will remain of $O(\epsilon)$ for a time of $O(-\ln \epsilon)$. Later on in the evolution the differences between the two interfaces will be of $O(1)$: the asymptotic shape of the $\epsilon = 0$ case will be two

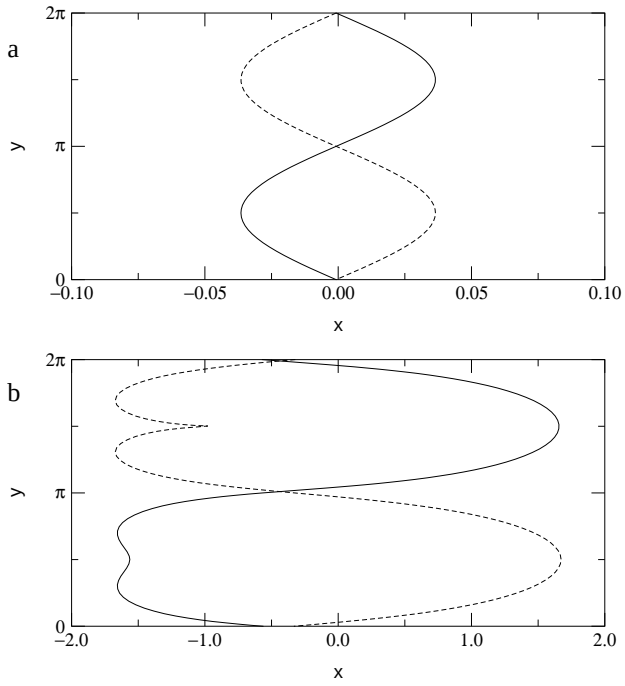


Figure 3.10: Evolution of two interfaces symmetric to linear order (see text), with $\lambda = \frac{1}{2}$, $\epsilon = 0.1$, $\alpha(0) = 0.02724 + i0.03104$ for the solid line and $\alpha(0) = 0.02724 - i0.04193$ for the dashed line. The upper plot corresponds to $t = 0$ and the lower to $t = 4.19$, when a cusp develops.

unequal fingers while the shape of the $\epsilon \to 0$ will be a single Saffman-Taylor finger. Similarly, for two initial conditions symmetrical to linear order such as in Example 2, with $\epsilon \to 0$, the differences between their interfaces will remain symmetric to $O(\epsilon)$ for a time of $O(-\ln \epsilon)$, but later they will lose symmetry and finally both will end up at the same fixed point, say the right one, even though one of the two evolutions has been favoring the other one, say the left one, for a long time (up to well developed fingers).

*Example 3.* In Fig. 3.11 we illustrate the effect of changing $\epsilon$ in initial conditions which are equivalent to linear order. Notice that in one case a cusp is generated at the secondary finger. In others the small finger rapidly overcomes the large one, while for the smallest $\epsilon$ the initial finger seems to lead the competition. Remarkably, in this last case the smaller finger will also take over after a much longer time.

All the above examples have been chosen to emphasize the caution that is required when trying to use exact solutions to approximate the dynamics of the problem. A direct comparison of these solutions with numerical integration for very small surface tension is required in order to make a more

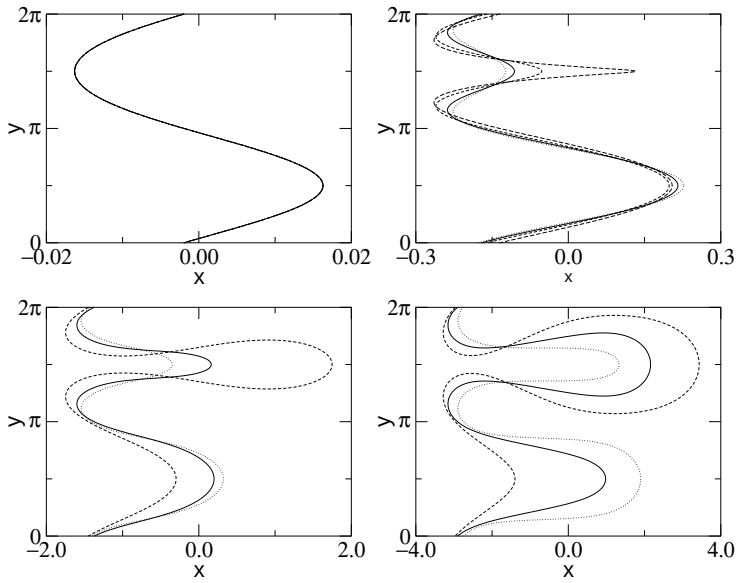


Figure 3.11: Evolution of four interfaces equal to linear order, with $\lambda = \frac{1}{2}$. $\epsilon = 0.01$ and $\alpha(0) = 0.04671 - i0.01291$ for the dotted line, the solid line is $\epsilon = 0.1$ and $\alpha(0) = 0.04619 - i0.01913$, the short-dashed line is $\epsilon = 0.3$ and $\alpha(0) = 0.04260 - i0.03137$ and the long-dashed is $\epsilon = 0.6$ and $\alpha(0) = 0.03472 - i0.04345$. (a) $t = 0$, (b) $t = 2.4$, (c) $t = 3.5$, (d) $t = 5.0$. Note that at $t = 2.4$ the $\epsilon = 0.6$ interface develops a cusp.

quantitative assessment of the issue. This is presented in next Chapter and in Ref. [PSC02].

In any case, it must also be stated that the class of logarithmic solutions does provide also qualitatively correct evolutions, not only of single finger configurations as stated in [MC98], but also with two-finger configurations showing successful competition. An example of this is plotted in Fig. 3.3: starting from the planar interface, during the linear regime a bump starts to grow, followed generically by a second bump as the evolution enters the nonlinear regime. The two fingers keep on growing for some time, until later on in the evolution, one of the fingers is dynamically eliminated of the competition process and the other finger approaches asymptotically the ST finger solution. This general scenario is illustrated in Fig. 3.12a, where the individual growth rates of the two fingers $\Delta\psi_1$ and $\Delta\psi_2$ are plotted versus time, for two different initial conditions.

For other initial conditions as generic as the previous one, however, the following phenomenon is observed: the small finger (with initially zero flux) of a configuration with two significantly unequal fingers increases its flux

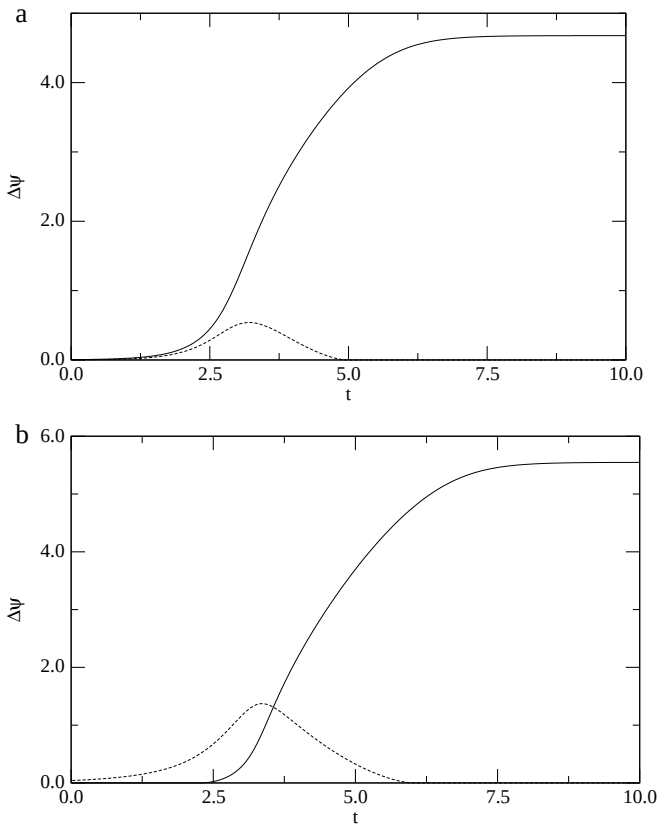


Figure 3.12: Individual growth rates $\Delta\psi_1(t)$ and $\Delta\psi_2(t)$ of the two fingers for the modified minimal model with $\lambda = \frac{1}{2}$ and $\epsilon = 0.1$, for two different initial conditions showing successful competition. For the (a) case the finger which initially has larger growth rate (and larger length too) wins the competition. For the (b) case the finger which initially has lower growth rate (and lower length too) wins the competition, in opposition to the evolution with the regularized dynamics (small surface tension).

while the flux of the large finger decreases, until the flux of the initially small finger is higher than the flux of the other finger and finally the flux of the initially large finger reaches zero: it has been suppressed from the competition. This is opposite to what it would expected *a priori* from simple physical considerations. In fact, one would expect that for well developed fingers the larger one wins the competition, at least if the distance between the two finger tips is large before the process begins. This anomalous competition dynamics is illustrated in Fig. 3.12b, where it can be seen that initially only one finger has a finite $\Delta\psi_1$, and it grows until a second finger develops and begins to grow, as indicated by the appearance of a nonzero $\Delta\psi_2$. The sec-

ond finger grows together with its growth rate and surpasses the first one, which is eventually suppressed from the competition process. This is indicated by $\Delta\psi_1$ going to zero. This example is important as a case where there is successful competition (finger coalescence) to the Saffman-Taylor asymptotic solution but with a completely wrong dynamics. In fact it can be seen that the zero surface tension evolution departs from the regularized trajectory much before the small finger takes over the competition (through the impact of a daughter singularity, as will be discussed in next Chapter). The winning finger with the regularized dynamics is thus the losing finger with the zero surface tension one.

Again, in the limit $\epsilon \to 0$ these phenomena appear even more dramatically, as a consequence of the structural instability of the minimal model. In this limit, for a $O(-\ln\epsilon)$ time we will observe two unequal fully developed fingers advancing with a fixed tip distance, but eventually the presence of finite $\epsilon$ will 'activate' the competition process and one of the two fingers will reduce its growth rate until fully suppressed from the competition. If $\alpha''(0) > 0$ the suppressed finger will be the small one (physically 'right' dynamics), but if $\alpha''(0) < 0$ the dynamically suppressed finger will be the large one (physically 'wrong' dynamics).

### 3.2.3 Comparison with the regularized dynamics.

In order to compare the $B = 0$ dynamics with the physical case of $B \neq 0$, we use the construction introduced in Sec. 3.1.2. Consider a one dimensional set of initial conditions ($t = 0$) of the form Eq. (3.2) surrounding the planar interface (PI) fixed point $\alpha' = 0$, $\alpha'' = 0$, for a fixed $\lambda$ and $\epsilon$. We choose the points of this set infinitesimally close to $\alpha = 0$, and therefore the interface is in the linear regime. The $B \neq 0$ time evolution from $t = -\infty$ to $t = \infty$ of this set spans a compact two dimensional phase space and defines a two-dimensional dynamical system $S^2(B)$ on a surface $\mathcal{S}^2(B)$, which is tangent, by construction, to the zero surface tension counterpart $\mathcal{L}^2(1/2, \epsilon)$ at the PI fixed point. $S^2(B)$ is embedded in the infinite dimensional dynamical system $S^\infty(B)$. We can also define the limiting case $S^2(0^+)$ as the limit of $S^2(B)$ for $B \to 0$. From the results of Ref. [ST96] it follows that $\mathcal{L}^2(1/2, \epsilon)$ and $\mathcal{S}^2(0^+)$ intersect not only at the 1ST(R) and 1ST(L) (selection theory) but have in common the full evolution of the $B = 0$ time-dependent single-finger solution (line $\alpha' = 0$).

For the set of dynamical systems $S^2(B)$ defined for different values of $B$ the basins of attraction of 1ST(R) and 1ST(L) are two-dimensional and finite, and therefore there must be at least one separatrix trajectory between the two basins. This separatrix must end at a saddle fixed point (which

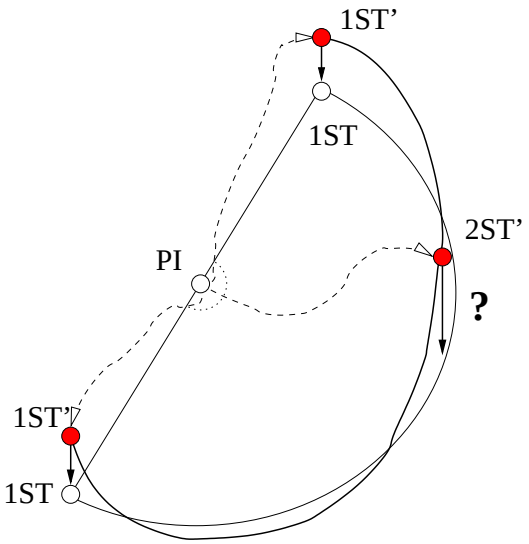


Figure 3.13: Schematic representation of the construction used to define $S^2(B)$ (see text). In this scheme the two-dimensional phase space $S^2(B)$ is embedded in a three-dimensional phase space instead of the infinite-dimensional one $S^\infty(B)$. The dashed semicircle represents the one dimensional set of initial conditions, and the dashed lines represent trajectories on $S^2(B)$.

does not exist in the phase portrait of the $B = 0$ solution). It is reasonable to assume that this fixed point is the double ST finger fixed point (2ST). Thus, the topology of the flow defined by the dynamical system with $B = 0$, $L^2(1/2, \epsilon)$ is not equivalent to the flow of the dynamical system as $B \to 0$, $S^2(0^+)$: the flow for the regularized problem contains a trajectory and a fixed point that it is not contained in the flow defined by the modified minimal model, the trajectory starting at the planar interface PI fixed point and ending up at the 2ST fixed point (see Fig. 3.13). The phase flow of the modified minimal model with $B = 0$ is qualitatively different from the phase flow of the regularized problem, $B \to 0$, and therefore the solution Eq. (3.2) is unphysical in a global sense, what is to say, when a sufficiently large set of initial conditions (spanning evolutions towards 1ST(R) and 1ST(L)) is considered simultaneously. Again it is important to state that the strict limit $B \to 0$ is not necessary in order to reach our basic conclusion on the topological inequivalence of the regularized and the idealized systems. The limit is taken to emphasize that the manifold $\mathcal{S}^2(B)$ is indeed close to $\mathcal{L}^2(1/2, \epsilon)$ and subsets of it do converge to $\mathcal{L}^2(1/2, \epsilon)$ (see discussion in Sec. 3.1.2).

We have shown that the introduction of a finite $i\epsilon$ term to the minimal model Eq. (3.1) fails to provide an unfolding of its nonhyperbolic fixed point structure. It has dramatically changed the topology of the flow obtained for $\epsilon = 0$, but the flow for $\epsilon \neq 0$ does not have the expected structurally stable flow of the physical problem (for two-finger configurations): an unstable fixed point, two (equivalent) stable fixed points and one saddle fixed point. Moreover, instead of this, the evolution of Eq. (3.2) with $\epsilon \neq 0$ presents finite-time singularities for a nonzero measure set of initial conditions. This can be understood as a consequence of the absence of the 2ST saddle point, which should control the competition regime. Without this fixed point the separatrix trajectory between the basins of attraction of ST(L) and ST(R) is not present and the only possible way to split the flow is through the existence of finite time singularities. This is not a particularity of the mapping Eq. (3.2) but a more general feature of $B = 0$ solutions. Below we will prove that, within the N-logarithms class, finite $\epsilon$ implies finite-time singularities in the evolution of a nonzero measure set of initial conditions (see Sec. 3.3.3). Besides the existence of finite-time singularities we have seen that, unlike the case $\epsilon = 0$, solutions exhibiting successful competition are possible with $\epsilon \neq 0$ for $\lambda = 1/2$. However, part of those evolutions are unphysical in the sense the winning finger may differ from the one with the regularized dynamics.

## 3.3 Generalization to higher dimensions

This section is devoted to the study of solutions that define a dynamical system of dimensionality greater than two. We will show that the discussion of previous sections is not peculiar of dimension 2 but is extendable to higher dimensions. The relevance of perturbations that change the finger width will be discussed. A general proof of the existence of finite time singularities within the N-logarithm class of solutions will be given. The relationship between rigid wall and periodic boundary, and its relevance to the dynamics will be discussed in depth.

### 3.3.1 Non-axisymmetric fingers

The solutions that have been studied so far, Eq. (3.1) and Eq. (3.2), have two pole-like singularities $\omega_{1,2}$ located at $\omega_1 = 1/\alpha$ and $\omega_2 = -1/\alpha^*$. The property $\omega_1 = -\omega_2^*$ reduces the dimensionality of the dynamical system to two and also forces the axisymmetry of the fingers. If the singularities $\omega_{1,2}$ are not related, then the phase space has one additional dimension and the fingers are not axisymmetric.

We will now recall the results of Magdaleno [Mag00] with respect the ansatz

$$f(\omega,t) = -\ln\omega + d(t) + (1-\lambda)\ln[1-\alpha_1(t)\omega] \\ +(1-\lambda)\ln[1-\alpha_2(t)\omega] \tag{3.8}$$

where $\alpha_j(t) = \alpha_j'(t) + i\alpha_j''(t)$ are two complex quantities satisfying $|\alpha_j| < 1$. This ansatz is an exact solution of Eq. (2.8) and it can be proved that the evolution is free of finite time singularities.

From the evolution equations for $\alpha_{1,2}$ in the case $\lambda = 1/2$ it is found that the dynamics satisfy

$$\frac{\alpha_1'\alpha_2' - \alpha_1''\alpha_2''}{\alpha_1'\alpha_2'' + \alpha_1''\alpha_2'} = \text{Const.} \tag{3.9}$$

Writing $\alpha$ in polar coordinates, $\alpha_j = r_j e^{i\theta_j}$, this constraint reduces to the simpler form

$$\theta_1 + \theta_2 = \text{C}. \tag{3.10}$$

The constant C depends on the initial condition, but its value can be fixed arbitrarily using the property of rotational invariance of the ansatz Eq. (3.8): the transformation $\alpha_1 \to \alpha_1 e^{i\phi}$ and $\alpha_2 \to \alpha_2 e^{i\phi}$ is equivalent to a translation of the interface a distance $\phi$ in the $y$ axis direction. For the minimal class studied previously (Eq. (3.1)) the value of C was $\text{C} = \pi$. The existence of the constraint Eq. (3.10) reduces the dimensionality of the problem from four to three, with variables $r_1$, $r_2$ and $\theta_1 - \theta_2$, implying that the dynamical system is actually three-dimensional.

In order to study the dynamical system defined by the substitution of the ansatz Eq. (3.8) into the evolution equation (2.8) we introduce the variables $z = r\exp i\theta = \alpha_1 + \alpha_2$ and $\rho = \alpha_1\alpha_2$. Moreover, we use the arbitrariness of C to choose the simpler value $\text{C} = 0$. Then, the dynamical system in the variables $(r,\theta,\rho)$ reads

$$\begin{aligned} \dot r &= 4r\frac{1 - r^2 + \rho(2+r^2)\cos(2\theta) - 3\rho^2}{4 - r^2} \\ \dot\rho &= 4\rho\frac{2(1-\rho^2) + r^2[\rho\cos(2\theta) - 1]}{4 - r^2} \\ \dot\theta &= -2\rho\sin(2\theta). \end{aligned} \tag{3.11}$$

With these variables the axisymmetric case studied in previous sections is contained as a the particular case $\theta = 0$. From the last equation it is immediate to see that $\theta$ decreases monotonically with time (since, for $\text{C} = 0$, $\rho > 0$), and tends to zero for long times, $\theta \to 0$, converging to the axisymmetric case $\theta = 0$. Therefore, we can conclude that the axisymmetric case is

attracting the dynamics of the nonaxisymmetric one and, asymptotically, its dynamics reduces to the axisymmetric one.

Therefore, we have shown that the dynamics of the minimal model is not a particularity of a zero-measure subset but the general behavior of the nonaxisymmetric neighborhood of the original axisymmetric class. This neighborhood has a nonzero measure within the three dimensional system. Similarly, it can be shown that the basin of attraction of the Saffman-Taylor finger for the ansatz Eq. (3.8) is also relatively small.

It is worth noting that nonaxisymmetric fingers can be obtained also in 2d. A conformal mapping describing nonaxisymmetric fingers is

$$f(\omega,t) = -\ln\omega + d(t) + (1-\lambda+p+i\epsilon)\ln[1-\alpha(t)\omega] \\ +(1-\lambda-p-i\epsilon)\ln[1+\alpha^*(t)\omega] \tag{3.12}$$

where $0 < p < 1-\lambda$. However, the lack of axisymmetry caused by the introduction of $p$ does not change qualitatively the phase portraits obtained for $p = \epsilon = 0$, the continuum of fixed points present for $\epsilon = 0$ is not removed by the introduction of a finite $p$ and the finite-time singularities that appear for $\epsilon \neq 0$ are also present when $p \neq 0$. Therefore, the results obtained for 2d in the previous sections are not modified at all if we relax the condition of finger axisymmetry.

### 3.3.2 Perturbations which change finger widths

The second type of modification of the ansatz (3.1) we have studied is the following. Consider

$$f(\omega,t) = -\ln\omega + d(t) + 2(\lambda-\lambda_s)\ln[1-\delta(t)\omega] + \\ (1-\lambda)\{\ln[1-\alpha_1(t)\omega] + \ln[1-\alpha_2(t)\omega]\} \tag{3.13}$$

with initial conditions $\alpha_1(0) = -\alpha_2^*(0) = \alpha(0)$, $0 < \lambda, \lambda_s < 1$ and $|\delta(0)| \ll 1$. Note that for $\delta(0) = 0$ this ansatz reduces to the minimal model (3.1). From substitution of this ansatz into the evolution equation (2.8) it is obtained that Eq. (3.13) is a solution with $\lambda$ and $\lambda_s$ constants. From the dynamical equations it can be proved that the asymptotic configuration of this ansatz consists of one or two fingers, with asymptotic filling fraction equal to $\lambda_s$. But if $|\delta(0)| \ll |\alpha(0)|$ then the interface will be initially almost identical to the one obtained within the class (3.1) with the same $\alpha(0)$ and $\lambda$, and its evolution will remain close to the one obtained with the minimal class for a time that will increase with decreasing $|\delta(0)|$. Therefore, given a small enough $|\delta(0)|$, starting from the planar interface a configuration with one or

two fingers (depending on the initial conditions) of total width $\lambda$ will develop. Later on, as $|\delta|$ grows and approaches 1, the total width will change from $\lambda$ to $\lambda_s$ for long enough time. The ansatz (3.13) thus describes an interface that changes the filling fraction of the fingers from $\lambda$ to $\lambda_s$. The same phenomenon will appear with any other of the solutions described in this paper (and in general in pole-like solutions) if a term of the type $2(\lambda - \lambda_s)\ln[1 - \delta(t)\omega]$ is added, and in particular it will appear in the single finger configurations obtained setting $\alpha(0)$ and $\delta(0)$ purely imaginary. Note that in this case if $\delta(0) = 0$ the ansatz describes exactly the time-dependent Saffman-Taylor finger [Saf59]. This changing-width phenomenon of $B = 0$ solutions has been known for long [How86], but it has been recently claimed [MW97] to be responsible of the known width selection observed with finite surface tension both experimentally and numerically. The idea was that, although solutions of arbitrary $\lambda$ exist in the absence of surface tension, these are unstable under some perturbations which trigger the evolution towards the $\lambda = 1/2$ solution. Since the present work is basically emphasizing the unphysical dynamics of the idealized ($B = 0$) problem, in direct contradiction with Ref. [MW97], we feel compelled to briefly comment on this respect here. The basic argument of Ref. [MW97] is as follows, in terms of the parameterization of the interface used by the author: a term of the form $i\mu\phi$ in the conformal mapping is always unstable under the substitution $i\mu\phi \to \mu\ln(e^{i\phi} - \epsilon)$. The introduction of such perturbation then leads to the $\mu = 0$ case, which corresponds to $\lambda = 1/2$. In Refs. [CM98, Alm98] it was pointed out that, with the same degree of generality, equivalent perturbations exist which lead to any desired $\lambda$, and therefore the conclusion that $\lambda = 1/2$ is the only attractor is incorrect. It is argued[MW98] that the latter class of perturbations is different from the former since they increase the number of logarithmic terms in the conformal mapping and therefore modify the dimension of the subspace of solutions. This objection is somewhat misleading since such partitioning of classes of solutions in terms of the number of logarithms is arbitrary and not intrinsic. This can be seen by choosing a different reference region to conformally map the physical fluid. Instead of mapping it into the semi-infinite strip [MW97], the mapping into the interior of the unit circle avoids the confusion on the dimension of the subspace of solutions. Thus, the perturbation proposed in Ref. [MW97] is equivalent to choosing $\lambda_s = 1/2$ in the ansatz (3.13), but it is manifest in this formulation that there is nothing special with this particular choice of $\lambda_s$. Perturbations leading to any finger width $\lambda_s$ occur with the same generic nature. Therefore the instability of the point $\delta = 0$ is *not* related to the steady state selection phenomenon.

### 3.3.3 Finite-time singularities within N-logarithms solutions

In this section we will prove that any solution of the N-logarithm class [PMW94] that does not have only real constant parameters presents finite time singularities, that is, it contains a nonzero measure set of initial conditions which develop singularities at finite time.

Consider a conformal mapping function $f(\omega,t)$

$$\begin{aligned} f(\omega,t) = -\ln\omega + d(t) + (\Lambda_1 + i\epsilon)\ln[1-\alpha_1(t)\omega] \\ +(\Lambda_2 - i\epsilon)\ln[1-\alpha_2(t)\omega] \end{aligned} \tag{3.14}$$

where $\Lambda_1+\Lambda_2 = 2(1-\lambda)$, $\epsilon > 0$ and $\alpha_{1,2}$ are complex with $|\alpha_{1,2}| < 1$. The mapping $f(\omega,t)$ must satisfy $\partial_\omega f(\omega,t) \neq 0$ for $|\omega| \leq 1$. If any zero $\omega_0$ of $\partial_\omega f(\omega,t)$ hits the unit circle $|\omega| = 1$ then the interface develops a cusp. For the ansatz (3.14) $\partial_\omega f(\omega,t)$ reads

$$\partial_\omega f = -\frac{1}{\omega} - \frac{(\Lambda_1+i\epsilon)\alpha_1}{1-\alpha_1\omega} - \frac{(\Lambda_2-i\epsilon)\alpha_2}{1-\alpha_2\omega}. \tag{3.15}$$

Thus, the position of the zero $\omega_0$ of $\partial_\omega f(\omega_0,t)$ is

$$\begin{aligned} \omega_0 = \frac{-(\Lambda_1+i\epsilon-1)\alpha_1 - (\Lambda_2-i\epsilon-1)\alpha_2}{2\alpha_1\alpha_2(2\lambda-1)} \\ \pm\frac{\sqrt{[(\Lambda_1+i\epsilon-1)\alpha_1+(\Lambda_2-i\epsilon-1)\alpha_2]^2 - 4\alpha_1\alpha_2(2\lambda-1)}}{2\alpha_1\alpha_2(2\lambda-1)} \end{aligned} \tag{3.16}$$

If, for some value of $\alpha_{1,2}$, $|\alpha_{1,2}| \leq 1$, the zero $\omega_0$ is inside the unit circle, then the ansatz Eq. (3.14) will present finite time singularities for some sets of initial conditions. Therefore, if $|\omega_0| < 1$ the interface will develop a cusp. Setting $\alpha_{1,2} = \alpha e^{i\theta_{1,2}}$ and $\theta_2 - \theta_1 = -2\delta$ with $\delta \ll 1$ the position of the zero (keeping up to linear terms in $\delta$) is:

$$\begin{aligned} \omega_0 \;=\; & e^{-i\theta_2}\frac{\lambda \pm (1-\lambda)}{\alpha(2\lambda-1)} + \\ & \frac{i\delta e^{-i\theta_2}}{\alpha(2\lambda-1)}\left[\Lambda_2 - 1 - i\epsilon \pm \frac{\lambda - 1 + \lambda(\Lambda_2 - i\epsilon)}{1-\lambda}\right] + O(\delta^2) \end{aligned} \tag{3.17}$$

and the modulus of the minus solution (the one with smaller modulus) reads

$$|\omega_0| = \frac{1}{\alpha}\left[1 - \frac{\epsilon\delta}{1-\lambda} + O(\delta^2)\right]. \tag{3.18}$$

In consequence, for $\alpha$ close to 1 we obtain $|\omega_0| < 1$, one of the zeros is inside the unit circle in a neighborhood of $\alpha_1 = \alpha_2 = e^{i\theta}$. Thus, the mapping Eq. (3.14) presents finite time singularities for some initial conditions independently of the value of $\epsilon$ and $\Lambda_{1,2}$, and the measure of this set is nonzero.

Now we consider a generic mapping with $N > 2$ logarithmic terms of the form:

$$f(\omega, t) = -\ln\omega + d(t) + \sum_{j=1}^{N} \gamma_j \ln[1 - \alpha_j(t)\omega] \tag{3.19}$$

where $\gamma_j = \Lambda_j + i\Gamma_j$ are constants of motion with the restriction $\sum_{j=1}^{N} \gamma_j = 2(1-\lambda)$. If we choose $\alpha_j = \alpha_1$ for $1 \le j \le k$ and $\alpha_j = \alpha_2$ for $k+1 \le j \le N$ we recover the mapping Eq. (3.14). Therefore, the N-logarithm solution (3.19) contains initial conditions that develop a cusp with this subset of $\alpha_j$, but the dimension of this subset is lower than the dimension of the phase space, implying that the measure of the set is zero compared to the whole phase space. To prove that the subset that develops a cusp has nonzero measure we choose now the following values for $\alpha_j$: $\alpha_j = \alpha_1 + \eta_j$ for $1 \le j \le k$ and $\alpha_j = \alpha_2 + \eta_j$ for $k+1 \le j \le N$, with $|\eta_j| \ll 1$, where $|\omega_0| < 1$ if $\eta_j = 0$. The equation $\partial_\omega f(\omega, t) = 0$ reads

$$\frac{1}{\omega} + \sum_{j=1}^{k} \frac{\gamma_j(\alpha_1 + \eta_j)}{1 - (\alpha_1 + \eta_j)\omega} + \sum_{j=k+1}^{N} \frac{\gamma_j(\alpha_2 + \eta_j)}{1 - (\alpha_2 + \eta_j)\omega} = 0. \tag{3.20}$$

This equation (3.20) reduces to Eq. (3.16) if all $\eta_j = 0$ and it has $N$ zeros if $\eta_j \neq 0$. Defining $g(\omega) = \partial_\omega f(\omega, t)$ for $\eta_j = 0$ and $G(\omega, \vec{\eta}) = \partial_\omega f(\omega, t)$ for $\eta_j \neq 0$ then $G(\omega, \vec{\eta}) = g(\omega) + \delta G(\omega, \vec{\eta})$ where $|\delta G(\omega, \vec{\eta})| < K|\vec{\eta}|$ for $|\omega| < R$, with $K$ and $R$ constants, and $g(\omega_0) = 0$. One zero $\omega_0'$ of $G(\omega, \vec{\eta})$ can be written $\omega_0' = \omega_0 + \delta\omega$, and assuming $|\delta\omega| < C|\vec{\eta}|$ with $C$ constant the substitution of $\omega_0'$ in $G(\omega, \vec{\eta}) = 0$ yields

$$g(\omega_0) + \left.\frac{\partial g}{\partial \omega}\right|_{\omega_0} \delta\omega + \delta G(\omega_0, \vec{\eta}) = 0. \tag{3.21}$$

The position of the zero is then:

$$\omega_0' = \omega_0 - \frac{\delta G(\omega_0, \vec{\eta})}{\left.\frac{\partial g}{\partial \omega}\right|_{\omega_0}} \tag{3.22}$$

where $\left.\frac{\partial g}{\partial \omega}\right|_{\omega_0} \neq 0$. Therefore, the zero $\omega_0'$ of Eq. (3.20) is inside a ball of radius $\mathcal{O}(|\vec{\eta}|)$ centered in $\omega_0$. If $|\omega_0| < 1$, then choosing $|\vec{\eta}|$ small enough the

zero will satisfy $|\omega_0'| < 1$: in a neighborhood of $(\alpha_1, \alpha_2)$ at least one zero of $\partial_\omega f(\omega, t)$ is inside the unit circle, and the dimension of this neighborhood will be the same of the phase space. So we can conclude that any mapping of the form (3.19) presents finite time singularities for some sets of initial conditions of nonzero measure, provided that at least one pair of $\gamma_j$ has a nonzero imaginary part.

Thus, the requirement that a mapping function of the form Eq. (3.19) is free of finite time singularities for any initial condition $\alpha_j(0)$ is fulfilled if and only if $\mathrm{Im}[\gamma_j] = 0$, $j = 1, ..., N$. But this restriction implies [MWK99] that for a wide range of initial conditions the asymptotic configuration is a N-finger interface with unequal fingers advancing at a constant speed, a situation fully analogous to the one discussed in Sec. 3.1. Then, if a mapping of the form Eq. (3.19) with $\mathrm{Im}[\gamma_j] = 0$ is chosen, then the dynamical system $L^{2N}(\gamma_j)$ will have nonhyperbolic fixed-points (continua of fixed points) and will lack the saddle-point structure of the regularized problem. In order to completely remove the continua of fixed points it is necessary to set $\mathrm{Im}[\gamma_j] \neq 0$ [MWK99], but in this case we will encounter finite-time singularities and the saddle-point structure will not be present anyway.

To sum up, we have shown that the features of the minimal model and its extensions that make them unphysical (in a global sense) are not specific of their low dimensionality. The features that make the solutions studied in previous sections ineligible as a physical description of low surface tension dynamics for a sufficiently large class of initial conditions, are also present within the much more general N-logarithm family of solutions, and the conclusions drawn in previous sections can be generalized to that class.

### 3.3.4 Rigid-wall boundary conditions

It is worth stressing that the use of periodic boundary conditions throughout this study, as opposed to the physically more natural rigid-wall boundary conditions, is not essential to the basic discussion. In connection with the discussion of multifinger steady solutions, this point was raised in Ref. [Vas01a] and addressed in Ref. [MC01]. Here we will just recall that the choice of periodic boundary conditions is not only the simplest in terms of symmetry and dimensionality, but it is the relevant one if one is interested in general mechanisms of finger competition in finger arrays. In this sense, the study of the two-finger configurations in this work refers to an alternating mode of two-finger periodicity in an infinite array of fingers, in the spirit of Ref. [KL86]. For finite size-systems one can also argue that rigid-wall boundary conditions are included as a particular case of periodic boundary conditions in an enlarged system. That is, a channel with width $W$ with rigid walls in

mathematically equivalent to a channel of width $2W$ with periodic boundary conditions where auxiliary channel of with $W$ is constructed as the mirror image of the physical one. The competition of two fingers in a channel with rigid walls at a distance $W$ is in practice equivalent to a four-finger problem with periodic boundary conditions in a double channel.

The only subtle point which we would like to stress is the apparent degeneracy of the single-finger attractor into a left ST finger and a right ST finger, as already pointed out in Sec. 3.2.2, and the possible relevance of this fact in connection with the saddle-point structure of the phase space flow. This degeneracy is inherited from the trivial continuous degeneracy associated to translation invariance in the transversal direction, when periodic boundary conditions are assumed. In fact an arbitrary shift in the transversal direction yields a physically equivalent configuration. When an initial condition is fixed, such continuous degeneracy is broken into two discrete spatial positions which are separated a distance $W/2$. The whole dynamical system is then invariant under translations of $W/2$. This is the reason why we only plotted a half of the disk in the phase portraits of Sec. 3.2. Technically, the resulting dynamical system must be defined 'modulo-W/2', that is, identifying any configuration with the resulting of a $W/2$ shift. In the phase space defined by the variables $(\alpha', \alpha'')$ one should identify any point with the resulting of a $\pi$ rotation. In this way the two single-finger attractors do correspond to the same fixed point. With this identification, the ST finger is not degenerate and the flow becomes topologically equivalent to the corresponding one in a channel with rigid-wall boundary conditions. The two-finger configurations have thus the same structure, regardless of the type of sidewall boundary conditions. The flow starts at the PI fixed point and ends up at the 1ST fixed point. Between them there is a saddle point corresponding to the 2ST fixed point. This separates the flow in two equivalent regions, namely 'from the left' and 'from the right' of the saddle point. With zero-surface tension, the case of rigid walls exhibits the same problems, namely the occurrence of a (nontrivial) continuum degeneracy of multifinger solutions, and the existence of finite-time singularities. The important point we want to stress is thus that all the general conclusions drawn in this work are valid if rigid-wall boundary conditions are considered.

## 3.4 Dynamical Solvability. General discussion

In this section we discuss the precise role of zero surface tension solutions and their relevance to an understanding of the dynamics of Hele-Shaw flows. A Dynamical Solvability Scenario is proposed and discussed as a generalization of MS theory.

### 3.4.1 The physics of zero-surface tension

The role of the zero surface tension solutions in the description of the dynamics of the nonzero but vanishingly small surface tension problem is now clearer. The $B = 0$ dynamics is in general incorrect in a global sense, even if we choose solutions with the asymptotic width $\lambda$ given by selection theory. However, they have an important place in the description of the physical problem. It has been proved in Refs. [Tan93, STD96, ST96] that the solutions with $B = 0$ converge to the $B \to 0$ during a time $O(1)$, before the impact with the unit circle of the so-called *daughter singularity* at time $t_d$. In practice this implies that the $B = 0$ dynamics is not only correct in the linear regime (where $B$ acts as regular perturbation) but also quite deep into the nonlinear regime. After $t_d$ nothing can be said *a priori*: as we have shown, there are regions of the $B = 0$ phase space corresponding to smooth interfaces that are physically wrong, but other regions are a good description of the evolution with finite (but very small) surface tension. For instance, in the neighborhood of the time-dependent Saffman-Taylor finger (the line $\alpha' = 0$ in the solutions Eqs. (3.1,3.2)) the $B = 0$ evolution is qualitatively correct for finite surface tension, and even quantitatively correct in the limit $B \to 0$ (for $\lambda = 1/2$). However, a question remains open: given a $B = 0$ evolution smooth for all time and consistent with the results of selection theory, is it the limit of a $B \to 0$ evolution? This question can be explored numerically and is the subject of the following Chapter.

It has been shown that exact zero-surface tension solutions taken in a global sense as families of trajectories in phase space are unphysical because the multifinger fixed points are nonhyperbolic, and an unfolding does not exist within the same class of solutions. This implies that there are sets of initial conditions within zero-surface tension solutions whose dynamics do not converge to the regularized dynamics with $B \to 0$, even if its asymptotic width is compatible with selection theory. In particular this means for the two-finger solution Eq. (3.2) that the outcome of the competition, that is, which one of the two competing fingers will survive at the end, when an

infinitesimally small surface tension is introduced may be the opposite of that of the zero surface tension case. This is not an instability of a particular trajectory, but a generic behavior in a finite (nonzero measure) range of initial conditions within the integrable class. For that region of phase space, it is clear that the dynamics of finger competition is completely wrong for the class of integrable solutions. Nevertheless, our results do not rule out the existence of a class of initial conditions which have a qualitatively correct evolution including 'successful' finger competition in the sense defined in sections above. Although strict convergence of the regularized solution to the idealized one may not occur in these cases, the quantitative differences may be moderately small. Actual convergence of some type can only be expected at most when there is only one finger along the complete time evolution. In summary, according to this scenario there are basically four classes of initial conditions within the most general integrable solutions, once those *a priori* incompatible with selection theory are excluded:

1. finite-time singularities forward or backward (or both) in time;

2. asymptotically correct ST finger with wrong dynamics (the incorrect finger wins);

3. asymptotically correct ST finger with qualitatively correct evolution (the correct finger wins although shapes may differ during a transient);

4. (unphysical) evolution towards multifinger fixed points.

It has to be added that, all of the above solutions plus those which are incompatible with selection theory are qualitatively and quantitatively correct in the limit of small surface tension, until a time of order one which is always in the deeply nonlinear regime.

As a general consideration it is worth remarking that fingers emerging from the instability of the planar interface when this is subject to noise are necessarily in the range of dimensionless surface tension of order one. A simple way to argue this point is that it is precisely surface tension which selects the size of the emerging fingers, since the fastest growing mode is that in which both stabilizing and destabilizing forces are of the same order. In these cases, surface tension is felt necessarily in the linear regime, and the usefulness of the zero surface tension solutions in the early stages of the evolution is obviously more limited.

Finally, from a physical point of view it is appropriate to recall that the presence of noise does modify the general picture of the fingering dynamics in the limit of small surface tension, as pointed out in Ref. [KL01]. Although

the ST finger is the universal attractor of the problem, the *linear* basin of attraction decreases with dimensionless surface tension. In practice this implies that the interface approaches the ST finger but when it gets too close, noise triggers its nonlinear instability and the interface makes a long excursion (typically a tip splitting) before approaching again the ST finger. The considerations made in this work concerning the limit of small surface tension thus imply that noise must be taken as sufficiently small.

### 3.4.2 A Dynamical Solvability Scenario

In Ref. [MC98] it was pointed out for the first time the dynamical implications of the MS analysis when extended to multifinger fixed points. The idea of the Dynamical Solvability Scenario (DSS) was already latent in that discussion. In Ref. [MC99, CM00] it was found that, in direct analogy to the single-finger case, the introduction of surface tension did select a discrete set of multifinger stationary states, in general with coexisting unequal fingers. Here we would like to discuss in what sense that analysis does provide a Dynamic Solvability Scenario.

Before doing that, let us briefly consider an alternative view of a possible DSS proposed by Sarkissian and Levine [SL98]. In Ref. [SL98], it was explicitly discussed with examples that exact solutions of the zero-surface tension problem did behave differently from numerical integration of the small surface tension problem. At the end, the authors speculated with the possibility that surface tension could play a selective role in the sense that it could basically pick up the physically correct evolutions out of the complete set of solutions without surface tension, in direct analogy with the introduction of a small surface tension selecting a unique finger width out of the continuum of stationary solutions. Since the class of nonsingular integrable solutions is indeed vast and infinite-dimensional, it is not unreasonable to expect that one could approximate any particular evolution with finite surface tension with one of those solutions for all time. However, as recently pointed out in Ref. [KL01], there is no simple way to determine which of those solutions is selected by any macroscopic construction. Furthermore, even if this were possible, one should still face the rather uncomfortable fact that the base of solutions defined by the superposition of logarithmic terms in the mapping, would itself correspond to unphysical (nonselected) solutions, as we have seen throughout this work. Indeed, an initial condition defined exactly by a finite number of logarithms would have to be replaced in general by a solution with an infinite number of logarithms as the 'selected' solution which the (small) finite surface tension system tracks.

From a more general point of view, a dynamical selection principle un-

derstood as 'selection of trajectories' has an important shortcoming when considered within the perspective of a broader class of interfacial pattern forming systems. In fact, the solvability theory of steady state selection has turned into a general principle because its applicability to a large variety of systems, most remarkably in the context of dendritic solidification [Lan87, Pel88, KKa88, BM91, GL99]. However, it is only for Laplacian growth problems that exact time-dependent solutions are known explicitly, so there would be no hope to extend the above DSS as a general principle to those other problems.

The DSS we propose here has a weaker form but it is susceptible of generalization to other interfacial pattern forming systems. The basic idea can be best expressed in similar words to those recently used by Gollub and Langer [GL99] to describe solvability theory in a general context. They have nicely synthesized the singular role of surface tension in the language of dynamical systems as to 'whether or not there exists a stable fixed point' [GL99]. In this context, our DSS extends the (static) solvability scenario in the sense that the singular role of surface tension is precisely to guarantee the existence of multifinger fixed points with a saddle-point (hyperbolic) structure. We have seen that the continuum of multifinger fixed points is directly related to a nonhyperbolic structure of the equal-finger fixed points. They imply directions in phase space were the flow is marginal. While in the traditional solvability scenario the introduction of surface tension does isolate a stable fixed point (a continuum of single-finger fixed points turns into a stable one and a discrete set of unstable ones), now it isolates multifinger saddle points out of continua of multifinger solutions, as discussed in Ref. [MC99, CM00] (a continuum of N-finger fixed points turns into a hyperbolic fixed point with stable and unstable directions, and a discrete set of unstable ones). Since the saddle fixed points are defined by the degenerate N-equal-finger solutions, the stable directions of the saddle-point are directly related to the stable directions of the single-finger fixed point, while the unstable directions correspond to all perturbations which break the N-periodicity of the equal-finger solution. The most important stable and unstable directions, however, are those depicted in the two-dimensional phase portraits discussed in the above section, namely the 'growth' direction connecting the planar interface and the N-finger fixed point, and the 'competition' direction connecting the N-finger fixed point to the single-finger fixed point[2]. Notice that arrays of fingers emerging from the morphological instability of the planar interface

[2]The observed hierarchical elimination of fingers in stages which reduce them in number approximately by a factor one half [KL86, CM89] could have here direct implications on the structure of the connections among the N-equal-finger fixed points.

are relatively close to N-periodic solutions as long as the noise in the initial conditions is weak and white, which guarantees that the most unstable (fastest growing) mode dominates in the early nonlinear regime. In these conditions, the system feels the attraction to the corresponding N-equal finger fixed point. This stage is what we called 'growth'. When the fingers are relatively large they start to feel the deviations form exact periodicity and start the 'competition' process.

Note that, despite the formal analogy to the single-finger solvability theory, the reference to a the restoring of multifinger hyperbolicity by surface tension as *dynamical* solvability scenario is fully justified. Indeed, the local structure of the multifinger fixed point has a dramatic impact on the global (topological) structure of the phase space flow, as we have seen in simple examples. The existence of a small but finite surface tension thus determines a global flow structure and it is in this sense that it 'selects' the dynamics of the system.

The possibility of extension of this analysis to other interfacial pattern forming problems relies on the existence of a continuum of unequal multifinger stationary solutions with zero surface tension. The fact that in the ST case the existence of those can be associated to a simple relationship between screening due to relative tip position and relative finger width (that is, a slower areal growth rate of the screened finger is compensated by its smaller width, resulting in an equal tip velocity), one is tempted to conjecture that similar classes of solutions must exist in other problems, for instance in the growth of needle crystals in the channel geometry [BM91]. Although this point should be more carefully addressed, it seems reasonable to expect that a DSS as presented above could be generalizable, to some extent, to other physical systems.

# Chapter 4

# Singular effects of surface tension in multifinger dynamics

In this chapter we study the singular effects of vanishingly small surface tension on the dynamics of finger competition in the Saffman-Taylor problem, using the asymptotic techniques developed by S. Tanveer and co-workers, as well as direct numerical computation. We demonstrate the dramatic effects of small surface tension on the late time evolution of two-finger configurations with respect to exact (nonsingular) zero-surface tension solutions. The effect is present even when the relevant zero surface tension solution has asymptotic behavior consistent with selection theory. Such singular effects therefore cannot be traced back to steady state selection theory, and imply a drastic global change in the structure of phase-space flow.

## 4.1 Applying asymptotic theory to two finger solutions

Little is known about the effect of finite (but small) surface tension $B$ on the dynamics of zero surface tension multifinger solutions, and in particular on the class of exact solutions Eq. (3.2) studied in previous chapter. For single finger configurations, steady state selection theory predicts that the finger cannot have an arbitrary width. Indeed, for vanishing surface tension $B \to 0$ the width $\lambda = 1/2$ is selected, asymptotically in time. Thus, it is clear that surface tension has a critical influence on single finger solutions with $\lambda \neq 1/2$. The nature of this influence in the limit $B \to 0$ has been investigated by Siegel, Tanveer and Dai [STD96, ST96], who present evidence that zero surface tension single finger solutions with $\lambda < 1/2$ are significantly perturbed by the inclusion of an arbitrarily small amount of surface tension

in order one time. The effect of surface tension is an increase of the finger width to reach the width predicted by selection theory. However, the effect of small surface tension on two-finger $B = 0$ exact solutions is not known, in particular on solutions whose asymptotic width $\lambda$ is compatible with Microscopic Solvability theory.

We will follow the approach of Refs. [STD96, ST96] to the exact solution given by Eq. (3.2), and study it by means of the asymptotic perturbation theory described in Sec. 2.3. The solution, within the formalism used in Sec. 2.3, reads

$$f(\zeta,t) = -\frac{2}{\pi}\ln\zeta + \frac{1}{\pi}(1-\lambda+i\epsilon)\ln(1-\frac{\zeta^2}{\zeta_s(t)^2}) + \frac{1}{\pi}(1-\lambda-i\epsilon)\ln(1-\frac{\zeta^2}{\bar{\zeta}_s(t)^2}) + d(t) + i. \tag{4.1}$$

The singularity locations are given by the complex parameter $\zeta_s(t)$, related to $\alpha$ used in previous chapters through $\alpha(t) = 1/(i\zeta_s^2(t))$. Analyticity of $f(\zeta,t)$ in the unit circle implies that $|\zeta_s(t)| > 1$. We employ the convention that $\zeta_s(t)$ is a complex number in the first quadrant. For the family of exact $B = 0$ solutions the mapping function Eq. (4.1) has four pole-like singularities: $\pm\zeta_s$ and $\pm\overline{\zeta}_s$, and four zeros $\pm\zeta_{0+}$ and $\pm\zeta_{0-}$ of $f_\zeta$ located at

$$\zeta_{0+}^2 = \frac{-(\lambda+i\epsilon)\zeta_s^2 - (\lambda-i\epsilon)\overline{\zeta}_s^2}{2(1-2\lambda)} + \frac{\sqrt{\left[(\lambda+i\epsilon)\zeta_s^2 + (\lambda-i\epsilon)\overline{\zeta}_s^2\right]^2 + 4(1-2\lambda)|\zeta_s|^4}}{2(1-2\lambda)} \tag{4.2a}$$

$$\zeta_{0-}^2 = \frac{-(\lambda+i\epsilon)\zeta_s^2 - (\lambda-i\epsilon)\overline{\zeta}_s^2}{2(1-2\lambda)} - \frac{\sqrt{\left[(\lambda+i\epsilon)\zeta_s^2 + (\lambda-i\epsilon)\overline{\zeta}_s^2\right]^2 + 4(1-2\lambda)|\zeta_s|^4}}{2(1-2\lambda)}. \tag{4.2b}$$

For the particular case $\lambda = 1/2$ this solution presents only one pair of zeros $\pm\zeta_0$ located at

$$\zeta_0^2 = \frac{|\zeta_s|^4}{2[(\lambda+i\epsilon)\zeta_s^2 + (\lambda-i\epsilon)\overline{\zeta}_s^2]}. \tag{4.3}$$

In the following it will be useful to define the real quantity $\beta = -(\lambda+i\epsilon)\zeta_s^2 - (\lambda-i\epsilon)\overline{\zeta}_s^2$ which appears in Eqs. (4.2) and (4.3).

Depending on the value of $\lambda$ the initial data may have zeros on both the real and imaginary axes, or all the zeros may lie on a single axis. This difference has significant consequences in the finite surface tension dynamics. More specifically, when $\lambda < 1/2$ the zeros described in Eqs. (4.2a) and (4.2b) are located on both the real and imaginary axes of $|\zeta| > 1$, namely at $\pm|\zeta_{0+}|$ and $\pm i|\zeta_{0-}|$. The situation is different for $\lambda > 1/2$, which is further divided into two cases, depending on whether $\beta^2 + 4(1-2\lambda)|\zeta_s|^2 > 0$ or $< 0$. In the former case all four singularities lie on the real axis (for $\beta > 0$) or on the imaginary axis (for $\beta < 0$). In the latter case the four zeros are located off the axes in conjugate pairs, i.e. at $\pm\zeta_0$ and $\pm\bar{\zeta}_0$. Finally, when $\lambda = 1/2$ the solution Eq. (4.1) has only two zeros, located on the real axis at $\pm|\zeta_s|^2/\sqrt{-2\beta}$ when $\beta < 0$ and on the imaginary axis at $\pm|\zeta_s|^2/\sqrt{2\beta}$ when $\beta > 0$. Note that for $\lambda = 1/2$ the $B = 0$ solution has two less zeros than for $\lambda \neq 1/2$.

The initial zero locations described above have a critical bearing on whether the daughter singularity will impact the unit disk[1]. Although all daughter singularities approach the unit disk, their impact may be shielded by the presence of an inner region corresponding to a pole singularity. More precisely, since $\zeta_d$ and $\zeta_s$ obey the same dynamical equation, they will move together if they get close enough to each other. However, the inner region around a pole moves to leading order like the $B = 0$ pole, i.e., it moves exponentially slowly toward $|\zeta| = 1$ when $|\zeta_s| - 1 << 1$, and does not impinge upon the unit disk in finite time [How86]. In this case the $O(B^{1/3})$ inner region around the daughter singularity will not affect the dynamics on $|\zeta| = 1$, at least until $t = O(-\ln B)$. Before this time, we expect the interface to be uninfluenced by the presence of the daughter singularity. This shielding mechanism is discussed in the context of single fingers in [ST96].

Knowledge of the $t \to \infty$ asymptotic state and the initial locations of zeros can be used to ascertain whether shielding can occur. The $B = 0$ asymptotic state corresponds to $\zeta_s^2(t \to \infty) \to \pm 1$. Thus, for $\lambda < 1/2$, only one pair of daughter singularities may be shielded—never both— so at least one pair of daughter singularities will impinge on the unit disk. The daughter singularities will also not be shielded when $\lambda > 1/2$ and $\beta^2 + 4(1-2\lambda)|\zeta_s|^2 < 0$. However, for $\lambda > 1/2$ and $\beta^2 + 4(1-2\lambda)|\zeta_s|^2 > 0$ it is possible for all the daughter singularities to be shielded, since they lie on a single axis. The daughter singularities can also be completely shielded when $\lambda = 1/2$. The different possibilities are schematically depicted in Fig. 4.1.

We have numerically computed the daughter singularity impact time $t_d$

[1] Although the daughter singularity is said to impact the unit disk when $|\zeta_d(t)| = 1$, the singularities comprising the cluster do not actually impinge upon the unit disk. However, at $t_d$ the singularities are close enough to influence the interface shape, in the sense that $|f_\zeta(\zeta_d, t_d) - f_\zeta^0(\zeta_d, t_d)| = O(1)$.

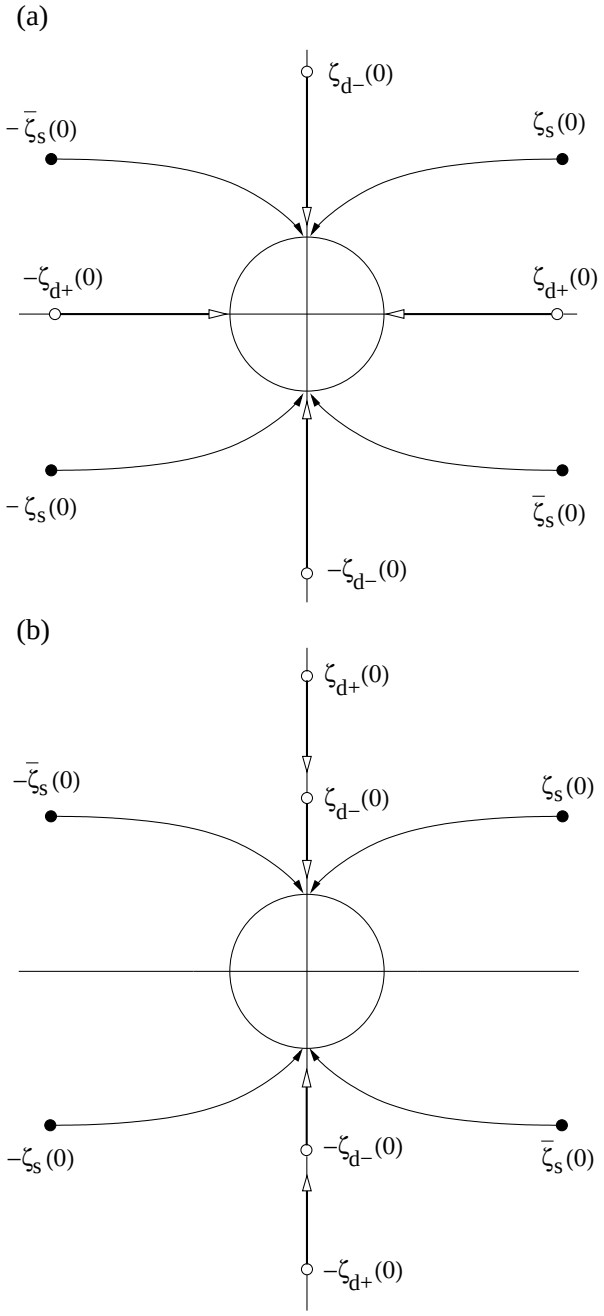


Figure 4.1: (a) Schematic representation of the dynamics of pole ($\zeta_s$) and daughter ($\zeta_d$) singularities for $\lambda < 1/2$. (b) Schematic representation of one of the two possible dynamics of pole ($\zeta_s$) and daughter ($\zeta_d$) singularities for $\lambda > 1/2$.

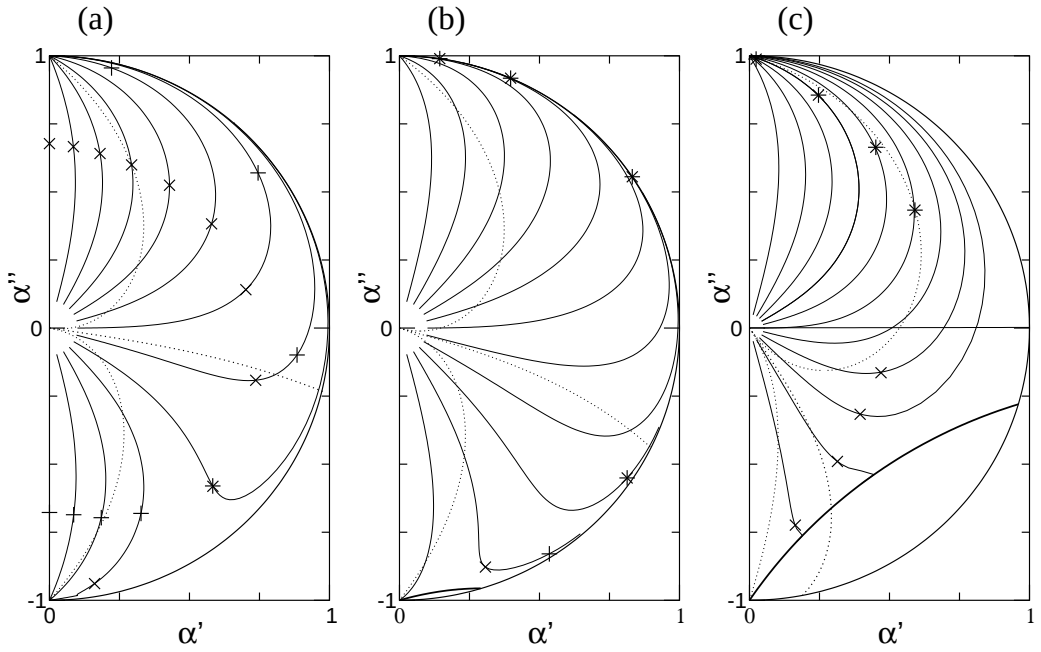


Figure 4.2: Phase portraits for (a) $\lambda = 1/3$ and $\epsilon = 0.1$, (b) $\lambda = 2/3$ and $\epsilon = 0.1$, and (c) $\lambda = 1/3$ and $\epsilon = 1/2$. The daughter singularity impact is indicated by the symbols. The + symbol corresponds to the impact of $\zeta_{d+}$, $\times$ to the impact of $\zeta_{d-}$ and $*$ to the simultaneous impact of $\zeta_{d+}$ and $\zeta_{d-}$.

for various values of $\lambda$ and $\epsilon$, using initial conditions close to the planar interface, $|\zeta_s|^2 = 20$ and various values of $\mathrm{Arg}[\zeta_s^2]$. Figure 4.2 shows the phase portrait for different values of $\lambda$ and $\epsilon$ with the daughter singularity impact indicated. From the plots it is immediately seen that for $\lambda < 1/2$ at least one daughter singularity always hits the unit circle, and for $\lambda \geq 1/2$ some trajectories are free from daughter singularity impact. In addition, it is observed that for fixed $\lambda$ a larger value of $\epsilon$ causes the daughter singularities to hit in shorter times (or less developed fingers) than a smaller value of $\epsilon$, and for fixed $\epsilon$ larger $\lambda$ implies larger impact times. We have also checked that the daughter singularity impact occurs well before a finite time singularity, i.e., the impact of a zero of $f_\zeta$. Thus, the effect of surface tension is significant well before the curvature in the zero surface tension solution becomes large.

It is noted that the $\lambda$ dependence of the daughter singularity impact is consistent with the results of steady state selection theory [Shr86, HL86, CDH+86, Tan87a]. According to selection theory, for small $B$ the possible values of $\lambda$ are discretized: $\lambda$ must satisfy the relation $\lambda = \lambda_n(B)$, given to

leading order by

$$\lambda_n(B) = \frac{1}{2}\left\{1 + (\frac{1}{8}\pi^2 C_n B)^{2/3}\right\}, \quad n = 0, 1, 2, ... \tag{4.4}$$

where $n$ parameterizes the branch of solutions. Note that $\lambda_n > 1/2$ for all $n$. The steady finger shape is to leading order a Saffman-Taylor finger, with the above values of $\lambda_n$ substituted for the width $\lambda$. On the other hand for $\epsilon > 0$ the asymptotic state of Eq. (4.1) is a Saffman-Taylor finger of width $\lambda$. From Eq. (4.4) it is clear there exists a steady solution with width $\lambda_n(B)$ close to a Saffman-Taylor finger of arbitrary width $\lambda > 1/2$. Thus the shielding of the daughter singularity, which leads to the persistence of a Saffman-Taylor solution with $\lambda > 1/2$ over long times, is consistent with steady state selection theory[2]. In contrast for $\lambda < 1/2$ there are no nearby steady solutions. Thus, a Saffman Taylor finger with $\lambda < 1/2$ cannot persist over a long time. We see that the impact of a daughter singularity provides a mechanism for the onset of finger competition, finger widening, and selection of a width $\lambda > 1/2$.

For $\epsilon = 0$ the scenario is similar, except there is an added class of $B > 0$ steady state solutions. Magdaleno and Casademunt [MRC00] have shown that two-finger solutions composed of steadily propagating but unequal fingers do exist for small nonzero $B$. The introduction of a small nonzero surface tension selects a discrete set of solutions from the continuum of fixed points of the $B = 0$ phase portrait. The solutions are parameterized by the total width of the fingers $\lambda = \lambda_1 + \lambda_2$ and the relative width $q = \lambda_1/\lambda$, and the introduction of finite $B$ discretizes the possible values of the parameters. In particular, they must satisfy a condition of the form $\lambda = \lambda_n(B)$ and $q = q_{n,m}(B)$ where $n$ and $m$ are integers. The expression for $\lambda_n(B)$ at lowest order is equivalent to Eq. (4.4), but with different coefficients $C_n$. The shape of these solutions are given to leading order (in the limit $t \to \infty$) by Eq. (4.1) with allowed value of $\lambda_n(B)$ substituted for the width $\lambda$. Again, $\lambda_n(B) > 1/2$, and the consistency between daughter singularity impacts and steady state selection theory follows as above.

We conjecture that the outcome of interfacial shape evolution after the daughter singularity impinges is in general independent of the particular finger on which the impact first occurs i.e., independent of the point at which $\zeta_d(t)$ impacts on $|\zeta| = 1$. More specifically, we surmise that impact on either the shorter (trailing) or larger (leading) finger retards the velocity of that finger, and is accompanied by the widening of the leading finger, so

[2]The steady state with $\lambda > 1/2$ is unstable to tip splitting modes, although specifying the initial value problem in the extended complex plane precludes the presence of noise needed to activate the instability.

as to maintain a constant fluid flux at infinity. The widened leading finger then shields the trailing finger, preventing it from further growth. Thus, the finger which is leading at the time of the daughter singularity impact 'wins' the competition, in the sense that it will evolve for $t \to \infty$ to the ST steady finger. To examine this conjecture and study the dynamics of finger competition with finite (but small) surface tension we have numerically computed the evolution of an interface with initial conditions given by the conformal mapping Eq. (4.1) close to the planar interface ($|\zeta_s(0)|^{-2} \ll 1$). The results are reported in the next section.

## 4.2 Numerical Results

Numerical computations have been performed for $B > 0$, using an initial interface corresponding to the explicit $B = 0$ solutions discussed in Secs. 3.1, 3.2 and 4.1. The effect of positive surface tension on this class of solutions is explored for various values of $\epsilon$ and a variety of initial pole positions.

We employ the numerical method introduced by Hou *et al.* [HLS94] and used in other studies of small surface tension effects in Hele-Shaw flow [STD96, ST96, CHS99, CH00]. The method is described in detail in Sec. 2.4. It is a spectral boundary integral method in which the interface is parameterized at equally spaced points by means of an equal-arclength variable $\alpha$. Thus, if $s(\alpha, t)$ measures arclength along the interface then the quantity $s_\alpha(\alpha, t)$ is independent of $\alpha$ and depends only on time. The interface is described using the tangent angle $\theta(\alpha, t)$ and the interface length $L(t)$, and these are the dynamical variables instead of the interface $x$ and $y$ positions. The evolution equations are written in terms of $\theta(\alpha, t)$ and $L(t)$ in such a way that the high-order terms, which are responsible of the numerical stiffness of the equations, appear linearly and with constant coefficients. This fact is exploited in the construction of an efficient numerical method, i.e., one that has no time step constraint associated with the surface tension term yet is explicit in Fourier space. We have used a linear propagator method that is second order in time, combined with a spectrally accurate spatial discretization. Results in this section are specified in terms of the nondimensional variables used in previous chapters, obtained scaling length with $W/(2\pi)$, instead of the ones used in previous sections of the present chapter.

The number of discretization points is chosen so that all Fourier modes of $\theta(\alpha, t)$ with amplitude greater than roundoff are well resolved, and as soon as the amplitude of the highest-wavenumber mode becomes larger than the filter level the number of modes is increased, with the amplitude of the additional modes initially set to zero. The time step $\Delta t$ is decreased until

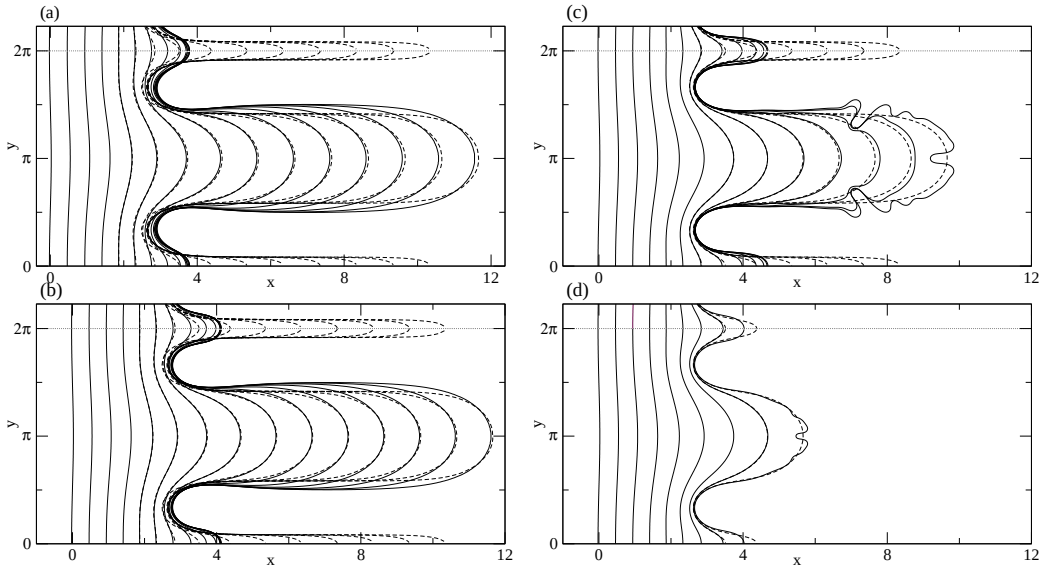


Figure 4.3: Evolution of an initial condition of the form Eq. (4.1) with $\lambda = 1/2$, $\epsilon = 0$ and $\zeta_s^2(0) = 20\exp(i\pi/6)$. The solid lines correspond to surface tension $B$ values (a) 0.01, (b) 0.005, (c) 0.001 and (d) 0.0005. The dashed lines correspond to the zero surface tension evolution. The time difference between different curves is 0.5. The physical channel in the $y$ direction extends from the origin to the dotted line, and the region above is plotted for better visualization of the lateral finger.

an additional decrease does not change the solution to plotting accuracy, nor lead to any significant differences in any quantities of interest. In a typical calculation 512 discretization points are initially used, and the initial time step is $\Delta t = 5 \cdot 10^{-4}$. For small values of surface tension numerical noise is a major problem, and the spurious growth of short-wavelength modes induced by roundoff error must be controlled. To help prevent this noise-induced growth at short wavelengths spectral filtering [Kra86] is applied. Additionally, we minimize noise effects and also assess the time at which these effects become prevalent by employing extended precision (128-bit) calculations, as described in the next section.

Our main interest is to uncover the role of surface tension in the dynamics of finger competition. To isolate the features of finger competition from those of width selection, we will concentrate on $B = 0$ solutions with $\lambda = 1/2$, the value selected by surface tension in the limit $B \to 0$. Since the $B = 0$ dynamics for $\epsilon = 0$ and $\epsilon \neq 0$ is quite different the numerical results for the two cases will be presented separately.

### 4.2.1 Solutions with $\epsilon = 0$

We first consider parameter values $\lambda = 1/2$ and $\epsilon = 0$. A typical set of interfacial profiles is shown in Fig. 4.3. The initial data is given by the mapping function Eq. (4.1), with $\lambda = 1/2$, $\epsilon = 0$, $d(0) = 0$ and $\zeta_s^2(0) = 20\exp(i\pi/6)$. With this value of $\zeta_s^2(0)$ the initial interface is well inside the linear regime. Evolutions are shown for different values of $B$, and the $B = 0$ interface evolution is also plotted for comparison. In all these evolutions the filter level is set to $10^{-13}$, although later we shall make comparisons to profiles computed at higher precision.

For the largest value of surface tension the computed $B > 0$ and the exact $B = 0$ solutions first differ appreciably at the seventh curve, corresponding to $t \approx 3$. At this point the velocity of the small finger (at the channel sides) begins to decrease and it is clearly left behind when compared with the small finger evolution in the $B = 0$ solution. Eventually, the advance of the small finger is completely suppressed and the larger finger widens to attain a width close to $1/2$ of the channel. For a smaller value of surface tension, for instance $B = 0.001$, the evolution displays qualitatively the same behavior. The $B > 0$ interface differs appreciably from the $B = 0$ sightly later than before (i.e., at the eighth curve) and the region where the two solutions differ most is to some extent more localized around the small finger than for larger values of $B$. Additionally, for this value of surface tension the effect of numerical noise is clearly exhibited in the interfacial profiles. Here the tip-splitting and side-branching activities are a clear effect of numerical noise, as can be easily checked redoing the computation with a different noise filter level.

In order to suppress or delay the branching induced by numerical noise that appears for small values of surface tension it is necessary to use higher precision arithmetic, e.g. quadruple precision (128-bit arithmetic). The filter level can then be reduced by a large amount and the outcome of spurious oscillations is substantially delayed. Figure 4.4 shows the effect of reducing the filter level to $10^{-27}$. The $B = 0$ solution is plotted, as well as the computation with double precision. For $B = 0.001$ the branching is totally suppressed, at least for the times we have computed, but for smaller values of $B$ the use of quadruple precision is only able to delay the branching and not totally suppress it. The quadruple precision computation confirms the results observed with lower precision: the introduction of finite (but small) surface tension results in the suppression of the small finger. From Fig. 4.4 one can also see that for long times, when the interface is clearly affected by numerical noise (in the double precision curve), the noise-induced branching is restricted to the large finger, and the small finger is basically unaffected by noise. This observation suggests that the small finger shape, as well as

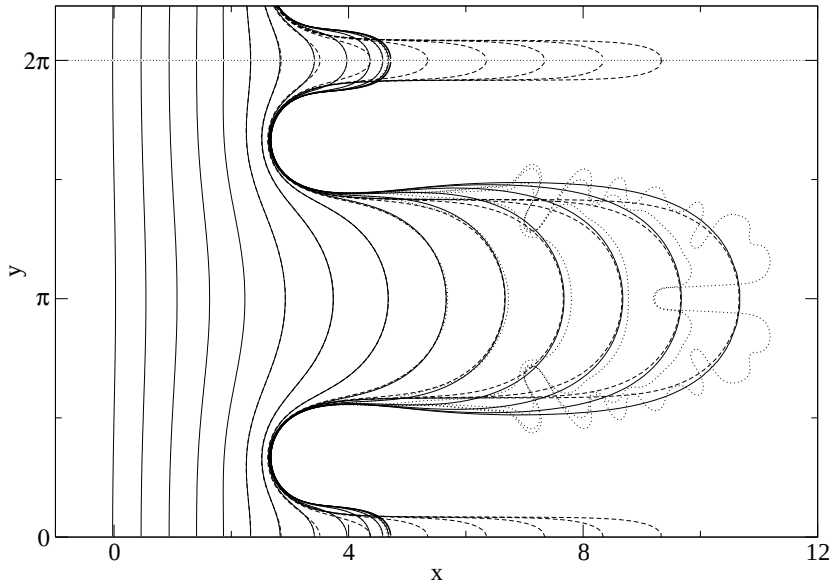


Figure 4.4: Evolution of an initial condition of the form (4.1) with $\lambda = 1/2$, $\epsilon = 0$ and $\zeta_s^2(0) = 20\exp(i\pi/6)$. The solid line correspond to $B = 0.001$ with a filter level equal to $10^{-27}$, the dotted line corresponds to the same $B$ but with the filter level equal to $10^{-13}$ and the dashed line corresponds to the zero surface tension solution. The time difference between curves is 0.5. As in Fig. 4.3, the physical channel in the $y$ direction extends from the origin to the dotted line.

its tip velocity and tip curvature, can be trusted even when the large finger has developed tip-splittings and side-branchings due to the spurious growth of roundoff error.

Figure 4.5 shows the tip velocity of both fingers versus $t$ for decreasing values of surface tension. It can be seen that the velocity of the large finger is only slightly affected by surface tension, whereas the velocity of the small finger is substantially reduced by the inclusion of finite $B$. As $B$ is decreased the tip velocity of the small finger is more faithful to the $B = 0$ evolution before the daughter singularity impact (shown by a cross), and clearly veers away from the $B = 0$ velocity later in the evolution, consistent with asymptotic theory. Note that at the smallest value of $B$ the tip velocity of the large finger drastically differs from the $B = 0$ velocity at late times. This discrepancy is a manifestation of noise effects in the neighborhood of the large finger tip. However, as previously seen, the small finger is basically unaffected by noise at the times we have plotted.

In order to further verify that the daughter singularity impact is responsi-

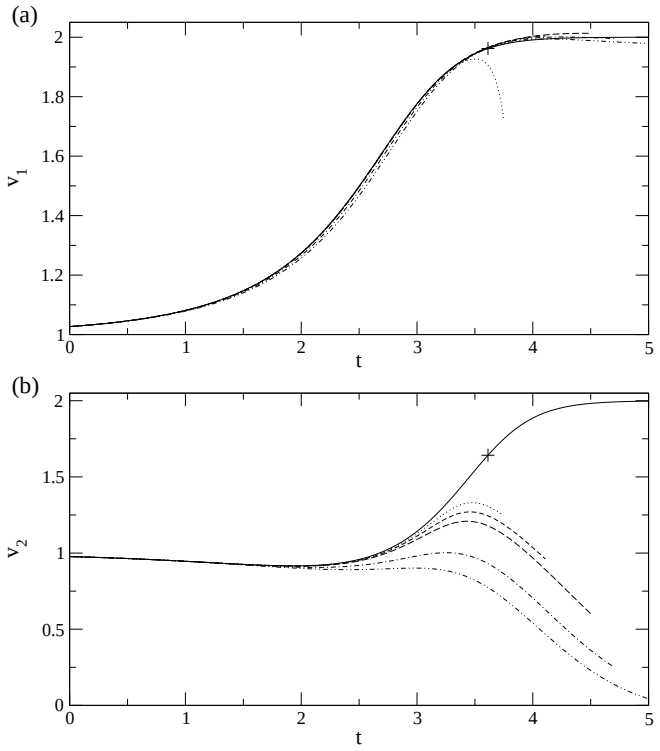


Figure 4.5: Computed tip velocities for the initial condition of Fig. 4.4 , (a) corresponds to the central (large) finger and (b) to the lateral (small) finger. The daughter singularity impact time $t_d$ is indicated by the + symbol. The value of $B$ is: 0 (solid line), 0.0002 (dotted line), 0.0005 (dashed line), 0.001 (long dashed line), 0.005 (dot-dashed line) and 0.01 (dot-dot-dashed line).

ble for the observed change in the small finger tip speed we follow the scheme introduced in [ST96]. Define $t_p$ as the time when the computed tip velocity differs by $p$ from the $B = 0$ tip velocity. According to asymptotic theory this $t_p$ will be a linear function of $B^{1/3}$ in the limit $B \to 0$ as long as $p$ is small enough. Figure 4.6 shows $t_p$ versus $B^{1/3}$ for various values of $p$, and it can be seen that $t_p$ exhibits the predicted behavior. Moreover, we have extrapolated the $B = 0$ value of $t_p$ using the two points of lowest $B$ and the result is very close to $t_d$, whose value is represented by a cross. We conclude that the impact of the daughter singularity is associated with the dramatic change of the $B > 0$ solution when compared to the zero surface tension solution, reducing the velocity of the small finger and eventually suppressing it. In contrast, for the $B = 0$ dynamics the small finger 'survives', propagating with the same asymptotic speed as the larger finger. Note that the average interface advances at unit velocity, and a tip velocity below 1 implies that

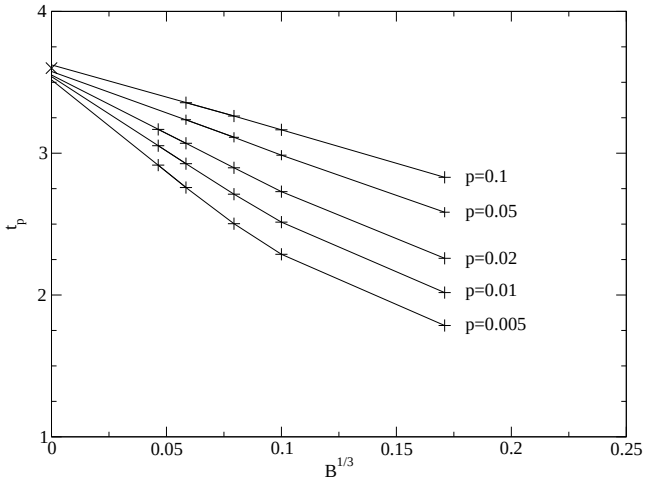


Figure 4.6: The time $t_p$ (defined in the text) versus $B^{1/3}$. From top to bottom, p=0.1, 0.05, 0.02, 0.01, 0.005. The daughter singularity impact time $t_d$ is indicated by a $\times$ symbol, and the curves are linearly extrapolated for comparison.

the finger is *retreating* in the reference frame of the average interface.

In summary then, our numerical results show that the computed interface for $B \neq 0$ follows the $B = 0$ evolution for an $O(1)$ time interval—roughly corresponding to the daughter singularity impact time—and that at further times the velocity of the small finger decreases while the large finger widens. The small finger eventually comes to a halt and the larger (leading) finger reaches an asymptotic width slightly above 1/2, the width singled out by selection theory. It is noted that for the initial condition we have studied the daughter singularity impact takes place on the tip of the small finger. Therefore, the influence of surface tension on the interface should be significant first around the impact point, that is, the small finger tip. Our numerical results show that in fact this is the case; the initial effect of the daughter singularity impact is to slow and then completely stop the growth of the small finger. Later on, as the singularity cluster centered in $\zeta_d$ spreads over the unit circle, the effect of surface tension is felt by the whole interface and the large finger widens to reach the selected width.

We have also studied the finite surface tension dynamics for a more general class of initial conditions. More precisely, we have studied initial conditions of the form $\zeta_s^2(0) = 20\exp(i\ n\pi/12)$ where $n = 0, \pm 1, ..., \pm 6$, and have obtained the same qualitative results as in the case previously studied, namely that the presence of small surface tension suppresses the growth of the finger which is trailing at the time of daughter singularity impact. In

order to compare the $B = 0$ and the $B \neq 0$ dynamics in a compact and global way we have plotted the phase portrait for $B = 0$ using the the tip velocities $v_1$, $v_2$ as dynamical variables. In the laboratory frame they read

$$v_1 = \frac{1 + \mathrm{i}(\zeta_s^2 - \bar{\zeta}_s^2) + \zeta_s^2 \bar{\zeta}_s^2}{\zeta_s^2 \bar{\zeta}_s^2 + \mathrm{i}(\zeta_s^2 - \bar{\zeta}_s^2)/2} \tag{4.5a}$$

$$v_2 = \frac{1 - \mathrm{i}(\zeta_s^2 - \bar{\zeta}_s^2) + \zeta_s^2 \bar{\zeta}_s^2}{\zeta_s^2 \bar{\zeta}_s^2 - \mathrm{i}(\zeta_s^2 - \bar{\zeta}_s^2)/2}. \tag{4.5b}$$

Now a comparison between dynamics for $B = 0$ and $B \neq 0$ is straightforward since the trajectories can be plotted together and compared. In addition, the tip velocity is a useful variable because it contains geometric information; specifically the inverse of the tip velocity is equal to the width of the finger in the asymptotic ($t \to \infty$) regime. It is important to note that $(v_1, v_2)$ are dynamical variables for the $B = 0$ problem, so that the plot of the zero surface tension trajectories onto the space $(v_1, v_2)$ is a true phase portrait. On the other hand $(v_1, v_2)$ are not state variables of the problem with finite surface tension, so in this case we simply obtain a projection onto the $(v_1, v_2)$ space of the original $B \neq 0$ trajectory, which is embedded in the infinite-dimensional phase space of interface configurations.

Figure 4.7 shows the phase portrait for $B = 0$ together with the tip velocities obtained from the initial conditions described above for $B = 0.01$. From the figure it is evident that the introduction of finite surface tension has substantially changed the global phase dynamics of the problem. Only one $B = 0.01$ trajectory connects the planar interface $(1, 1)$ and the 2ST point $(2, 2)$, corresponding to the unsteady double Saffman-Taylor finger. Any other $B = 0.01$ trajectory ends in one of the two ST finger points, ST(L) at $(2, 0)$ and ST(R) at $(0, 2)$. In contrast, the $(2, 2)$ point, equivalent to the continuum of fixed points present with the $(\alpha', \alpha'')$ or $(\mathrm{Re}\zeta_s, \mathrm{Im}\zeta_s)$ variables, has a finite basin of attraction for $B = 0$. The introduction of finite surface tension has dramatically changed the zero surface tension $(v_1, v_2)$ trajectories, to the extent that the $B = 0$ phase portrait and the $B \neq 0$ projection are not topologically equivalent. This result is not a complete surprise, since it was anticipated from the structural instability of the dynamical system governing the evolution of Eq. (4.1) for $\epsilon = 0$ [MC98]. A more dramatic example of topological inequivalence of phase portraits will be given in the next subsection, when we consider the case $\epsilon \neq 0$.

Although the use of the variables $(v_1, v_2)$ has allowed us to project the finite surface dynamics onto the zero surface tension phase portrait this projection has one major limitation: it only considers a local quantity, the tip velocity. We have also considered a projection that takes more global properties of the interface into account. Specifically, given a computed $B \neq 0$

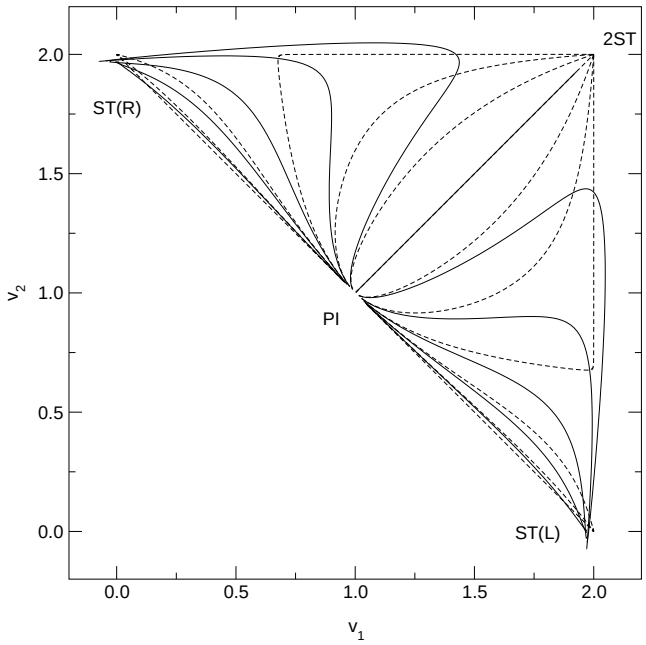


Figure 4.7: Plot of the evolution of initial conditions of the form (4.1) with $\lambda = 1/2$, $\epsilon = 0$ and $\zeta_s^2(0) = 20\exp(i\ n\pi/12)$ and $n = 0, \pm 1, ..., \pm 6$ in the $(v_1, v_2)$ or tip speed space. The solid line corresponds to $B = 0.01$ and the dashed line to $B = 0$.

solution for an initial condition of the form (4.1), one can use a suitable norm to define a 'distance' between the computed interface and the $B = 0$ interface obtained from the mapping function Eq. (4.1). We choose this 'distance' to be the area enclosed between the two interfaces at a given time. Additionally, we define a projection of the $B \neq 0$ interface onto the $B = 0$ phase space (with phase space variables $(\mathrm{Re}\,\zeta_s, \mathrm{Im}\,\zeta_s)$) by selecting the value of $\zeta_s$ that minimizes the 'distance' between the two interfaces, with the restriction that the position of the two mean interfaces must be the same. The latter condition ensures that the projection satisfies mass conservation.

Figure 4.8 shows the $B = 0$ phase portrait and the corresponding projected evolution for surface tension $B = 0.01$. Again, the plot clearly shows that the introduction of finite surface tension modifies the phase portrait of $B = 0$. The projected trajectories are initially close to the $B = 0$ dynamics, but for well developed fingers (corresponding to $|\alpha| \sim 1$) the projection departs from the $B = 0$ trajectory towards the Saffman-Taylor fixed point, located at $\alpha' = 0, \alpha'' = 1$. The projected trajectory only remains close to the corresponding $B = 0$ trajectory when the latter evolves towards the Saffman-Taylor fixed point. More precisely, the continuum of fixed points present for

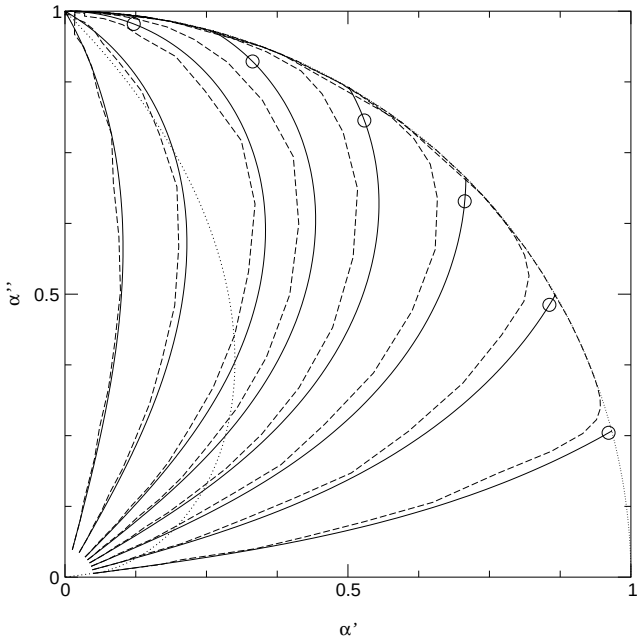


Figure 4.8: Comparison between the $B = 0$ trajectories and the projected evolutions with $B = 0.01$, for the initial conditions of Fig. 4.7. The solid line corresponds to $B = 0$ and the dashed lines to the projection of the $B = 0.01$ evolutions. The daughter singularity impacts are indicated by a circle.

$B = 0$ has been removed by surface tension and the Saffman-Taylor fixed point is the universal attractor of the dynamics for finite surface tension.

In Fig. 4.9 the projection for decreasing values of $B$ is plotted, using the initial condition $\zeta_s^2(0) = 20\exp(i\pi/6)$. As $B$ is decreased the projected trajectory gets closer to the $B = 0$ trajectory, but as it approaches the point when the daughter singularity impinges the unit circle (this point is signaled by a cross) the projection departs from the $B = 0$ trajectory and approaches the Saffman-Taylor fixed point, consistent with asymptotic theory.

### 4.2.2 Solutions with $\epsilon \neq 0$

The continuum of fixed points present for $\epsilon = 0$ is absent for $\epsilon \neq 0$, but in this case finite-time singularities in the form of zeros of $f_\zeta$ impinging on the unit disk do appear for some initial conditions. Therefore, we can expect that the effect of finite surface tension will be somewhat different than for $\epsilon = 0$. Firstly, the presence of surface tension should eliminate finite-time singularities, and secondly, finite $B$ could modify the basin of attraction for the two attractors of the $B = 0$ dynamical system, namely the side Saffman-

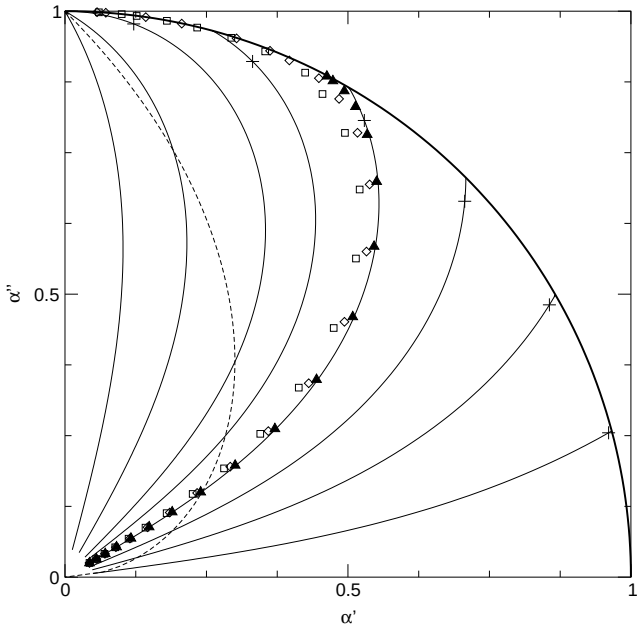


Figure 4.9: Comparison between the $B = 0$ trajectories and the projection of the evolution of the initial condition given by Eq. (4.1) with $\lambda = 1/2$, $\epsilon = 0$ and $\zeta_s^2(0) = 20\exp(i\pi/6)$, where ▲ corresponds to $B = 0.001$, ⋄ to $B = 0.005$, □ to $B = 0.01$ and × to $B = 0$. The daughter singularity impacts are indicated by a plus.

Taylor finger and the center Saffman-Taylor finger.

To explore this, we have performed computations with $\lambda = 1/2$ and $\epsilon = 0.1$ with initial conditions $\zeta_s^2(0) = 20\exp(\mathrm{i}\, n\pi/12)$ and $n = 0, \pm1, ..., \pm6$. Initially we set $B = 0.01$ and use a value of the noise filter level equal to $10^{-13}$, which suffices due to the relatively large value of $B$. The easiest way to compare both dynamics, finite $B$ and $B = 0$, is to plot their trajectories in velocity space. Thus, in Fig. 4.10 the tip velocities $(v_1, v_2)$ of the $B = 0.01$ computation are plotted together with the tip velocities for $B = 0$. For arbitrary $\epsilon$ and $\lambda$ the tip velocities of the $B = 0$ solution read

$$v_1 = \frac{1 + \mathrm{i}(\zeta_s^2 - \bar{\zeta}_s^2) + \zeta_s^2\bar{\zeta}_s^2}{\zeta_s^2\bar{\zeta}_s^2 - \epsilon(\zeta_s^2 + \bar{\zeta}_s^2) + \mathrm{i}\lambda(\zeta_s^2 - \bar{\zeta}_s^2) - (1 - 2\lambda)} \tag{4.6a}$$

$$v_2 = \frac{1 - \mathrm{i}(\zeta_s^2 - \bar{\zeta}_s^2) + \zeta_s^2\bar{\zeta}_s^2}{\zeta_s^2\bar{\zeta}_s^2 + \epsilon(\zeta_s^2 + \bar{\zeta}_s^2) - \mathrm{i}\lambda(\zeta_s^2 - \bar{\zeta}_s^2) - (1 - 2\lambda)}. \tag{4.6b}$$

From the plot one can see that most $B = 0.01$ velocity trajectories follow (at least qualitatively) their $B = 0$ counterparts, in the sense that they end up in the same fixed point. However, the second, third and fourth

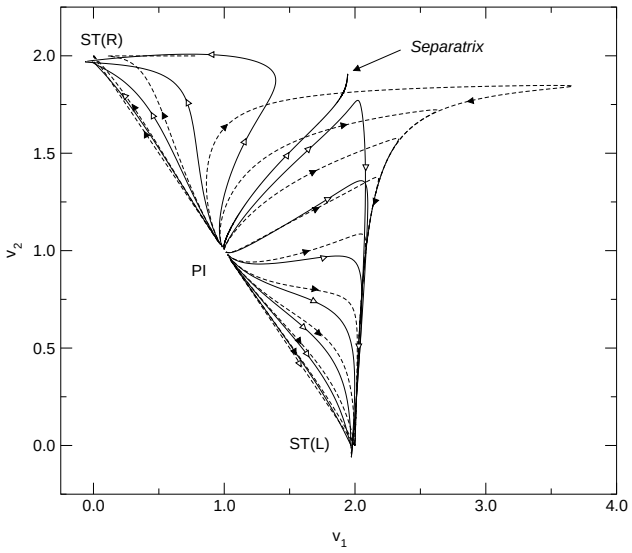


Figure 4.10: Plot of the evolution of initial conditions of the form (4.1) with $\lambda = 1/2$, $\epsilon = 0.1$ and $\zeta_s^2(0) = 20\exp(i\ n\pi/12)$ and $n = 0, \pm 1, ..., \pm 6$ in the $(v_1, v_2)$ or tip speed space. The solid line corresponds to $B = 0.01$ and the dashed line to $B = 0$. The computed trajectory that most nearly separates the two basins of attraction is also plotted. Note that the long time behavior of the third and fourth $B = 0.01$ curves (counting from the upper left trajectory in clockwise direction) is dramatically different from the corresponding $B = 0$ solutions.

trajectories (counting from the upper left trajectory in clockwise direction) differ significantly from their $B = 0$ counterparts. The second $B = 0.01$ trajectory moves apart from the $B = 0$ solution simply because the latter develops a finite-time singularity, which is regularized by the introduction of finite surface tension. However, the third and fourth trajectories exhibit a quite surprising behavior: the computed interface with $B = 0.01$ ends up in a different fixed point than the exact $B = 0$ solution, despite the fact that the $B = 0$ solution is smooth for all time and has the asymptotic width that would be selected by vanishing surface tension.

In order to get further insight into this behavior we have computed the evolution for decreasing values of $B$ using the specific initial pole position $\zeta_s^2(0) = 20\exp(-\mathrm{i}\pi/6)$, with $\lambda = 1/2$ and $\epsilon = 0.1$. Quadruple precision has been used when it has been necessary. The differences between the two interfaces for long times are readily apparent. When $B = 0$ the finger in the central position stops growing and the side finger wins the competition, whereas for $B > 0$ we encounter the opposite situation—namely, the central

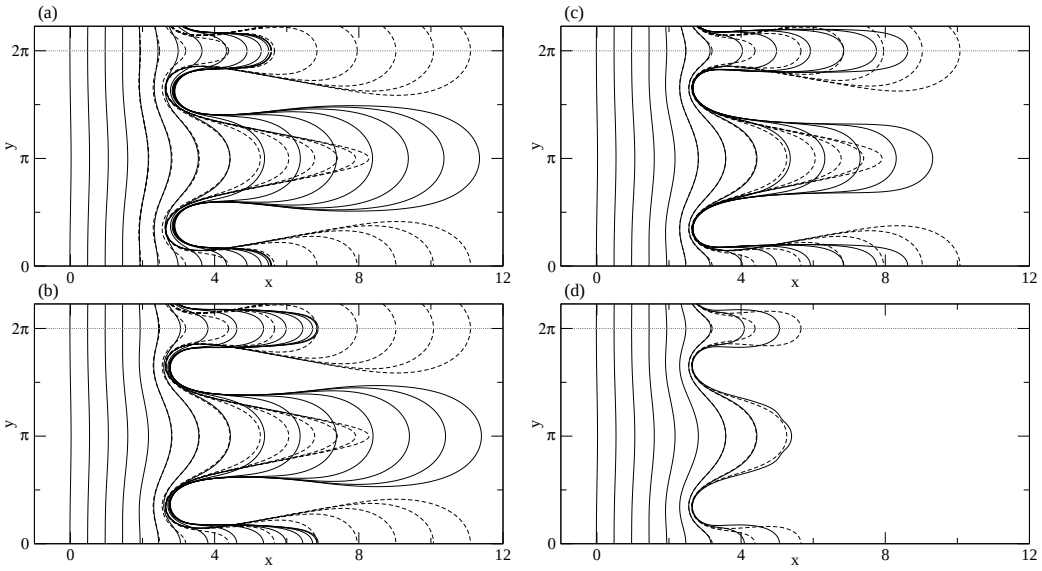


Figure 4.11: Evolution of an initial condition of the form Eq. (4.1) with $\lambda = 1/2$, $\epsilon = 0.1$ and $\zeta_s^2(0) = 20\exp(-i\pi/6)$. The solid lines correspond to surface tension $B$ values (a) 0.01, (b) 0.005, (c) 0.001 and (d) 0.0005. The dashed lines correspond to the zero surface tension evolution. The time difference between different curves is 0.5.The physical channel in the $y$ direction extends from the origin to the dotted line.

finger surpasses the side finger and wins the competition. For the smaller values of $B$ the finger on the sides has not quite stopped growing when the computation is stopped, although its tip speed shows a marked decrease over that for $B = 0$ and is less than that of the central finger.The side finger tip speed is also decreasing at the final stage of the computation. Figure 4.11 shows its evolution for four values of the surface tension parameter, together with the $B = 0$ solution. The tip speed trend in the limit $B \to 0$ is further illustrated in Fig. (4.12). This figure shows the tip speed versus time of each finger for a sequence of decreasing $B$. The plot suggests that upon impact of the daughter singularity the side finger velocity levels off and eventually decreases, whereas the velocity of the center finger is nearly unaffected and continues to increase. The trend is indicative of the center finger "winning" the competition in the $B > 0$ dynamics, while the opposite occurs for $B = 0$. Finally, it is noted that the influence of surface tension is first felt by the smaller finger, which is the recipient of the daughter singularity impact. Afterwards the leading finger begins to widen, in a manner consistent with the conjecture in Sec. 4.1. Further remarks on this point are made in Sec. 4.3.

The projection method described in the previous section has been also

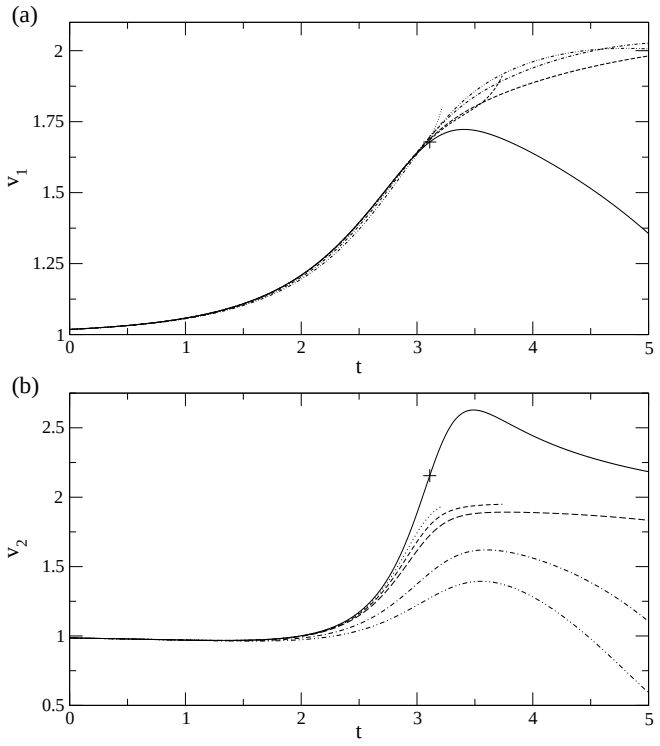


Figure 4.12: Computed tip velocities for the initial condition of Fig. 4.11, (a) corresponds to the central finger and (b) to the lateral finger. The daughter singularity impact time $t_d$ is indicated by the + symbol. The value of $B$ is: 0 (solid line), 0.0002 (dotted line), 0.0005 (dashed line), 0.001 (long dashed line), 0.005 (dot-dashed line) and 0.01 (dot-dot-dashed line). The deviations observed at late times for $B = 0.0002$ and $B = 0.0005$ in (b) are due to numerical noise.

applied to this case, and the results are displayed in Fig. 4.13 in the particular case $B = 0.01$. It can be seen that for most trajectories the projection stays close to the $B = 0$ curves, even for long times. The daughter singularity impact still leads to $O(1)$ differences between the $B = 0$ and $B > 0$ solutions, although the impact does not produce changes in the outcome of finger competition. However, as expected some of the trajectories (namely the third and fourth as measured clockwise from the bottom) do indicate significant qualitative differences in the long time evolution. The plot provides a simple depiction of the topological inequivalence of the $B > 0$ and $B = 0$ dynamics[3].

[3]It is noted that the $B > 0$ interfacial profile and the projection profile do differ significantly in small scale features. This is another indication of the difficulties in using

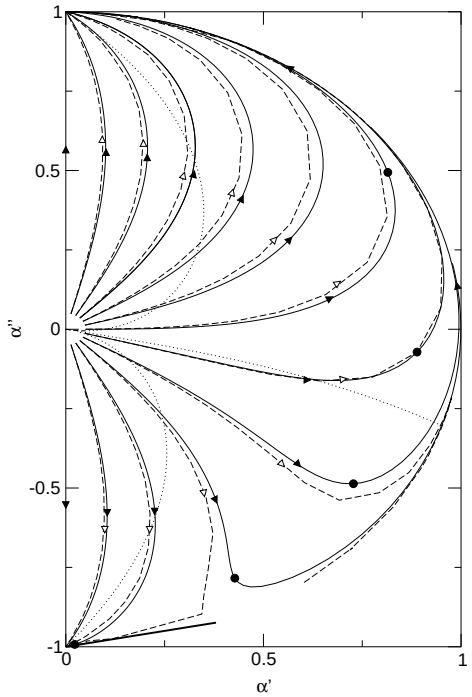


Figure 4.13: Comparison between the $B = 0$ trajectories and the projected evolutions with $B = 0.01$, for the initial conditions of Fig. 4.11. The solid line corresponds to $B = 0$ and the dashed lines to the projection of the $B = 0.01$ evolutions. The daughter singularity impacts are indicated by a circle. Note that the fourth $B > 0$ trajectory (as measured counterclockwise from the bottom) reverses direction and heads toward the fixed point (-1,0).

It has been shown that the introduction of a finite $B$ has not changed the attractors of the problem, but it has changed their basins of attraction. Interestingly, in the $B = 0$ case there does not exist a single separatrix trajectory between the two Saffman-Taylor attractors, but rather a finite region, corresponding to the set of trajectories ending in cusps, that acts as an effective separatrix. Since for finite surface tension there are no cusps, it can be assumed that there is a single trajectory that separates the two basins of attraction. Obviously, this trajectory will depend on the value of the surface tension parameter. More precisely, the initial condition $\zeta_s^2(0)$ corresponding to the separatrix trajectory will be a function of the surface tension $B$. To quantitatively characterize this set of initial conditions we have studied the dependence of the separatrix trajectory in a neighborhood

zero surface tension solutions to describe, even qualitatively, the finite surface tension dynamics.

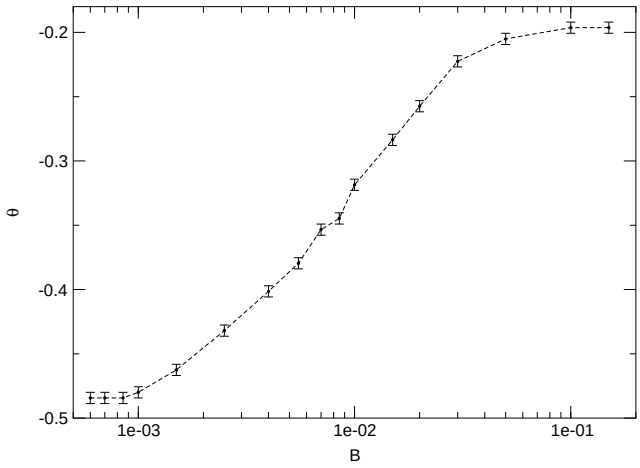


Figure 4.14: Plot of $\theta_{sep}$ vs. $B$ for initial conditions of the form Eq. (4.1) with $\lambda = 1/2$, $\epsilon = 0.1$ and $\zeta_s^2(0) = 20\exp(i\theta)$.

of the planar interface fixed point as a function of $B$, using initial conditions of the form $\zeta_s^2(0) = 20\exp(i\theta)$. For a given initial condition $\zeta_s(0)$ introduce the parameter $\theta_{sep}(B)$, defined as the unique value for which the evolution is attracted toward the fixed point ST(L) when $\theta > \theta_{sep}$ and to the fixed point ST(R) when $\theta < \theta_{sep}$.

Figure 4.14 shows the plot of $\theta_{sep}$ versus $B$, and it is observed that as $B$ decreases, $\theta_{sep}$ saturates to a fixed value, namely $\theta_{sep}(B \to 0) = -0.4843 \pm 0.0009$. It is interesting to compare this value to the position of the separatrix region for $B = 0$, which is located between $\theta_+^{B=0} = -0.95758$ and $\theta_-^{B=0} = -1.04796$. The separatrix for finite $B$ lays outside and far away from the separatrix region for $B = 0$, even for vanishing surface tension. Our evidence therefore suggests that any $B = 0$ trajectory located between the trajectories defined by $\theta_{sep}(B \to 0)$ and $\theta_+^{B=0}$ will not describe, even qualitatively, the regularized dynamics in the limit $B \to 0$, since the finger that will 'win' the competition under the $B = 0$ dynamics will 'lose' under the $B \to 0$ dynamics. Thus, there exists a positive measure set of initial conditions of the form Eq. (4.1) such that the evolution with $B \to 0$ cannot be qualitatively described by its evolution under $B = 0$ dynamics. This is a dramatic consequence of the singular nature of surface tension on the dynamics of finger competition which is not related to steady state selection, but confirms the ideas of Dynamical Solvability Scenario proposed in Chapter 3.

## 4.3 Summary and concluding remarks

The asymptotic theory developed in Refs. [Tan93, ST96] predicts the existence of regions of the complex plane where the zero surface tension solution and the finite surface tension solution differ by $O(1)$. These regions are the daughter singularity clusters, and their influence is felt in the physical interface when they are close to the unit circle. Daughter singularities move towards the unit circle, and when their motion is not impeded by other singularities they reach the unit circle in $O(1)$ time. When the distance between the daughter singularity and the unit circle is $O(B^{1/3})$ the interface can display $O(1)$ discrepancies with respect the interface of the $B = 0$ solutions. However, the asymptotic theory does not predict the nature of the discrepancies caused by daughter singularity impact.

Since the precise effect of the daughter singularity cannot be established by the asymptotic theory it is necessary to use numerical computation in order to establish the effects of daughter singularity on the dynamics of the interface. We have focused our efforts on uncovering the role of surface tension in the dynamics of two finger configurations, which is the simplest situation exhibiting nontrivial finger competition. Numerical computations with small surface tension show that the introduction of a small $B$ in the $\epsilon = 0$ solutions removes the continuum of fixed points and triggers the competition process which was absent for $B = 0$ by restoring the saddle-point (hyperbolic) structure of the appropriate multifinger fixed point. The other type ($\epsilon \neq 0$) of two-finger solution we have studied exhibits finger competition for $B = 0$, but the numerical computation with small $B$ has shown that the long time configuration of the computed interface may be *qualitatively* different from the $B = 0$ solution for a broad set of initial conditions, in the sense that the finger that 'wins' the competition is not the same with and without surface tension. Thus, the presence of surface tension seemingly can change the outcome of finger competition even in configurations that are well behaved and smooth for all time and whose asymptotic width is fully compatible with the predictions of selection theory for vanishing surface tension. This unexpected result shows that surface tension is not only necessary to select the asymptotic width and to prevent cusp formation, but plays also an essential role in multifinger dynamics through a drastic reconfiguration of the phase space flow structure.

Our calculations support the conjecture that impact on either the shorter or larger finger retards the velocity of that finger, and is accompanied by the widening of the larger finger. As a consequence, in general the outcome of finger competition is independent of the particular finger on which the impact first occurs, and the finger which is leading at the time of the daughter

singularity impact 'wins' the competition. This recipe fails only for interfacial configurations with very similar fingers, when not only the position of the finger (which finger is leading) but also the tip velocities (a trailing finger can have for a certain time a larger velocity than the leading one) at the impact time may play a role.

The main conclusion of the present chapter is that surface tension is essential to describe multifinger dynamics and finger competition, even when the corresponding zero surface tension evolution is well behaved and compatible with selection theory. That is, we have detected singular effects of surface tension on the dynamics of finger competition that are not directly related to steady state selection. These can be properly interpreted in the context of the Dynamical Solvability Scenario described in Chapter 3 where the reconfiguration of phase space flow by surface tension can be traced back to the restoring of hyperbolicity of multifinger fixed points.

The general picture emerging from this Part II of the thesis is thus the following. The $B = 0$ problem does coincide with the limiting one $B = 0^+$ only in a finite region of phase space. This includes finite time evolutions departing from the planar interface fixed point, and the full infinite time evolution of trajectories ending at fixed points if these are the ones consistent with selection theory ($\lambda = 1/2$). The boundary of the region of phase space where the manifolds of $B = 0$ and $B = 0^+$ coincide is defined by the impact of daughter singularities. For later times, the two manifolds span disjoint regions of the full phase space of possible interface configurations. Trajectories which overlap in the common region of $B = 0$ and $B = 0^+$ follow different paths in phase space for later times. Remarkably, two trajectories which coincided at early times may go far apart from each other, even if they eventually evolve to the same asymptotic attractor. In particular, which finger wins the competition may be different for the two cases, not just for a single 'borderline' trajectory but for an appreciably broad range of initial conditions. This is a rather subtle effect since the fact that the evolution is always smooth and to the correct attractor makes it virtually impossible *a priori* to anticipate such dramatic differences between $B = 0$ and $B = 0^+$.

# Part III

# Viscosity contrast

# Chapter 5

# Multifinger dynamics with arbitrary viscosity contrast. Fingers versus bubbles

Finger competition with arbitrary viscosity contrast is studied by means of numerical computation. An initial condition appropriate to study the size of the basin of attraction of the Saffman-Taylor finger is identified, and used to characterize the dependence of the ST basin of attraction on the viscosity contrast $c$, obtaining that its size decreases for decreasing $c$. An alternative class of attractors is identified as the set of Taylor-Saffman bubble solutions, and the implications of this result are discussed in detail.

## 5.1 Introduction

Tryggvason and Aref in their numerical study of multifinger dynamics [TA83] observed that the viscosity contrast has a deep influence in the dynamics of Hele-Shaw flows and in the morphology of the fingering patterns formed. This numerical evidence was later confirmed by the experimental results obtained by Maher [Mah85] using a experimental setup where the instability was driven by gravity and the fluid used was the binary-liquid mixture isobutyric acid plus water at critical composition, that allowed to reach very low values of the viscosity contrast parameter. Simple (two finger) configurations were also studied [TA85] by means of direct numerical integration that confirmed the dramatic differences between high $c$ and low $c$ dynamics. The conclusion was very qualitative though, and no systematics was ever used, to some extent due to the computer limitations of that time. The essential difference in the dynamics between high and low viscosity contrast is

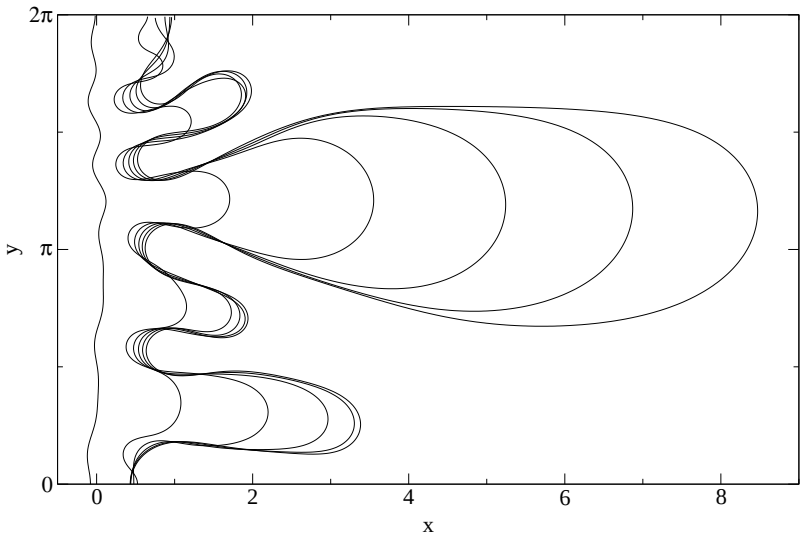


Figure 5.1: Temporal evolution of an noisy initial condition with $c = 1$ and $B = 0.01$, using rigid wall boundary conditions.

illustrated in Fig. 5.1 and Fig. 5.2. For low viscosity contrast the finger competition process is strongly inhibited, and the coarsening process observed for high viscosity contrast [CM89, VnJ92] that leads to the formation of a single finger does not take place (see Figs. 1.4 and 5.2). In an attempt to clarify the issue on more rigorous grounds Casademunt and Jasnow [CJ91, CJ94] developed a topological approach to study finger competition that allowed them to get new insights on the dynamics of low $c$. They conjectured that the size of the basin of attraction of the Saffman-Taylor depended on the value of $c$. That is, the ST finger might *not* be the universal attractor of the dynamics for any viscosity contrast[1]. But then a new question arises: what is the long time behavior of the system when not attracted to a single finger? With the present computer power and the substantial progress made on the numerical algorithms for this kind of problems, it seem thus appropriate to reconsider those open questions and try to shed new light into the problem, both testing the scenario conjectured by Casademunt and Jasnow and providing a more quantitative characterization of the sensitivity to viscosity contrast. In addition, there is another fundamental reason to explore this issue with precise numerics, and is the relevance to the general question on the occurrence of topological singularities in interfacial problems. For low viscosity contrast, indeed, one observes both in experiments and simulations

[1]Note that the ST finger for $B = 0$ is an exact solution for *any* value of the viscosity contrast.

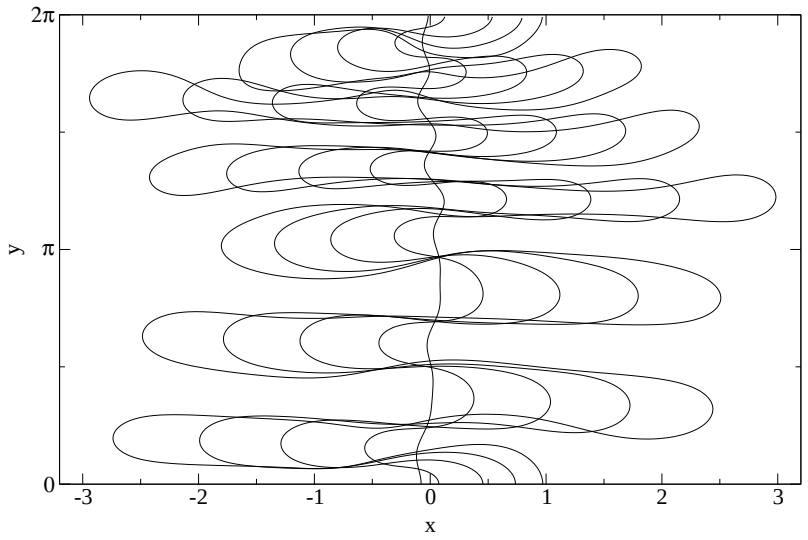


Figure 5.2: Temporal evolution of an noisy initial condition with $c = 0$ and $B = 0.01$, using rigid wall boundary conditions. The initial condition is the same of Fig. 5.1 and the curves are plotted in the mean-interface reference frame.

an enhanced tendency to interface pinchoff. While we will not specifically address the question of whether the dynamics leads spontaneously to finite-time pinchoff, we will push the idea that the tendency to pinchoff can be related to the fact that attractors with different topology coexist and compete.

Recently, the problem of Hele-Shaw flows with arbitrary viscosity contrast, that has been neglected in the literature in comparison to the high viscosity case, has received some attention also from a mathematical point of view. Howison [How00] has presented a formal technique for finding explicit solutions to the two-phase flow in a Hele-Shaw cell, with the confessed intention to drive the attention of the community to this fundamental problem.

## 5.2 The basin of attraction of the ST finger

The introduction of a viscosity contrast different from one makes the problem far more difficult to study both from a theoretical and experimental point of view. In the mathematical literature this is known as the Muskat problem [How00]. The wide classes of exact solutions for $c = 1$ (and $B = 0$) described in Chapters 2 and 3 are not available to study the dynamics with $c \neq 1$. For $c \neq 1$ the conformal mapping approach described in Appendix A only allows to obtain one time dependent exact solution, and the only avail-

able tool left to study the fully nonlinear regime is numerical computation. The reason for this increased difficulty of the $c \neq 1$ case in comparison to $c = 1$ is that, for arbitrary $c$, the two fluids are coupled, while for $c = 1$ the pressure of the fluid of negligible viscosity fluid is constant and the pressure of the viscous fluid is independent from the other one. The problem is then one-sided, as opposed to the $c \neq 1$ case, in which the pressure field in the two sides of the interface is coupled through the boundary conditions Eqs. (1.4, 1.5) and the problem is formally two-sided.

In opposition to the severe mathematical complications introduced by the viscosity contrast, an arbitrary $c$ does not introduce any special difficulties to the numerical computation, and the methods and code used for $c = 1$ can be easily generalized to $c \neq 1$. In this Chapter we will use the extension to arbitrary $c$ of the code used in Chapter 4 to study multifinger dynamics with $c \neq 1$.

The aim of the present section is to gain insights into the long time behavior of two finger dynamics with $c \neq 1$, and in particular it will focus on a partial, quantitative characterization of the basin of attraction of the Saffman-Taylor finger and the attractor (or attractors) that compete with the ST finger. To explore the basin of attraction of the ST finger it is necessary first to accurately choose appropriate initial conditions and the value of the surface tension parameter. Indeed it would be a hopeless task to aim at an exhaustive characterization of the phase space, due to its infinite dimension. It is thus crucial to devise an optimal strategy in selecting the class of interface configurations which will be most useful to elucidate the generic questions posed on the dynamics with a minimal numerical effort.

It seems clear that two-finger configurations will be adequate to study finger competition. We will choose initial conditions with two sinusoidal modes, with wave numbers $k$ and $2k$, with small amplitudes so that their growth is initially linear. Furthermore, we will choose surface tension in such a way that the two modes have exactly the same linear growth rate. This is always possible and has the great advantage that the ratio between the two mode amplitudes is kept constant as long as the dynamics is linear. Deviations of this constant ratio will directly signal nonlinear interactions. In addition, with this condition the linear growth yields a selfsimilar solution and the actual initial amplitude of the modes is thus irrelevant. The amplitude ratio is then the only parameter that spans the phase space. This one-dimensional projection is obviously a dramatic simplification but will provide useful insights. It will be made less restrictive *a posteriori* to assess the validity of the general conclusions. In any case, in this chapter we will deal with dimensionless surface tension of order unity ($B \approx 1$). Note that this range of values is the relevant one for configurations of fingers arising spontaneously

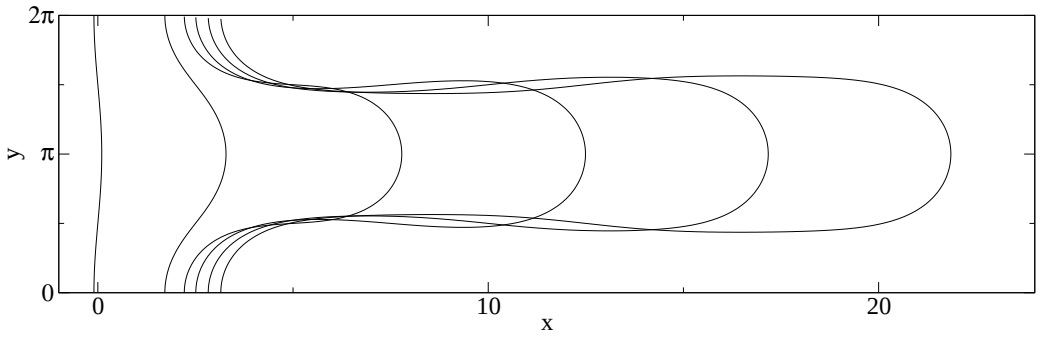


Figure 5.3: Evolution of the initial condition with a single mode ($a_1 = 0.1$ and $a_2 = 0$), with $B = 1/7$ and $c = 0.0$.

from the linear instability of the planar interface, which occur precisely at the scale where capillary and viscous forces are of the same order. We will not discuss the small surface tension limit for general viscosity contrast.

The simplest initial condition to study finger competition is thus a two-finger (or two-bump) interface, with two Fourier modes of the form

$$x(y) = -a_1 \cos(y) + a_2 \cos(2y), \tag{5.1}$$

where both $a_1$ and $a_2$ are real and positive. The form Eq. (5.1) describes an interface with one or two bumps, depending on the ratio $a_1/a_2$: if $a_1 < 4a_2$ the interface has two bumps, and one otherwise. The values of $a_1$ and $a_2$ are chosen small enough to guarantee that the initial interface is well inside the linear regime. The two modes present in Eq. (5.1) have equal growth rates for a surface tension value $B = 1/7$.

It is important to stress at this point that the evolution in the case where any of the two amplitudes is zero leads to the ST finger (single or double), regardless of viscosity contrast. The basin of attraction of the ST is thus always finite. The intrinsic differences between high and low viscosity contrast refer only to the process of finger competition, that is, they are manifest as long as unequal fingers coexist. In Fig. 5.3 we show the evolution towards the ST finger in a case with $c = 0$.

We have numerically computed the evolution of the initial condition Eq. (5.1) for various values of the viscosity contrast, surface tension and initial conditions. We have observed that for long times the interface exhibits two different kinds of configurations, illustrated in Fig. 5.4 and consistently with the two types of finger dynamics observed in Ref. [CJ91, CJ94] for the two extreme values of $c = 1$ and $c = 0$. The two types of dynamics give rise to two distinct morphologies as follows. As usually seen for high viscosity contrast, in what we call type I dynamics the leading finger screens out the

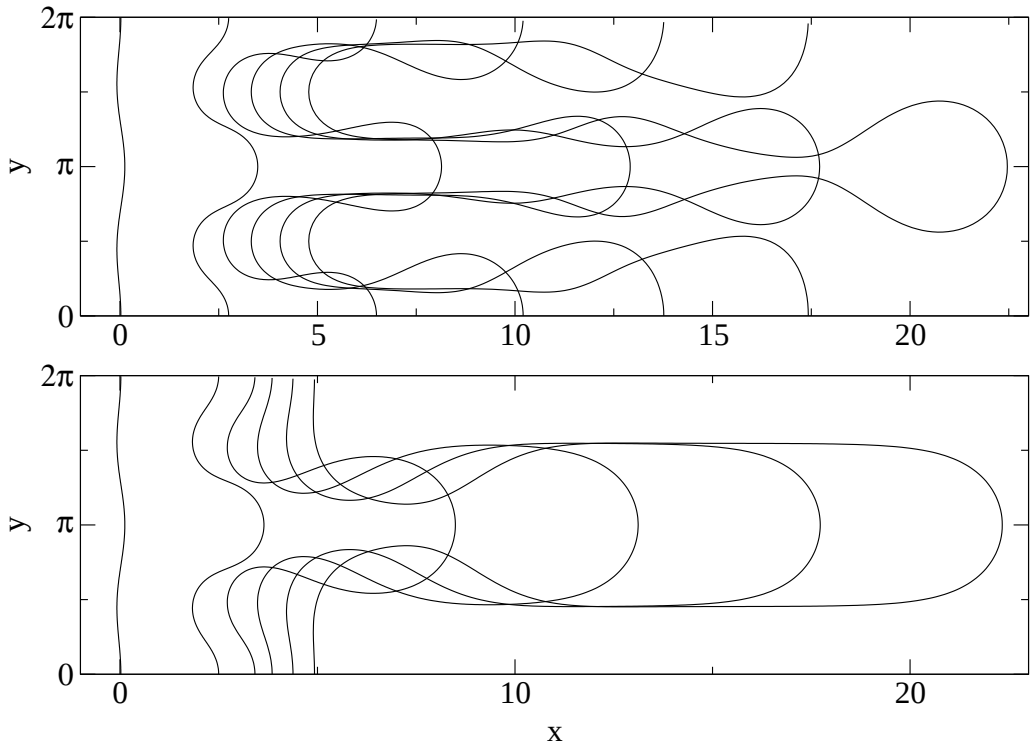


Figure 5.4: Evolution of the initial condition $a_1 = 0.05$ and $a_2 = 0.07285$, with $B = 1/7$ and $c = 0.0$ (upper plot) and $c = 0.8$ (lower plot).

trailing one by suppressing its growth rate to the point that the small finger is completely halted or exhibits a residual evolution driven by surface tension. The key defining point of type I dynamics is that the leading finger widens to attain a stationary shape close to the single-finger solution predicted by selection theory, thus absorbing all the injected flow, while the secondary finger is either completely suppressed or frozen.

In the second type of behavior (or type II), which is typical of lower viscosity contrast, the growth of the second finger is not halted, although its speed may decrease a considerable amount with respect to the speed of the large finger. At long times the large finger advances approximately at constant velocity, but with a substantial difference with respect the previous case: the finger sides bend to give rise to a narrow neck behind the leading head. This neck can become extremely narrow to the point of approaching a possible topological singularity in the form of interface pinchoff. The appearance of some sort of a neck is rather usual even for high viscosity contrast, since fingers typically develop overhangs. Indeed, at short times both fingers are substantially narrower than half the channel width, and later in

the evolution the region of the leading finger that is ahead widens also in type I competition. The key point here, however, is that the narrow neck in type II dynamics supports a vanishingly small inner flux, so that the leading head or bubble increases its area only very slowly. On the other hand, there is an amount of flux that feeds the secondary finger which then exhibits a nontrivial dynamics which persists in one way or another for all times. When a pronounced necking develops, the shape of the quasi-bubble formed is very close to the zero surface tension bubble shape described in [TS59], as will be shown in the following section. The second finger exhibits a variety of behaviors: it may or may not develop necking, and it can also present tip-splitting, but in any case it will exhibit some sort of 'persistent' dynamics. Note that the whole system is becoming more and more elongated with time so there is increasing space for the secondary finger to evolve independently of the leading tip. We have not observed any clear indication of a steady state behavior of the secondary finger in type II dynamics, although the tip region of the leading finger often reaches a practically stationary shape in a reasonably short time. The two morphologies and corresponding dynamics just introduced were described and characterized more precisely in Ref. [CJ91, CJ94] for the extreme values of $c$. Here we will see that for a given initial condition, the system will display unambiguously one of the two behaviors depending on the viscosity contrast. Remarkably the transition between the two behaviors is quite sharp, with slight changes in the value of the viscosity contrast driving the system from one kind of behavior to the other one. This is illustrated in Fig. 5.5.

With the simplest choice of surface tension $B$ described above to assure the same linear growth of the two modes, according to the linear dispersion relation Eq. (1.14), we are left, in our first analysis, with a uniparametric family of selfsimilar initial conditions in the linear regime. These are self-similar in the sense that rescaling the interface deviation from planarity by a given factor amounts to a time shift but does not change the dynamics[2], as long as the interface stays in the linear regime. The quantity we will use to parameterize the two-bump initial condition Eq. (5.1) is the ratio between the tip difference and the total width of the interface, measured as the length difference between the maximum and the minimum of the interface (see Fig. 5.6). This parameter will be called $d$, and according to its definition $d$ reads

$$d = \frac{1}{\frac{1}{2} + \frac{1}{16}\frac{a_1}{a_2} + \frac{a_2}{a_1}}. \tag{5.2}$$

[2]A rescaling of the interface height by a factor $F$ is compensated by shifting the initial time an amount $\frac{7}{6}\ln F$

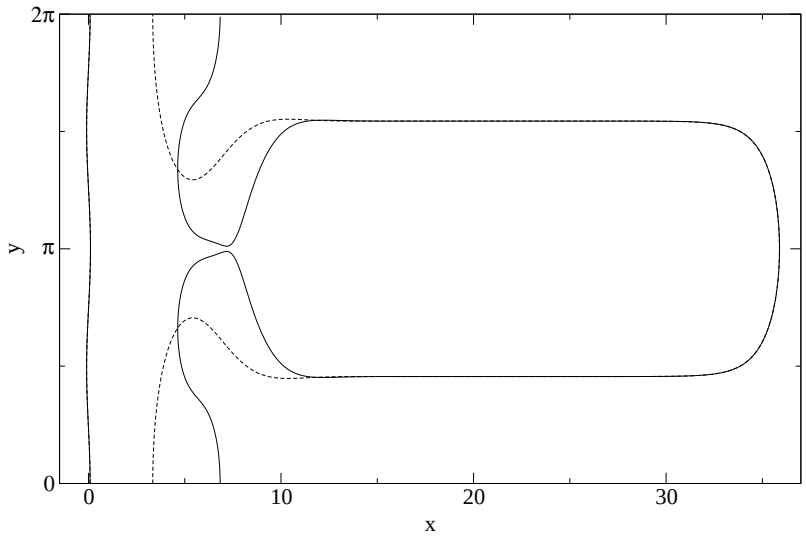


Figure 5.5: Evolution of the same two finger initial condition with $B = 1/7$, $c = 0.98$ (dashed line) and $c = 0.97$ (solid line). The width of the neck is decreasing for $c = 0.97$ but increasing for $c = 0.98$, and the secondary finger has disappeared for $c = 0.98$. The initial condition is $d = 0.1$.

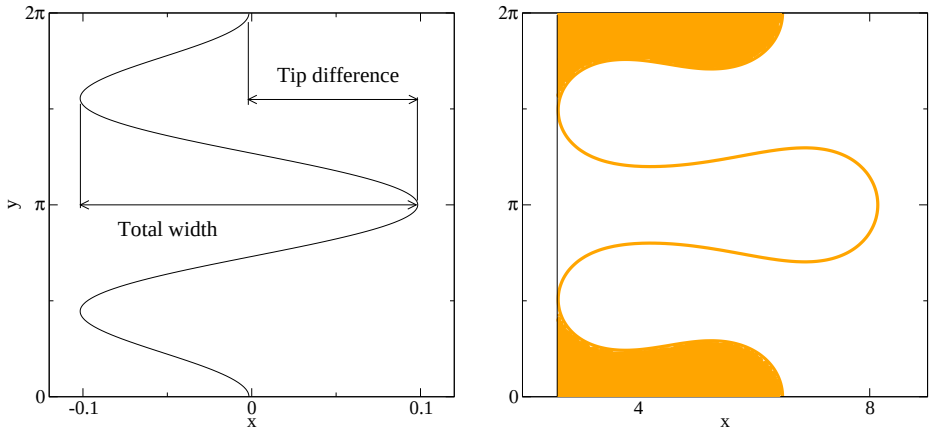


Figure 5.6: The left plot shows the distances involved in the definition of $d$: it is the ratio between the tip difference and the interface width. The right plot shows how the area of the small finger is defined (filled region).

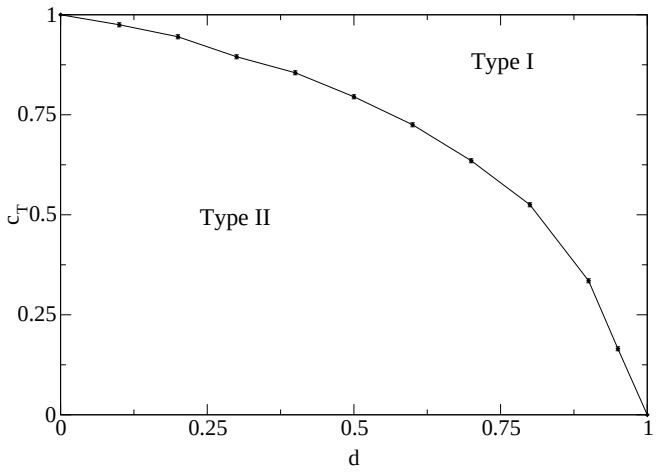


Figure 5.7: $c_T$ versus $d$, for an initial condition of the form Eq. (5.1) and surface tension $B = 1/7$.

$d$ is a function of the ratio $a_1/a_2$, and since the surface tension is chosen to make the growth rate of both $a_1$ and $a_2$ the same, $d$ remains constant throughout the linear regime. Then, the value of the viscosity contrast at which the transition between type I and type II dynamics takes place depends on the initial condition, or equivalently, is a function of the parameter $d$.

In order to study quantitatively the transition between the two types of dynamics and its dependence on the viscosity contrast it is convenient to use a precise criterion to decide whether an interface displays type I or type II dynamics. A useful quantity to measure this is the area of the small finger, or the ratio between the area of the small finger and the total area. To compute these areas the origin in the $x$ axis is placed at the minimum $x$ position of the interface, that is, the bottom of the groove (see Fig. 5.6). Then, the dynamics is of type I if the area of the small finger takes a constant value for long times, and type II otherwise. We have applied this criterion to study systematically the dependence of the viscosity contrast transition value $c_T$ on the initial condition. In Fig. 5.7 $c_T$ versus $d$ is plotted, for an initial condition of the form Eq. (5.1) and surface tension $B = 1/7$. $d = 0$ corresponds to two equal bumps, and $d = 1$ corresponds to a single bump. From the plot it can be seen that as the lengths of the two initial fingers become close to each other the viscosity contrast that drives the dynamics into the type I dynamics tends to $c = 1$. For $c = 1$, regardless of how small the initial difference in finger tip position is, the long time interface configuration consists of a steady Saffman-Taylor finger (type I). In opposition to this limit, when the length of the small finger tends to zero the type I dynamics is present for any value of

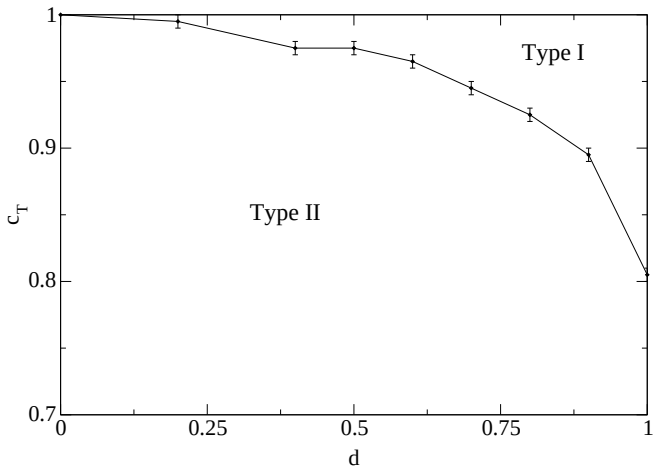


Figure 5.8: $c_T$ versus $d$, for an initial condition of the form Eq. (5.1) and surface tension $B = 1/14$.

the viscosity contrast. Then, if the initial interface consists in a single bump the long time interface will be a Saffman-Taylor finger. The convexity of the curve $c_T(d)$ shows that type II dynamics has a larger basin of attraction than type I dynamics. Furthermore, the very small slope of the boundary between the two behaviors in Fig. 5.7 when approaching $c = 1$ is telling us that the maximal sensitivity to viscosity contrast is precisely at $c \approx 1$. The physical picture of finger competition based upon laplacian screening, which is the common one for the high viscosity contrast case, happens to be less generic than the low contrast behavior. Fig. 5.7 describes the variation and sensitivity of the basin of attraction of the ST finger to viscosity contrast. It can also be viewed as a reduced, dynamical phase diagram: given a value of $c$ and $d$, it tells us whether the dynamics is attracted to the ST finger or not.

The weakly nonlinear approach developed in Ref. [ALCO01] can be applied to the present problem in order to gain some insight into the dependence of the dynamics on the viscosity contrast at the early nonlinear stages of the evolution. According to the weakly nonlinear equations, the amplitudes $a_1(t)$ and $a_2(t)$ of the two relevant modes obey the following equations

$$\frac{\dot{a}_1(t)}{a_1(t)} = \frac{6}{7}\{1 + 2c\, a_2(t) + \left[4c^2 - 1\right] a_2^2(t) - \frac{3}{4}a_1^2(t)\} \tag{5.3a}$$

$$\frac{\dot{a}_2(t)}{a_2(t)} = \frac{6}{7}\{1 + 4a_2^2(t)\}. \tag{5.3b}$$

From these equations it can be observed that the viscosity contrast reinforces

the growth of the mode $k = 1$ through a quadratic[3] coupling with the mode $k = 2$. On the contrary, for $c$ close to zero this quadratic term is small and the cubic term is negative, weakening the growth of the mode $k = 1$ in front of the mode $k = 2$. Hence, in the weakly nonlinear regime the reinforced growth of $a_1(t)$ pushes the interface towards the single finger configuration for $c$ large, and for $c$ small the growth of $a_1(t)$ is weakened and the dynamics tends to the two-finger configuration.

A change in the surface tension value yields qualitatively similar results, but now the two initial modes have different growth rates and the interface can suffer significant changes even in the linear regime: a second bump can develop from a configuration which initially had one bump if $B < 1/7$, or a bump of a two-bump configuration can be suppressed if $B > 1/7$. Then, from this simple linear regime considerations one can infer that a plot of $c_T$ versus $d$ will have a major difference from the plot depicted in Fig 5.7: for $d = 1$ (single bump) $c_T$ will be greater than zero if $B < 1/7$, one will observe both types of dynamics. In Fig. 5.8 $c_T$ versus $d$ is plotted for $B = 1/14$. As predicted, $c_T(d = 1)$ is larger than zero and for this value of $B$ it is closer to 1 than to 0. However, one must keep in mind that for $B \neq 1/7$ the linear growth rates for the two modes are different, and consequently the initial condition Eq. (5.1) is not described by a single parameter in the linear regime. Then, if we had computed $c_T(d)$ with different values of the ratio $a_1/a_2$ we would have obtained a curve different from the one of Fig. 5.8, but qualitatively equivalent. On the other hand, if $B > 1/7$ $c_T(d)$ will reach zero for $d < 1$.

An examination of Figs. 5.7 and 5.8 shows that type II dynamics occupies the larger part of the phase diagrams. In particular, for low values of $d$ the behavior of the system is type II except for viscosity contrasts very close to one. Taking into account that the fingers arising spontaneously from the linear instability of the planar interface have similar length, that is, $d$ is close to zero in real experiments, type II dynamics is the dominant behavior as long as the viscosity contrast is slightly below one. Thus, in generic situations with arbitrary viscosity contrast finger competition is absent or weak, and the ST finger may not be reached. Instead, a more complex situation arises, and attractors absent for high viscosity contrast appear. This will be discussed in the section below.

[3]Note that a quadratic term in the expression for $\dot{a}_{1,2}$ is a linear term in the RHS of Eqs. (5.3).

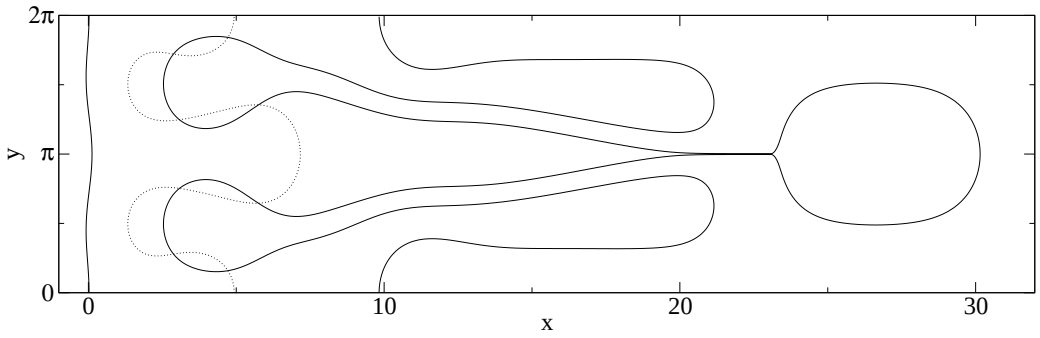


Figure 5.9: Evolution of an initial condition with $d = 0.5$, $c = 0.8$ and $B = 1/7$. The leftmost curve correspond to $t = 0$, the dotted one to $t = 4$ and $t = 16$ is the final time. Note that the secondary finger has undergone a tip-splitting.

## 5.3 Taylor-Saffman bubbles: the competing attractors

We have observed that within type II behavior in certain cases the leading finger evolves for long times to a configuration consisting of a bubble-shaped tip connected to the rest of the interface by a long, narrow neck, that can be extremely thin next to the bubble region. One of these situations can be seen in Fig. 5.9. This bubble formation process has been observed for a wide range of values of the viscosity contrast, except for values very close to 1. Formation of bubbles for low viscosity contrast has been previously reported by Ref. [TA83] in more complex interfacial configurations. Bubble shaped (closed) exact solutions do exist for $B = 0$ [TS59], and similarly to the ST finger, bubbles are also solutions with finite $B$ via a similar selection mechanism. Although the method used to compute the evolution of the interface is a sharp-interface method that does not allow the formation of a true (disconnected) bubble, the dynamics approaching the topological singularity is well described and it is thus possible that the dynamics be indeed attracted to such solutions with different topology. In this section we will compare the interfaces obtained to known bubble shaped solutions.

Taylor and Saffman [TS59] found a two-parametric family of exact solutions of the problem with zero-surface tension consisting of symmetric bubbles advancing with constant velocity $\mathcal{U}$. Its functional form is

$$x = \frac{2}{\pi}\frac{\mathcal{U}-1}{\mathcal{U}} \tanh^{-1}\left[\sin^2\left(\frac{\pi}{2}\mathcal{U}\lambda\right) - \cos^2\left(\frac{\pi}{2}\mathcal{U}\lambda\right)\tan^2\left(\frac{\mathcal{U}}{4}y - \frac{\pi}{2}\mathcal{U}\right)\right]^{\frac{1}{2}} \quad (5.4)$$

and contains two parameters, the (nondimensional) bubble velocity[4] $\mathcal{U}$ and the maximum width $\lambda$ of the bubble (measured in channel-width units). The area $S$ bounded by the interface reads [TS59]

$$S = 16\frac{\mathcal{U}-1}{\mathcal{U}^2}\tanh^{-1}\left[\tan^2\left(\frac{\pi}{4}\mathcal{U}\lambda\right)\right]. \tag{5.5}$$

In the limit $\mathcal{U}\lambda \to 1$ with $\mathcal{U}$ fixed, the area $S$ of the bubble diverges and the steady-state Saffman-Taylor finger solution is recovered. The area of the bubble does not specify $\mathcal{U}$ and $\lambda$ since Eq. (5.5) only provides one relation between them, and there exists a continuum of solutions with arbitrary speed that satisfy the area condition. Then, we encounter a selection problem fully analogous to the classical finger-width selection problem, where the zero-surface tension solution for a steadily translating Saffman-Taylor finger has an arbitrary width. Tanveer [Tan86, Tan87b] showed that the introduction of a finite surface tension removes the degeneracy in the bubble speed $\mathcal{U}$, and that families of bubbles that do not contain the symmetries present in the solution Eq. (5.4) exist.

Since the bubble-shaped region of the interface that forms for some parameter values resembles the Taylor-Saffman bubble solution, we have compared the bubble region of the computed interface with finite $B$ and the bubble given by solution Eq. (5.4). For convenience the conformal mapping version of Eq. (5.4) is used. The bubble shape in terms of the complex variable $z = x + iy$ reads [Tan87b]

$$z(s) = \ln\left(\frac{e^{is}-\alpha}{e^{is}+\alpha}\right) + \left(\frac{2}{\mathcal{U}}-1\right)\ln\left(\frac{1+e^{is}\alpha}{1-e^{is}\alpha}\right) + i\pi \tag{5.6}$$

where the constant parameter $\alpha$ takes values in the range $(0,1)$ and the interface shape is described by $0 < s < 2\pi$. The interface width is $2\pi\lambda$ and the bubble is centered along the mid-channel axis. The parameter $\alpha$ relates to $\lambda$ and $\mathcal{U}$ through the relation

$$\lambda = \frac{1}{\pi}\frac{4}{\mathcal{U}}\tan^{-1}\left(\frac{2\alpha}{1-\alpha^2}\right). \tag{5.7}$$

In Fig. 5.10 the bubble region of the computed interface with $c = 0.8$ and $B = 1/14$ is plotted together with the interface obtained from Eq. (5.6) with $\mathcal{U} = 1.8243$ and $\alpha = 0.938216$. The parameter values $\mathcal{U}$ and $\alpha$ have been chosen by imposing that $\lambda$ is equal to the computed width of the bubble

[4] If $c \neq 1$ the bubble velocity $\mathcal{U}$ has to be replaced in Eq. (5.4) by a more complicate expression, that can be found in Ref. [TS59].

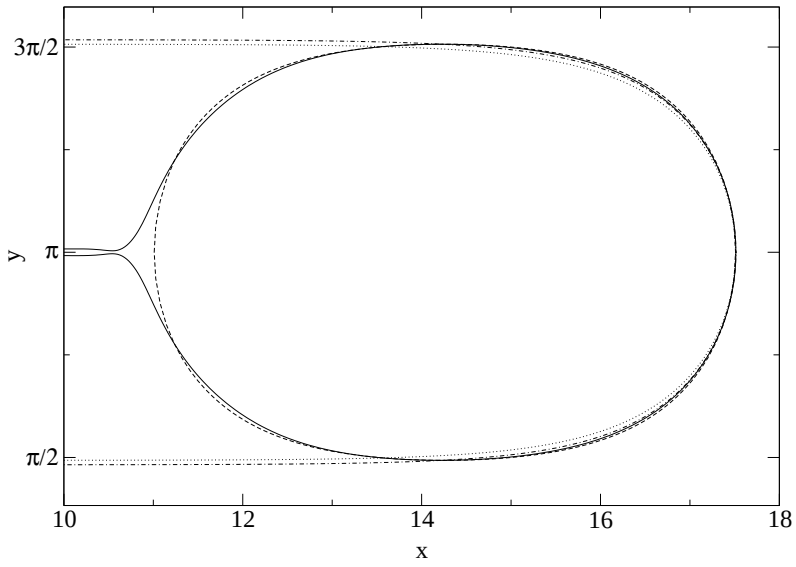


Figure 5.10: Bubble region of the computed interface with an initial condition $a_1 = 0.05$, $a_2 = 0.0788555$, $c = 0.8$ and $B = 1/14$ at time $t = 9.4$ together with the interface obtained from Eq. (5.6) with $\mathcal{U} = 1.8243$ and $\alpha = 0.938216$. The dotted curve is the profile of the ST finger with $\lambda = 0.50698$ and the dashed-dotted curve corresponds to $\lambda = 0.517863$. This last curve has the same tip curvature than the original interface.

and then the length of the analytical solution has been adjusted in order to get a good agreement between the two interfaces. From the plot it can be seen that the analytical solution Eq. (5.6) describes the computed interface to a high degree of accuracy, and the only part of the computed bubble that significantly differs from the solution is the tail that connects the bubble to the rest of the interface. The agreement between the two curves is remarkable taking into account that Eq. (5.6) is a zero-surface tension solution. We have also tried to fit the Saffman-Taylor finger to the right half of the computed bubble, but the agreement is not as good as the one obtained with the bubble solution. In Fig. 5.10 two Saffman-Taylor fingers are plotted, using two different criteria to choose the value of the asymptotic width of the finger. First, the asymptotic width has been chosen equal to the width of the bubble, and we have obtained a poor agreement between the two curves. A better agreement is obtained imposing that the curvature of the finger and the curvature of the bubble are equal at the tip, but even in this case the solution Eq. (5.6) is a better fit of the computed interface. However, for larger bubble areas the fit by a Saffman-Taylor finger improves since Eq. (5.4) tends to the Saffman-Taylor finger solution for $S \to \infty$. In addition, the region around

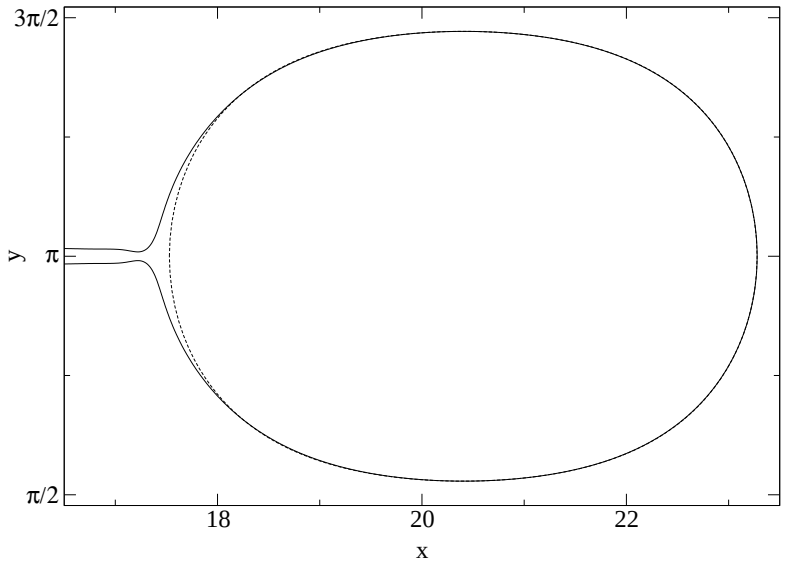


Figure 5.11: Bubble region of the computed interface with initial condition $a_1 = 0.038223$, $a_2 = 0.00972855$, $c = 0.5$ and $B = 0.01$ at time $t = 9.9$ together with the interface obtained from Eq. (5.6) with $\mathcal{U} = 1.975$ and $\alpha = 0.8969$

the tip is usually well fitted by ST fingers, but these do not fit well lateral walls of the bubble, except for very long ones.

In Fig. 5.11 the bubble region of an evolution with $c = 0.5$ and $B = 0.01$ is plotted together with the analytical bubble with $\mathcal{U} = 1.975$ and $\alpha = 0.8969$, and in this case the agreement between the two curves is much better than in the previous case because the value of the surface tension is smaller in this case. The excellent agreement between the bubble region of the computed interface and the Taylor-Saffman bubble indicates that the interface is being attracted to the Taylor-Saffman bubble fixed point. In addition, this also suggests that the dynamics of the bubble-shaped region is almost independent of the rest of the interface. Not, however, that through the neck that connects the two parts of the interface there is a residual finite flux of fluid that allows a slight increase of the bubble area. This variation is slow enough to keep it very close to a stationary solution on the time scale of interface displacement.

The area of the bubble shaped region, for a given $B$ and $c$ depends also on the particular initial condition. This is illustrated in Fig. 5.12, where the evolution of two different initial conditions but with same values of $B$ and $c$ is plotted. The area of the two bubble shaped areas, although not very well formed, is clearly distinct, showing that the two evolutions are being attracted, at least during a certain time, to different bubble fixed

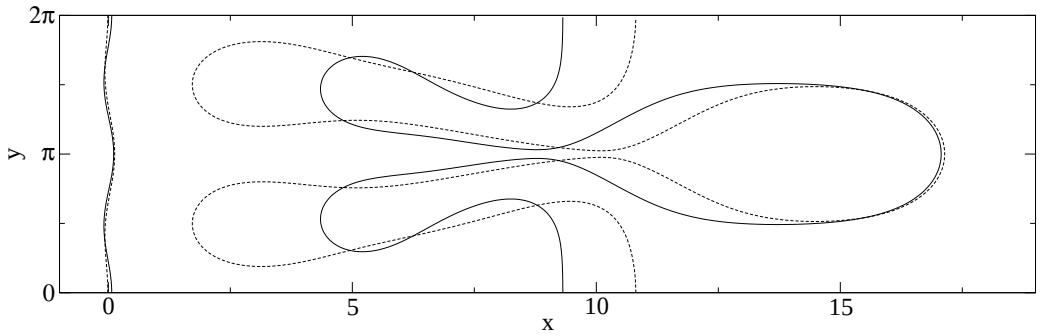


Figure 5.12: Evolution of two different initial conditions with $a_1 = 0.02$, $a_2 = 0.08972$ (solid line) and $a_1 = 0.07$, $a_2 = 0.05988$ (dashed line). The viscosity contrast is $c = 0.8$ and surface tension is $B = 1/14$. The final times are $t = 9.25$ (solid line) and $t = 8.0$ (dashed line).

points. Apparently, the area of the bubble changes continously with the initial condition, and the bubble region is being attracted to different points of the continuum of Taylor-Saffman solutions.

The fate of the bubble region is a critical issue to elucidate the long time asymptotics of the problem. Two relevant aspects of the bubble dynamics are its eventual, finite-time pinchoff from the rest of the interface and/or its asymptotic area (finite or infinite) at long times. If the bubble area tends to infinity as $t \to \infty$ then the attractor of the system is the Saffman-Taylor finger, not the Taylor-Saffman bubble, although the system follows a path in phase space that stays very close to the continuum of fixed points corresponding to the bubble solutions with varying area. This issue will be discussed in more detail in Sec. 5.4. The eventual pinchoff of the interface at finite time would obviously imply that the system will end up in one of the bubble solutions. However, even if the dynamics does not yield a finite-time pinchoff, the attractor could in practice be one of the bubble solutions as long as the enclosed area would be bounded. Interface pinchoff has been a subject of major interest in fluid dynamics in recent years [Egg97], not only for its relevance to practical applications but also as a problem where a high degree of universality is present. There exists strong evidence of the existence of finite time pinchoff of the interface in Hele-Shaw flows [GPS98, Alm96], but in setups different from the one studied here. It would be interesting then to get some insight concerning the possible existence of pinchoff in our system although a general answer to this question is much beyond the scope of this thesis.

In Fig. 5.13 it is plotted the evolution of the area of the bubble region for various values of the viscosity contrast. From the plot it is difficult to draw a

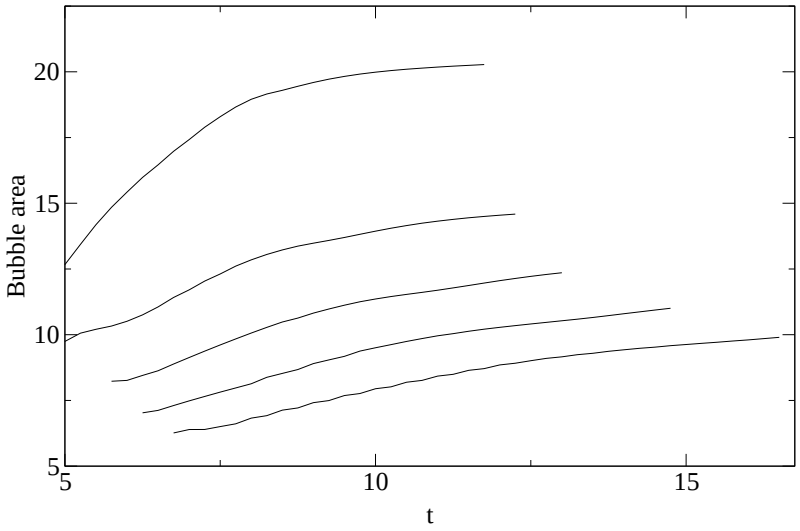


Figure 5.13: Area of the bubble region vs. time for $B = 1/14$, for various values of $c$. The curves correspond to the following values of viscosity contrast, from bottom to top: $c = 0.0$, $c = 0.2$, $c = 0.4$, $c = 0.6$ and $c = 0.8$. The initial condition is the same for the five curves: $a_1 = 0.07$, $a_2 = 0.0598861$.

clean conclusion. The area of the bubble is clearly increasing, and at the same time its growth rate decreases, but unfortunately the computational cost of running the code for even longer times makes not possible to elucidate if the area of the bubble will saturate or will diverge as $t \to \infty$. For high $c$, the area of the bubble is clearly increasing more slowly than for low $c$. The reason is that the bubble at a given time is better formed (the neck is narrower) for high $c$, and for low $c$ more time is necessary to form a narrow neck and the corresponding bubble. Our computations show that, for a given initial condition, as the viscosity contrast is decreased, the area of the bubble gets smaller, as can be seen in Fig. 5.13. A possible explanation for this behavior is the following: according to our results, the bubble gets formed in the region of the leading finger that is ahead, and its area will depend on the distance between the tips of the fingers, with larger bubbles forming when the tip distance is larger. Since for low viscosity contrast the velocity of the trailing finger is larger than for high viscosity contrast, the tip distance at the time when the fingers are well developed and the interface is in the fully nonlinear regime (when the bubble forms) is larger for high viscosity contrast, causing the formation of a larger bubble. In addition, we have also observed that large bubbles form sooner than small ones, and this also explains why for low $c$ the bubbles need more time to form than for large $c$.

As mentioned above, the occurrence of topological singularities is relevant

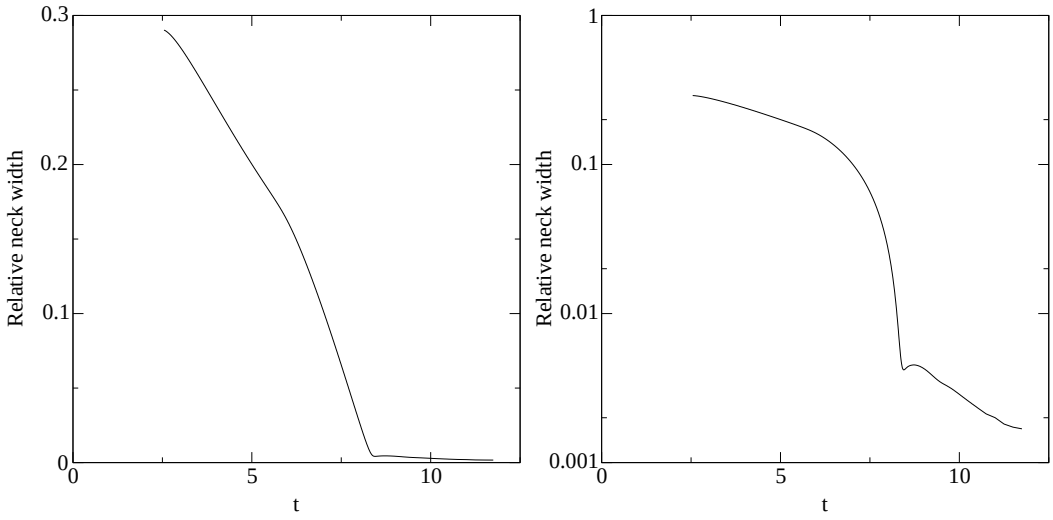


Figure 5.14: Relative neck width versus time, with initial condition $d = 0.5$, $c = 0.8$ and $B = 1/7$. The relative neck width is the ratio between the neck width and the channel width

in a much wider context. Unfortunately, the numerical approach we have used, although well-suited for computing the evolution of the whole interface in an efficient and accurate manner is not optimal to deal with the pinchoff[5] with the desired accuracy, and only can give information about how the (eventual) pinchoff of the interface is approached. An example of this is shown in Fig. 5.14, where the width of the neck that connects the bubble-region to the rest of the interface is plotted as a function of time. Two distinct regimes are observed. The first one starts as soon as the neck (or overhang) appears, and during this initial regime the width decreases quite fast until it reaches a value close to zero: this is the regime where the bubble gets formed. Next, the width reaches a local minimum and enters the second regime, characterized by the slow decrease of the neck width. This second regime corresponds to the situation where the area of the bubble is quasi-stationary and apparently the neck has no dynamical role. The computation cannot be continued much further because the numerical cost of increasing the number of points that describe the interface is too high.

The fate of the neck is unclear from our results and none of the three possible scenarios, namely, pinchoff at finite time, pinchoff at infinite time and no pinchoff can be discarded. On the other hand, Almgren [Alm96] has found strong evidence of the existence of finite time pinchoff in a situation

[5] If such pinchoff took place.

without fluid injection—the pinchoff is driven by surface tension. Then, it may be expected that in our situation pinchoff is probable. In any case, it is clear that the tendency towards pinchoff from a situation which is clearly far apart from it, seems indeed to be generic in the problem.

## 5.4 Discussion and concluding remarks

We have shown that the Saffman-Taylor finger is not the universal attractor of the problem with arbitrary viscosity contrast, in opposition to the $c = 1$ case, where the ST finger fixed point is the unique attractor. The size of its basin of attraction depends on the viscosity contrast, and drops very fast as one departs from the very neighborhood of $c \approx 1$, getting very small for $c = 0$. In particular, for fingers of similar length the ST finger is the attractor only for values of $c$ very close to one. Since in real situations the fingers arising from the planar interface are of comparable length, the Saffman-Taylor finger is not attained in generic situations with arbitrary viscosity contrast.

The alternative set of attractors to the Saffman-Taylor finger is a rather complicate object. First of all, it is not at all clear that the very concept of an attractor is justified in the problem, due to the fact that the system is unbounded in space. At most one can state that parts of the system (in this case the leading fingertips) do appear attracted to certain stationary solutions, but not the system as a whole. In many cases we have observed that the system evolves towards an interface configuration with a bubble-shaped leading 'finger' that is extremely similar to the $B = 0$ exact bubble solution found by Taylor and Saffman [TS59], but with trailing fingers that have some dynamics. In other cases the interface does not develop a clear bubble-shaped region, and apparently does not reach a steady state during the computation time. However, the latter behavior might not imply the existence of a different attractor, but only that the system needs a longer time to reach the Taylor-Saffman bubble attractor. The Taylor-Saffman attractors present also important differences from a conceptual point of view with respect to the well-known Saffman-Taylor finger: for the ST fixed point, given a value of $B$ and $c$ the fixed point is unique, only one value of the width $\lambda$ is observed. But the situation is different for the Taylor-Saffman bubbles: given $B$ and $c$, an additional parameter is needed to determine the width $\lambda$ (or equivalently, the velocity) of the bubble. This additional quantity is the area of the bubble, that in general depends on the initial condition and is a result of the details of the evolution. In Fig. 5.12 we have shown how two different initial conditions lead to bubble shapes apparently with different areas.

Therefore, the Taylor-Saffman bubble solutions constitute a continuum[6] of solutions the bubble region is attracted to, with the area of the bubble varying continously. In the case of two-finger configurations, depending on initial conditions and parameters the leading finger will generically be attracted to a bubble solution of a certain size. The existence of topological singularities, or at least the tendency to develop a narrow neck that approaches pinchoff can thus be related to the fact that the relevant attractor is a closed bubble, with a different topology (implying a transition between simple connected to multiply connected domains). Note that whether the area of the bubble approached saturates to a finite value or this area drifts slowly towards larger sizes is not particularly relevant to the discussion of the generic types of dynamics. The distinction between type I and type II dynamics occurs in a relatively short time scale (corresponding to reasonable observation times both in simulations and possible real experiments) and only if the pinchoff is somehow impeded or frustrated, an extremely slow dynamics may eventually drive the bubble towards the ST finger.

Finally, in the previous discussion we have only considered single-bubble isolated solutions but N-bubble exact[7] solutions do also exist [Vas01b], introducing further complexity to the scenario: an arbitrary initial condition (with an arbitrary number of fingers) could be attracted to one of these multibubble solutions, or even to solutions with coexisting bubbles and fingers.

[6]Here the continuum is referred to the uniparametric (with given $B$) family spawned by the bubble area. Each value thus corresponds to a different problem, and therefore the degeneracy is not the analogue of the continua of fixed points discussed in Part II.

[7]These are exact solutions for $B = 0$, but they should survive to the introduction of finite surface tension, probably through a reduction of the dimensionality of the parameter space of the exact solutions, analogously to what occurs with the Saffman-Taylor finger or bubble solutions [Tan86, Tan87b]

# Part IV

# Inhomogeneous gap

# Chapter 6

# Interface equation for an inhomogeneous Hele-Shaw cell

A theoretical model of viscous flows in a Hele-Shaw cell with arbitrary space-dependent gap between plates is developed. The formalism is exact within the assumption of local Darcy flow. An explicit fully nonlocal interface equation is derived for small displacements from planarity, which is systematic in the nonlinearities of a weakly nonlinear expansion of the problem (including both local and nonlocal nonlinear terms) and perturbative to first order in the gap fluctuations (noise). The equation contains both conserved and nonconserved noise terms. We also derive a contribution of the noise that exhibits long range correlations both in time and space. All different noise contributions are explicitly related to the 'microscopic' gap variations and the 'bare' parameters.

## 6.1 Formulation

Consider a Hele-Shaw cell with an inhomogeneous gap spacing $b = b(x, y)$ which fluctuates around a mean value $b_0$. If the gap $b$ varies slowly enough, that is, if $|\nabla b| \ll 1$ then we can assume that the usual Darcy's law for the flow in a Hele-Shaw cell is locally valid. This assumption of local Darcyan flow is the starting point of our formulation. This will allow us to derive explicitly the full interface equation in term of the original 'bare' parameters and the explicit space dependence of the gap, which may be controlled experimentally at the 'microscopic' level. In case of more abrupt variations of the gap one can presume that the same type of contributions will be present with the appropriate coarse-grained parameters. It is worth remarking here, however, that one of the big advantages of our formulation is precisely to

avoid a coarse-graining procedure, and therefore have a perfect control of the derivation. This will be useful to elucidate the different types of contributions that must be considered, and which may completely escape a phenomenological approach to the problem. The underlying philosophy of this approach is similar to the work of Cuerno *et al.* [CC01] in trying to clarify similar problems in the context of interface growth. The analysis is also directly motivated by the experiments made recently on Hele-Shaw cells with random but controlled gap variations by Soriano *et al.* [SOHM02b].

The assumption of local Darcy flow reads

$$\mathbf{v} = -\frac{b(x,y)^2}{12\mu}\nabla p. \tag{6.1}$$

If we now impose the incompressibility of the full 3D flow, which is the physical requirement in the usual case of incompressible fluids, then the requirement $\nabla \cdot \mathbf{v}_{3D} = 0$ yields, in terms of the two-dimensional (z-averaged) velocity field the condition

$$\nabla \cdot (b\mathbf{v}) = 0. \tag{6.2}$$

The consideration of the incompressibility of the flow in three dimensions has important consequences regarding the conservation of the interface displacement from planarity (hereinafter referred to as interface height) in the problem of fluid invasion, as shown in Sec. 6.2. Fluid conservation as described in Eq. (6.2) will imply that the interfacial height is *not* a conserved field variable, contrary to what is often assumed in the literature.

The substitution of Darcy's law into Eq. (6.2) yields the equation satisfied by the pressure $p$ in the bulk of the fluid

$$\nabla^2 p + \frac{3\nabla b}{b} \cdot \nabla p = 0. \tag{6.3}$$

Eq. (6.3) differs from Laplace equation valid in the usual case of homogeneous gap, so the pressure is not a harmonic function. The gap can be expressed as $b = b_0 + \delta b(x,y)$, where $b_0$ is the average value of the gap with $\nabla \delta b(x,y)$ small, and the pressure can be expressed as $p = p_0 + \delta p$ with $p_0$ being the value of the pressure computed with $b = b_0$ ($\delta b = 0$). The separation of the pressure in two contributions, a laplacian part ($p_0$), and the remaining (nonlaplacian) part of the pressure ($\delta p$) will make easier to obtain an approximate solution to Eq. (6.3). Eq. (6.3) then reads:

$$\nabla^2 (p_0 + \delta p) + \frac{3\nabla b}{b} \cdot \nabla (p_0 + \delta p) = 0, \tag{6.4}$$

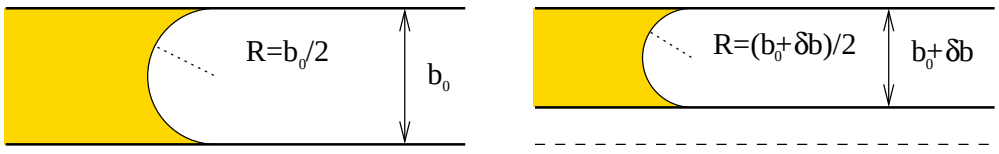


Figure 6.1: Scheme of the curvature variation due to a gap change

and taking into account that $\nabla^2 p_0 = 0$ and that the term $\frac{3\nabla b}{b}\cdot\nabla\delta p$ is negligible compared to the other terms since $\delta p$ is formally of order $|\nabla b|$, the bulk equations read

$$\nabla^2 p_0 = 0 \tag{6.5a}$$

$$\nabla^2\delta p + \frac{3\nabla b}{b}\cdot\nabla p_0 = 0. \tag{6.5b}$$

The term that has been neglected is of order $|\nabla b|^2$. This approximation is fully consistent with the fact that higher order corrections have already been neglected in the assumption of local Darcy flow.

The usual boundary condition on the interface is given by the Young-Laplace pressure jump condition, $p_2 - p_1 = \sigma\kappa$. Fluid 1 displaces fluid 2, and the curvature is defined with the criterion that a bubble has negative curvature. Curvature $\kappa$ contains both the curvature of the interface in the plane of the cell and in the plane perpendicular to the plates, that is, the curvature of the meniscus. If the gap is constant the latter term is also constant and can be absorbed in the definition of the pressure, but with inhomogeneous gap it has an important contribution. Fig. 6.1 depicts schematically the effect of the gap variation on the meniscus curvature. Then, the Laplace pressure drop condition reads

$$p_2 - p_1 = \sigma(\kappa_\parallel + \kappa_\perp) = \sigma\left(\kappa_\parallel + \frac{2\cos\theta}{b_0 + \delta b}\right) \tag{6.6}$$

where $\theta$ is the contact angle between the meniscus and the plates, with $\cos\theta = 1$ meaning perfect wetting of the invading fluid. From now on we will consider the static approximation for $\theta$: the contact angle is considered to be constant along the interface and throughout its evolution. Boundary condition Eq. (6.6) is supplemented by the kinetic boundary condition, that states that the normal velocity on the interface is the same for the two fluids, and equal to the velocity of the interface

$$v_n = -\frac{b^2}{12\mu_1}\partial_n p_1 = -\frac{b^2}{12\mu_2}\partial_n p_2. \tag{6.7}$$

To complete the problem an additional condition is needed, the velocity at $y \to \infty$ if we are considering constant injection rate or the pressure at $y = y_0$ if we are dealing with the constant pressure case.

Eqs. (6.5,6.6, 6.7) together with the boundary conditions at infinity[1] completely specify the free-boundary problem we are interested in. A common strategy is now to project the full dynamics into the interface degrees of freedom, writing a nonlocal equation for the interface location.

Eqs. (6.5) are solved using the following scheme: Eq. (6.5a) is solved applying the boundary condition Eq. (6.6) by any of the standard methods, since the only difference with the problem with constant gap is that the boundary condition Eq. (6.6) has an additional term containing the disorder $\delta b$. Once the pressure field $p_0$ is known, the Poisson equation (6.5b) for $\delta p$ can be solved, with the boundary condition $\delta p = 0$. Note that the simplest boundary condition $\delta p = 0$ can be used because the pressure drop due to surface tension was taken into account in the solution of $p_0$. Once $\delta p$ is known the velocity at the interface is determined using Darcy's law:

$$v_n = -\frac{(b_0 + \delta b)^2}{12\mu}\partial_n p_0 - \frac{(b_0 + \delta b)^2}{12\mu}\partial_n \delta p. \tag{6.8}$$

This last equation (6.8), together with Eqs. (6.5) and (6.6), completes our formulation of the interfacial evolution in a Hele-Shaw cell with inhomogeneous gap, where the only approximation considered is the local Darcy flow condition.

The solution of the Poisson equation (6.5b) can be obtained in terms of the Green function $\mathrm{G}(x - x', y - y')$ of the Laplace equation and $p_0$ as

$$\int dx'dy'\mathrm{G}(x - x', y - y')\frac{3\nabla b}{b}\nabla p_0 = \int_{\mathrm{int}} ds'\mathrm{G}[x - x(s), y - y(s)]\frac{\partial \delta p}{\partial n} \tag{6.9}$$

where it has been used that $\delta p$ is zero on the boundaries (including the interface). This will be used in the following section to obtain the explicit interface equation.

## 6.2 Forced fluid invasion

We are interested in the particular case of a more viscous fluid displacing the less viscous one at a constant injection rate $V_\infty$ in a cell with a noisy gap, being $\delta b$ a quenched disorder[2]. In this configuration of the problem

[1] Or at a given height if we are dealing with the constant pressure case.

[2] The case of fluid imbibition, with injection at constant pressure, will not be discussed explicitly here but most of our results can be easily adapted to that case

the planar interface is stable in the absence of disorder, but the presence of noise roughens the interface through different mechanisms associated to both capillary and viscous forces. We will restrict ourselves to quasi-planar interfaces with weak noise. The gap has the form $b^2 = b_0^2[1 + \zeta(x, y)]$ where the noise[3] has zero mean, $\langle \zeta(x, y) \rangle = 0$, and correlation $\langle \zeta(x, y)\zeta(x', y') \rangle = C(x - x', y - y')$. In addition, $|\zeta(x, y)|$ is assumed to be sufficiently small to keep only linear contributions in the noise. The gap variation $\delta b$ introduced in the previous section reads in terms of the noise as $\delta b \simeq b_0\zeta/2$.

### 6.2.1 Derivation of the interface equation

The linearized equation for the interface height $h(x, t)$ in the absence of noise is well known, see for instance Ref. [ALCO01], and reads

$$\frac{\mathrm{d}h(x,t)}{\mathrm{d}t} = cV_\infty \mathrm{H}\left[-\frac{\partial h(x',t)}{\partial x'} + \tilde{B}\frac{\partial^3 h(x',t)}{\partial^3 x'}\right](x) + V_\infty \tag{6.10}$$

where $c$ is the viscosity contrast[4], $\tilde{B}$ is a surface tension parameter defined as $\tilde{B} = \sigma b^2/[12(\mu_1 - \mu_2)V_\infty]$, and $\mathrm{H}[f](x)$ is the Hilbert Transform defined as

$$\mathrm{H}[f](x) = \frac{1}{\pi} P \int_{-\infty}^{\infty} dx' \frac{f(x')}{x' - x} \tag{6.11}$$

where $P$ denotes Cauchy's principal value. A systematic weakly nonlinear expansion of the full unperturbed problem has been developed recently in Ref. [ALCO01]. Since we are mostly focussed in determining the different noise contributions, we will restrict the deterministic part to the contributions linear in $h$ for simplicity, and add the nonlinear ones later. To obtain the linearized equations from the full equations with noise the method described in Ref. [ALCO01] will be used. A straightforward computation yields the following expression for $\dot{h}(x, t)$:

$$\begin{aligned}\frac{\mathrm{d}h(x,t)}{\mathrm{d}t} = V_\infty \left\{1 - c\mathrm{H}\left[\frac{\partial h(x',t)}{\partial x'} - \tilde{B}\frac{\partial^3 h(x',t)}{\partial^3 x'}\right](x)\right\} + \\ V_\infty \left\{\frac{\tilde{B}\cos\alpha}{b_0}\mathrm{H}\left[\frac{\partial \zeta(x',h)}{\partial x'}\right] + \zeta(x,h)\right\} + \delta v_\zeta(x,h),\end{aligned} \tag{6.12}$$

[3] We will refer to the gap variation as noise, characterized by its statistical properties just to adapt the language to the problem of fluid invasion of (random) porous media. However, the derivation is valid for any arbitrary form of $\zeta(x, y)$.

[4] Note that in Eq. (6.10) the viscosity contrast is negative since the more viscous fluid displaces the less viscous one.

where only linear terms on $h$ and $\zeta$ are considered.

The noise $\zeta$ appears in three different places in the above equation for the temporal evolution of $h(x,t)$. First, a term proportional to $\mathrm{H}[\frac{\partial\zeta(x',t)}{\partial x'}]$ that is the lowest order contribution from the pressure field $p_0$ resulting from the variation of the perpendicular curvature at the interface, that is, it comes from Eq. (6.6). This term will be named capillary noise. Its derivation is straightforward applying the formulation of Ref. [ALCO01]. The second contribution of the noise is the trivial multiplicative term that has its origin in the factor $\frac{\delta b^2}{12\mu}\nabla p_0$ in Eq. (6.8). This contribution will be termed permeability noise. The third noise term $\delta v_\zeta(x,h(x))$ comes from the term $\nabla\delta p$ in Eq. (6.8) and will be called bulk noise, since it contains the effect of the noise in the fluid region or bulk and not only on the interface. The derivation of this term will be shown next for $c=-1$.

First, we define $\mathbf{v}_0$ as $\mathbf{v}_0 = -\frac{b_0^2}{12\mu}\nabla p_0$ and the bulk noise $\delta v_\zeta$ as $\delta v_\zeta = -\frac{b_0^2}{12\mu}\frac{\partial\delta p}{\partial n}$. Using these definitions and recalling Eq. (6.9), the bulk noise satisfies:

$$\int_{int} ds'\mathrm{G}[x-x(s),y-y(s)]\delta v_\zeta(s) = \int dx'dy'\mathrm{G}[x-x',y-y']\frac{3\nabla b}{b}\cdot\mathbf{v}_0, \quad (6.13)$$

where the integration region of the rhs integral is the viscous fluid region and the integration path of the lhs integral is the interface, since we have $\delta v_\zeta = 0$ at at $y\to-\infty$. Now, since we are interested in the value of $\delta v_\zeta$ on the interface, we have $y=h(x)$ and $ds=\sqrt{1+(\partial_{x'}h)^2}dx'$. Moreover,

$$\frac{3\nabla b}{b}\mathbf{v}_0 \simeq \frac{3}{2}\nabla\zeta\cdot\mathbf{v}_0 \simeq \frac{3}{2}\nabla\zeta\cdot V_\infty\hat{\mathbf{y}} = \frac{3}{2}\frac{\partial\zeta}{\partial y}V_\infty \quad (6.14)$$

where we have considered only the leading order (linear) contribution, neglecting terms of order $\partial_x h\nabla\zeta$. Eq. (6.13) now reads

$$\int_{-\infty}^{\infty} dx'\sqrt{1+\left(\frac{\partial h(x')}{\partial x'}\right)^2}\mathrm{G}[x-x',h(x)-h(x')]\delta v_\zeta(x') = \frac{3V_\infty}{2}\int_{-\infty}^{\infty}dx'\int_{-\infty}^{h(x')}dy'\mathrm{G}[x-x',h(x)-y']\frac{3V_\infty}{2}\frac{\partial\zeta}{\partial y}. \quad (6.15)$$

We will use the expression of the Laplace Green function in the free space, that is, considering a channel of infinite width or equivalently assuming that the walls have a negligible influence on the dynamics. It reads $\mathrm{G}(x-x',y-y') = \frac{-1}{4\pi}\ln[(x-x')^2+(y-y')^2]$. Now we can integrate by parts the integral on $y$ of the RHS of Eq. (6.15) and imposing that the noise vanishes at infinity,

$\zeta(x, y \to -\infty) = 0$, the integral equation (6.15) reads

$$\int_{-\infty}^{\infty} dx' \sqrt{1 + \left(\frac{\mathrm{d}h(x')}{\mathrm{d}x}\right)^2} \ln\left[(x-x')^2 + (h(x) - h(x'))^2\right] \delta v_\zeta(x') = \frac{3V_\infty}{2} \int_{-\infty}^{\infty} dx' \ln\left[(x-x')^2 + (h(x) - h(x'))^2\right] \zeta(x', h(x')) - \frac{3V_\infty}{2} \int_{-\infty}^{\infty} dx' \int_{-\infty}^{h(x')} dy' \frac{2(h(x') - y')}{(x-x')^2 + (h(x) - y')^2} \zeta(x', y'). \quad (6.16)$$

We keep the lowest order in the interface deviation $h - V_\infty t$ with respect to the mean interface, dropping terms of order $(h - V_\infty t)\zeta$, and apply the substitution $y = y' - V_\infty t$

$$\int_{-\infty}^{\infty} dx' \ln|x - x'| \delta v_\zeta(s') = -\frac{3}{2} V_\infty \int_{-\infty}^{\infty} dx' \ln|x - x'| \zeta(x', h) - \frac{3}{2} V_\infty \int_{-\infty}^{\infty} dx' \int_{-\infty}^{0} dy \frac{-y}{(x-x')^2 + y^2} \zeta(x', y + V_\infty t). \quad (6.17)$$

Then, to obtain an explicit expression for $\delta v_\zeta$ the Fourier transform is applied to both sides of Eq. (6.17). First, we recall the following results: the Fourier transform $\mathcal{F}$ of $\ln|x|$ is [RY90]

$$\mathcal{F}[\ln|x|](k) = \frac{-\pi}{|k|} - 2\pi(\gamma + \ln\ 2\pi)\delta(k) \quad (6.18)$$

where $\gamma$ is Euler's constant, and the Fourier transform $\mathcal{F}$ of the other term of Eq. (6.17) reads

$$\mathcal{F}\left[\frac{-y'}{(x-x')^2 + y'^2}\right](k) = \pi e^{-ikx'} e^{y'|k|}, \quad (6.19)$$

where $y' < 0$. Using Eqs. (6.18) and (6.19) we obtain the following expression for $\widehat{\delta v_\zeta}(k)$, the Fourier transform of $\delta v_\zeta(x)$:

$$\widehat{\delta v_\zeta}(k) = \frac{3V_\infty}{2} \left\{ -\hat{\zeta}(k) + |k| \int_{-\infty}^{\infty} dx' \int_{-\infty}^{0} dy \zeta(x', y + V_\infty t) e^{-ikx'} e^{y|k|} \right\} \quad (6.20)$$

where $\hat{\zeta}(k)$ is the Fourier transform of $\zeta(x, h(x))$. $\widehat{\delta v_\zeta}(k)$ has two contributions, a local nonconserved noise term proportional to $\hat{\zeta}(k)$ whose form is the same of the permeability noise appearing in Eq. (6.12) but with opposite sign, and a nonlocal, long-ranged noise term $\hat{\Omega}_{LR}(k, t)$ defined as

$$\hat{\Omega}_{LR}(k, t) = \frac{3V_\infty}{2} |k| \int_{-\infty}^{\infty} dx' \int_{-\infty}^{0} dy \zeta(x', y + V_\infty t) e^{-ikx'} e^{y|k|}. \quad (6.21)$$

that contains the contribution of the noise in the fluid region below the (mean) interface. This means that the evolution of the interface has a contribution from the disorder in the bulk of the fluid and not just from the disorder at the interface. Note that $\hat{\Omega}_{LR}(k,t)$ is effectively an annealed (time-dependent) noise, and that it does not depend on $h$ but only on its mean value in the absence of disorder, that is $\bar{h} = V_\infty t$. The validity of this approximation will be discussed below. The noise $\hat{\Omega}_{LR}(k,t)$ can be better understood by computing the quantity $\langle \hat{\Omega}_{LR}(k,t)\hat{\Omega}_{LR}(k',t')\rangle$. It reads

$$\langle \hat{\Omega}_{LR}(k,t)\hat{\Omega}_{LR}(k',t')\rangle = \left(\frac{3V_\infty}{2}\right)^2 |k'k| \times$$
$$\iint_{-\infty}^{\infty} dx\, dx' \iint_{-\infty}^{0} dy\, dy' e^{|k|y-ikx} e^{|k'|y'-ik'x'} \langle \zeta(x, y+V_\infty t)\zeta(x', y'+V_\infty t')\rangle. \quad (6.22)$$

The quenched noise will typically be correlated on a microscopic scale $a$. Then, for $ka << 1$ the noise will be effectively white, that is, with correlations $\langle \zeta(x,y)\zeta(x',y')\rangle = \Delta\, \delta(x-x')\delta(y-y')$ which yields

$$\langle \hat{\Omega}_{LR}(k,t)\hat{\Omega}_{LR}(k',t')\rangle = \Delta \left(\frac{3V_\infty}{2}\right)^2 \pi|k|\delta(k+k')e^{-V_\infty|k||t-t'|}. \quad (6.23)$$

From the above expression it results that the nonlocal contribution of the bulk noise scales as $|k|^{1/2}$ and introduces also memory effects in the form of power-law time-correlations associated to the continuum of relaxation time scales $(V_\infty|k|)^{-1}$. $\hat{\Omega}_{LR}(k,t)$ is thus long-range correlated both in space (in the $x$-axis direction) and time. Similar power-law correlations have been postulated phenomenologically for different interfacial problems. To our knowledge this is the first one to be explicitly derived from first principles.

The derivation of $\widehat{\delta v}_\zeta$ above has been done for $c = -1$, that is, a viscous fluid displacing an inviscid one, but it can also be done in the general case of $-1 \leq c \leq 0$. The derivation is somewhat more involved, and can be found in Appendix B.

Remarkably, replacing $\widehat{\delta v}_\zeta(k)$ with its value from Eq. (6.20) into Eq. (6.12) the additive nonconserved noise contribution $\hat{\zeta}(k)$ reverses its sign. We thus obtain that the capillary noise contribution has the same sign that the joint contribution from permeability and conservation, contrary to naive expectation which could anticipate that capillarity and permeability of would oppose each other. We will see that this is true only in the case of persistent noise in next subsection.

Unlike local terms, the 'annealed' approximation[5] we have applied above

[5]By 'annealed' approximation we mean the lowest order approximation in $h - V_\infty t$ applied to Eq. (6.16) to get Eq. (6.17).

to derive $\widehat{\delta v}_\zeta$ is justified as a leading order, because of its integral form. Note that, while exchanging a quenched noise by a time-dependent one in the local noise terms is a bad approximation in situations where the interface is partially pinned and advances via avalanches, the case of the nonlocal noise is different. As a matter of fact, the noise acting on a pinned region of the interface may indeed change with time due to the motion of the interface elsewhere, because this is coupled through the bulk. Since in the case of forced fluid invasion the mean interface position is always advancing at constant velocity, one should expect that there is always an effective annealed noise acting on the interface even if this is partially pinned. Notice also that if one is not willing to assume the annealed approximation, then an explicit expression for the bulk noise cannot be found and one must rely on a full numerical approach from an earlier stage.

Finally we complete the interface equation with the leading nonlinear contributions obtained from the weakly nonlinear expansion. We include only the quadratic terms which are the only ones that may be relevant in the Renormalization Group sense (see discussion in Sec. 6.2.3). Our final interface equation then reads, in Fourier space,

$$\begin{aligned}\frac{\partial \hat{h}_k}{\partial t} &= V_\infty \left\{ \delta(k) + c|k|\hat{h}_k[1+(\ell_1 k)^2] - \hat{\zeta}(k)/2 - \ell_2|k|\hat{\zeta}(k) \right\} \\ &+\hat{\Omega}_{LR}(k,t) - V_\infty c^2|k| \int_{-\infty}^{\infty} dq[1-\mathrm{sgn}(kq)]\hat{h}_{k-q}\hat{h}_q|q|[1+(\ell_1 q)^2] \end{aligned} \tag{6.24}$$

with

$$\begin{aligned}\hat{\Omega}_{LR}(k,t) = &\frac{3V_\infty}{2}\frac{1-c}{2}|k| \int_{-\infty}^{\infty} dx' \int_{-\infty}^{0} dy \zeta(x', y+V_\infty t) e^{-ikx'} e^{y|k|} \\ &+\frac{3V_\infty}{2}\frac{1+c}{2}|k| \int_{-\infty}^{\infty} dx' \int_{0}^{\infty} dy \zeta(x', y+V_\infty t) e^{-ikx'} e^{-y|k|}. \end{aligned} \tag{6.25}$$

The above interface equation is the central result of this part of the thesis and will be studied in detail in some cases. The lengths $\ell_1$ and $\ell_2$ are defined in terms of the capillary number $\mathrm{Ca} = 12(\mu_1+\mu_2)V_\infty/\sigma$ as

$$\ell_1 = \frac{b_0}{\sqrt{|c|\mathrm{Ca}}} \quad \text{and} \quad \ell_2 = \frac{b_0 \cos\theta}{\mathrm{Ca}}. \tag{6.26}$$

In usual experiments [REDG89, HFV91, HKzW92, SOHM02b] a wetting fluid displaces air, then the contact angle $\theta$ satisfies $\cos\theta \simeq 1$, and viscosity contrast is $c = -1$. In this case, the lengths $\ell_1$ and $\ell_2$ satisfy $\ell_2 > \ell_1$, since $\mathrm{Ca} < 1$ to ensure that the Hele-Shaw approximation and the Darcy

law hold, but in the general case of arbitrary viscosities and wetting conditions the ratio $\ell_2/\ell_1$ can take any value between zero and infinity. The length scale $\ell_1$ has already been discussed in the literature (see for instance Dubé *et al.* [DRE+00]) as the one governing the crossover between capillary and viscous forces. This length scale is already present in the deterministic equation. On the contrary, the length scale $\ell_2$ is newly found and entirely related to fluctuation properties, controlling an additional crossover between conserved and nonconserved noise.

There is a particular case, that of $c = 0$ which will become specially relevant in the discussion of universality classes in sections below, and for which the interface equation takes a remarkably simple form since both nonlinearities and the deterministic viscous term drop out. In terms of a redefined $\tilde{\ell_1} = b_0/\sqrt{\mathrm{Ca}}$ this reads

$$\frac{\partial \hat{h}_k}{\partial t} = V_\infty \left[ \delta(k) - |k|(\tilde{\ell_1} k)^2 \hat{h}_k - \frac{\hat{\zeta}(k)}{2} - \ell_2 |k| \hat{\zeta}(k) \right] + \frac{3V_\infty}{4} |k| \int_{-\infty}^{\infty} dx' \int_{-\infty}^{\infty} dy \zeta(x', y + V_\infty t) e^{-ikx'} e^{-|yk|}. \tag{6.27}$$

### 6.2.2 The case of persistent noise

So far we have considered a gap with a disorder described by a general quenched noise $\zeta(x, y)$, and in the derivation of the expression for $\widehat{\delta v}_\zeta$ we have implicitly used that $\partial_y \zeta(x, y) \neq 0$ (see Eq. (6.14)). There is, however, an important particular case for which the problem is particularly simple both from theoretical and experimental points of view. We refer the case of persistent (or columnar) noise, corresponding to the particular case for which the disorder is translationally invariant in the propagation direction, namely $\zeta = \zeta(x)$. This has been studied experimentally by Soriano *et al.* [SRR+02]. We will see that, in this case, the bulk noise cancels out since $\partial_y \zeta(x) = 0$ and therefore[6] $\widehat{\delta v}_\zeta = 0$. However, in real experiments with persistent noise as those by Soriano *et al.* [SRR+02] the disorder does not extend all the way to infinity and important transient effects are expected from the memory contained in the long-ranged noise derived in the previous section.

We consider a disorder that is nonzero only above a fixed position $y = H_0 < 0$, with the form

$$\zeta(x, y) = \begin{cases} \zeta(x) & y \geq H_0 \\ 0 & y < H_0 \end{cases} \tag{6.28}$$

[6] If we consider the next order in $\partial_x h$ then it is found $\widehat{\delta v}_\zeta \neq 0$.

and then $\partial_y \zeta(x,y)$ reads

$$\frac{\partial \zeta(x,y)}{\partial y} = \delta(y - H_0)\zeta(x). \tag{6.29}$$

Using Eq. (6.29), $\widehat{\delta v}_\zeta(x)$ satisfies (see Eq. (6.15)

$$\int_{-\infty}^{\infty} dx' \sqrt{1 + \left(\frac{\partial h(x')}{\partial x'}\right)^2} \ln\left\{(x-x')^2 + [h(x) - h(x')]^2\right\} \delta v_\zeta(x') =$$
$$-\frac{3}{2} V_\infty \int_{-\infty}^{\infty} dx' \int_{-\infty}^{h(x')} dy' \ln\left\{(x-x')^2 + [h(x) - h(x')]^2\right\} \delta(y - H_0)\zeta(x') \tag{6.30}$$

and applying the same approximations of the general case, that is, with the replacement $h = V_\infty t$ wherever $h$ appears additively, we get

$$\int_{-\infty}^{\infty} dx' \ln(x-x')^2 \delta v_\zeta(x') =$$
$$-\frac{3}{2} V_\infty \int_{-\infty}^{\infty} dx' \ln\left[(x-x')^2 + (V_\infty t - H_0)^2\right] \zeta(x') \tag{6.31}$$

where we have assumed $h(x') > H_0$. To obtain the Fourier transform of $\widehat{\delta v}_\zeta(x)$ we split the logarithm in the rhs of Eq. (6.31) into two terms:

$$\int_{-\infty}^{\infty} dx' \ln(x-x')^2 \delta v_\zeta(x') =$$
$$-\frac{3}{2} V_\infty \left\{ \int_{-\infty}^{\infty} dx' \ln(x-x')^2 \zeta(x') + \int_{-\infty}^{\infty} dx' \ln\left[1 + \frac{(V_\infty t - H_0)^2}{(x-x')^2}\right] \zeta(x') \right\} \tag{6.32}$$

and now it is straightforward to apply the Fourier transform. The transformation of Eq. (6.32) reads

$$-\frac{\widehat{\delta v}_\zeta(k)}{|k|} + 2(\gamma + \ln 2\pi)\delta(k)\widehat{\delta v}_\zeta(0) =$$
$$\frac{3}{2} V_\infty \left\{ \frac{\hat{\zeta}(k)}{|k|} + 2(\gamma + \ln 2\pi)\delta(k)\hat{\zeta}(0) - \frac{\hat{\zeta}(k)}{|k|}\left[1 - e^{-(V_\infty t - H_0)|k|}\right] \right\} \tag{6.33}$$

and $\widehat{\delta v}_\zeta(k)$ is then

$$\widehat{\delta v}_\zeta(k) = -\frac{3}{2} V_\infty \hat{\zeta}(k) e^{-(V_\infty t - H_0)|k|}. \tag{6.34}$$

The main difference with the general case of quenched noise $\zeta(x,y)$ is that for long times (and $k \neq 0$) $\widehat{\delta v}_n(k)$ vanishes and therefore there is no contribution from the bulk to the interface dynamics for long times, at least to the lowest order we have computed here. For $k = 0$ the bulk noise term is $\widehat{\delta v}_n(0) = -\frac{3}{2}V_\infty \hat{\zeta}(0)$, the same value obtained in the general case with $\zeta = \zeta(x,y)$.

Using the result of Eq. (6.34) the interfacial equation (with quadratic nonlinearities in $h$) for columnar noise, as defined in Eq. (6.28), reads

$$\begin{aligned}\frac{\mathrm{d}\hat{h}_k}{\mathrm{d}t} &= V_\infty \delta(k) - V_\infty c|k| \left[1 + (\ell_1 k)^2\right] \hat{h}_k \\ &\quad -V_\infty c^2 |k| \int_{-\infty}^{\infty} dq[1 - \mathrm{sgn}(kq)]\hat{h}_{k-q}\hat{h}_q |q| [1 + (\ell_1 q)^2] \\ &\quad -V_\infty \hat{\zeta}(k)\ell_2 |k| - V_\infty \hat{\zeta}(k) \left[1 - \frac{3}{4}(1+c)e^{-(V_\infty t - H_0)|k|}\right] \end{aligned} \tag{6.35}$$

where for $k = 0$ the rightmost term in brackets has to be replaced with $1/2$, and the total nonconserved contribution is then $-V_\infty \hat{\zeta}(k)/2$. We have introduced the viscosity contrast and assumed that the noise vanishes at $y \to +\infty$ to obtain the above expressions.

### 6.2.3 Discussion of nonlinear terms

In the interfacial equations we have derived, Eqs. (6.24) and (6.35), we have included only quadratic nonlinear contributions for the deterministic part of the equation and linear contributions on the noise. Multiplicative noise terms coupling the interface displacement and the noise have also been neglected except for the strong nonlinearity which is inherent to the quenched noise through the dependence $\zeta = \zeta(x, h(x))$. In this section we will elaborate more on the justification of our handling of nonlinearities.

Let us first consider the nonlinear terms of the deterministic (zero noise) part of the problem. The weakly nonlinear formalism of Hele-Shaw flows developed in Ref. [ALCO01] provides the second and third order on $h$, but we will consider the second order only. Then, the second order nonlinear contribution $\mathcal{N}_h(x)$ to the interfacial equation from the deterministic terms reads in real space

$$\mathcal{N}_h(x) = c^2 V_\infty \left(\mathrm{H}\left\{h_{x'}\mathrm{H}[f]\right\} + \mathrm{H}\left\{h\mathrm{H}[f_{x''}]\right\} + (hf)_x\right) \tag{6.36}$$

where $f(x) = -h_x + \ell_1^2 h_{xxx}$. Note that $\mathcal{N}_h(x)$ has both local[7] and nonlocal terms, in comparison to the linear order that has only nonlocal terms. The

[7] One of the (local) nonlinear terms is the familiar KPZ term [KPZ86].

exact form of $\mathcal{N}_h(x)$, and in particular of the nonlocal terms is not at all obvious *a priori*. From dimensional considerations it can be seen that terms with two derivatives and terms with four derivatives times $\ell_1^2$ appear, but combinations of local terms fail to satisfy the required symmetries: a term such as $\partial_x(h\partial_x h)$ has zero mean, as required by volume conservation, but is not translation invariant: to satisfy this symmetry nonlocal terms are necessary. This is easily verified computing the Fourier transform of $\mathcal{N}_h(x)$:

$$\mathcal{N}_h(k) = -V_\infty c^2|k| \int_{-\infty}^{\infty} dq[1-\mathrm{sgn}(kq)]\hat{h}(k-q)\hat{h}(q)|q|(1+\tilde{B}q^2). \quad (6.37)$$

$\mathcal{N}_h(k)$ does not contain any coupling between the zero mode $\hat{h}(0)$ and any other mode, satisfying the translation invariance requirement, and $\mathcal{N}_h(0) = 0$ as necessary to account for volume conservation. Cubic nonlinearities can also be obtained but in no case may be relevant in the RG sense so we do not include them for the purposes of studying scaling and universality of interface growth.

The nonlinear terms associated to the noise can be separated in two types. The nonlinear couplings of the noise with itself, and the crossed couplings with the interface height $h$ (multiplicative noise). In all cases the nonlinear contributions from the noise can be neglected on the assumption of sufficiently weak noise. However, some of such contributions can be derived explicitly. The leading multiplicative noise term, of order $\zeta h$ comes from the permeability noise in Eq. (6.8) and reads

$$-cV_\infty\zeta(x,h(x))\mathrm{H}[\frac{\partial h(x',t)}{\partial x'} - \tilde{B}\frac{\partial^3 h(x',t)}{\partial^3 x'}](x). \quad (6.38)$$

The other multiplicative noise term of order $\zeta h$ comes from the noise in the capillarity (Eq. (6.6)) and reads

$$c\frac{\ell_2\cos\theta}{\pi b_0}\mathrm{H}\left\{\frac{1}{\pi}\mathrm{P}\int_{-\infty}^{\infty}dx'\frac{h(x')-h(x)}{(x-x')^2}\frac{\partial\zeta(x',h)}{\partial x'} - \frac{\partial h}{\partial x}\mathrm{H}\left[\frac{\partial\zeta(x',h)}{\partial x'}\right]\right\}. \quad (6.39)$$

Again, this is a nonlocal term, like the linear capillary term.

Nonlinear noise terms of arbitrary order $\zeta^n$ coming from capillary noise can all be determined exactly from the expansion of the denominator in Eq. (6.6). However, other nonlinear noise contributions cannot be derived explicitly, most remarkably those from the bulk noise. The second order contribution from bulk noise can be expressed in closed form, but in terms of an integral equation. The complete description of quadratic nonlinearities containing the noise could in principle be included in the formalism but is too involved in practice.

The RG relevance of the nonlinear terms will be discussed in detail in the following chapter.

### 6.2.4 Discussion of the physical content

In the derivation of the interface equation we have seen that a unique source of noise, the spatial gap variations give rise to different types of noise terms, all of them related to the original noise source and therefore mutually correlated. These different noise terms are associated to different physical effects of the gap variation. The derivation of the explicit form these physical effects take in the interface equation and the knowledge of all parameters may thus provide useful insights in the physics of the problem and hopefully help clarify the different regimes that may be partially responsible for the existing confusion and controversy in the literature.

From a physical point of view, one can foresee at least two types of effects, namely those related to capillarity and those related to the viscous flow. The former are the simplest ones to account for, and are the only ones considered for instance in Dubé *et al.* [DRE+99, DRE+00] or Ganesan and Brener [GB98], although they both formulated them from a phenomenological perspective. Ref. [DRE+00] does explicitly neglect noise in the permeability, which is justified for the case of asymptotically small imbibition. However they recognized their importance for the general case. A phenomenological attempt to model permeability noise was also presented by Hernandez-Machado *et al.* [HMSL+01] but did not include all nonlocal effects associated to the viscous flow. An important point to emphasize in the context of the above references is the importance of the interplay between permeability variations and mass conservation. As emphasized above, the consideration of 3d conservation has crucial consequences and rules out for instance the conserved phase-field formulation such as those of Refs. [DRE+00, HMSL+01]. In addition, phase-field formulations based on conserved order parameter Ginzburg-Landau equations are only valid for the high viscosity contrast limit. However, it has been recognized that viscosity contrast and wetting conditions have an important effect on the resulting scaling and morphologies of growing interfaces [HHZ95].

Let us focus on the more subtle physics of the interplay between permeability and conservation. Consider a capillary tube of radius $r$ at fixed pressure drop between the two extremes. At constant $r$ the velocity of the fluid is $v$, but a variation of the radius implies a change in the velocity of the same sign, a relative velocity fluctuation scales as $\delta v/v \sim 2\delta r/r$. This occurs because permeability is increased (resp. decreased) when the radius is increased (decreased) since larger radius implies less resistance to flow. Now consider the same capillary tube at fixed flow injection (constant mass per unit time of an incompressible fluid): in this case a variation of the radius is accompanied by a variation of the velocity of opposite sign! More precisely,

$\delta v/v \sim -2\delta r/r$, that is, mass conservation slows down (resp. speeds up) the flow if there is more (less) volume available. In this simple example one sees that variation of permeability and conservation have opposite effects. Of course none of the boundary conditions used in the argument will be locally satisfied in our system. The effective conditions acting at a given region will require the solution of the full nonlocal problem for the pressure and will in any case depend on the spatial scale. For low $k$ (long length scales) one expects that conservation becomes dominant, since we are dealing with the case of overall constant injection rate, while for large $k$ the detailed consideration of the full nonlocal problem is necessary. In fact, if the fluid enters a narrow region, the possibility of permeability to overcome the speeding up due to conservation will depend on the ability of the flow to redirect to the sides, and to the degree of persistence of the flow entering the region. The two effects require the knowledge of the flow field in the neighborhood which in turns depends on the actual spatial dependence of the gap throughout a large region. The combined effect is what is exactly captured by our explicit derivation of permeability and bulk noise, which contain both local and nonlocal contributions. Direct numerical computation of both terms in the bulk noise shows that the local part is typically larger, but it is unclear to what extent neglecting the long range tern may miss important details of local interface pinning which may eventually affect the scaling. Furthermore, for $k\lambda \sim 1$ where $\lambda$ is the noise correlation length, both local and nonlocal parts of the bulk noise are comparable but then the annealing approximation may not be justified, and a more careful analysis of bulk noise based in Eq. (6.16) may be necessary. In Fig. 6.2 we plot $|\hat{\Omega}_{LR}(k,t_0)|$ and $|\hat{\zeta}(k)|$ computed for a particular realization of noise, for a system of size $L = 128$ and correlation length of the noise $\lambda = 0.0625$. We observe that $\hat{\zeta}$ overcomes $\hat{\Omega}_{LR}$ at small $k$ but $\hat{\Omega}_{LR}$ has a larger amplitude for large $k$. In addition, $|\hat{\Omega}(k,t_0)|$ grows with $\sqrt{k}$, as predicted from Eq. (6.23).

Capillary effects are much simpler. As stated before, if the cell becomes narrower, the pressure drop at the meniscus will increase pulling the interface ahead (in the case of a wetting fluid). Similarly, a wider gap will tend to slow down the interface. The effect is thus naively opposite to that of permeability. This turns to be the case for instance for persistent noise, when the bulk noise contributions vanishes. However, in the general case we have seen that the local term in the bulk noise has opposite sign to that of the permeability noise and it actually reverses the sign of the total nonconserved noise contribution, which then has the same sign as capillary (conserved) noise.

All the combined local, nonlocal, conserved and nonconserved noise contributions are properly taken into account in our central result Eq. (6.24). First, it preserves fluid mass in three dimensions (not in two!): at $k = 0$

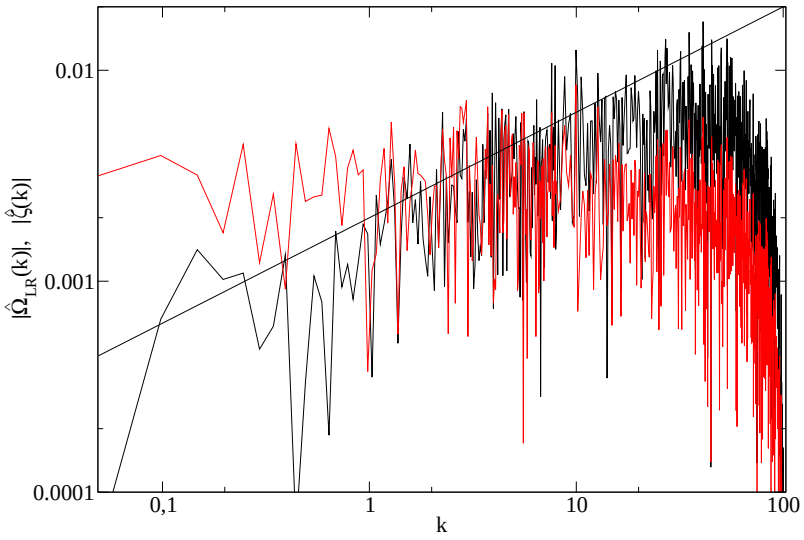


Figure 6.2: $|\hat{\Omega}_{LR}(k,t_0)|$ (black line) and $|\hat{\zeta}(k)|$ (red line) for a particular realization of noise, with system size $L = 128$ and correlation length of the noise $\lambda = 0.0625$. The straight line has a slope $1/2$.

the only noise term is $-V_\infty\hat{\zeta}(k)/2$, with a sign opposite to gap variation, as discussed above. This term (at $k = 0$) can be easily obtained independently from our derivation using the conservation of the fluid, imposing $\zeta(x, y \to -\infty) = 0$ and keeping only linear terms. The capillary noise term proportional to $-|k|\hat{\zeta}(k)$ has, as expected, the same sign than the nonconserved noise term just discussed. The nontrivial interplay between permeability and conservation is properly quantified by the bulk noise terms. Its interpretation at small length scales is indeed not so obvious. The integral term $\hat{\Omega}_{LR}$ scales as $|k|^{1/2}$, and then it is more relevant for large $k$ or small length scales, as expected for the permeability effects, and also involves the noise in a neighboring region. However, a word of caution is in order about this point: $\hat{\Omega}_{LR}$ gets relevant at large $k$, but it is precisely at small length scales where the annealed approximation used to obtain it may fail. Although we do not expect this to have significant implication for the use of our equation in the study of scaling, a definitive check of this point can only be carried out from direct numerical computation of the problem at a stage prior to the annealed assumption. As a final conclusion, let us remark that from the consideration above, the long ranged noise will be typically subdominant with respect to the local noises if the original quenched noise is short-ranged (effectively white). In these cases the nonlocal noise will be negligible to study the asymptotic low-$k$ scaling. In other cases, such as for

persistent noise, the local and nonlocal parts of the bulk noise are exactly of the same order. They cancel out for an infinite system, leaving capillary and permeability noises to oppose each other, but in general the nonlocal term generates explicit transients in the equation. In general, even if the long-ranged noise may not contribute to the asymptotic scaling, it is crucial in introducing transients and consequently to help interpreting experiments. In summary, the nonlocal noise must be taken into account as a fundamental part of the (linear) response of the system to gap perturbations, but a part that will typically not affect the scaling properties.

In the next chapter we will address the physics of the interface equation in what respects to scaling and universality classes.

# Chapter 7

# Application to kinetic roughening in porous media

In this chapter we study the scaling properties of the interface equation for a Hele-Shaw cell with random gap derived in previous chapter. We obtain analytically the scaling exponents for two types of noise: dynamical and persistent. The interface equation is simulated with quenched noise in different regimes, and its scaling behavior at different ranges of parameters is obtained. The results obtained are discussed and compared with experimental results.

## 7.1 Scaling concepts

A rough interface is described from an statistical point of view in terms of its scaling properties [BS95]. The relevant magnitude in order to study the scaling behavior of a rough interface is its width or roughness $W(t)$, which is defined as the root mean square (rms) value of the deviations of the interfacial height $h(x)$ with respect the mean value $\overline{h}$. More precisely,

$$W(t) = \langle \overline{[h(x,t) - \overline{h}]^2} \rangle^{1/2} \tag{7.1}$$

where the overline denotes average over all $x$ in a system of size $L$ and the brackets denote the average over different realizations. In a typical experiment the interface width grows as

$$W(t) \sim t^{\beta} \tag{7.2}$$

at short times, $t \ll t_{\times}$, but this power-law growth does not continue indefinitely, but it halts and is followed by a saturation regime where $W(t)$ has a constant value $W_{sat}$ known as saturation width. The exponent $\beta$ is known

as *growth* exponent. The crossover between the two regimes takes place at a crossover time $t_\times$. The saturation width $W_{sat}$ increases with the system size $L$, and the dependence also follows a power law,

$$W_{sat}(L) \sim L^\alpha \tag{7.3}$$

for $t \gg t_\times$, where the exponent $\alpha$ is the roughness exponent. In addition, the crossover time $t_\times$ increases with $L$ according to $t_\times \sim L^z$, being $z$ the *dynamic* exponent.

Family and Vicsek [FV85] observed that the three scaling exponents $\alpha$, $\beta$ and $z$ are not independent, and obtained that the interface width satisfies the scaling relation

$$W(L,t) = L^\alpha f\left(\frac{t}{L^z}\right), \tag{7.4}$$

where the scaling function $f(u)$ reads

$$f(u) \sim \begin{cases} u^\beta & u \ll 1 \\ \text{const} & u \gg 1. \end{cases} \tag{7.5}$$

The growth regime takes place for $u \ll 1$, and the saturation regime for $u \gg 1$. To show that the three scaling exponents are not independent note that the crossover point $(t_\times, W(t_\times))$ obeys $W(t_\times) \sim t_\times^\beta$ approaching from small $u$, and $W(t_\times) \sim L^\alpha$ approaching from large $u$, and together with the scaling relation $t_\times \sim L^z$ implies

$$z = \frac{\alpha}{\beta}. \tag{7.6}$$

This scaling law is valid for any growth process that obeys the Family-Vicsek scaling hypothesis given by the scaling relation Eq. (7.4).

A key concept to describe kinetic roughening of growing interfaces is the *correlation length* $\xi$, the characteristic distance over which the points of the interface are correlated. The existence of such correlation length means that the heights are not independent, but 'know' of each other. At the beginning of the growth, the points of the interface are uncorrelated, but during the growth $\xi$ increases with time until it reaches its maximum possible value, the system size $L$. Then, at saturation, the whole interface is correlated. The correlation length satisfies

$$\xi \sim \begin{cases} t^{1/z} & t \ll t_\times \\ L & t \gg t_\times. \end{cases} \tag{7.7}$$

A useful quantity to determine the scaling exponents of a growing interface and that provides more information on the scaling is the structure factor $S(k,t)$, defined as [Kru97]

$$S(k,t) = \langle h_k(t) h_{-k}(t) \rangle, \tag{7.8}$$

where $h_k(t)$ is the $k$-th mode of the Fourier transform of $h(x,t)$. $S(k,t)$ is related to the interface width through the simple relation [Kru97]

$$W^2(t) = \sum_{k \neq 0} S(k,t), \tag{7.9}$$

and the Family-Vicsek scaling hypothesis Eq. (7.4) translates to the structure factor to yield

$$S(k,t) = k^{-1-2\alpha} g(t/|k|^{-z}) \tag{7.10}$$

where the scaling function $g(u)$ satisfies

$$g(u) \sim \begin{cases} u^{(2\alpha+1)/z} & u \ll 1 \\ \text{const} & u \gg 1. \end{cases} \tag{7.11}$$

The structure factor is useful to determine the value of the roughness exponent $\alpha$ with a fixed system size $L$.

In addition, one may calculate other quantities related to correlations over a distance $l$ as the height-height correlation function $G(l,t)$ defined as

$$G(l,t) = \langle \overline{[h(x+l,t) - h(x,t)]^2} \rangle \tag{7.12}$$

or the local width $w(l,t)$ of the interface, which is defined as the root mean square (rms) value of the deviations of the interfacial height $h(x)$ with respect the mean value $\overline{h}_l$ over a length scale $l$. More explicitly,

$$w(l,t) = \langle \overline{[h(x,t) - \overline{h}_l]^2}_l \rangle^{1/2} \tag{7.13}$$

where $\overline{\phantom{x}}_l$ stands for averaging over all segments of length $l$ that may be defined in the $x$ (horizontal) direction, and the brackets denote the average over different realizations. It obeys a power law behavior at long times,

$$w(l) \sim l^{\alpha_{loc}} \tag{7.14}$$

where $\alpha_{loc}$ is the *local* roughness exponent, that coincides with the roughness exponent $\alpha$ within the Family-Vicsek scaling hypothesis, but may differ otherwise, in the so-called anomalous roughening scenarios [RLR00]. The scaling of both quantities is related through $w(l,t) \sim \sqrt{G(l,t)}$.

## 7.2 Scaling properties

The presence of the two lengths $\ell_1$ and $\ell_2$ in our problem has important implications regarding the scaling properties of Eq. (6.24). In experiments one usually finds $Ca \ll 1$ and $\ell_1 \ll \ell_2$, so we will focus the discussion on this case, but in general, with arbitrary viscosity contrast and wetting conditions the opposite situation could also be obtained. From the linear equation one can argue the existence of different scaling regimes (the consideration of nonlinearities may further complicate the analysis and will be discussed later). During the growth regime, depending on the value of the correlation length $\xi(t)$ the terms of Eq. (6.24) dominant for the scaling of the interface will be different. For short times such that $\xi \ll \ell_1$ the dominant terms of Eq. (6.24) are the two capillary terms: the deterministic one proportional to $|k|^3\hat{h}_k$ and the noisy one proportional to $|k|\hat{\zeta}(k)$. In this case the interface is in the capillary regime, and the exponent $\beta$ observed for these short times would be the corresponding to this regime. As $\zeta(t)$ increases with time, a different situation will be encountered where $\ell_1 \ll \xi \ll \ell_2$ and the dominant terms are the deterministic one proportional to $|k|\hat{h}_k$ (viscous term) and the disorder term $|k|\hat{\zeta}(k)$. Finally, for long times $\ell_2 \ll \xi$ and the dominant terms are the one proportional to $|k|\hat{h}_k$ and the additive noise term $\hat{\zeta}(k)$. Thus, the interface equation (6.24) can exhibit up to *three* different scaling regimes with the corresponding crossovers during the growth stage, or in other words, up to three different values of $\beta$ could be observed. However, these three regimes will be actually observed in an experiment or simulation of Eq. (6.24) only if the spatial scales are clearly separated and well resolved: $\ell_1 \ll \ell_2 \ll L$. Otherwise only one or two of the regimes might be observed, or a combination of them. In most existing experiments one usually has $\ell_2 \gg L$ and $\ell_1 \approx L$, and this implies that only the first capillary regime would be observed. At saturation the situation is equivalent: the scaling for instance of the structure factor $S(k,t)$ would show different behaviors at different values of $k$, although this is difficult to observe experimentally for the reasons cited above.

The integral term $\hat{\Omega}_{LR}$ cannot be easily compared to the other noise terms because of its integral form. It can be shown that $|\hat{\Omega}_{LR}| \sim |\lambda k|^{1/2}$, where $\lambda$ is the correlation length of the noise, and then it follows that $\hat{\Omega}_{LR}$ will be the dominant one for the scaling for $|k| \ll \lambda/\ell_2^2$ and $|k| \gg \lambda^{-1}$, and these relations imply $\lambda \gg \ell_2$ for the term $\hat{\Omega}_{LR}$ to be felt in the scaling. We recall that $\ell_2 = \cos\theta\, b_0 Ca^{-1}$, so in normal experimental situations with $\cos\theta \approx 1$ we find $\ell_2 \approx b_0 Ca^{-1}$. Then, if $b_0$ and $\lambda$ are of similar magnitude and $Ca \ll 1$ (as in usual experiments) we find $\lambda \ll \ell_2$: the long range noise $\hat{\Omega}_{LR}$ will not modify the asymptotic scaling. But, if the two fluids wet equally well, then $\ell_2 \approx 0$ and $\hat{\Omega}_{LR}$ will be crucial for small wave numbers satisfying $\lambda|k| \gg 1$.

### 7.2.1 Exact results

The scaling of the interface equation Eq. (6.24) can be determined exactly in the particular cases of persistent and annealed noise, if the quadratic nonlinearities are neglected (see discussion in next section). For persistent noise the bulk contribution can be integrated, making the problem far more simpler, and for annealed noise $\zeta(x,t)$ the integral term does not make sense, so we must omit it. We will study the different regimes separately for sake of clarity, but the same analysis can be done with the whole equation. The results of this section will be useful to interpret the results obtained in next section, devoted the numerical simulation of the interfacial equation with quenched noise.

Let us first focus on the viscous regime, that satisfies $\ell_2|k| \ll 1$. Dropping the terms of Eq. (6.24) that are subdominant in this regime the equation to solve for persistent noise is

$$\frac{\mathrm{d}\hat{h}_k}{\mathrm{d}t} = -V_\infty \left[ |k|\hat{h}_k + \frac{1}{2}\hat{\zeta}(k) \right], \tag{7.15}$$

where $\hat{\zeta}(k)$ has no implicit dependence on $h$ (noise in real space is $\zeta = \zeta(x)$). Eq. (7.15) can be easily solved, and after some algebra we find

$$W^2(t) = \frac{\Delta}{8} \int_{2\pi/L}^{\pi/a} dk \frac{1 - 2e^{-V_\infty kt} + e^{-2V_\infty kt}}{k^2} \tag{7.16}$$

where $a$ is a microscopic cutoff. The integral can be evaluated to yield

$$W^2(t) = \frac{\Delta}{8} \left\{ \frac{L}{2\pi} \left[ 1 - e^{-\frac{2\pi V_\infty t}{L}} \right] - \frac{a}{\pi} \left[ 1 - e^{-\frac{\pi V_\infty t}{a}} \right] + 2V_\infty t \int_{2\pi/L}^{\pi/a} \frac{dk}{k} (e^{-V_\infty kt} - e^{-2V_\infty kt}) \right\}. \tag{7.17}$$

For very short times, $\frac{2\pi V_\infty}{L} t \ll 1$ and $\frac{\pi V_\infty}{a} t \ll 1$, the width of the interface grows as $W^2(t) \sim t^2$ and we identify $\beta = 1$. This first time regime is extremely short since its duration is directly related to the cutoff $a$. A second time regime is given by $\frac{2\pi}{L} t \ll 1$ but $\frac{\pi}{a} t \gg 1$, for which the width grows as $W^2(t) \sim t$ and therefore in this regime $\beta = 1/2$. The power spectrum $S(k,t)$ is

$$S(k,t) = \frac{\Delta}{4L} \frac{(1 - e^{-|k|t})^2}{k^2} \tag{7.18}$$

and comparing Eq. (7.18) to the general scaling form for the power spectrum,

$$S(k,t) \sim |k|^{-(1+2\alpha)} g(|k|^z t), \tag{7.19}$$

the scaling exponents in the persistent noise case are $\alpha = 1/2$ and $z = 1$.

The time dependent term Eq. (6.34) due to the bulk noise can be included in the analysis, and we have also solved Eq. (7.15) adding the bulk noise term Eq. (6.34). We have obtained that the introduction of this term does not alter the scaling properties of the interface, and the exponents are the same obtained above for Eq. (7.15).

The scaling of Eq. (7.15) with a dynamical noise $\zeta(x,t)$ (that translates to $\hat{\zeta}(k,t)$ in Fourier space) can also be computed exactly [KM91]. The scaling behavior is in this case $W^2(t) \sim \ln t$ and $W^2_{sat}(L) \sim \ln L$, so the exponents are $\alpha = 0$ and $\beta = 0$.

In the capillary regime $\ell_1|k| \gg 1$, the interface is described by the equation

$$\frac{\mathrm{d}\hat{h}_k}{\mathrm{d}t} = -V_\infty \left[ |k|(\ell_1 k)^2 \hat{h}_k + \ell_2 |k| \hat{\zeta}(k) \right] \tag{7.20}$$

that can be solved both for annealed and persistent noise. The integration of Eq. (7.20) is straightforward, and the structure factor $S(k,t)$ is easily computed to yield

$$S(k,t) = \frac{(1 - e^{-V_\infty \ell_1^2 |k|^3 t})^2}{\ell_1^4 |k|^4} \frac{\Delta}{L} \tag{7.21}$$

for quenched noise. Comparing Eq. (7.21) and the general expression for the scaling of $S(k,t)$ in Eq. (7.10) results in a roughness exponent $\alpha = 3/2$ and a growth exponent[1] $\beta = 1/2$. In the case of annealed white noise we find $\alpha = 0$ and $\beta = 0$.

In the intermediate regime $\ell_1|k| \ll 1 \ll \ell_2|k|$ the equation is

$$\frac{\mathrm{d}\hat{h}_k}{\mathrm{d}t} = -V_\infty \left[ |k| \hat{h}_k + \ell_2 |k| \hat{\zeta}(k) \right], \tag{7.22}$$

and the structure factor for quenched noise obtained from its integration is

$$S(k,t) = \ell_2^2 \left(1 - e^{V_\infty |k| t}\right)^2 \frac{\Delta}{L}. \tag{7.23}$$

From Eq. (7.23) the exponents are $\alpha = -1/2$ and $\beta = -1/2$, implying that the interface is not rough.

### 7.2.2 RG-Relevance and the zero-contrast universality class

In the section above the quadratic nonlinearities Eq. (6.37) have been neglected, and will be also neglected in the following section devoted to the

[1] For very short times, $\left(\frac{\pi}{a}\right)^3 V_\infty \ell_2 t \sim 1$, the width grows as $W(t) \sim t$

scaling properties of the interface equation with quenched noise. The relevance or nonrelevance of nonlinearities in the Renormalization Group (RG) sense can be naively studied using power counting arguments in the case of time dependent or persistent noise. Thus, we have studied the relevance of the quadratic terms to the scaling of the linear equations Eqs. (7.15), (7.20), and (7.22). Power counting arguments show that quadratic terms are irrelevant to the scaling of the interface in both the last (viscous dominated) regime characterized by $\ell_2|k| \ll 1$ and in the intermediate regime characterized by $\ell_1|k| \ll 1 \ll \ell_2|k|$, but are relevant in the capillary regime $\ell_1|k| \gg 1$. Therefore, the exponents obtained in the capillary regime $\alpha = 3/2$ and $\beta = 1/2$ (persistent noise) and $\alpha = 0$ and $\beta = 0$ (annealed noise) could indeed be modified by the inclusion of nonlinearities.

Power counting arguments cannot be taken too seriously with quenched noise, but if one naively applies them to the (linear) interface equation in each of the three regimes, one finds results equivalent to those obtained for persistent or annealed noise. That is, nonlinearities are irrelevant in the viscous dominated regime and in the intermediate one, but relevant in the capillary regime. This result from power counting for quenched noise is reinforced by the results for persistent and annealed noise, taking into account that the latter types of noise can be considered limiting cases of quenched noise.

In next section we numerically study the scaling of the interface equation with quenched noise keeping only linear terms, in the three regimes. It is fully justified to neglect quadratic nonlinearities in the viscous and intermediate regimes, but to drop nonlinearities in the capillary regime needs to be justified. We have simulated the equation in the capillary regime with and without the quadratic terms, and have not observed a significative change in the scaling exponents. Note that, contrary to what is usual in phenomenological equations, we know all bare parameters, including those of the nonlinearities so we can really weight the importance of nonlinearities during realistic simulation times. In addition, the results of Ref. [DRE+00] support the fact that nonlinearities do not affect the scaling, because Dubé *et al.* simulated the full problem (in the capillary regime) and found exponents compatible with ours, when a comparison is possible. More details will be given in next section. In any case, the above considerations do not at all rule out the possibility that the effect of nonlinearities does modify the exponents if much longer times are computed (as is well established for the KPZ equation when the coefficient of the nonlinear term is taken not too large [BC94]). In our case, however, it must be taken into account that the problem will eventually crossover to a different regime so most likely the corresponding nonlinear capillary fixed point will not be observed in real experiments. The

pursue of this nonlinear fixed point remains as a rather academic question.

There is a particular case where the nonlinear terms are strictly absent, that is, for zero viscosity contrast ($c = 0$). An examination of the quadratic term Eq. (6.37) shows that it vanishes for $c = 0$. Then, to neglect them is not approximate but exact in this case. In addition, the viscous linear term proportional to $|k|$ also vanishes, and the only terms that remain in the equation are both capillary terms (deterministic and random) and the nonconserved and long range noise terms, that is Eq. (6.27). Thus, from the three different regimes present for arbitrary $c$ only the capillary regime survives for $c = 0$, and a new regime appears where the deterministic capillary term and the nonconserved (viscous) noise term are dominant. In addition, the capillary regime extends longer than for $c \neq 0$ and is exact, in the sense that both the nonlinearities and the viscous term are exactly zero. We can talk then of a *zero-viscosity-contrast universality class* in the problem, and this is precisely the class that seems to govern the scaling in the capillary regime because nonlinearities apparently do not modify the scaling. As argued in the previous chapter, the long-range noise is not expected to affect the scaling for originally short-range gap variations. Accordingly, we define the zero-contrast universality class by the scaling of the equation

$$\frac{\partial \hat{h}_k}{\partial t} = V_\infty \left[ \delta(k) - |k|(\tilde{\ell_1} k)^2 \hat{h}_k - \ell_2 |k| \hat{\zeta}(k) \right] \tag{7.24}$$

which we define with conserved noise, dominant in the early stages of interface growth. A real system with $c = 0$ would eventually undergo a crossover to permeability (nonconserved) noise not described by the equation above.

Typical experiments usually take place (as will be discussed later) in the capillary regime, and this makes the zero-contrast universality class the relevant one also from an experimental point of view. Note that this fixed point is a saddle point in the RG flow, since any (arbitrarily small) finite $c$ will flow towards $c = 1$. We thus find that, in the capillary regime, while the deterministic viscous term $c|k|$ is negligible, the system is attracted to the zero-contrast fixed point, and then, as long as $c \neq 0$, it crosses over to a different regime.

In the above discussion we have not addressed the possibility that the inherent nonlinearity that is present through the quenched (multiplicative) character of the noise may generate, under the renormalization flow, new terms in the renormalized interface equation. A detailed study of this question is deferred to future work. With respect to this point, however, a similar comment to that made for the neglect of nonlinearities may be invoked, in the sense that the generation of the asymptotic regime where these terms

will start playing a role may well be beyond the actual validity of the analyzed equation, due to the crossover to a different regime of the full problem. In any case, it is worth remarking that, even if the RG flow is capable to generate new terms, such as a local one of the usual diffusive type $\partial_x^2 h$, and despite the fact that the KPZ nonlinearity, $(\partial_x h)^2$ is present in our equation, we cannot expect the scaling of the Quenched KPZ equation, because of the presence of the deterministic viscous term $c|k|$ and/or the presence of a conserved noise. For $c = 0$ the deterministic viscous term is indeed absent but so are the quadratic nonlinearities, so the only case in which QKPZ scaling may be observable is for $c = 0$ and assuming that both linear and nonlinear local terms were generated. This would then occur after the crossover from capillary (conserved) noise to permeability (nonconserved) noise. Generically, however, in our problem one should not expect the scaling of the QKPZ equation.

### 7.2.3 Numerical results

Now we would like to obtain the scaling properties of the linearized equation, Eq. (6.24) with quenched noise $\zeta(x, h)$ in the three relevant regimes, by means of numerical simulation of the equation. To simplify the calculations the numerical integration of Eq. (6.24) in each regime will be done separately, that is, including in the computation only the dominant terms, instead of choosing the parameters of the system to exhibit the three regimes.

#### Capillary regime

The scaling behavior of the linearized interface Eq. (6.24) in the capillary or initial regime characterized by $\ell_1|k| \gg 1$ has been studied numerically. In this regime the scaling of the interface is given by the scaling of Eq. (7.20), with $\hat{\zeta}(k) = \mathcal{F}[\zeta(x, h)]$, that is, the term $|k|\hat{h}_k$, the nonconserved noise term and the integral noise term originally present in Eq. (6.24) have been neglected since they do not affect the scaling. Eq. (7.20) has been simulated in a variety of systems sizes ranging from $L = 32$ to $L = 1024$, using a grid spacing in the $x$ direction $\Delta x = 32^{-1} = 0.03125$. The noise values are uniformly distributed between the values $-0.5$ and $0.5$, with an average value $\zeta_0 = 0$. The unit cell of the noise is a square of size twice the grid, $(2\Delta x) \times (2\Delta x)$. The time step has been chosen small enough to ensure stability and convergence.

The values of the characteristic lengths have been chosen with the criteria $\ell_1 \ll \ell_2$ and $\ell \gg \Delta x$, and various values have been used yielding slightly different behaviors. An example of a roughened interface is depicted in Fig. 7.1. From the plot it can be seen that the interface does not advance simultane-

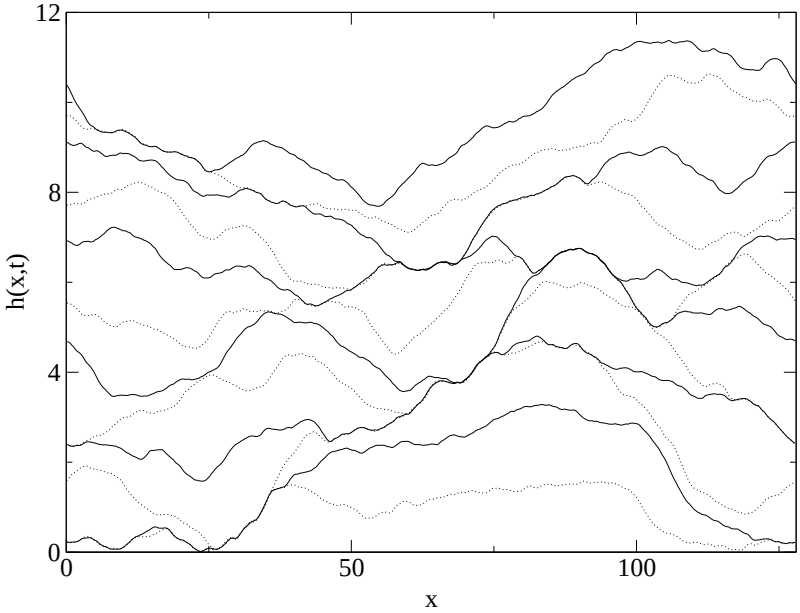


Figure 7.1: Configurations of a rising interface at equal time intervals $\Delta t = 0.8$, with $\ell_1 = 50$ and $\ell_2 = 3000$. Dotted and solid lines alternate for better visualization of the advancing interface.

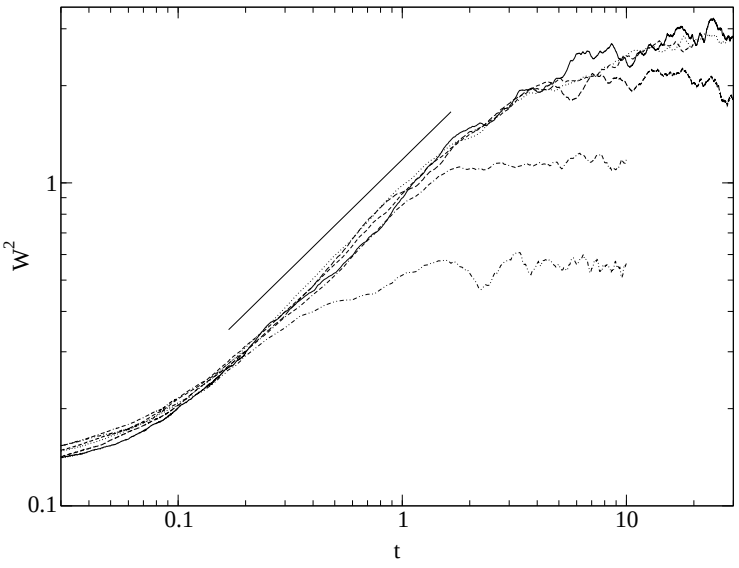


Figure 7.2: Width $W^2$ of the interface as a function of time, for system sizes $L = 32$ (lowest line), 64 (next line), 128 (dashed line), 256 (solid line), 512 (dashed line) and 1024 (dotted line). The straight line is a fit with a slope corresponding to $\beta = 0.68$. Note that the $L = 512$ and $L = 1024$ have not reached the saturation regime at the final time shown in the plot.

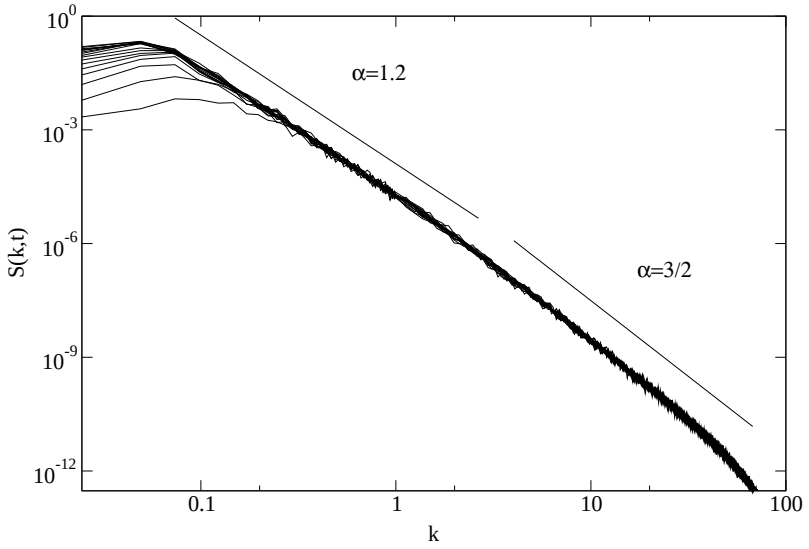


Figure 7.3: Structure factor for a system with $L = 256$. The data are for times $t = 0.5$ (lower curve) to $t = 12.0$, and the time interval is $\Delta t = 0.5$. The straight line with slope $-3.3$ ($\alpha = 1.2$) is a fit, and the other straight line has slope $-4$ ($\alpha = 3/2$).

ously in all its extent, but a large portion of it is pinned a fraction of the time while other portions advance. Note that the interface as a whole cannot get pinned because the flow rate is fixed, and in the regime we are studying the zero mode increases at a constant rate. The interface is quite smooth at small length scales but rough at large ones. This can be easily interpreted looking at Eq. (7.20): for small length scales (large values of $k$) the term $|k|^3$ dominates and smoothes the interface, while for small $k$ or large length scales is the noisy $|k|$ term the dominant one and the interface gets roughened.

The width $W$ of the interface is plotted versus time in Fig. 7.2 for various system sizes $L$, $\ell_1 = 50$ and $\ell_2 = 3000$. At very short times a transient that does not exhibit a power law behavior is observed. Later, a power low behavior $W(t) \simeq t^\beta$ becomes apparent, with an observed value of the growth exponent $\beta = 0.68 \pm 0.01$. In the plot we also observe the saturation of the width for the three smaller values of the system size, but the growth has not saturated yet at the final time of the simulation for other values of $L$. The structure factor has also been computed at various times, and in Fig. 7.3 $S(k,t)$ for $L = 128$ is shown for $\ell_1 = 50$ and $\ell_2 = 3000$. First of all, it is seen that, for very small wave numbers, saturation is not reached at the end of the simulation, and it is approached very slowly. Two slightly different scaling regimes can be distinguished in the plot, one at large $k$ and another at

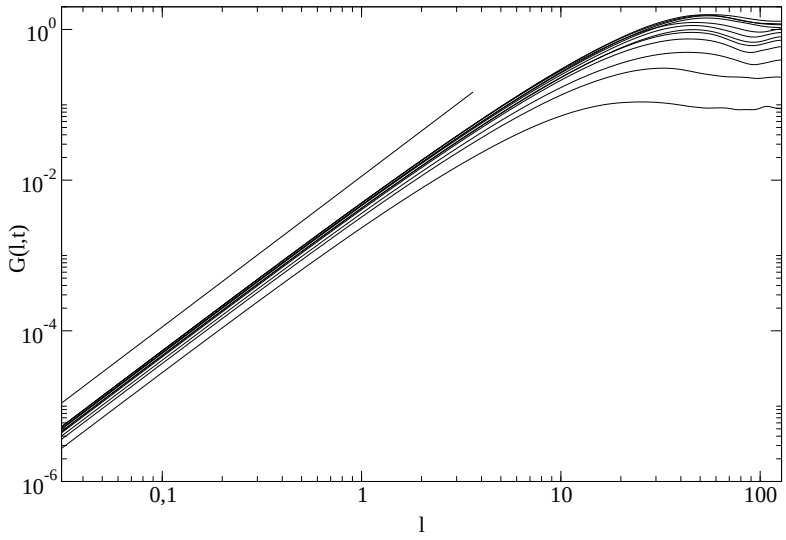


Figure 7.4: Correlation function $G(l,t)$ vs. $l$, for a system with $L = 256$. The data are for times $t = 0.5$ (lower curve) to $t = 12.0$, and the time interval is $\Delta t = 0.5$ for the eight first curves and $\Delta t = 2.0$ for the rest. The straight line has slope $-2$, corresponding to $\alpha_{\rm loc} = 1$.

small $k$. In the small $k$ regime we have fitted a power law $S(k,t) \sim k^{-3.4\pm0.1}$, corresponding to $\alpha = 1.2 \pm 0.05$. This value is compatible with the value reported by Dubé *et al.* [DRE+00], $\alpha \simeq 1.25$. The problem they study is slightly different since they impose constant pressure instead of constant flow rate, but for long times their linearized equation (Eq. (11) in their paper) is basically the same than Eq. (7.20). In their work Dubé *et al.* found $\alpha \simeq 1.25$ computing not the linearized equation but a phase-field model that contained all the nonlinear contributions to the deterministic terms, and therefore this is a clear indication that the deterministic nonlinearities Eq. (6.37) do not affect the scaling, at least for the times we have simulated. For short length scales the observed scaling is very close to $\alpha = 3/2$, the value obtained for Eq. (7.20) with persistent noise. This value is not a surprise, since short segments of the interface span also small heights, thus effectively 'feeling' a persistent noise most of the time. The height-height correlations of the interface have been also studied, and in Fig. 7.4 $G(l,t)$ is plotted for various times and $L = 128$. Since the obtained value of the roughness exponent is $\alpha > 1$ corresponding to a superrough interface, we expect $G(l,t)$ to obey a power law $G(l,t) \sim l^{2\alpha_{\rm loc}}$ for small $l$, with $\alpha_{\rm loc} = 1$. This is precisely the behavior observed in Fig. 7.4, confirming the theoretically predicted scaling. Dubé *et al.* [DRE+00] observed a slightly smaller value, $\alpha_{\rm loc} \simeq 0.9$, that

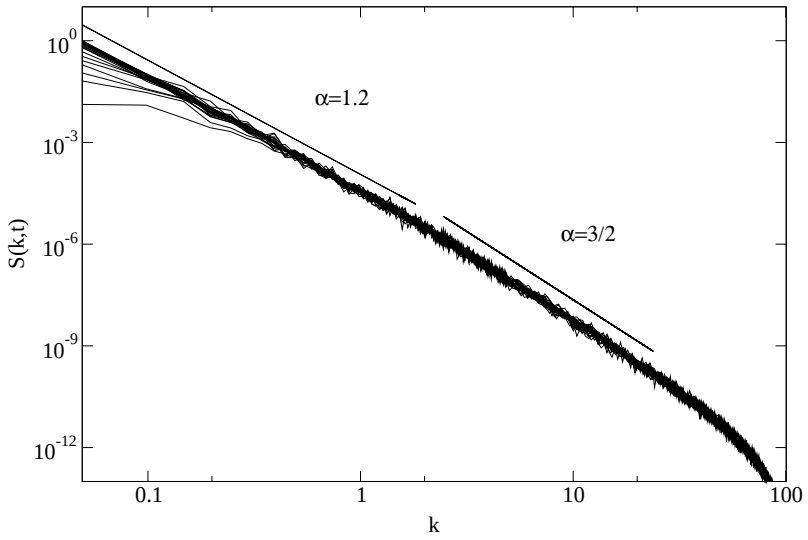


Figure 7.5: Structure factor for a system with $L = 128$. The data are for times $t = 2$ (lower curve) to $t = 50$, and the time interval is $\Delta t = 2$. The straight line with slope $-3.3$ ($\alpha = 1.2$) is a fit, and the other straight line has slope $-4$ ($\alpha = 3/2$). The characteristic lengths are $\ell_1 = 250\sqrt{2}/3$ and $\ell_2 = 50000/3$, with $V_\infty = 0.18$.

they attributed to finite size effects. The value of the growth exponent $\beta$ we have found cannot be compared with the value obtained in Ref. [DRE+00] because their model only reduces to Eq. (7.20) for large time, beyond the growth regime.

The results presented so far have been obtained using the values $\ell_1 = 50$, $\ell_2 = 3000$ and $V_\infty = 1$, yielding $Ca = 3600^{-1} = 2.78 \times 10^{-4}$ (and $b_0 = 5/6$). Experiments are usually done with varying values of $Ca$ and $b_0$, and the method used to change $Ca$ is a change in the injection velocity $V_\infty$ with the remaining physical magnitudes unchanged [SOHM02b]. Therefore, we have repeated the simulations presented above with different injection velocities. In Fig. 7.5 the structure factor is plotted for a system with $L = 128$ and $V_\infty = 0.18$. The capillary number is then $Ca = 5 \times 10^{-5}$ with the lengths $\ell_1$ and $\ell_2$ modified accordingly. The scaling behavior observed in Fig. 7.5 is basically the same found with $V_\infty = 1$ (see Fig. 7.3), with the only difference being that the region where $\alpha = 1.2$ holds extends to lower values of $k$.

Larger injection velocities have also been simulated. Fig. 7.6 shows $S(k,t)$ obtained with $V_\infty = 36$, resulting in $Ca = 10^{-2}$, $\ell_1 = 25/3 = 8.33$ and $\ell_2 = 250/3 = 83.3$. In this case the scaling at small wave numbers is very close to $\alpha = 0$, while the scaling $\alpha \simeq 1.35$ at intermediate wave numbers

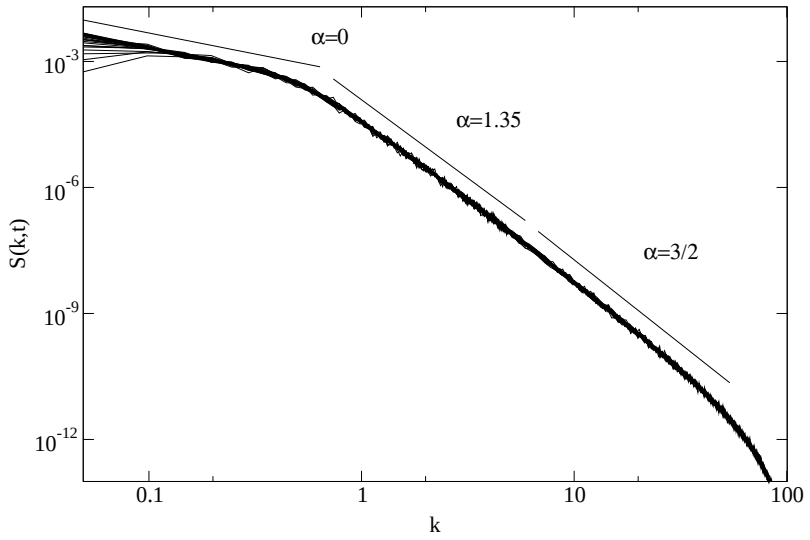


Figure 7.6: Structure factor for a system with $L = 128$. The data are for times $t = 0.2$ (lower curve) to $t = 5.0$, and the time interval is $\Delta t = 0.2$. The straight line with slope $-3.7$ ($\alpha = 1.35$) is a fit, and the other two lines have slopes $-1$ ($\alpha = 0$) and $-4$ ($\alpha = 3/2$). The characteristic lengths are $\ell_1 = 25/3$ and $\ell_2 = 250/3$, with $V_\infty = 36$.

is slightly above the value $\alpha \simeq 1.2$ obtained for lower injection velocities. To interpret the change of scaling behavior that accompanies the change of the injection velocity we recall the results obtained in Sec. 7.2.1: in the capillary regime (described by Eq. (7.20)) the roughness exponent obtained for annealed noise is $\alpha = 0$, and for persistent noise it is $\alpha = 3/2$. We have discussed above the scaling of the interface at large $k$ as a manifestation of the persistent nature of noise at small length scales, but we have just observed that a change in the injection velocity implies also a change in the scaling of large length scales: for large $V_\infty$ the scaling of $S(k,t)$ at small $k$ is the corresponding to annealed noise. Thus, at large length scales the noise effectively 'felt' by the interface is not quenched but annealed. This seems reasonable from a physical standpoint since at larger velocities the interface tends to be less (locally) pinned and the advancing segments of the interface are larger. Larger velocities also imply that the time a noise 'pixel' is occupied by the interface is smaller, and the time intervals the interface spends in each noise 'pixel' are more similar. In other words, at higher velocities the interface pushes harder, and the quenched character of the noise is weaker.

Eq. (7.20) has also been simulated with parameters $\ell_1$ and $\ell_2$ chosen

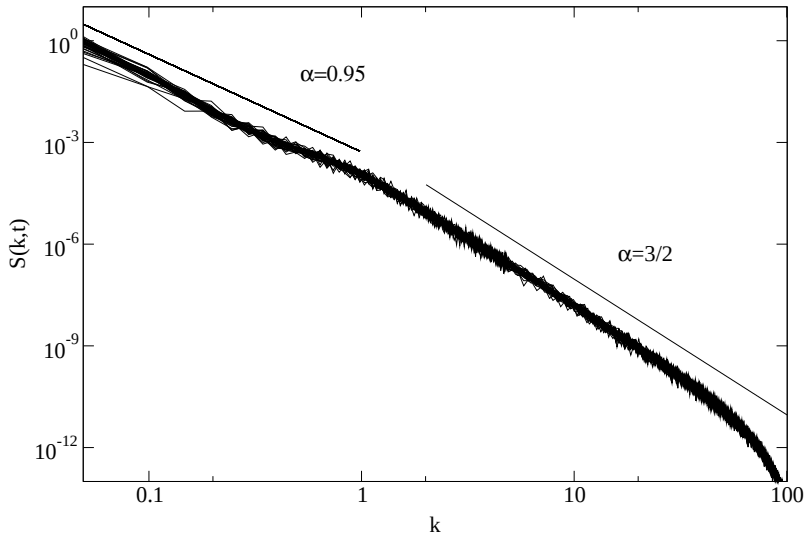


Figure 7.7: Structure factor for a system with $L = 128$. The data are for times $t = 0.4$ (lower curve) to $t = 14.8$, and the time interval is $\Delta t = 0.4$. The straight line with slope $-2.9$ ($\alpha = 0.95$) is a fit, and the other one has slope $-4$ ($\alpha = 3/2$). The characteristic lengths are $\ell_1 = 5 \times 10^5$ and $\ell_2 = 500$, with $V_\infty = 1$.

to yield a different value of $b_0$ than in the cases described above. More precisely we have also simulated evolutions with $b_0 = \ell_1^2/\ell_2 = 1/2$. With these parameters the results we have obtained are similar to the ones obtained with the previous set of parameters, except that in some cases the behavior at small wave numbers is different from the ones described above. One case illustrating this different behavior can be seen in Fig. 7.7, that shows $S(k,t)$ obtained using $\ell_1 = 5 \times 10^5$, $\ell_2 = 500$ and $V_\infty = 1$ (the capillary number is $Ca = 10^{-6}$). The exponent at small $k$ is not very clear, in the sense that it does not exhibit a distinct power law behavior. If we adjust a power law to the small $k$ area we find $\alpha \simeq 0.95$, but this exponent is not very robust. Simulating with different (smaller) values of the velocity we have found a different value for $\alpha$, but clearly below 1. More numerical work is necessary to uncover this small $k$ behavior, using larger system sizes, larger times and more realizations.

### Viscous regime

The long time or viscous regime is characterized by $\ell_2|k| \ll 1$ (the correlation length satisfies $\ell_2 \ll \xi$), and in this case the dominant terms are the nonconserved noise term and the deterministic $|k|$ term. The equation to study is

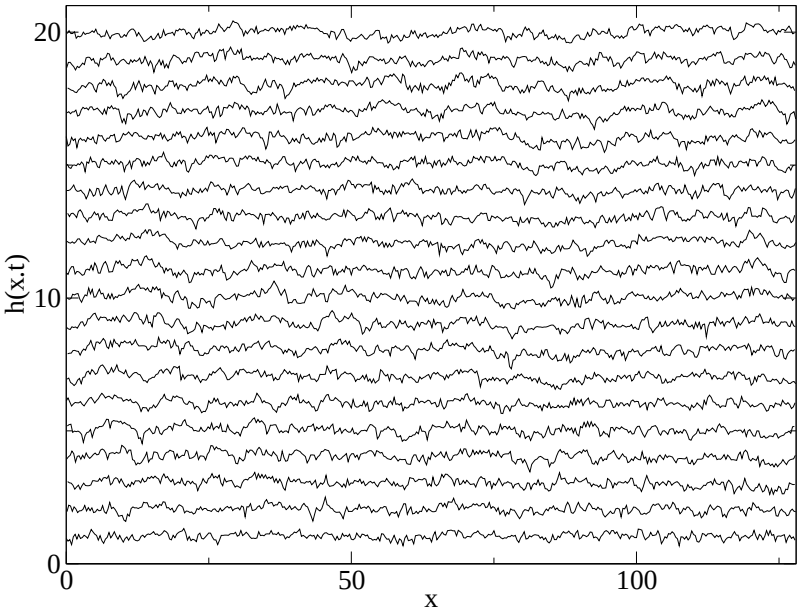


Figure 7.8: Configurations of a rising interface at equal time intervals $\Delta t = 1$.

given by Eq. (7.15), where in this case $\hat{\zeta}(k)$ is the Fourier transform of $\zeta(x, h)$. We have numerically integrated Eq. (7.15) for various system sizes ranging from $L = 2$ to $L = 512$, and two different quenched noise types, using two different values of the grid spacing in the $x$ direction, $\Delta x = 16^{-1} = 0.0625$ and $\Delta x = 8^{-1} = 0.125$. The disorder $\zeta(x, y)$ is an independently distributed random variable in unit cells of size $2 \times 2$ of the grid spacing, with average $\zeta_0$. Two different types of distribution have been used, Gaussian distribution with standard deviation $\Delta\zeta$ and uniform distribution in a finite interval of half width $\Delta\zeta$.

A typical evolution of the interface is shown in Fig. 7.8, where qualitative differences can be clearly seen with respect to the interfaces obtained in the capillary regime (see Fig. 7.1). The interfaces look less rough at large scales but much more rough at short length scales. The reasons for that are twofold: first, the stabilizing effect of the deterministic terms is more important in the capillary regime than in the viscous one, since in the former the deterministic term is proportional to $|k|^3$ and in the latter to $|k|$, making the short length scales more rough. Second, in the capillary regime the stochastic term has a larger amplitude than the deterministic term because $l_2 \gg l_1$, making the interface more rough at large length scales. The intensity of the noise $\zeta$ is similar in both plots, Fig. 7.1 and Fig. 7.8.

Figure 7.9 shows $W^2(t)$ in a case with $\zeta_0 = 0$ and $\Delta\zeta = 0.75$, using a

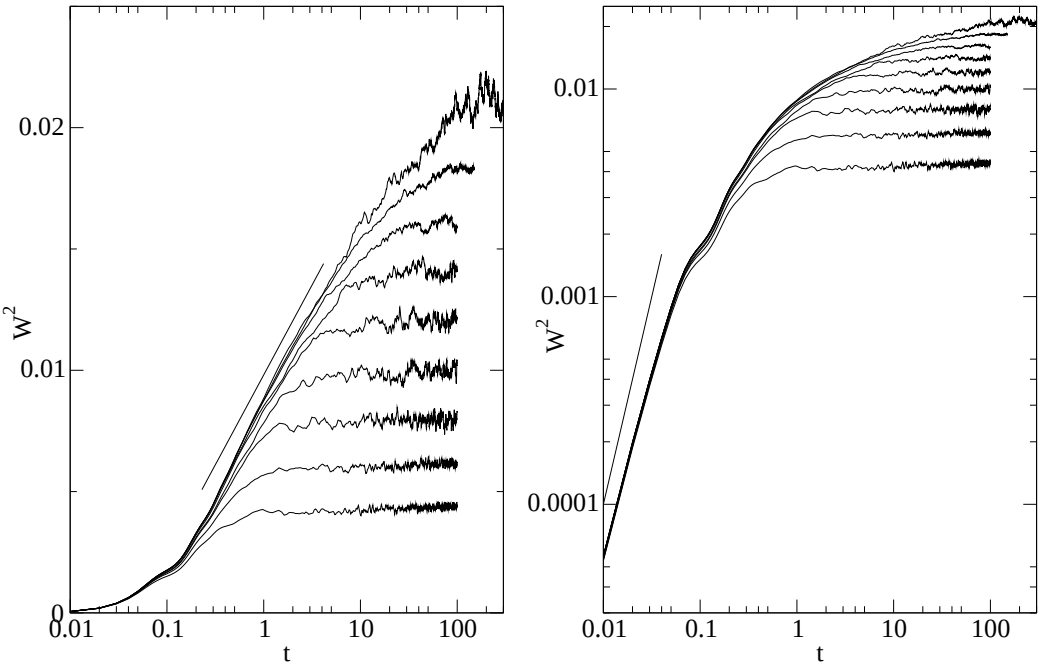


Figure 7.9: Width $W^2$ of the interface as a function of time, for system sizes $L = 2$, 4, 8, 16, 32, 64, 128, 256, and 512, from bottom to top, and $\Delta = 0.75$. (a) Log-linear plot, the straight line is a fit of $W^2 = A + B \ln t$. (b) Log-log plot, the straight line has a slope 2 ($\beta = 1$).

Gaussian distribution for the noise, for a wide range of system sizes $L$. The observation of Fig. 7.9 shows the existence of two different growth regimes before saturation. The first, short-time regime obeys a power law characterized by $\beta \simeq 1$, while the second regime exhibits a logarithmic behavior, $W^2(t) \sim \ln t$ ($\beta = 0$). The structure factor $S(k,t)$ for the same parameters with $L = 256$ is shown in Fig. 7.10. Two different scalings apply for the structure factor at long and short wave numbers. For small $k$ the observed $\alpha$ is $\alpha \simeq 0$, while for large wave numbers $\alpha \simeq 1/2$ is found. Finally, Fig. 7.11 plots $W^2_{sat}$ versus the system size $L$. From the figure it is seen that $W^2_{sat} \sim \ln L$, consistent with $\alpha \simeq 0$ obtained from the structure factor.

The scaling behavior observed in Figs. 7.9 and 7.10 can be interpreted recalling the exact results obtained in Sec. 7.2.1 for persistent noise, and the results of Krug [KM91] for annealed noise. Since in the numerical computation the quenched noise is realized on a square grid, a segment of the interface with a vertical extent significantly smaller than the size of the noise box will effectively 'feel' a persistent noise for a certain time. In particular, at $t = 0$

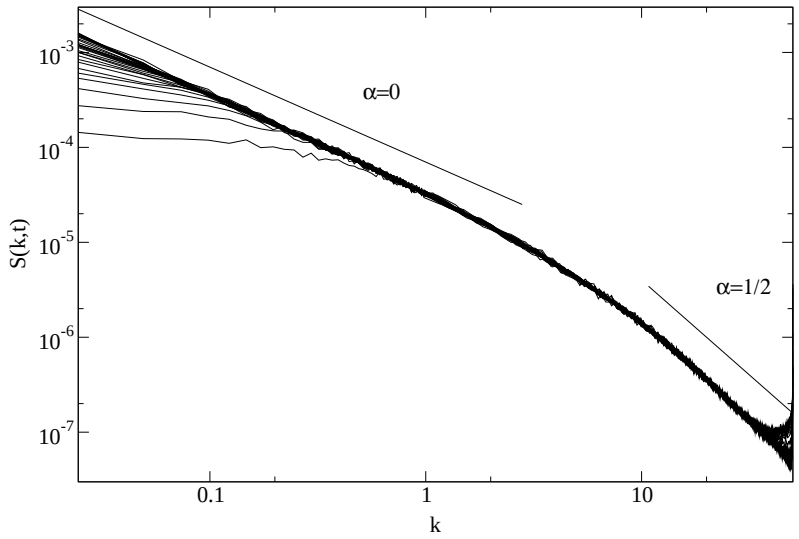


Figure 7.10: Structure factor for a system with $L = 256$ and $\Delta = 0.75$. The data are for times $t = 2.0$ (lower curve) to $t = 150.0$, and the time interval is $\Delta t = 2$ for the first 20 curves and $\Delta t = 10$ for the rest. The straight lines have slopes $-1$ ($\alpha = 0$) and $-2$ ($\alpha = 1/2$).

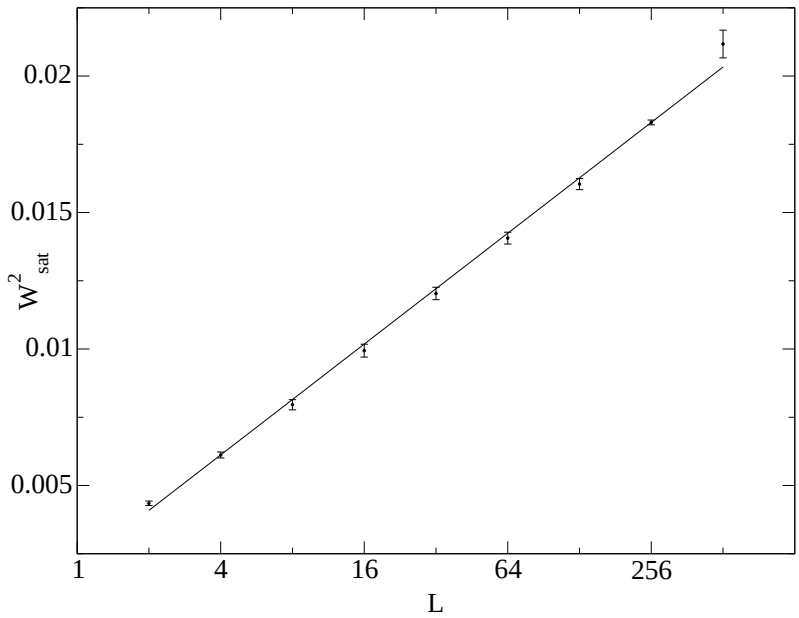


Figure 7.11: Saturation width $W^2_{sat}$ as a function of the system size $L$. The straight line is a fit of $W^2_{sat} = A + B \ln L$. The deviation of the last point with respect the straight line is probably due to the poor statistics available for that system size.

the interface is flat and for a short time $\Delta t_p$ the noise is effectively persistent not only on short segments of the interface but in all its extent. Thus, the roughening of the interface is governed by a persistent noise during a time interval $\Delta t_p$ that can be evaluated as $\Delta t_p \simeq V_\infty d$, where $d$ is the lateral size of the noise boxes, and since $d$ is similar to the microscopic cutoff $a$ the exponent $\beta$ observed for $t < t_p$ will be $\beta = 1$, corresponding to the very short time regime for persistent noise. This value of $\beta$ at very short time is fully consistent with our numerical results, as can be seen in Fig. 7.9. On the other hand, even at long times any short segment of the interface will be subject to persistent noise, and we expect that for large wave numbers the scaling behavior of persistent noise will manifest. This explains the observed value of $\alpha \simeq 1/2$ found for large wave numbers.

From Fig. 7.9 it is seen that the width of the interface grows with time as $W^2(t) \sim \ln t$ beyond the initial short time regime, and it has been shown before that $\alpha = 0$ for large length scales and $W^2_{sat} \sim \ln L$. This is precisely the scaling behavior of annealed noise [KM91], and appears because the quenched character of the noise is not sufficiently strong to manifest, in the sense that different points of the interface have velocities not much different from the average velocity, and the interface 'feels' an annealed noise with a temporal correlation $\Delta t = \mathcal{O}(d/V)$ where $V$ is the average velocity of the interface. The quenched character of the noise can be enhanced increasing its amplitude, but then the interface can become totally pinned when using the simplified interface equation (the full problem does not allow complete pinning because of constant overall injection rate). The possibility of a total pinning of the interface is not allowed by the original model since we are dealing with the constant flux rate boundary condition, but it appears in the simulation of the linear equation because in its derivation the weak noise condition has been assumed, and the nonlinear contribution that comes from the bulk noise would account for mass conservation, preventing interface pinning.

To overcome this problem the following strategy has been adopted: we have increased the intensity of the noise but using an average value different from zero. Pinning can be avoided using a noise with a positive mean, $\langle \zeta(x,y) \rangle = \zeta_0$, allowing the noise to reach values well above one[2]. Eq. (6.24) has been numerically integrated with $\zeta_0 = 4.1$ and $\Delta = 8.0$ for various values of the system size $L$, and the results for the interface width are shown in Figure 7.12. From the plot a growth exponent $\beta = 0.36 \pm 0.02$ can be derived. However, for the system sizes $L$ used it can not be found a clear roughness exponent $\alpha$ since it varies depending on the value of $L$, getting

[2]In the original model, $\zeta(x,y) > -1$ to prevent negative values of the gap spacing $b$.

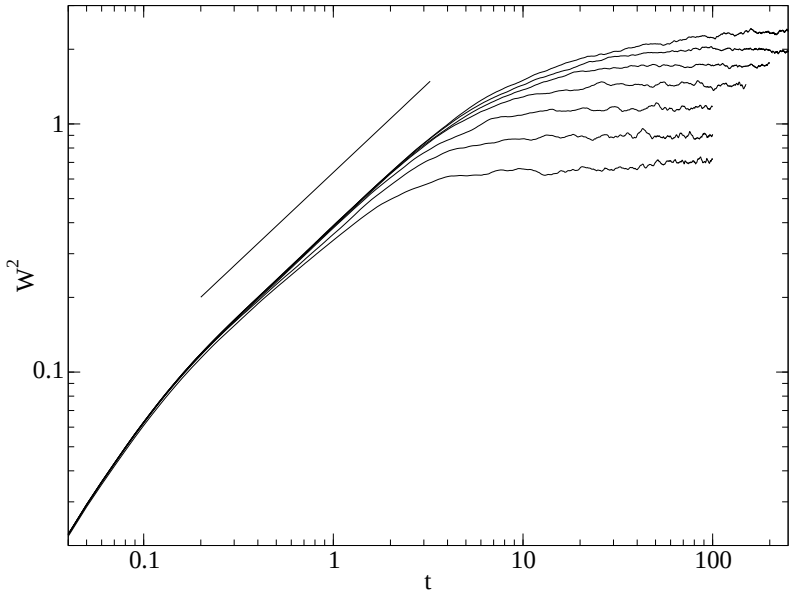


Figure 7.12: Width $W^2$ of the interface as a function of time, for system sizes $L = 16$, 32, 64, 128, 256, 512 and 1024, from bottom to top, $\Delta = 8.0$ and $\zeta_0 = 4.1$. The straight line is a fit with a slope corresponding to $\beta = 0.36$.

smaller as $L$ is increased, and presumably it would reach the value $\alpha = 0$ for larger system sizes. Unfortunately, to check this conjecture is beyond our computing capabilities.

#### Intermediate regime

The intermediate regime $\ell_1|k| \ll 1 \ll \ell_2|k|$ has also been numerically studied, using Eq. (6.24) and neglecting the capillary term $|k|^3$, the nonconserved noise term and the integral noise term. It has been obtained that $W(t)$ does not have a power law behavior, and neither does $W_{sat}(L)$. Thus, the interface is not self-affine. This result could be anticipated because for both annealed $\zeta(x,t)$ and persistent noise $\zeta(x)$ the interface is not rough.

## 7.3 Summary and comparison with experiments

Our results with respect to the scaling behavior are summarized as follows. In the capillary regime various scalings coexist: at small length scales (large wave-numbers) the observed exponent is $\alpha \simeq 1.5$, that corresponds to the

scaling of Eq. (7.20) with columnar noise. At intermediate and large length scales the observed roughness exponent is in the range $\alpha \simeq 1.2 - 1.3$ and in some cases a scaling behavior compatible with $\alpha = 0$ also appears at large length scales, in particular at large injection velocities (and large $Ca$). The exponent $\alpha = 0$ corresponds to the scaling of Eq. (7.20) with dynamical noise. At small $Ca$ (around $10^{-6} - 10^{-7}$) we also observe a different scaling for small $k$, but the power law behavior is not very strong. However, power law fits yield exponents below 1 and clearly above 1/2.

In the viscous regime described by Eq. (7.15) the interface is logarithmically rough, with $\alpha = \beta = 0$. At short length scales the scaling $\alpha \simeq 0.5$ corresponding to Eq. (7.15) with columnar noise appears. If the noise intensity is increased to values beyond the intensity where pinning appears, the scaling behavior changes, and an exponent $\beta \simeq 0.36$ is observed, but in this case the roughness exponent is not clear. Finally, in the intermediate regime we have found that the interface is not rough.

The scaling behavior of the interface in forced fluid invasion of a Hele-Shaw cell with random gap spacing has been experimentally studied by Soriano and co-workers [SRR+02, SOHM02b, SOHM02a]. In the experimental setup used by these authors the gap can take two values, and the transition from one to the other is sharp. Then, the condition $|\nabla b| \ll 1$ necessary to ensure the local validity of Darcy's law (that is the basis of our derivation) is not satisfied. However, it seems reasonable to assume that at large length scales or after a coarse-graining of the system our model and the interface equation derived from it can be a good description of the experimental setup. For quenched noise (SQ disorder in Ref. [SOHM02b]) they distinguish three different scaling behaviors depending on the parameter values, that are the injection velocity and the mean gap[3]. They also observe different roughness exponents at different length scales. In summary, at small velocities and small gap (strong disorder) they observe a roughness exponent in the range $\alpha \simeq 0.6 - 0.9$, and at large velocities they report $\alpha \simeq 0$ at large length scales and $\alpha \simeq 1.3$ otherwise. They also find an intermediate parameter regime with $\alpha \simeq 0.6$ at large length scales and $\alpha \simeq 1$ at short ones.

We have computed the length scales $\ell_1$ and $\ell_2$ of the experiments of Ref. [SOHM02b], and obtained that $\ell_2$ is much larger than the system size $L$ but $\ell_1$ is of the order of $L$, and depending on the particular values of the injection rate and the gap spacing it falls above or below $L$. Then, experiments take place in the capillary regime except at long length scales (and large times) where the influence of the intermediate regime could be felt. If the scaling behavior of the capillary regime is compared with the

[3]The noise intensity is approximately inversely proportional to the mean gap.

experiments, we see that it reproduces the experimental roughness exponents of the large velocity regime, except the small length scale exponent $\alpha \simeq 1.5$, which does not show up in experiments. The agreement between the experiment and the theory is remarkable given the differences between the model and the actual experiments. However, at smaller velocities and gap spacings (weaker noise) the accordance between experiments and theory is not so good. We do obtain exponents below 1, but do not reproduce the various regimes and crossovers. This poor agreement is not surprising if the experimental interfaces are examined: at smaller injection rates the interface is wider and the derivative $\partial_x h$ is clearly much larger, and even points where the interface is parallel to the channel walls can be distinguished. Since the linear equation assumes that $|\partial_x h|$ is small, the discrepancy between theory and experiments can be explained by this difference. At small values of the gap our theory and experiments also give different exponents, and this can be explained considering that our derivation of the interface equation assumes weak noise[4], but the noise present in the experiment at small gap is strong. Note also that the sharp edges of the regions with different gap in the experiment introduce additional effects not present in our formalism through the phenomenon of anchoring of the interface to those edges. The extent to which this ingredient may affect the scaling is yet to be explored.

Soriano *et al.* have also conducted experiments using columnar or persistent noise in the direction of advance of the interface, but in this case the accordance between theory and experiment is weaker because even at large velocities and large gaps they differ. For persistent noise, our interface equation predicts $\alpha = 3/2$ and $\beta = 1/2$, but Soriano *et al.* found (for large velocities or large gaps) $\alpha \simeq 0$ at large length scales and $\alpha \simeq 1.3$ otherwise, and $\beta \simeq 0.5$. The discrepancy might be caused by the difference between the model and the disorder used in experiments. Another explanation could be the influence of the intermediate scaling regime (that is not rough) at large length scales (for the larger velocities used in the experiment $\ell_1 < L$) that could modify the scaling at small wave numbers. On the other hand, it is difficult from experimental spectra to clearly distinguish a 1.5 exponent from a 1.3, and this could account for the discrepancy. In addition, we note that experiments found an exponent $\beta \simeq 0.5$ fully compatible with our results. Finally, it is worth remarking that our model of random Hele-Shaw cell does not predict the anomalous roughening observed in experiments for columnar noise by Soriano *et al.* [SRR+02]. In this case the discrepancy can be clearly

[4]The weak noise requirement is not necessary to model a random Hele-Shaw cell, but only to derive a linear interface equation. Strong noise could be easily introduced in the capillary regime equation, by the substitution of $\frac{|k|}{2}\hat{\zeta}$ by $-|k|\mathcal{F}\left(\frac{1}{\sqrt{1+\zeta}}\right)$.

attributed to the interface anchoring at the edges of the tracks. These act as effective walls (absorbing a finite range of pressure drops) and therefore introducing nondarcyan effects in relatively long parts of the interface.

One of the main reasons to study kinetic roughening in Hele-Shaw cells with random gap is to provide an explanation to the experiments with Hele-Shaw cells filled with glass beads [REDG89, HFV91, HKzW92]. In these experiments it was found a roughness exponent in the range $\alpha = 0.6 - 0.9$, and a dependence of $\alpha$ with $Ca$. The similarity between these exponents and the ones found by Soriano *et al.* in one of the parameter regimes suggests that a Hele-Shaw cell with random gap contains essentially the same physics than the model porous medium consisting in a Hele-Shaw cell with glass beads in the gap. Unfortunately, for strong noise and small velocities our results are not clear, and although we obtain roughness exponents below one more numerical work is required to reach a conclusive result.

# Part V

# Conclusion

# Chapter 8

# Conclusion

This chapter gives a general overview on the main results and strengths of the thesis within a historical perspective, lists the main original results obtained and suggests possible natural continuations of it. At the end of the chapter there is a list of publications.

## 8.1 Overview

In this thesis we have studied various *dynamical* aspects of Hele-Shaw flows, in particular surface tension effects on zero surface tension solutions for high viscosity contrast, the influence of the viscosity contrast in the dynamics of viscous fingering and finally the effect on the interface dynamics of an inhomogeneous gap. The two first topics do close, to some extent, issues that are relatively old, while the third topic is the one that more clearly opens new and promising perspectives. In all cases, part of the originality of the work is in the effort to develop new approaches, and reformulate old questions in different ways. The topic related to the effects of surface tension is the one that can be put in a longer historical perspective, since it is an extension to the dynamics of the classical selection problem. It originates on the one hand in the work of Kadanoff and co-workers in the early nineties, who first posed the question of the selective role of surface tension in the dynamics, and on the other hand on the later results by Tanveer and co-workers who made the crucial steps to formalize the problem in the small surface tension limit in a precise mathematical framework. The pursue of a dynamical solvability scenario has been after all, that of finding the right way to pose the question, one that allows a precise and useful answer. On hindsight it appears that, more than the answer itself, it is the development of a new way of thinking the problem and the general picture resulting from it what may be most valuable

of our work. The second topic of the thesis participates also of this spirit of finding precise formulations of problems for which there was only a qualitative feeling. In this case it originated directly on a conjecture of Casademunt and Jasnow which has been put to the test and confirmed at a quantitative level. Along the way, new concepts have also arisen. Finally, the study of a Hele-Shaw cell with inhomogeneous gap has also been proposed as a new approach to the problem of viscous flow in porous media. The idea of studying the universal properties of interface roughening by means of model systems goes back to the pioneering work of Rubio and co-workers, which did trigger an intense research activity for many years in the field. The idea of introducing controlled modifications to the Hele-Shaw cell to gain understanding of other more complicated problems was strongly pushed by Maher and co-workers, who were also the first to study the problem of an inhomogeneous gap. The recent experimental results by Ortín and co-workers in random Hele-Shaw cells further motivated the interest and potential of this strategy and the need of an appropriate theoretical modeling. We believe that there is still a long way to go both theoretically and experimentally along this line, and we hope the open perspective will contribute to our understanding of many open issues in the field.

From a general point of view, it may be considered that one of the strengths of the thesis is methodological in what refers to the development of a powerful numerical code which has played a crucial role in achieving clear conclusions in some parts of the thesis. Numerical integration of free-boundary problems is always a delicate and demanding task, but the limit of small surface tension in Hele-Shaw flows offers particularly severe difficulties due to strong stiffness and, most importantly, extreme noise sensitivity. It has been only rather recently that sophisticated numerical strategies have overcome those numerical difficulties, mostly thanks to the major steps made by Hou, Lowengrub and Shelley. We hope that this numerical tool will contribute also in the future to clarify some confusions existing in the literature originated in poor numerical studies.

Before proceeding to list the main original results of the thesis, we would like to draw some very general conclusions. From the study of small surface tension there is a clear warning message in the use of well-behaved solutions of the problem without surface tension. We have shown that those are unphysical when taken in a global sense as families of trajectories. Remarkably, this applies to trajectories which are not only physically acceptable (no singularities) but even have the correct asymptotics. The order one time breakdown of the validity of zero surface tension dynamics discovered by Siegel and Tanveer for trajectories with the incorrect asymptotics (those inconsistent with selection theory) is now shown to be more general, implying that sufficiently

generic trajectories which have the correct asymptotics are *not* the limit of vanishingly small surface tension dynamics, and may indeed be radically different (for instance changing which one of the fingers reaches the asymptotic state). The singular effects of surface tension in the dynamics, which can be phrased as restoring hyperbolicity to multifinger fixed points (or unfolding the structural instability), are thus responsible of dramatic changes in the phase space flow structure. At the same time, these results provide the means to establish criteria to identify the classes of initial conditions and time regimes in which the zero surface tension dynamics may be accurate either quantitatively or qualitatively.

The sensitivity of viscous fingering dynamics to viscosity contrast has been known at a qualitative level for a long time. Our general conclusion is that the two types of dynamics pointed out for the extreme values $c = 1$ and $c = 0$ Ref. [CJ91] are still present for arbitrary $c$ and sharply define a nontrivial basin of attraction of the Saffman-Taylor finger depending on $c$, which we have determined for a representative class of initial conditions. We have also identified the relevant attractors which compete with the ST finger as the so-called Taylor-Saffman bubbles. Remarkably, these have a different topology than the finger, and this fact has been related to the pinching tendency that is characteristic of low viscosity contrast. These has also been characterized quantitatively but the issue of possible finite-time topological singularities remains open. We have also shown that the low-contrast behavior is the generic one and that, typically, one must have a $c$ very close to $c = 1$ to systematically observe the finger competition scenario which is commonly described in the literature, that in which the ST is the only attractor and where fingers compete via a mechanism of screening of the laplacian field. In other words, the sensitivity of the dynamics to $c$ is maximal precisely at $c = 1$. For most values of $c$, indeed, one observes generically that trailing fingers are not necessarily suppressed (even though the field is still laplacian!), while leading fingers tend to pinch and approach bubble solutions. The general scenario is more complicated since only parts of the system attain stationary shapes, and these depend on initial conditions (bubbles of all sizes are available).

Finally, the topic which opens more promising perspectives has been the study of inhomogeneous Hele-Shaw cells. On the one hand, it is known that noise has a great influence in finger dynamics at very low values of surface tension, and as a side-branching mechanism in dendrites when anisotropy is present. The main source of experimental noise is probably gap and wetting variations. Only for this reason a formulation of Hele-Shaw flows with inhomogeneous gap and wetting conditions is fully justified. But in addition, a random gap introduces the possibility to study a completely different prob-

lem: the kinetic roughening of the interface when a viscous fluid displaces a less viscous one. Thus, we have formulated the problem with inhomogeneous gap and derived *ab initio* a nonlocal and nonlinear interface equation containing all noise terms with their microscopic coefficients and without any unknown parameter. This has been done in full generality of parameters (including viscosity contrast) and wetting conditions. We have identified new crossovers, such as that between capillary dominated noise and permeability dominated one, and have analyzed in detail the relevance of nonlinearities and the possible universality classes. We conclude that the early time regime that is relevant to most experimental studies, is governed by a new universality class defined by the zero-contrast fixed point defined by the $c = 0$ dynamics, which differs from the so-called Quenched KPZ universality class. The predictive power of our basic equations is yet to be fully explored and we expect it will not only help clarifying the interpretation of existing numerical and experimental results, but most importantly designing new experiments to better elucidate the open issues and presumably finding new growth regimes.

## 8.2 Summary of original results

The results of this thesis can be grouped in three different parts, namely a part concerning the singular effects of surface tension, a part devoted to the effects of viscosity contrast, and a part addressing the effects of a random gap as quenched disorder.

**Surface tension**

- We have analyzed explicit zero surface tension solutions of the Saffman-Taylor problem presenting nontrivial finger competition, and from its phase-space flow it has been concluded that they are generically unphysical in a global sense, when sufficiently large classes of initial conditions are considered simultaneously, because they lack the correct topology of the physical phase-space flow. The unphysical behavior of zero surface tension solutions is a consequence of the nonhyperbolicity of the multifinger fixed points of the finite-dimensional dynamical system that they define, as opposed to the saddle point structure of the regularized problem, which we argue it captures the essential physics as a crossover between *growth* (stable directions) and *competition* (unstable directions). We have proved that the N-logarithms class of solutions presents finite-time singularities if the continua of fixed points are removed thus confirming the generality of the conclusions reached

in low-dimensional models, namely, that for $B = 0$ either the flow is structurally unstable or it contains finite-time singularities, implying that no unfolding exists within the integrable class. The global failure of this class does not completely rule out all specific solutions.

- We propose a Dynamical Solvability Scenario (DSS) relevant in principle not only for viscous fingering but also of applicability to other pattern forming problems. Within this DSS the role of surface tension as a singular perturbation is to isolate multifinger saddle points out of the continua of multifinger fixed points. This extends the traditional solvability theory applied to steady state selection, where surface tension did also isolate a unique stable hyperbolic fixed point out of a continuum of nonhyperbolic ones. In the present extension, the introduction of surface tension does isolate a unique N-equal finger (saddle) fixed point out of each continuum of N-finger fixed points. By restoring this saddle point local structure the topology of the phase space flow is modified, so the introduction of surface tension has a deep impact on the global phase-space structure of the dynamics. It is in this sense that this scenario can be considered as a *dynamical* solvability theory.

- The effects of small surface tension on the zero surface tension solutions previously analyzed have been studied by means of the asymptotic perturbative theory for $0 < B \ll 1$ developed by Tanveer and coworkers. The evolution of the so-called daughter singularities has been studied both theoretically and numerically, and their impact times have been computed in relevant cases. It has been shown that surface tension has an effect of order one in an order one time in all cases with $\lambda < 1/2$, and for $\lambda \geq 1/2$ surface tension manifests either at order one or at a time of order $-\ln B$. In particular, surface tension manifests at order one when the asymptotic configuration belongs to the continuum of fixed points or when a clearly trailing finger wins the competition.

- A code to numerically solve the evolution equations of Hele-Shaw flows with arbitrary $B$ and $c$ has been developed. This code treats efficiently the numerical stiffness, is spectrally accurate and can deal with very small values of surface tension. It includes noise filtering to prevent the spurious growth of high order modes induced by roundoff noise, and can use quadruple (128-bit arithmetic) precision. The development of this code has been crucial to explore the small surface tension limit and in general, to establish the conclusions throughout this thesis on firm grounds.

- The above code has been used to study the evolution under small surface tension of the classes of integrable solutions studied previously. The effect of finite surface tension on exact solutions is dramatic since it modifies the topology of the phase space flow, including the removal of the continuum of fixed points (and the consequent restoring of hyperbolicity) and the change of the size of the basins of attraction of the problem (in the case where no continuum is present). At a quantitative level, surface tension manifests at order one when the asymptotic configuration belongs to the continuum of fixed points or when a clearly trailing finger wins the competition. Our calculations show that the impact of daughter singularities on either the shorter or larger finger retards the velocity of that finger, and is accompanied by the widening of the larger finger. As a consequence, in general the outcome of finger competition is independent of the particular finger on which the impact first occurs, and the finger which is leading at the time of the daughter singularity impact 'wins' the competition. We provide explicit criteria to establish when the zero-surface tension dynamics is quantitatively or qualitatively correct, for the studied explicit solutions. In general, we conclude that the $B = 0$ problem and the $B = 0^+$ one coincide only for *finite-time* evolutions departing from the planar interface and only up to infinite time for some trajectories going to fixed points consistent with selection theory ($\lambda = 1/2$). Remarkably, sufficiently generic and smooth configurations evolving with $B = 0$ to the correct asymptotic state may follow completely different paths in phase space for $B = 0^+$, changing for instance which finger wins the competition.

**Viscosity contrast**

- Finger competition with arbitrary viscosity contrast has been studied by means of numerical computation, using the code we have developed. A uniparametric initial condition with two modes has been chosen together with a value of surface tension in such a way that both modes grow at the same rate in the linear regime, and this initial condition has been used to precisely quantify the size of the basin of attraction of the Saffman-Taylor fixed point as a function of the viscosity contrast. The result we have obtained is that the basin of the ST fixed point decreases rapidly with decreasing values of the viscosity contrast, being practically very small for zero viscosity contrast. Similarly, the sensitivity of the dynamics to viscosity contrast is maximal at $c \approx 1$.

- We have identified a class of attractors which compete with the ST

finger as that of closed (Taylor-Saffman) bubbles. We have pointed out that the different topology of the two types of attractors explains the phenomenon of pinching, observed generically and which we have characterized quantitatively. The existence of actual finite-time topological singularities remains an open issue.

- A conformal mapping formulation of Hele-Shaw flows with zero viscosity contrast has been developed. This formalism takes advantage of the local character of vorticity for zero viscosity contrast. Explicit solutions for the evolution equation for the mapping have been sought, but only previously known solutions have been found. We have explicitly checked that the families of known solutions in the high viscosity contrast limit are not solution in the zero viscosity contrast one.

**Inhomogeneous gap**

- We have formulated the equations for Hele-Shaw flows with inhomogeneous gap, upon the assumption that Darcy law is locally valid. This formulation has been used to derive *ab initio* an interface equation for the problem of forced fluid invasion of a Hele-Shaw cell with random gap. This equation takes into account the nonlocality of the problem, is linear in the randomness and quadratic in the interfacial height, contains all noise effects and includes a noise term that has long range correlations both in space and time.

- The scaling properties of the rough interfaces that appear in forced fluid invasion of a Hele-Shaw cell with random gap have been studied by means of the interface equation we have derived. Two crossovers separating the corresponding regimes have been identified, in particular a new crossover between capillary noise and nonconserved noise has been found. The scaling of the interface has been studied in each of the regimes. The interface equation has been analytically solved for some particular types of noise, and numerically simulated in the case of quenched noise. From the simulation various roughness exponents at different length scales and parameter values have been determined. The obtained scaling properties are in good agreement with experimental results in one of the experimental regimes.

- A new universality class has been identified which governs the scaling in early time (capillary) regime, relevant to most experiments. The corresponding fixed point is that of the zero viscosity contrast problem, and its scaling properties differ from those of the Quenched KPZ

equation. We argue that the QKPZ fixed point does not describe any of the identified regimes of the problem.

## 8.3 Open questions and perspectives

Some of the results of this thesis have opened lines of research with a wide scope perspective. Other more specific open questions can also be listed which deserve further attention in the near future but correspond to tasks of more limited scope. Among the more general perspectives we quote three main lines:

- The formulation of Hele-Shaw flows with inhomogeneous gap has been applied to the forced fluid invasion problem, but there is a similar problem that we have not explicitly addressed and that is suitable to be dealt with our formulation, namely, spontaneous imbibition (constant pressure driving). The formulation could be applied to derive an interface equation with not only all the noise terms but also with the correct zero mode fluctuations, as a step beyond the existing phenomenological treatments with the aim at the study of pinning and avalanche phenomena.

- The interface equation for forced fluid invasion presents scaling behaviors that we have not completely uncovered, in particular in the capillary regime. More numerical work is necessary to provide further insight in this point. The effects of quadratic terms could be studied systematically in the regime where they might change the scaling properties, and nonlinear noise terms could also be added to the analysis. It would also be interesting to design new experiments to look for the new scaling regimes predicted.

- The existence of finite time pinchoff in the configurations studied in Chapter 5 needs further investigation, but the numerical scheme used seems inadequate to give additional information on the existence of the pinchoff. An alternative approach would be to use the lubrication approximation to Hele-Shaw equations in the pinching region and the computation of the full problem in the rest of the interface, matching the solutions in an appropriate way. This is a major task but the promise of universality makes the effort justified. The existence of nonforced, spontaneous pinchoff is also relevant in the more general context of topological singularities in fluid dynamics.

Among the more specific open questions that could deserve further study in the near future we have selected the following:

- The exact solution studied in Chapter 3 exhibits finite time pinchoff for some initial conditions, in the stable configuration of the problem where the viscous fluid displaces the nonviscous one. This is an exact prediction of a topological singularity. It would be of great interest to study if that pinchoff survives to the introduction of finite surface tension, using the tools of Chapter 4, namely the asymptotic perturbation theory and direct numerical computation with finite $B$.

- The long time behavior of Hele-Shaw flows with low viscosity contrast needs further investigation in the situation when the dynamics is not attracted to the Saffman-Taylor finger. Extending the numerical computations to larger times would be useful for a better understanding of the problem, but probably not conclusive unless the extension of the computation shows clear evidence of pinching. A different approach would be to look for exact composite steady-state solutions with zero surface tension consisting of a bubble and one or two fingers. Solutions (for $c = 1$) of a finger plus a bubble do exist, but on the same axis. If such solutions exist, they could shed new light into the long time asymptotics of the problem.

- One aspect of the evolution with small surface tension that has not been studied is the fate of exact solutions with $\lambda > 1/2$. In this case the asymptotic theory is not of much use, but numerical computation could answer the question. The possible phenomena that could arise are a tip splitting followed by the formation of a double ST finger, or simply the narrowing of the finger, by either a side-branching-like phenomenon or through a direct narrowing of the finger.

- We have observed that the evolution under very small $B$ is very sensitive to noise, but the noise present in the numerical computations is of numerical origin, caused by roundoff. It would be interesting to implement the noise contributions obtained in Chapter 6 into the code and then study the effect of noise of physical origin on the small $B$ evolution, in a fully controlled way.

## 8.4 List of publications and papers in preparation

**Included in the thesis**

- E. Pauné, F.X. Magdaleno, and J. Casademunt. Dynamical Systems approach to Saffman-Taylor fingering. A Dynamical Solvability Scenario. *Physical Review E*, 65:056213, 2002.
- E. Pauné, M. Siegel, and J. Casademunt. Effects of small surface tension in Hele-Shaw multifinger dynamics: an analytical and numerical study. *Physical Review E*, 66:, 2002. In press.
- E. Pauné and J. Casademunt. Multifinger dynamics in two-sided Hele-Shaw flows: fingers versus bubbles. Submitted to *Physics of Fluids*.
- E. Pauné and J. Casademunt. Kinetic roughening in two-phase fluid flow through a random Hele-Shaw cell. Submitted to *Physical Review Letters*. arXiv:cond-mat/0207673.
- E. Pauné and J. Casademunt. Interface equation for Hele-Shaw flows with quenched disorder. General derivation and numerical simulation. In preparation
- E. Pauné, R. Folch, and J. Casademunt. Hele-Shaw flows with arbitrary viscosity contrast. Conformal mapping approach. Preprint.

**Other publications**

- E. Alvarez-Lacalle, E. Pauné, J. Casademunt, and J. Ortín. Systematic weakly nonlinear analysis of radial viscous fingering. Submitted to *Physical Review E*.

# Appendix

# Appendix A

# Conformal mapping approach to zero viscosity contrast

The conformal mapping method used to study Hele-Shaw flows when one of the two fluids has negligible viscosity ($c = 1$) is generalized to zero viscosity contrast ($c = 0$). We derive an integro-differential equation for $c = 0$ and use the formalism to recover in a straightforward way the only time dependent solution known for arbitrary viscosity contrast and zero surface tension. Moreover, it is shown that any other solution of the $c = 1$ case is not a solution of the $c = 0$ case.

## A.1 Derivation

The arbitrary viscosity contrast case has received very little theoretical attention in comparison to the high viscosity contrast limit, mainly due to the lack of a suitable scheme for its analytical study. In the high viscosity contrast limit the conformal mapping approach is the tool that has made possible most of the progress achieved on the understanding of the problem, and for this reason we have developed a conformal mapping formulation of the $c = 0$ case, which takes a relatively compact form. For general $c$ this is also possible but much more involved.

The evolution equation for the time-dependent conformal mapping $f(\omega, t)$ of the interior of the unit circle in the complex plane $\omega$ into the region occupied by the fluid 2 in the physical plane $z = x + iy$ can be written as [BKL+86]

$$\partial_t f = \omega \partial_\omega f \, A \left\{ \frac{\mathrm{Re}[\omega \partial_\omega \Phi]}{|\omega \partial_\omega f|^2} \right\}, \tag{A.1}$$

and the normal velocity $U$ of the interface reads

$$U = -\frac{\mathrm{Re}[\omega\partial_\omega\Phi]}{|\omega\partial_\omega f|} \tag{A.2}$$

where $\Phi = \varphi + i\psi$ is the complex potential, $\varphi$ is the real velocity potential and $\psi$ the stream function. $A$ is an integral operator applied to a real-valued function $F(s)$, $0 \leq s < 2\pi$ defined on the unit circle, giving the complex-valued analytic function on the unit disk whose real part on the unit circle is $F(s)$, $\omega = e^{is}$. $A$ can be written as

$$A\{F\}(\omega) = a_0 + 2\sum_{n=1}^{\infty} a_n\omega^n \tag{A.3}$$

where the $a_n$'s are the Fourier coefficients of $F(s)$:

$$F(s) = a_0 + \sum_{n=0}^{\infty}\left(a_n e^{ins} + a_n^* e^{-ins}\right). \tag{A.4}$$

We recall the expression of $A$ in terms of its integral representation, given in Eq. (2.2):

$$A\{F\}(\omega) = \frac{1}{2\pi}\int_0^{2\pi} ds\, F(s)\frac{e^{is}+\omega}{e^{is}-\omega}. \tag{A.5}$$

The evolution equation Eq. (A.1) can be rewritten as

$$\mathrm{Re}\{i\,\partial_t f\,\partial_s f^*\} = \mathrm{Re}\{\omega\partial_\omega\Phi\} \tag{A.6}$$

on the unit circle, $\omega = e^{is}$.

To obtain a closed equation for the mapping $f$ we just need to express the complex potential $\Phi$ in terms of $f$, and replace it in Eqs. (A.1) or (A.6). In order to find $\Phi$ as a function of the mapping we will take advantage of the formulation of the problem in terms of the interface vorticity. In general, the vorticity depends on the velocity of the interface and its local geometry, but since the velocity is related to the vorticity through an integral expression, it is necessary to solve an integral equation to obtain the vorticity. However, for zero viscosity contrast the situation is different: for $c = 0$ the dependence of $\gamma$ on the velocity disappears and the vorticity $\gamma$ is only a function of the local geometry of the interface, as can be seen setting $c = 0$ in Eq. (1.13). We can use this property to obtain an expression for the stream function $\psi$ using the Green function method. Once $\psi$ is known we can calculate $\Phi$ using that $\psi$ is the imaginary part of the analytic function $\Phi$. For $c = 0$ fluid injection only introduces an homogenous advance of the interface without any other

dynamic consequence on the interface, and from now on it will be considered the case without injection, $V_\infty = 0$. The stream function $\psi$ can be obtained using the appropriate Green function $G(x - x', y - y')$ as

$$\begin{aligned}\psi(x,y) &= \int dx'\, dy'\, \Omega(x',y')\, G(x-x', y-y') \\ &= \int ds'\, \Omega\left[x(s'), y(s')\right] G\left[x - x(s'), y - y(s')\right] \end{aligned} \tag{A.7}$$

where the interface (and the vortex sheet) is parameterized by $(x(s'), y(s'))$. From now on, we will use complex variable techniques and the complex potential $\Phi$ will be a function of the complex variable $z = x + i\,y$. Moreover, within the context of the conformal mapping method, $z = f(\omega)$ and the interface is then described by $f(\omega = e^{is})$ with $s \in [0, 2\pi)$.

For the channel geometry the Green function appropriate to the problem must satisfy periodic boundary conditions along the $y$ axis, the one perpendicular to the channel walls. The Green function of an infinite channel of width $2\pi$ with periodic boundary conditions can be written as

$$G(z - z') = \frac{1}{2\pi}\left\{\ln[\mathrm{sign}(x - x')] + \ln\left[\sinh\left(\frac{z - z'}{2}\right)\right]\right\}. \tag{A.8}$$

Therefore, the complex potential $\Phi$ is

$$\Phi(s) = -i \int_0^{2\pi} ds' \gamma(s') G\left[f(s) - f(s')\right]. \tag{A.9}$$

We replace Eq. (A.8) into the previous equation and then calculate the quantity $\mathrm{Re}[\omega\partial_\omega\Phi]|_{\omega=e^{is}} = \mathrm{Im}[\partial_s\Phi]$, to obtain

$$\mathrm{Re}\left[\omega\partial_\omega\Phi\right]|_{\omega=e^{i\,s}} = \frac{-1}{4\pi}\mathrm{Re}\left\{\partial_s f\, P\int_0^{2\pi} ds'\gamma(s')\mathrm{cotgh}\left[\frac{f(s) - f(s')}{2}\right]\right\}. \tag{A.10}$$

$P$ stands for Cauchy's principal value and the vorticity $\gamma(s)$ can be written in terms of the mapping $f$ and the nondimensional surface tension $B$ as:

$$\gamma(s) = 2\mathrm{Re}(\partial_s f) + 2B\partial_s\kappa(s) \tag{A.11}$$

where $\kappa(s)$, the local curvature of the interface, is [BKL+86]

$$\kappa(s) = -\mathrm{Im}\frac{\partial_s^2 f/\partial_s f}{|\partial_s f|}. \tag{A.12}$$

Replacing Eq. (A.10) with $\gamma(s)$ given in Eq. (A.11) yields an integro-differential equation for the mapping:

$$\partial_t f = -\frac{1}{4\pi}\omega\partial_\omega f\, A\left(\frac{\mathrm{Re}\left\{\partial_s f\, P\int_0^{2\pi} ds'\gamma(s')\mathrm{cotgh}\left[\frac{f(s)-f(s')}{2}\right]\right\}}{|\omega\partial_\omega f|^2}\right) \tag{A.13}$$

and using the integral representation for $A$, Eq. (A.5)

$$\partial_t f = -\frac{1}{8\pi^2}\omega\partial_\omega f\int_0^{2\pi} d\theta\frac{e^{i\theta}+\omega}{e^{i\theta}-\omega}\frac{\mathrm{Re}\left\{\partial_s f\, P\int_0^{2\pi} ds'\gamma(s')\mathrm{cotgh}\left[\frac{f(\theta)-f(s')}{2}\right]\right\}}{|\omega\partial_\omega f|^2} \tag{A.14}$$

Eq. (A.14) is the evolution equation for the mapping $f(\omega,t)$ for zero viscosity contrast, together with the expression for the vorticity $\gamma$ given by Eq. (A.11). Eq. (A.14) is analogous to Eq. (2.7) for $c=1$, but more difficult to solve, as it will be shown in next section.

For arbitrary viscosity contrast a conformal mapping formulation [PFC02] of the problem is also possible but couples two different mapping functions. In general, a system of four integro-differential equations has to be solved, so the formulation is far more complicate than for the limiting cases $c=0$ and $c=1$, and does not seem to help analytical insights with respect to other more standard formulations of the problem.

## A.2 Exact solutions

We have checked that Eq. (A.13) reproduces the correct linear dispersion relation, Eq. (1.14). From now on we will concentrate on the zero-surface tension case, $B=0$, because for $B=0$ the expression for $\gamma$ is simpler, and in addition all relevant exact solutions found for $c=1$ have zero surface tension.

Large families of Eq. (A.1) are known in the high viscosity contrast limit (c=1), when one of the fluids has negligible viscosity (see for instance Refs. [How86, PMW94]), but only two nontrivial explicit solutions are known for arbitrary viscosity contrast: the stationary Saffman-Taylor finger [ST58] and the unsteady finger of width 1/2 found by Jacquard and Séguiner [JS62]. In our notation the mapping $f_{ST}$ of the Saffman-Taylor finger which moves with velocity $\mathcal{U}$ relative to the walls reads

$$f_{ST}(\omega,t) = -\ln\omega + \mathcal{U}t + 2(1-\lambda)\ln(1+\omega) \tag{A.15}$$

where the constant $\lambda$ is the ratio of the finger width to the width of the channel and takes real values in the interval $(0,1)$. Replacing $f_{ST}(\omega,t)$ in

Eq. (A.13) it is found that $\lambda$ and $\mathcal{U}$ are related through $\mathcal{U} = 2(1-\lambda)$, the known result from Ref. [ST58].

From the large families of exact time-dependent solutions known for $c = 1$ we have tested if the polynomial and logarithmic maps described in Chapter 2 are solutions of Eq. (A.14). The answer is negative in all cases but one. We have found only one nontrivial solution in the $c = 0$ case. This solution describes the temporal evolution of a finite finger of width $\lambda = \frac{1}{2}$ and reads:

$$f(\omega, t) = -\ln \omega + a(t) + \ln(b(t) + \omega) \tag{A.16}$$

with $a(t)$ and $b(t)$ real functions of time and $b(t) \geq 1$. This is the solution found by Jacquard and Séguier using a more complex method. Replacing Eq. (A.16) into Eq. (A.13) it is found that Eq. (A.16) is an exact solution, and $a(t)$ and $b(t)$ have the following form

$$a(t) = t + a(0) \quad \text{and} \quad b(t) = \sqrt{1 + (b(0)^2 - 1)e^{-2t}}. \tag{A.17}$$

This solution describes the evolution of the finger from an initial condition in the form of a small perturbation of the planar interface ($b \gg 1$) until it asymptotically approaches the ST finger shape ($b \to 1$, $t \to \infty$).

# Appendix B

# Derivation of bulk noise for arbitrary viscosity contrast

In this Appendix we derive an expression for the bulk noise contribution $\delta v_\zeta$ for arbitrary viscosity contrast $c \neq -1$.

First, we recall that the pressure $p = p_0 + \delta p$ in each fluid satisfies (see Eq. (6.5))

$$\nabla^2 p_0 = 0 \tag{B.1a}$$

$$\nabla^2 \delta p + \frac{3\nabla b}{b} \cdot \nabla p_0 = 0. \tag{B.1b}$$

On the interface, the pressure jump reads

$$p_2 - p_1 = \sigma\kappa \tag{B.2}$$

where $\kappa$ is the total mean curvature. To solve Eq. (B.1) we impose

$$p_{0,2} - p_{0,1} = \sigma\kappa \tag{B.3a}$$

$$\delta p_2 - \delta p_1 = 0. \tag{B.3b}$$

For $c = -1$, that is, when the displaced fluid has negligible viscosity, $p_2$ is constant and can be taken to be zero. Then, in this simpler case $\delta p_2 = 0$. But for $c \neq -1$ the more complicated boundary condition at the interface $\delta p_2 - \delta p_1 = 0$ has to be applied, and the method used in Section 6.2.1 to derive $\delta v_\zeta$ cannot be used. Then, in this case we will use an alternative method based on the formulation of Casademunt *et al.* in Ref. [CJHM92].

To solve Eq. (B.1b) we apply Green's theorem

$$\delta p_1(s) = \int_{\text{int}} ds' \left\{ \delta p_1(s') \frac{\partial \mathrm{G}[x(s)-x(s'), y(s)-y(s')]}{\partial n'} + \right. \\ \left. - \mathrm{G}[x(s)-x(s'), y(s)-y(s')] \frac{\partial \delta p_1(s')}{\partial n'} \right\} \\ + \int_1 dx'\, dy' \frac{3\nabla b}{b} \nabla p_{0,1} \mathrm{G}[x(s)-x', y(s)-y'] \tag{B.4a}$$

$$\delta p_2(s) = -\int_{\text{int}} ds' \left\{ \delta p_2(s') \frac{\partial \mathrm{G}[x(s)-x(s'), y(s)-y(s')]}{\partial n'} + \right. \\ \left. - \mathrm{G}[x(s)-x(s'), y(s)-y(s')] \frac{\partial \delta p_2(s')}{\partial n'} \right\} \\ + \int_2 dx'\, dy' \frac{3\nabla b}{b} \nabla p_{0,2} \mathrm{G}[x(s)-x', y(s)-y']. \tag{B.4b}$$

Now, the two equations are added and it is used that $\delta p_2(s) - \delta p_1(s) = 0$. Applying the partial derivative with respect to the normal component, $\frac{\partial}{\partial n}$, the resulting equation reads

$$(\mu_1+\mu_2)\delta v_\zeta(s) = \int ds' \left\{ \frac{\partial \mathrm{G}^{(2)}[x(s)-x(s'), y(s)-y(s')]}{\partial n} \mu_1 \delta v_\zeta(s') \right. \\ \left. - \frac{\partial \mathrm{G}^{(1)}[x(s)-x(s'), y(s)-y(s')]}{\partial n} \mu_2 \delta v_\zeta(s') \right\} \\ + \int_1 dx'\, dy' \frac{3\nabla b}{b} \mu_1 \mathbf{v}_{0,1} \frac{\partial \mathrm{G}[x(s)-x', y(s)-y']}{\partial n} \\ + \int_2 dx'\, dy' \frac{3\nabla b}{b} \mu_2 \mathbf{v}_{0,2} \frac{\partial \mathrm{G}[x(s)-x', y(s)-y']}{\partial n}, \tag{B.5}$$

where we have used $\mathbf{v}_{0,i} = -\frac{b_0^2}{12\mu_i}\nabla p_{0,i}$ and $\delta v_\zeta = -\frac{b_0^2}{12\mu_i}\nabla p_i$. $\frac{\partial \mathrm{G}^{(2)}}{\partial n}$ and $\frac{\partial \mathrm{G}^{(2)}}{\partial n}$ denote the limit from fluid 1 and 2 respectively, of the first order normal derivative.

Now we introduce the disorder in the gap: $\frac{\nabla b}{b} = \frac{1}{2}\frac{\nabla \zeta}{1+\zeta}$ and consider that the interface is quasiplanar $ds' = \sqrt{1+h'^2(x')}dx' \simeq dx'$. We will use the expression of the Green function in the free space, that is, considering a channel of infinite width or equivalently assuming that the walls have a negligible influence on the dynamics. It reads $\mathrm{G}(x-x', y-y') = \frac{-1}{4\pi}\ln[(x-x')^2+(y-y')^2]$. To evaluate the partial derivatives of the Green function we apply the results of Ref. [CJHM92], and consider $x(s) \simeq x$, $y(s) = h$

$$\frac{\partial \mathrm{G}^{(1,2)}[x(s)-x(s'), y(s)-y(s')]}{\partial n} = \mp\frac{1}{2}\delta(x-x') + \mathcal{O}(h) \tag{B.6}$$

and we consider

$$\frac{3\nabla b}{b}\mathbf{v}_0 \simeq \frac{3}{2}\nabla\zeta\cdot\mathbf{v}_0 \simeq \frac{3}{2}\nabla\zeta\cdot V_\infty\hat{\mathbf{y}} = \frac{3}{2}\frac{\partial\zeta}{\partial y}V_\infty \tag{B.7}$$

where we have kept only the leading order (linear) contribution. Replacing Eqs. (B.6) and (B.7) into Eq. (B.5) and integrating by parts the bulk integrals yields

$$\begin{aligned}(\mu_1+\mu_2)\delta v_\zeta(x) = &-\mu_1\int_{-\infty}^{\infty}dx'\delta(x-x')\frac{3}{2}V_\infty\zeta(x',y')\Big|_{-\infty}^{h(x')}\\ &+\mu_2\int_{-\infty}^{\infty}dx'\delta(x-x')\frac{3}{2}V_\infty\zeta(x',y')\Big|_{h(x')}^{\infty}\\ +\frac{\mu_1}{\pi}\int_{-\infty}^{\infty}dx'\int_{-\infty}^{h(x')}dy'&\frac{3}{2}V_\infty\zeta(x',y')\frac{\partial}{\partial y'}\frac{h(x)-y'}{(x-x')^2+(h(x)-y')^2}\\ +\frac{\mu_2}{\pi}\int_{-\infty}^{\infty}dx'\int_{h(x')}^{\infty}dy'&\frac{3}{2}V_\infty\zeta(x',y')\frac{\partial}{\partial y'}\frac{h(x)-y'}{(x-x')^2+(h(x)-y')^2}\end{aligned} \tag{B.8}$$

We keep the lowest order in the interface deviation $h-V_\infty t$ with respect to the mean interface, dropping terms of order $(h-V_\infty t)\zeta$, and apply the substitution $y=y'-V_\infty t$ and consider $\zeta(x',y'\to-\infty)=0$. Then, in terms of the viscosity contrast, $c=\frac{\mu_2-\mu_1}{\mu_2+\mu_1}$

$$\begin{aligned}\delta v_\zeta(x) = -\frac{3}{2}V_\infty\Big\{&\zeta(x,h(x))\\ -\frac{1-c}{2\pi}\int_{-\infty}^{\infty}dx'\int_{-\infty}^{0}dy'&\zeta(x',y'+V_\infty t)\frac{\partial}{\partial y'}\frac{-y'}{(-y')^2+(x-x')^2}\\ -\frac{1+c}{2\pi}\int_{-\infty}^{\infty}dx'\int_{0}^{\infty}dy'&\zeta(x',y'+V_\infty t)\frac{\partial}{\partial y'}\frac{-y'}{(-y')^2+(x-x')^2}\Big\}\end{aligned} \tag{B.9}$$

where the kernel has been rewritten in terms of the derivative to ease the evaluation of the Fourier transform of $\delta v_\zeta(x)$. The above equation is the main result of this Appendix, and to facilitate its comparison with the result for $c=-1$, Eq. (6.20) we compute its Fourier transform, that reads

$$\begin{aligned}\widehat{\delta v}_\zeta(k) = \frac{3V_\infty}{2}\Big\{&-\hat{\zeta}(k)+\frac{1-c}{2}|k|\int_{-\infty}^{\infty}dx'\int_{-\infty}^{0}dy\zeta(x',y+V_\infty t)e^{-ikx'}e^{y|k|}\\ &+\frac{1+c}{2}|k|\int_{-\infty}^{\infty}dx'\int_{0}^{\infty}dy\zeta(x',y+V_\infty t)e^{-ikx'}e^{y|k|}\Big\}\end{aligned} \tag{B.10}$$

and the result obtained in Sec. 6.2.1 for $c=-1$ is recovered. To obtain the full interface equation for arbitrary $c$ it is most convenient to start with the formulation of Ref. [CJHM92].

# Bibliography


[ABB+95] L. A. N. Amaral, A.-L. Barabási, S. V. Buldyrev, S. Havlin, R. Sadr-Lahijany, and H. E. Stanley. Avalanches and the directed percolation depinnig model: Experiments, simulation and theory. *Phys. Rev. E*, 51:4655, 1995.

[ALCO01] E. Alvarez-Lacalle, J. Casademunt, and J. Ortín. Systematic weakly nonlinear analysis of interfacial instabilities in Hele-Shaw flows. *Phys. Rev. E*, 64:016302, 2001.

[Alm96] R. Almgren. Singularity formation in Hele-Shaw bubbles. *Phys. Fluids*, 8(2):344–352, 1996.

[Alm98] R. F. Almgren. Comment on "Selection of the Saffman-Taylor finger width in the absence of surface tension: an exact result". *Phys. Rev. Lett.*, 81:5951, 1998.

[BACC93] M. Ben Amar, R. Combescot, and Y. Couder. Viscous fingering with adverse anisotropy — a new Saffman–Taylor finger. *Phys. Rev. Lett.*, 70:3047, 1993.

[BBC+92] S. V. Buldyrev, A.-L. Barabási, F. Caserta, S. Havlin, H. E. Stanley, and T. Vicsek. Anomalous interface roughening in porous media: Experiment and model. *Phys. Rev. A*, 45:R8313, 1992.

[BC94] M. Beccaria and G. Curci. Numerical simulation of the Kardar-Parisi-Zhang equation. *Phys. Rev. E*, 50:4560, 1994.

[Ben86] D. Bensimon. Stability of viscous fingers. *Phys. Rev. A*, 33:1302, 1986.

[Ben91] M. Ben Amar. Viscous fingering in a wedge. *Phys. Rev. A*, 44:3673, 1991.

[BHLS93] J. T. Beale, T. Y. Hou, J. S. Lowengrub, and M. J. Shelley. On the well-posedness of two fluid interfacial flows with surface tension. In R. Caflisch and G. Papanicolaou, editors, *Singularities in fluids, plasmas and optics*, page 11. Kluwer Academic, Amsterdam, 1993. Nato Adv. Sci. Inst. Ser. A.

[Bir54] G. Birkhoff. Taylor instability and laminar mixing. Technical Report LA-1862, Los Alamos Scientific Laboratory, December 1954.

[BKL+86] D. Bensimon, L. Kadanoff, S. Liang, B. I. Shraiman, and C. Tang. Viscous flows in two dimensions. *Rev. Mod. Phys.*, 58:977, 1986.

[BM91] E. A. Brener and V. I. Mel'nikov. 2-Dimensional dendritic growth at arbitrary Peclet number. *Adv. Phys.*, 40:53, 1991.

[BS95] A.-L. Barabási and H.E. Stanley. *Fractal Concepts in Surface Growth*. Cambridge University Press, Cambridge, UK, 1995.

[BST95] G. Baker, M. Siegel, and S. Tanveer. A well-posed numerical method to track isolated conformal map singularities in Hele-Shaw flow. *J. Comp. Phys.*, 120:348, 1995.

[Bur74] J. M. Burgers. *The Nonlinear Diffusion Equation*. Riedel, Boston, UK, 1974.

[CC01] R. Cuerno and M. Castro. Transients due to instabilities hinder Kardar-Parisi-Zhang scaling: a unified derivation for surface growth by electrochemical and chemical vapor deposition. *Phys. Rev. Lett.*, 87:23610, 2001.

[CCR92] B. Caroli, C. Caroli, and B. Roulet. Instabilities of planar solidification fronts. In C. Godrèche, editor, *Solids Far from Equilibrium*. Cambridge University Press, Cambridge, 1992.

[CDH+86] R. Combescot, T. Dombre, V. Hakim, Y. Pomeau, and A. Pumir. Shape selection of Saffman-Taylor fingers. *Phys. Rev. Lett.*, 56:2036, 1986.

[CH93] M.C. Cross and P.C. Hohenberg. Pattern formation outside of equilibrium. *Rev. Mod. Phys.*, 65:851, 1993.

[CH00] H.D. Ceniceros and T.Y. Hou. The singular perturbation of surface tension in Hele-Shaw flows. *J. Fluid Mech.*, 409:251, 2000.

[CHD+88] R. Combescot, V. Hakim, T. Dombre, Y. Pomeau, and A. Pumir. Analytic theory of the Saffman-Taylor fingers. *Phys. Rev. A*, 37:1270, 1988.

[CHS99] H.D. Ceniceros, T.Y. Hou, and H. Si. Numerical study of Hele-Shaw flows with suction. *Phys. Fluids*, 11:2471, 1999.

[CJ91] J. Casademunt and David Jasnow. Defect dynamics in viscous fingering. *Phys. Rev. Lett.*, 67:3677, 1991.

[CJ94] Jaume Casademunt and David Jasnow. Finger competition and viscosity contrast in viscous fingering. A topological approach. *Physica D*, 79:387, 1994.

[CJHM92] J. Casademunt, D. Jasnow, and A. Hernández-Machado. Interface equation and viscosity contrast in Hele-Shaw flow. *Int. J. Mod. Phys. B*, 6:1647, 1992.

[CL85] J. B. Collins and H. Levine. Diffuse interface model of diffusion-limited crystal growth. *Phys. Rev. B*, 31:6119–6122, 1985.

[CM89] S. A. Curtis and J. V. Maher. Racetrack of competing viscous fingers. *Phys. Rev. Lett.*, 63:2729, 1989.

[CM98] J. Casademunt and F. X. Magdaleno. Comment on "Selection of the Saffman-Taylor finger width in the absence of surface tension: an exact result". *Phys. Rev. Lett.*, 81:5950, 1998.

[CM00] J. Casademunt and F. X. Magdaleno. Dynamics and selection of fingering patterns. Recent developments in the Saffman-Taylor problem. *Phys. Rep.*, 337:1, 2000.

[Cra91] J.D. Crawford. Introduction to bifurcation theory. *Rev. Mod. Phys.*, 63:991, 1991.

[Cvv59] R. L. Chuoke, P. van Meurs, and C. van der Poel. The instability of slow, immiscible, liquid-liquid displacements in permeable media. *Pet. Trans. AIME*, 216:188, 1959.

[DKZ91] W. Dai, L. P. Kadanoff, and S. Zhou. Interface dynamics and the motion of complex singularities. *Phys. Rev. A*, 43:6672, 1991.

[DM87] A.T. Dorsey and O. Martin. Saffman–Taylor fingers with anisotropic surface-tension. *Phys. Rev. A*, 35:3989, 1987.

[DRE+99] M. Dubé, M. Rost, K.R. Elder, M. Alava, S. Majaniemi, and T. Ala-Nissila. Liquid conservation and nonlocal interface dynamics in imbibition. *Phys. Rev. Lett.*, 83:1628, 1999.

[DRE+00] M. Dubé, M. Rost, K.R. Elder, M. Alava, S. Majaniemi, and T. Ala-Nissila. Conserved dynamics and interface roughening in spontaneous imbibition: a phase field model. *Eur. Phys. J. B*, 15:701, 2000.

[DS85] A.J. DeGregoria and L.W. Schwartz. Finger breakup in Hele-Shaw cells. *Phys. Fluids*, 28:2313, 1985.

[DS86] A.J. DeGregoria and L.W. Schwartz. A boundary-integral method for two-phase displacement in Hele-Shaw cell. *J. Fluid Mech.*, 164:383, 1986.

[DS93] W. Dai and M. J. Shelley. A numerical study of the effect of surface tension and noise on an expanding Hele-Shaw bubble. *Phys. Fluids A*, 5:2131, 1993.

[Egg97] J. Eggers. Nonlinear dynamics and breakup of free-surface flows. *Rev. Mod. Phys.*, 69:865–929, 1997.

[EW82] S. Edwards and D.R. Wilkinson. The surface statistics of a granular aggregate. *Proc. Roy. Soc. London Ser. A*, 381:17, 1982.

[FCHMRP99a] R. Folch, J. Casademunt, A. Hernández-Machado, and L. Ramírez-Piscina. Phase field model for Hele-Shaw flows with arbitrary viscosity contrast. I. Theoretical approach. *Phys. Rev. E*, 60:1724, 1999.

[FCHMRP99b] R. Folch, J. Casademunt, A. Hernández-Machado, and L. Ramírez-Piscina. Phase field model for Hele-Shaw flows with arbitrary viscosity contrast. II. Numerical study. *Phys. Rev. E*, 60:1734, 1999.

[FPD01] M.J. Feigenbaum, I. Procaccia, and B. Davidovich. Dynamics of finger formation in laplacian growth without surface tension. *J. Stat. Phys.*, 103:973, 2001.

[FV85] F. Family and T. Vicsek. Scaling of the active zone in the Eden process on percolation networks and the ballistic deposition model. *J. Phys. A: Math. Gen.*, 18:L75, 1985.

[GB98] V. Ganesan and H. Brenner. Dynamic of two-phase fluid interfaces in random porous media. *Phys. Rev. Lett.*, 81:578, 1998.

[GH83] J. Guckenheiner and P. Holmes. *Nonlinear Oscillations, Dynamical Systems and Bifurcations of Vector Fields*. Applied Mathematical Sciences. Springer-Verlag, New York, 1983.

[GL99] J.P. Gollub and J.S. Langer. Pattern formation in nonequilibrium physics. *Rev. Mod. Phys.*, 71:S396, 1999.

[GPS98] R. E. Goldstein, A. I. Pesci, and M. J. Shelley. Instabilities and singularities in Hele-Shaw flow. *Phys. Fluids*, 10:2701, 1998.

[Hel98] H.S. Hele-Shaw. The flow of water. *Nature*, 58(1489):33, 1898.

[HFV91] Viktor K. Horváth, Fereydoon Family, and Tamás Vicsek. Dynamic scaling of the interface in two-phase viscous flows in porous media. *J. Phys. A: Math. Gen.*, 24:L25–L29, 1991.

[HHZ95] Timothy Halpin-Healy and Yi-Cheng Zhang. Kinetic roughening phenomena, stochastic growth, directed polymers and all that. aspects of multidisciplinary statistical mechanics. *Phys. Rep.*, 254(4–6):215–414, 1995.

[HKzW92] Shanjin He, Galathara L. M. K. S. Kahanda, and Po zen Wong. Roughness of wetting fluid invasions fronts in porous media. *Phys. Rev. Lett.*, 69(26):3731–3734, 1992.

[HL86] D. C. Hong and J. S. Langer. Analytic theory of the selection mechanism in the Saffman-Taylor problem. *Phys. Rev. Lett.*, 56:2032, 1986.

[HL87] D. C. Hong and J. S. Langer. Pattern selection and tip perturbations in the Saffman-Taylor problem. *Phys. Rev. A*, 36:2325, 1987.

[HLS94] T.Y. Hou, J.S. Lowengrub, and M.J. Shelley. Removing the stiffness from interfacial flows with surface tension. *J. Comp. Phys.*, 114:312, 1994.

[HLS01] T.Y. Hou, J.S. Lowengrub, and M.J. Shelley. Boundary integral methods for multicomponent fluids and multiphase materials. *J. Comp. Phys.*, 169:302, 2001.

[HMSL+01] A. Hernández-Machado, J. Soriano, A. M. Lacasta, M.-A. Rodríguez, L. Ramírez-Piscina, and J. Ortín. Interface roughening in Hele-Shaw flows with quenched disorder: Experimental and theoretical results. *Europhys. Lett.*, 55(5):194–200, 2001.

[How86] S.D. Howison. Fingering in Hele-Shaw cells. *J. Fluid Mech.*, 167:439, 1986.

[How00] S.D. Howison. A note on the two-phase Hele-Shaw problem. *J. Fluid Mech.*, 409:243, 2000.

[HS95] Viktor K. Horváth and H. Eugene Stanley. Temporal scaling of interfaces propagating in porous media. *Phys. Rev. E*, 52(5):5166–5169, 1995.

[JS62] P. Jacquard and P. Séguier. Mouvement de deux fluides en contact dans un milieu poreux. *J. de Mécanique*, 1:367, 1962.

[Kep11] J. Kepler. *De nive sexangula godfrey tampach.* Godfrey Tampach, Frankfurt am Main, 1611.

[KH88] A.R. Kopf–Sill and G.M. Homsy. Nonlinear unstable viscous fingers in Hele–Shaw flows. 1: Experiments. *Phys. Fluids*, 31:242, 1988.

[KKa88] D. A. Kessler, J. Koplik, and H. and, Levine. Pattern selection in fingered growth fenomena. *Adv. Phys.*, 35:255, 1988.

[KL86] D. A. Kessler and H. Levine. Coalescence of Saffman-Taylor fingers: A new global instability. *Phys. Rev. A*, 33:R3625, 1986.

[KL01] D. A. Kessler and H. Levine. Microscopic selection of fluid fingering patterns. *Phys. Rev. Lett.*, 86:4532, 2001.

[KM91] J. Krug and P. Meakin. Kinetic roughening of laplacian fronts. *Phys. Rev. Lett.*, 66:703, 1991.

[Kob93] R. Kobayashi. Modelling and numerical simulations of dendritic crystal growth. *Physica D*, 63:410, 1993.

[KPZ86] M. Kardar, G. Parisi, and Y.-C. Zhang. Dynamic scaling of growing interfaces. *Phys. Rev. Lett.*, 56:889, 1986.

[KqZFzW92] Galathara L. M. K. S. Kahanda, Xiao qun Zou, Robert Farrell, and Po zen Wong. Columnar growth and kinetic roughening in electrochemical deposition. *Phys. Rev. Lett.*, 68:3741, 1992.

[Kra86] R. Krasny. A study of singularity formation in a vortex sheet by the point-vortex approximation. *J. Fluid Mech.*, 167:65, 1986.

[Kru97] J. Krug. Origins of scale invariance in growth processes. *Adv. Phys.*, 46:139, 1997.

[Lan80] J. S. Langer. Instabilities and pattern formation in crystal growth. *Rev. Mod. Phys.*, 52:1, 1980.

[Lan86] J. S. Langer. Models of pattern formation in first-order phase transitions. In G. Grinstein and G. Mazenko, editors, *Directions in Condensed Matter Physics*, page 165. World Scientific, Singapore, 1986.

[Lan87] J. S. Langer. Lectures in the theory of pattern formation. In J. Souletie, J. Vannimenus, and R. Stora, editors, *Chance and Matter, 1986 Les Houches Lectures*. North-Holland, Amsterdam, 1987.

[Les96] H. Leschhorn. Anisotropic interface depinning: Numerical results. *Phys. Rev. E*, 54:1313, 1996.

[LSSC+97] M.Q. López-Salvans, F. Sagués, J. Claret, , and J. Bassas. Fingering instability in thin-layer electrodeposition: general trends and morphological transitions. *J. Electroanal. Chem*, 421:205, 1997.

[Mag00] Francesc Xavier Magdaleno. *Singular effects of surface tension in Saffman-Taylor dynamics*. PhD thesis, Universitat de Barcelona, 2000.

[Mah85] J. V. Maher. Development of viscous fingering patterns. *Phys. Rev. Lett.*, 54:1498, 1985.

[Man77] B.B. Mandelbrot. *Fractals: form, chance and dimension*. Freeman, San Francisco, 1977.

[Man90] P. Manneville. *Dissipative structures and weak turbulence*. Academic Press, New York, 1990.

[Mar51] G.H. Markstein. Experimental and theoretical studies of flame-front stability. *J. Aero. Sci.*, 18:199, 1951.

[Max87] T. Maxworthy. The nonlinear growth of a gravitationally unstable interface in a Hele-Shaw cell. *J. Fluid Mech.*, 177:207, 1987.

[MC98] F. X. Magdaleno and J. Casademunt. Surface tension and dynamics of fingering patterns. *Phys. Rev. E*, 57:R3707, 1998.

[MC99] F. X. Magdaleno and J. Casademunt. Two-finger selection theory in the Saffman-Taylor problem. *Phys. Rev. E*, 60:R5013, 1999.

[MC01] F. X. Magdaleno and J. Casademunt. Reply to "Comment on 'Two-finger selection theory in the Saffman-Taylor problem"'. *Phys. Rev. E*, 63:043102, 2001.

[MHKZ89] E. Medina, T. Hwa, M. Kardar, and Y.-C. Zhang. Burgers equation with correlated noise: Renormalization-group analysis and applications to directed polymers and interface growth. *Phys. Rev. A*, 39:3053, 1989.

[MM92] S. Matsuura and S. Miyazima. Self-affine fractal growth front of Aspergillus oryzae. *Physica A*, 191:30, 1992.

[MM95] K. V. McCloud and J. V. Maher. Experimental perturbations to Saffman-Taylor flow. *Phys. Rep.*, 260:139, 1995.

[MRC00] F. X. Magdaleno, A. Rocco, and J. Casademunt. Interface dynamics in Hele-Shaw flows with centrifugal forces: Preventing cusp singularities with rotation. *Phys. Rev. E*, 62:R5887, 2000.

[MS64] W.W. Mullins and R.F. Sekerka. The stability of a planar interface during solidification of a dilute binary alloy. *J. App. Phys.*, 3:444, 1964.

[MS81] J. W. McLean and P. G. Saffman. The effect of surface tension on the shape of fingers in a Hele-Shaw cell. *J. Fluid. Mech.*, 102:455, 1981.

[MW97] M. Mineev-Weinstein. Selection of the Saffman-Taylor finger width in the absence of surface tension: an exact result. *Phys. Rev. Lett.*, 80:2113, 1997.

[MW98] M. Mineev-Weinstein. Mineev-weinstein replies. *Phys. Rev. Lett.*, 81:5952, 1998.

[MWD94] M. Mineev-Weinstein and S. P. Dawson. Class of nonsingular exact solutions of laplacian pattern formation. *Phys. Rev. E*, 50:R24, 1994.

[MWK99] M. Mineev-Weinstein and O. Kupervasser. Finger competition and formation of a single Saffman-Taylor finger without surface tension: an exact result. patt-sol/9902007, 1999.

[NP77] G. Nicolis and I. Prigogine. *Self-Organization in Nonequilibrium Systems: From Dissipative Structures to Order through Fluctuations*. Wiley, New York, 1977.

[PA92] Y. Pomeau and M. Ben Amar. Dendritic growth and related topics. In C. Godrèche, editor, *Solids Far from Equilibrium*. Cambridge University Press, Cambridge, 1992.

[Pat81] L. Paterson. Radial fingering in a Hele–Shaw cell. *J. Fluid Mech.*, 113:513, 1981.

[PC82] P. Pelcé and P. Clavin. Influence of hydrodinamics and diffusion upon the stability limits of laminar premixed flames. *J. Fluid Mech.*, 124:219, 1982.

[Pel88] P. Pelcé, editor. *Dynamics of Curved Fronts*. Perspectives in Physics. Academic Press, Boston, 1988.

[PFC02] E. Pauné, R. Folch, and J. Casademunt. Hele-Shaw flows with arbitrary viscosity contrast. Conformal mapping approach. Preprint, 2002.

[PH84] C.W. Park and G.M. Homsy. Two-phase displacement in Hele–Shaw cells: theory. *J. Fluid Mech.*, 139:291, 1984.

[PH85] C.W. Park and G.M. Homsy. The instability of long fingers in Hele–Shaw flows. *Phys. Fluids*, 28:1583, 1985.

[PMC02] E. Pauné, F. X. Magdaleno, and J. Casademunt. Dynamical systems approach to Saffman-Taylor fingering: Dynamical solvability scenario. *Phys. Rev. E*, 65:056213, 2002.

[PMW94] S. Ponce Dawson and M. Mineev-Weinstein. Long time behavior of the n-finger solution of the laplacian growth equation. *Physica D*, 73:373, 1994.

[PSC02] E. Pauné, Michael Siegel, and J. Casademunt. Singular effects of surface tension in the dynamics of two finger competition in Hele-Shaw flows. *Phys. Rev. E*, 66, 2002. In press.

[Rai91] Y. P. Raizer. *Gas discharge physics*. Springer, Berlin, 1991.

[REDG89] M. A. Rubio, C. A. Edwards, A. Dougherty, and J. P. Gollub. Self-affine fractal interfaces from immiscible displacement in porous media. *Phys. Rev. Lett.*, 63:1685–1688, 1989.

[RLR00] J.J. Ramasco, J.M. López, and M.A. Rodríguez. Generic dynamics scaling in kinetic roughening. *Phys. Rev. Lett.*, 84:2199, 2000.

[Rog77] R. Rogallo. An Illiac program for the numerical simulation of homogeneous incompressible turbulence. NASA Tech. Report TM-73203, NASA Ames Research Center, 1977.

[RY90] I. Richards and H. Youn. *Theory of distributions: a non-technical introduction*. Cambridge University Press, Cambridge, UK, 1990.

[Saf59] P. G. Saffman. Exact solutions for the growth of fingers from a flat interface between two fluids in a porous medium or Hele-Shaw cell. *Quart. J. Mech. and Applied Math.*, 12:146, 1959.

[Sar85] K.S. Sarkar. Generalization of singularities in nonlocal interface dynamics. *Phys. Rev. A*, 31:3468, 1985.

[SB84] B. I. Shraiman and D. Bensimon. Singularities in nonlocal interface dynamics. *Phys. Rev. A*, 30:2840, 1984.

[Shr86] B. I. Shraiman. Velocity selection and the Saffman-Taylor problem. *Phys. Rev. Lett.*, 56:2028, 1986.

[SL98] K. S. Sarkissian and H. Levine. Comment on "Selection of the Saffman-Taylor finger width in the absence of surface tension: an exact result". *Phys. Rev. Lett.*, 81:4528, 1998.

[SOHM02a] J. Soriano, J. Ortín, and A. Hernández-Machado. Anomalous roughening in experiments of interfaces in Hele-Shaw flows with strong quenched disorder. cond-mat/0208432, 2002.

[SOHM02b] J. Soriano, J. Ortín, and A. Hernández-Machado. Experiments of interfacial roughening in Hele-Shaw flows with weak quenched disorder. *Phys. Rev. E*, 66:031603, 2002.

[SRR+02] J. Soriano, J. J. Ramasco, M. A. Rodríguez, A. Hernàndez-Machado, and J. Ortín. Anomalous roughening of Hele-Shaw flows with quenched disorder. *Phys. Rev. Lett.*, 89:026102, 2002.

[SS86] Youcef Saad and Martin H. Schultz. GMRES: a generalized minimal residual algorithm for solving nonsymmetric linear systems. *SIAM J. Sci. Stat. Comp.*, 7:856, 1986.

[ST58] P.G. Saffman and G. Taylor. The penetration of a fluid into a porous medium or Hele-Shaw cell containing a more viscous liquid. *Proc. R. Soc. Lond. A*, 245:312, 1958.

[ST96] M. Siegel and S. Tanveer. Singular perturbation of smoothly evolving Hele-Shaw solutions. *Phys. Rev. Lett.*, 76:419, 1996.

[STD96] M. Siegel, S. Tanveer, and W.-S. Dai. Singular effects of surface tension in evolving Hele-Shaw flows. *J. Fluid Mech.*, 323:201, 1996.

[TA83] G. Tryggvason and H. Aref. Numerical experiments on Hele-Shaw flow with a sharp interface. *J. Fluid Mech.*, 136:1, 1983.

[TA85] G. Tryggvason and H. Aref. Finger-interaction mechanisms in stratified Hele-Shaw flow. *J. Fluid Mech.*, 154:287, 1985.

[Tan86] S. Tanveer. The effect of surface tension on the shape of a Hele-Shaw bubble. *Phys. Fluids*, 29:3537, 1986.

[Tan87a] S. Tanveer. Analytic theory for the linear-stability of the Saffman–Taylor finger. *Phys. Fluids*, 30:2318, 1987.

[Tan87b] S. Tanveer. New solutions for steady bubbles in a Hele-Shaw cell. *Phys. Fluids*, 30:651, 1987.

[Tan91] S. Tanveer. Saffman-Taylor finger problem with thin film effects. In M. Ben Amar et al., editors, *Growth and Form*. Plenum Press, New York, 1991.

[Tan93] S. Tanveer. Evolution of Hele-Shaw interface for small surface tension. *Phil. Trans. R. Soc. Lond. A*, 343:155, 1993.

[Tan00] S. Tanveer. Surprises in viscous fingering. *J. Fluid Mech.*, 409:273, 2000.

[Tho17] D'Arcy Wentworth Thompson. *On growth and form*. Cambridge University Press, Cambridge, 1917.

[TL86] P. Tabeling and A. Libchaber. Film draining and the Saffman–Taylor problem. *Phys. Rev. A*, 33:794, 1986.

[TRHC89] H. Thome, M. Rabaud, V. Hakim, and Y. Couder. The Saffman-Taylor instability: from the linear to the circular geometry. *Phys. Fluids A*, 1:224, 1989.

[TS59] G. Taylor and P.G. Saffman. A note on the motion of bubbles in a Hele-Shaw cell and porous medium. *Quart. J. Mech. Applied Math.*, 12:265, 1959.

[TZL87] P. Tabeling, G. Zocchi, and A. Libchaber. An experimental study of the Saffman–Taylor instability. *J. Fluid Mech.*, 177:67, 1987.

[Vas01a] G. L. Vasconcelos. Comment on "Two-finger selection theory in the Saffman-Taylor problem". *Phys. Rev. E*, 63:043101, 2001.

[Vas01b] G. L. Vasconcelos. Exact solutions for steady bubbles in a Hele-Shaw cell with rectangular geometry. *J. Fluid Mech.*, 444:175, 2001.

[VB83] J. M. Vanden-Broeck. Fingers in a Hele-Shaw cell with surface tension. *Phys. Fluids*, 26:2033, 1983.

[VCH90] T. Vicsek, M. Cserzo, and V.K. Horváth. Self-affine growth of bacterial colonies. *Physica A*, 167:315, 1990.

[VnJ92] J. Viñals and D. Jasnow. Coarsening following a morphological instability in the one-sided model. *Phys. Rev. A*, 46:7777, 1992.

[Wal97] D. Walgraef. *Spatio-temporal pattern formation.* Springer-Verlag, Heidelberg, 1997.

[WS81] T. A. Witten and L. M. Sander. Diffusion-limited aggregation, a kinetic critical phenomenon. *Phys. Rev. Lett.*, 47:1400, 1981.

[Zha90] Y.-C. Zhang. Non-universal roughening of kinetic self-affine interfaces. *J. de Physique*, 51:2129, 1990.

[ZOM98] O. Zik, Z. Olami, and E. Moses. Fingering instability in combustion. *Phys. Rev. Lett.*, 81:3868, 1998.

[ZZAL92] J. Zhang, Y.C. Zhang, P. Alstrom, and M.T. Levinsen. Modeling forest-fire by a paper-burning experiment, a realization of the interface growth mechanism. *Physica A*, 189:383, 1992.